UNIVERSITY OF OKLAHOMA

GRADUATE COLLEGE

CARBON NANOTUBES AS CATALYST SUPPORTS IN BIPHASIC SYSTEMS

A DISSERTATION

SUBMITTED TO THE GRADUATE FACULTY

in partial fulfillment of the requirements for the

Degree of

DOCTOR OF PHILOSOPHY

By

NICHOLAS M. BRIGGS
Norman, Oklahoma
2016

CARBON NANOTUBES AS CATALYST SUPPORTS IN BIPHASIC SYSTEMS

A DISSERTATION APPROVED FOR THE
SCHOOL OF CHEMICAL, BIOLOGICAL AND MATERIALS ENGINEERING

BY

_____
Dr. Steven P. Crossley, Chair

_____
Dr. Daniel E. Resasco

_____
Dr. Brian P. Grady

_____
Dr. Walter E. Alvarez

_____
Dr. David A. Sabatini

The author dedicates this work to his brother Evan Briggs, mother Ann Briggs, and father Paul Briggs.

Acknowledgements

My brother Evan for being the best brother I can ever ask for. I never cease to be amazed by his belief in me and how he supports me anyway he can.

My mother for helping me become the man I want to be by teaching me to be considerate of others, treat everyone as equal, not to take advantage of others when they are vulnerable, her unwavering support, and indomitable belief in me.

My father who taught me what an engineer is, how exciting the field of engineering can be, for teaching me to take a holistic approach to solving problems, and for his continual support and belief that I can achieve my goals.

My grandparents Carlyle Briggs and Maxine Briggs who inspire me by operating their own engineering firm, B & A Engineer, Inc, and always believe in a positive outcome for me when I face challenges.

My mothers and fathers family members who have always believed in me.

My best friend Valeria Herrera Araque for her unwavering belief in me, always supporting me however she can, and reminding me life is a balance of many aspects. Her extra help at the end of this journey was invaluable.

My advisor Dr. Steven Crossley who made time for me to discuss research ideas with him and for letting me explores my ideas in the lab. The freedom I was given made the experience fun and exciting. He taught me how to conduct research in an effective, professional, and safe manner. Importantly, Dr. Crossley gave me a great foundation to build from as a scientist and engineer.

Dr. Daniel Resasco for teaching me to be on the lookout for new opportunities during my time as a graduate student and how critical engineers and scientist must be of

our results. I learned how to be critical of my results and to validate my results with different methods to ensure my conclusion was correct. In addition, to always look at published articles critically and look for alternative explanations, even when the articles are authored by the experts. I greatly appreciated him allowing me to work with his group and sharing resources; it has been a tremendous benefit for me.

Dr. Brian Grady for collaborating with Dr. Crossley and myself on the first project I worked on. From this project I was able to branch off into many different areas and work on many exciting projects. For also going with Javen Weston and I to do neutron scattering at Oakridge National Laboratories, which gave me an opportunity to learn about neutron scattering.

Dr. David Sabatini for providing a great class on emulsions and surfactants and teaching in a way which made what I learned in the class highly applicable to my research. I was able to use what I learned in his class many times during my research.

Dr. Walter Alvarez for giving me perspective on how research is performed in industry and the importance of safety.

For the help and suggestions from, Dr. Tawan Sooknoi, Dr. Bin Wang, Dr. Rolf Jentoft, Dr. Clint Aichele, Dr. Lance Lobban, Dr. Friederike Jentoft, and Dr. Richard Mallinson.

Preston Larson and Greg Strout for their help with scanning electron microscopy, transmission electron microscopy, sample preparation and sharing their knowledge and expertise with me.

Jimmy Faria, Wesley Tennyson, and Dachuan Shi for taking the time to teach and mentor me at the beginning of my graduate studies. From each I learned a different way of approaching research as a graduate student.

Chase Brown for the many discussions we had on carbon nanotubes, emulsions, and reactions. He is a good friend and shared in the experience of being a graduate student with me.

My friends and colleagues: Javen Weston, Lawrence Barrett, Zheng Zhao, Abhishek Gumidyala, Manasa Godavarthy, Santiago Umbarilla Garcia, Daniel Santhanaraj, Felipe Anaya Saltarin, Mohammed Reda Bababrik, Mohannad Kadhum, Duong Ngo, Yen Pham, Tu Pham, Rajiv Janupala, Puridej Warakunwit, Nhung Duong, Tuong Bui, Tyler Vann, J. J. Hamon, Qiaohua Tan, Cristian Jimenez Rojas, Ali Mehdad, Taiwo Omotoso, and Tania Vitery Erazo.

Everyone part of the biofuel and nanotube groups.

The undergraduates who have worked with me: Brian Li, Devlin Leavitt, Paulina Del Rio, Alex Schwans, Brandon Bonk, Issac Schneberger, Nick Bray, Jared Dopp, Dillon Kang, and Bree Cooper. Many of whom I enjoyed working with and by working with them gave us the opportunity to explore new research ideas.

Terri Colliver, Wanda Gress, Vernita Farrow, Donna King, and Madena McGinnis, for making the department feel like home, helping with purchasing equipment, setting up conferences, and arranging travel.

Alan Miles for helping me with construction and repair of reactors and for sharing his invaluable electrical and mechanical knowledge.

Southwest Nanotechnologies and Dr. Ricardo Prada Silvy for providing carbon nanotubes used in many of the following studies.

Table of Contents

List of Tables

List of Figures

Abstract

Carbon nanotubes are studied as catalyst supports in biphasic (oil and water) systems. In the first part the relationships between a carbon nanotubes properties before and after functionalization and the influence those properties have on emulsions characteristics is studied. Emulsion characteristics studied were emulsion type, droplet size, interfacial area, and quantity of carbon nanotubes at the oil-water interface. Emulsions stabilized with carbon nanotubes are compared with emulsions stabilized with silica nanoparticles to further understand how material properties influence emulsion characteristics. The relationship between carbon nanotubes and silica nanoparticles properties and emulsion characteristics is utilized to control reaction selectivity, further understand the particles environment at the oil-water interface, and create a responsive system where reaction selectivity can be tuned as the reaction proceeds. Finally, with the ability to synthesize carbon nanotubes with different properties a novel catalyst is made which can determine the location of the active site for bifunctional catalysts.

Keywords - Carbon nanotubes, surfactant, hydrogen spillover, Pickering emulsions, bifunctional catalysts, biphasic, responsive, and catalysis.

Chapter 1: Introduction

Biphasic systems are composed of two chemically similar, but physically distinct phases. Common examples of these are two immiscible liquids, such as oil and water, liquid and gas, such as a bubble, and two physically distinct solids, such as a metal alloy under certain conditions or a polymer blend with two immiscible polymers. The use of two distinct phases can be creatively taken advantage as in biology,[1,2] carbon nanotube separation based on chirality,[3] cosmetics industry,[4] food industry,[5] enhanced oil recovery,[9] homogenous catalysis,[6] and heterogeneous catalysis.[7,8] The basis for this work is the last example where heterogeneous catalysis is performed in biphasic systems composed of oil and water.

Conducting heterogeneous catalysis in biphasic systems offers several advantages. These advantages are: (1) controlling selectivity by operating under mass transfer conditions wherein molecules in a specific phase are reacted with catalyst solely in that phase, (2) effective separation of products and reactants by utilizing the differences in solubility of oil and water, (3) phase transfer of molecules between the oil and water phases which can be made facile with a emulsion which increases the interfacial area, and (4) the combination of a reaction system and separation process. These advantages can have use in production of specialty chemicals, pharmaceuticals, enhancement of oil recovery,[9] Fischer-Tropsch synthesis,[143,144] and biomass conversion to fuels.[7,8]

Due to the many advantages gained by performing heterogeneous catalysis in biphasic systems, several aspects are explored. The particles properties on emulsion characteristics and the effect these characteristics have on reaction selectivity are examined. To explore these aspects carbon nanotubes are used as emulsion stabilizers

and catalyst supports for several reasons. Carbon nanotubes can be functionalized to have a variety of different functional groups on the surface.[27,33] The van der Waals forces which cause carbon nanotubes to agglomerate together have been shown to create rigid networks which helps stabilize emulsions.[63] The conductive nature of carbon nanotubes makes them capable of hydrogen spillover, which is an important phenomenon in many catalytic applications.[271,272,274] Carbon nanotubes can be grown in a random,[254,255] horizontal,[253] or vertical[251,255] orientation with chemical vapor deposition, which provides flexibility when making catalysts. The structure of carbon nanotubes provides a large external surface area and catalyst particles reside on the outside of the carbon nanotubes which eliminates internal mass transfer limitations and makes studying particles at the oil-water interface facile. With this combination of properties carbon nanotubes are suitable for understanding the relationship between a particles properties and emulsion characteristics and using that knowledge for controlling chemical reactions in biphasic systems.

In this work, carbon nanotubes are functionalized to tune their wettability to understand the relationship between carbon nanotubes wettability and emulsion characteristics. Emulsion type, droplet size, interfacial area, and quantity of carbon nanotubes at the oil-water interface are measured. The knowledge gained from this is then tied with reactions to further understand the environment of the carbon nanotubes at the oil-water interface and how reaction selectivity can be tuned. Carbon nanotubes are compared with silica nanoparticles, due to their wide use in research and industry, to act as a comparison and to understand a materials influence on emulsion characteristics. Using the knowledge gained from the behavior of carbon nanotubes and silica

nanoparticles at the oil-water interface a responsive system is created where the particles environment at the oil-water interface is tuned while the reaction proceeds. Tuning the particles environment as the reaction proceeds allows for the reaction selectivity to be controlled as the reaction proceeds, thereby creating a responsive system. Finally, utilizing the ability to synthesize catalyst which can control selectivity in biphasic systems, a novel catalyst using carbon nanotubes is created which can determine the location of the active site when using bifunctional catalysts.

Chapter 2: Stable Pickering Emulsions using Multi-Walled Carbon Nanotubes of Varying Wettability

Introduction

Pickering emulsions have found uses in catalysis,[7,8,9] Janus particle synthesis[10,11,12,13,14,15], oil recovery[16], food applications[17], drug delivery[18], and templates[19]. With the many uses for Pickering emulsions, the ability to control their properties offers many attractive commercial applications. Emulsion droplet size and type of emulsion can be controlled by tuning the wettability of fumed silica (by varying the percent of SiOH) which in turn allows for control over the emulsion's properties[20]. In addition, silica particles fused with single-walled carbon nanotubes (SWNTs) can also be tuned to change emulsion droplet size and type of emulsion when the SWNTs are oxidized[21].

Results from silica experiments have indicated that minimum emulsion droplet size is achieved when the silica particles are amphiphilic[20,43]. The relationship of droplet size to particle wettability is determined by the free energy of a spherical particle adsorption at a planar interface. For a spherical particle at a planar interface the free energy is [20,22,23,43]

$$E = \pi R^2 \gamma_{ow} (1 \pm cos\theta)^2$$

where R is the particle's radius, γ_{ow} is its interfacial tension, θ is its contact angle, and E is the energy required for the particle to be adsorbed at the interface. By plotting the equation, while holding both the radius and interfacial tension constant and varying the

contact angle, it can be seen that the energy required to remove the particle from the interface is greatest when the contact angle is at 90°.

The same trend that is seen for spheres is also seen for cylinders, with the greatest energy required for adsorption/desorption of a cylinder at the interface when the contact angle is at 90°[24,25,26]. Because of this, adsorption of cylinders at the interface is most favorable in the parallel orientation, not the perpendicular orientation[24]. Our recent work has shown the majority of multi-walled carbon nanotubes (MWNTs) orient themselves parallel to the interface of the emulsion droplet[27].

Despite extensive work done with Pickering emulsions stabilized with silica, few studies have focused on MWNTs being used as Pickering emulsion stabilizers. The first study with carbon nanotubes in Pickering emulsions was with SWNTs[28], which was followed up by work showing that SWNTs wrapped with DNA are also capable of stabilizing emulsions[29]. Pickering emulsions with SWNTs have been used to remove SWNT bundles from individual SWNTs,[30,31] for the purpose of achieving a scalable separation of SWNTs. Oxidized MWNTs were also used to make water in oil (w/o) emulsions that could then be dried out to create carbon nanotube microcapsules[32]. MWNTs oxidized through plasma treatment were also shown to stabilize oil in water (o/w) emulsions[33]. Recently it was shown that attractive van der Waals forces between carbon nanotubes makes them agglomerate together and create a rigid network of carbon nanotubes at the emulsion interface that enhance emulsion stability[34]. Our recent work also found that the addition of a surfactant creates a repulsive force between carbon nanotubes that decreases emulsion stability[27]. Other studies that we reviewed, however, provided little information on how emulsion droplet size and emulsion type

can be tuned by varying MWNT wettability, oil to water ratios and the mix of MWNTs with different wettability characteristics. To the best of our knowledge, there has been no effort made to control the degree of MWNT functionalization to see if higher emulsion stability could be obtained. Due to the vast use of Pickering emulsions in industry, the ability to be able to have greater control over emulsion properties and their stability could have an impact in many industrial fields.

The main objective of this study is to examine Pickering emulsions stabilized with MWNTs of different wettability characteristics and the potential impact on emulsion stability. In addition to this, the effects of using different oils, oil to water ratios, concentrations of MWNTs, mixes of MWNTs with different wettability characteristics were studied, along with the phase in which the MWNTs were initially dispersed. Studying these effects allows for further comparisons to be drawn between MWNTs and other emulsion stabilizers. This study shows how MWNT wettability can be changed to tune emulsion properties and shows the effects these changes have on MWNT stability. We hope that as a result of the many parameters tested in this study, that comparisons can be made between MWNTs and other emulsion stabilizers used in the literature that will be of value to the community.

Experimental Details

MWNTs were obtained from SouthWest Nanotechnologies, Inc. that were designated by the company as type SMW100. The MWNTs were less than one micron long with diameters between 6 to 9 nm, and contained from 3 to 6 walls. Nitric acid

(70%), dodecane (99%), heptane (99%), and toluene (99%) were purchased from Sigma Aldrich. 18 MΩ water was obtained from a Cole Parmer filtration system.

Oxidation of the MWNTs was completed by adding one gram of MWNTs to a round bottom flask and using either 6 M or 12 M of HNO_3 to control the number of functional groups. The solution was then refluxed at 110°C for either 1.5 hours or 24 hours to control the number of functional groups. After oxidation, the MWNT solution was filtered using a 0.22 μm PTFE filter. After this, the filtered material was then rinsed with 18 MΩ water until the pH was neutral.

MWNT Pickering emulsions were made by horn sonication using a Fisher Scientific Model 505 Sonic Dismembrator with a 0.5-inch horn tip. Between 0.03% and 0.26% by weight with respect to water of MWNTs were then added to a 100 mL beaker. A concentration of 0.07 wt% of MWNTs was used for all emulsions, unless otherwise stated. Except for emulsions where the oil to water ratio was changed, an equal volume of dodecane was then added to the same amount water used. The solution was then sonicated for 5 minutes at 75% amplitude to disperse the MWNTs since they are typically highly agglomerated and bundled naturally in their solid state. After this, the opposite phase, either oil or water, was then added and emulsification was performed by horn sonicating the solution for 5 minutes at 100% amplitude. Twenty-four hours after emulsification, emulsion droplet size, volume fraction of oil, emulsion, and water were measured and then the emulsions were left undisturbed for one month. After one month, the emulsion droplet size and volume fraction of oil, emulsion, and water were measured again and emulsion stability was determined by comparing emulsion droplet size and interfacial area one month and 24 hours after emulsification.

Optical microscopy was used to obtain the average emulsion droplet size for each emulsion by depositing a drop of the emulsion phase on a microscope slide and viewing it under an optical microscope, which allowed for capturing the images shown in this study. ImageJ software was used to measure the diameter of one hundred emulsion droplets from the captured images, which was then used to make a histogram of droplet size and determine average droplet size.

Two methods were used to test if the resulting emulsion was of type o/w or w/o. If an aliquot of the emulsion dispersed in a beaker of pure water, then the test indicated that it was an o/w type of emulsion. If the aliquot did not disperse, then it was determined to be a w/o type of emulsion. The second method utilized the opposite phase in the same manner. If an aliquot of the emulsion dispersed in a beaker of pure dodecane, then the test indicated it was a w/o type of emulsion, and similarly, if it did not disperse, it was determined to be an o/w type of emulsion.

All temperature programmed desorption (TPD) experiments were performed in a Thermcraft Furnace (Model SST-0.75-0-12-1C-D2155-A). Each MWNT sample was prepared by drying it at 120◦C in a vacuum oven to remove any moisture, adjusting its weight to 50 mg, and then placing it in a quartz tube (3mm inner diameter, 5mm outer diameter, 50cm length). An Omega thermocouple was placed in the quartz tube at the surface of the CNT material to ensure that the heating rate was maintained at 10◦C/min. Quartz wool (~300 ml) was used at the inlet and outlet of the furnace around the sample tube in order to minimize heat loss. These samples were heated programmatically from room temperature to 900◦C at a heating rate of 10◦C/min in the Thermcraft furnace with a helium flow of 35 ml/min. After the samples reached 900◦C, after approximately 90

minutes, the temperature was held isothermal for an additional 30 minutes with a helium flow of 35 ml/min. The outlet gas from the furnace was then mixed with a hydrogen stream (45 ml/min) and fed into a nickel (aluminum supported) catalyst held at 400◦C, which converted all of the carbon containing gases to methane. This gas stream was then sent to a flame ionizing detector (FID) (SRI 110 Detector Chassis) where it was mixed with oxygen (80 ml/min) and hydrogen (10 ml/min) to produce combustion for the detector.

Total integrated TPD signals were used in order to determine the atomic percentage of the Oxygen groups on the MWNT sample material. This was achieved by using Simpson's rule for integration of the FID signal over time. The total moles of carbon desorbed were calculated by multiplying the integrated area by a constant, which was determined by injecting CO2 (in 64 micoliter pulses) through the TPD system under the same conditions and flow rates used for all of the other gases described above. Treating this CO2 as an ideal gas provided a molar value associated with the total integrated TPD signal, $1.3x10^{-13}$ mol C/area. It was assumed that the carbon desorbed from the CNT material during the TPD experiments was equivalent to the oxygen functional groups created by the acid treatments, due to the lower thermal stability of these groups which convert to CO or CO_2. Based on this assumption, The atomic percentage of the thermally destable oxygen groups was calculated to be the ratio of total molar carbon desorbed (found by the process above) and the total molar carbon in the initial sample.

The TPD experimental data suggests that the four samples tested above had 0.8%, 2.3%, 3.1% and 4.4% by weight of thermally unstable carbon on their surfaces.

These four samples were then designated as follows: sample 0.8MWCNT, which was the as-received sample?; sample 2.3MWCNT, which had been oxidized for 1.5 hours with 6M HNO_3 at 110°C; sample 3.1MWCNT, which had been oxidized for 24 hours with 6M HNO_3 at 110°C; and sample 4.4MWCNT, which had been oxidized for 24 hours with 12M HNO_3 at 110°C.

Results and Discussion

MWNT Sample Characterization

MWNTs are inherently hydrophobic and tend to agglomerate due to van der Waals forces. A typical method to increase the hydrophilicity and decrease agglomeration is to oxidize the MWNTs with nitric acid or a mix of nitric and sulfuric acid to create hydrophilic functional groups[35,36,37]. By varying the MWNTs treatment with nitric acid, the number of hydrophilic functional groups can be controlled, which was determined using TPD methods, Figure 1. TPD plots showing the carbon desorbed as a function of temperature for each sample are included in the appendix, Figure 79.

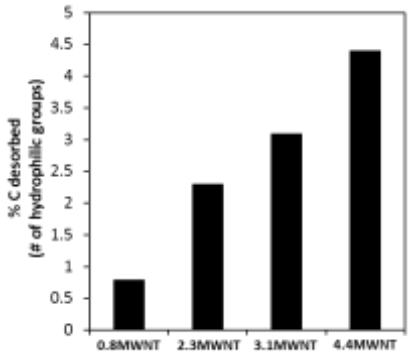

Figure 1: TPD results of MWNT samples. Percent carbon desorbed for each MWNT sample.

Previous work by Binks et al. has shown the emulsion inversion point will change at different oil to water ratios depending on the hydrophobicity of spherical silica particles[20,46]. Hydrophobic particles favor w/o emulsions at a one to one oil to water ratio, while hydrophilic particles favor o/w emulsions[20,46]. A high oil to water ratio is required for emulsion inversion of particles with a high amount of hydrophobic groups, while a low oil to water ratio is required for particles with a low amount of hydrophobic groups. It also follows that a roughly equal oil to water ratio is required for emulsion inversion of particles with an intermediate amount of hydrophobic groups. Since particles of different hydrophobicity have different emulsion inversion points when changing oil to water ratios, a quick characterization of the particles' hydrophobicity can be accomplished using this phenomenon. Using this characterization method, it was found that different oil to water ratios were required for emulsion inversion for each MWNT sample, as shown in Table 1. This indicates the hydrophilicty of each MWNT sample is unique, which correlates with the TPD experimental results. Initially no inversion in emulsion was obtained, due to the MWNTs' inherent hydrophobicity. As the number of hydrophilic functional groups increased on the MWNTs, the emulsion inversion points required higher oil to water ratios. For the most hydrophilic MWNT sample, 4.4MWNT, no emulsion inversion was observed, which indicated that the MWNTs changed from being hydrophobic to hydrophilic. It appears that the most hydrophobic and hydrophilic MWNTs may invert at higher or lower oil to water ratios respectively, but this was not considered to be a factor in determining the relative wettability of the oil to water ratios tested for this study.

O:W Ratio	Sample			
	0.8MWNT	2.3MWNT	3.1MWNT	4.4MWNT
1:4	w/o	o/w	o/w	o/w
2:3	w/o	o/w	o/w	o/w
1:1	w/o	w/o	o/w	o/w
3:2	w/o	w/o	o/w	o/w
4:1	w/o	w/o	w/o	o/w

Table 1: Emulsion type for each O:W ratio of the MWNT samples.

Role of MWNT Wettability

It was found by this study that emulsion droplet size and interfacial area change based on the MWNTs wettability, Figure 2. This is the same trend as seen with fractal silica with different wetability[20]. This study found that the emulsion droplet diameter was largest with hydrophobic and hydrophilic MWNTs and smallest with amphiphilic MWNTs, and that the emulsion type changed within the range of the amphiphilic MWNTs, Figure 2 and Figure 3. The type of emulsion has been shown to change when silica particles of intermediate wettability were initially dispersed in oil or water, with the continuous phase of the emulsion being the phase the particles are initially dispersed in[38]. For MWNTs in the amphiphilic range, however, it was found that the emulsion type changed if the MWNTs were not dispersed in water, Figure 2 (a), or oil, Figure 2 (b),which may have been due to not having MWNTs of the required wettability. Regardless of whether the MWNTs were dispersed in the oil or water, the change in

droplet size with MWNT wettability remained the same. At this point, it can be concluded that changes in interfacial area result from amphiphilic MWNTs creating the largest interfacial area from having the smallest emulsion droplet size. It can also be concluded that the most hydrophobic and hydrophilic MWNTs have the smallest interfacial area, Figure 2 (a).

The reason emulsion droplet size changes with MWNT wettability may be similar to the reason emulsion droplet size changes with fractal silica particles of different wettability.[43,39] Depending on the oil-water contact angle of the particle the orientation of the fractal silica particle can change. The hydrophobic and hydrophilic are loosely held at the oil-water interface and can change orientation with respect to the oil-water interface, while amphiphilic particles are strongly held at the oil-water interface and maintain a parallel orientation to the oil-water interface. For hydrophilic and hydrophobic particles at the oil-water interface when two droplets collide the loosely held particles at the oil-water interface change orientation and droplet coalescence continues until the enough particles are at the oil-water interface to keep the particles from no longer changing orientation. Amphiphilic particles are held strongly at the oil-water interface in a parallel orientation. This minimizes the amount of droplet coalescence from occurring keeping emulsion droplet small. Molecular dynamic studies have shown the orientation of ellipsoidal Janus nanoparticles varies depending on the particles oil-water contact angle.[40] This ability to change orientation depending on the particles oil-water contact angle may also explain why emulsion droplet size varies with MWNT wettability.

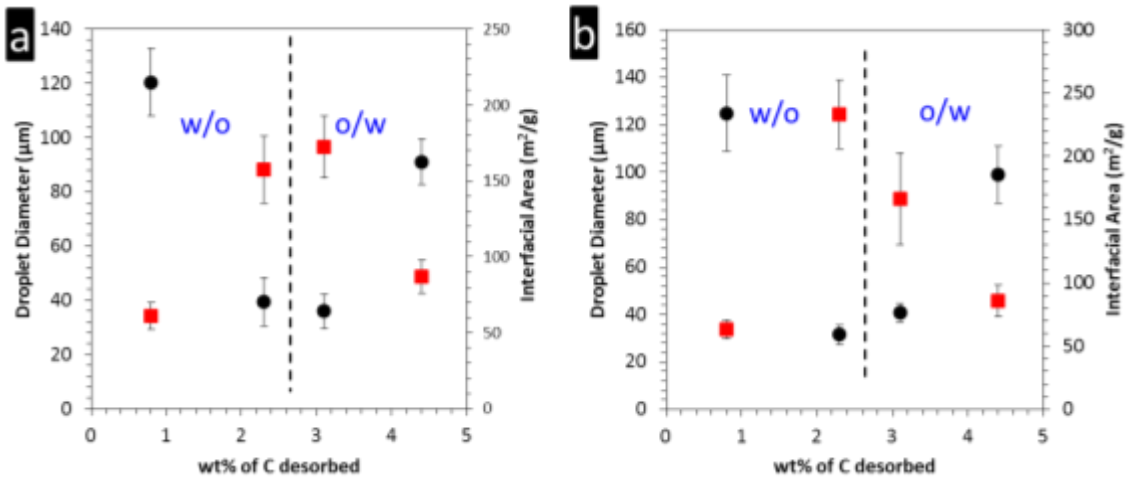

Figure 2: For dodecane and water systems, (a) shows change in droplet diameter as a function of MWNT wettability when dispersing MWNTs in water while (b) shows change in droplet size as a function of MWNT wettability when dispersing MWNTs in dodecane. 0.07wt% of MWNTs was used in both cases. Circles represent droplet diameter and squares represent interfacial area divided by the amount of MWNTs used.

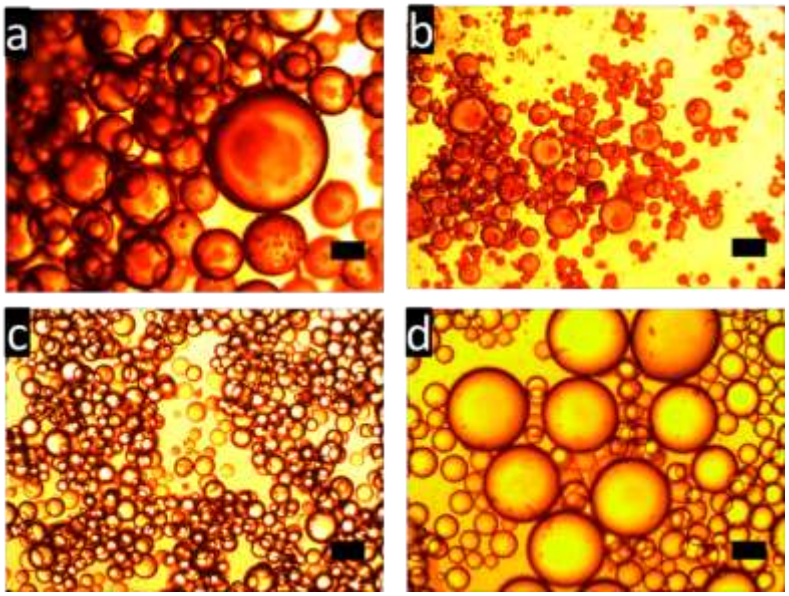

Figure 3: Optical microscope for dodecane and water systems (a) sample 0.8MWNT, (b) sample 2.3MWNT, (c) sample 3.1MWNT, and (d) sample 4.4MWNT. 0.07wt% of MWNTs were used in all cases. The scale bar shown in the images is 100 µm.

The results of studying the variation in MWNT concentration showed the same trend as shown in Figure 2 for MWNTs of different wettability. Previous work by others showed that the concentration of particles in an emulsion system increases as the emulsion droplet size decreases until a point is reached where concentration then plateaus[41]. The initial decrease in emulsion droplet size is dependent on the number of particles to stabilize and stop the coalescence of the droplets. It was found that at a particular point, there were sufficient particles to cover the emulsion droplets and droplet sizes no longer changed. For all of the MWNT samples, it was found that the emulsion droplet size decreased until reaching a plateau at which point the emulsion droplet size no longer changed significantly.

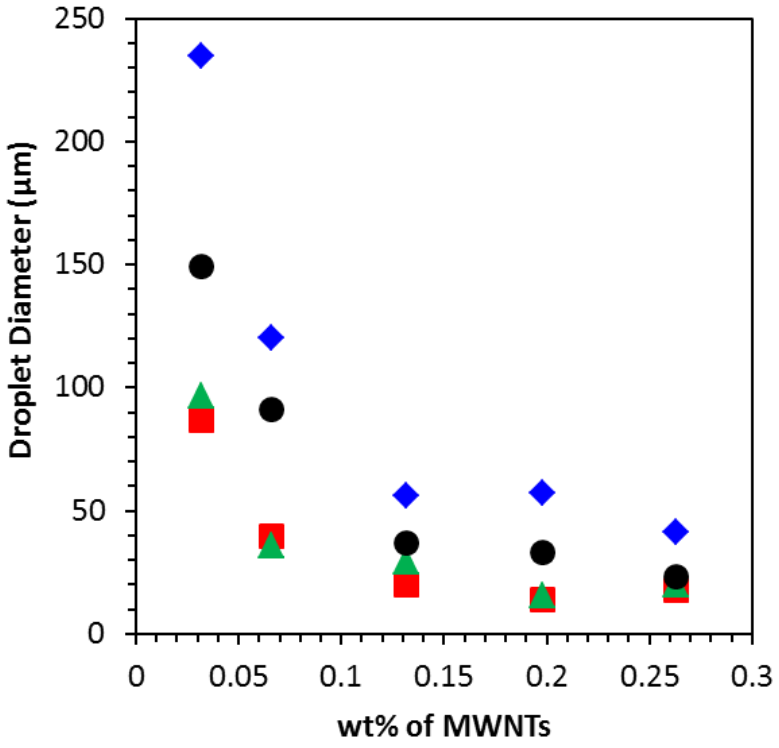

Figure 4: Effect of concentration of MWNTs on emulsion droplet size for each sample. Diamonds are for sample 0.8MWNT, squares are for sample 2.3MWNT, triangles are for sample 3.1MWNT, and circles are for sample 4.4MWNT.

Different Oils

To further study the extent to which the change in MWNT wettability could be used to tune emulsion droplet size, two additional oils, toluene and heptane, were used and tested in addition to dodecane. Heptane has an oil–water interfacial tension of 50.7 mN/m and contact angle of 105°and dodecane has an oil-water interfacial tension of 52.5 mN/m and contact angle of 122°.[54,42] Heptane and dodecane vary in the oil-water contact angle. Toluene has an oil-water interfacial tension of 36.0 mN/m and contact angle of 125°.[54,42] Dodecane and toluene vary the most in interfacial tension, however, both interfacial tension and oil-water contact angle affect the energy of adsorption/desorption for a particle at the oil-water interface, which leads to the same results regardless of which oil is used[20,22,23]. Because of this, it was, expected that the emulsion droplet size would be different depending on which oil was used, but the relative results would remain unchanged. As expected, this study found that the emulsion droplet size and interfacial area varied depending on if heptane, Figure 5 (a), toluene, Figure 5 (b), or dodecane, Figure 2, was used as the oil. The point at which the emulsion type changed with respect to MWNT wettability changes depended on the type of oil. This study found that with heptane the emulsion type changed from w/o to o/w between sample 0.8MWNT and sample 2.3MWNT and with toluene between sample 3.1MWNT and sample 4.4MWNT. The point at which emulsion type changes with respect to silica wettability has been found to change when using toluene[20] and limonene[43].

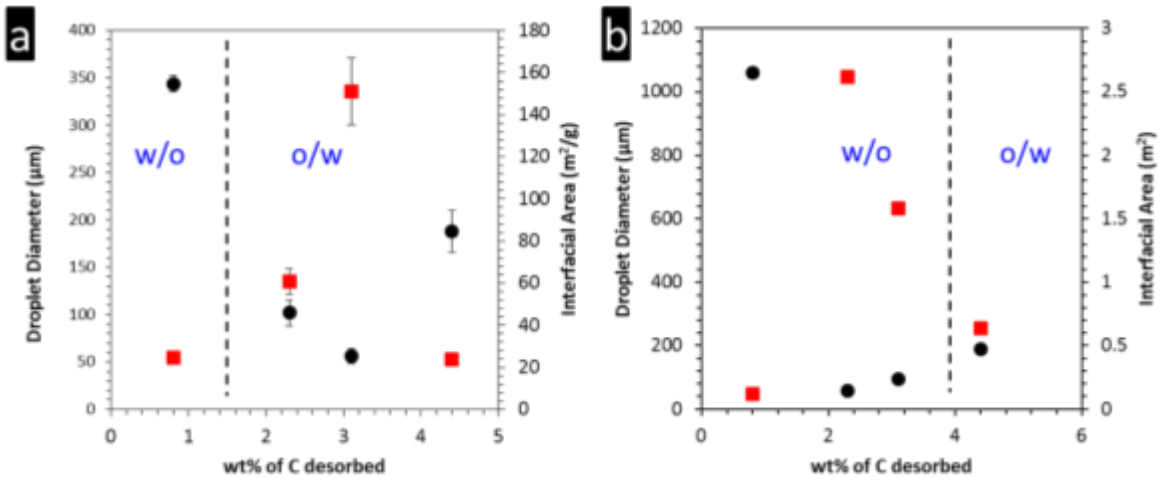

Figure 5: Use of different oils. Change in emulsion droplet size and interfacial area for (a) heptane and (b) toluene. Circles represent droplet diameter and squares represent interfacial area divided by the amount of MWNTs used.

Emulsion Stability

Agglomeration of carbon nanotubes has been shown to enhance emulsion stability over silica particles because of the strong van der Waals forces between carbon nanotubes[44]. Van der Waals forces between carbon nanotubes form a rigid network at the interface of an emulsion droplet that keep emulsion droplets from coalescing. Charge repulsion between silica particles creates a weak network at the interface of an emulsion droplet that allows for the rate of coalescence to increase. Emulsions stabilized with silica particles with different wettability properties have been shown to have different emulsion stability characteristics[20]. The most unstable emulsions were made with hydrophobic and hydrophilic silica particles while stable emulsions were made with silica particles with intermediate wettability properties.

Emulsion stability tests done for this study with MWNTs showed small changes in the interfacial area 24 hours and one month after emulsification, Figure 6, indicating that the MWNT network was maintained even though the MWNT wettability

characteristics had been changed. Treatment of the MWNTs with nitric acid added oxygen-containing functional groups that helped disperse the MWNTs by creating repulsion. In this case, however, the functionalization was enough to change the MWNT wettability characteristics but not enough to weaken the MWNT network that inhibited droplet coalescence. It can be concluded that for applications requiring high emulsion stability, MWNTs of different wettability characteristics allow for greater flexibility.

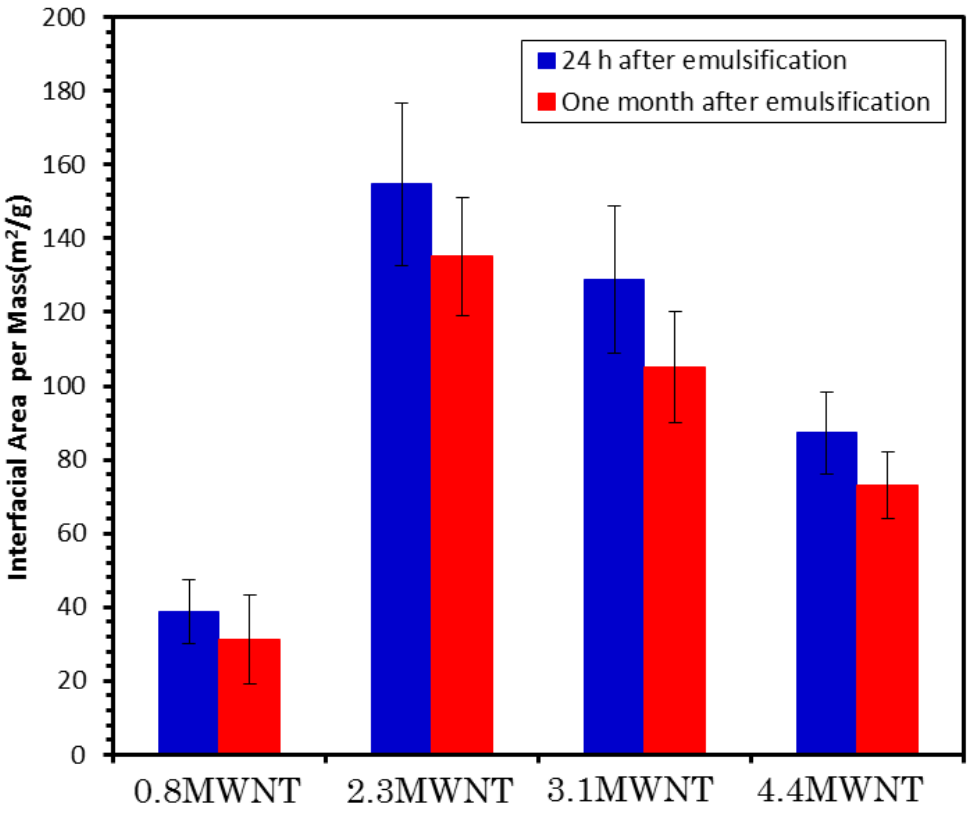

Figure 6: Change in interfacial areas per mass of MWNTs 24 hours and one month after emulsification. Emulsions were made with dodecane and water.

Oil to Water Ratio

This study found that changing the oil to water ratio of an emulsion allowed for tuning the emulsion characteristics without having to change particle properties, or the

oil or aqueous phase. When changing the oil to water ratio for hydrophobic MWNTs, a decrease in emulsion droplet size was observed as the oil fraction increased with no change in emulsion type, sample 0.8MWNT, Figure 7(a). Stiller et al. showed a similar trend for hydrophilic titanium dioxide, except the emulsion droplet size increased with increasing oil fraction due to the hydrophilic nature of the titanium dioxide[45]. This study found that holding the amount of MWNTs constant and decreasing the volume of water the number of emulsion droplets increased. With this increase in the number of emulsion droplets and the decrease in droplet size, their was an increase in interfacial area.

This study found that for MWNTs with intermediate wettability characteristics , the emulsion droplet size and interfacial area tapered off at high and low oil fractions, sample 2.3MWNT, Figure 7 (b). Because emulsion inversion occurs close to an oil fraction of 0.5, the MWNTs are roughly, equally wet by both oil and water. This may be why the greatest interfacial area is obtained at an oil fraction close to 0.5, and that the change in emulsion droplet size at the inversion point is not catastrophic.

Test results from sample 3.1MWNT shows that since the emulsion droplet size is small, catastrophic phase inversion does not occur as until an oil fraction of 0.8 is reached Figure 7 (c). This type of catastrophic phase inversion has also been observed with hydrophobic and hydrophilic silica particles[46]. This study found that emulsion droplet size increases significantly after reaching the oil fraction that causes emulsion inversion from o/w to w/o and that the significant change in emulsion droplet size corresponds with a decrease in interfacial area.

The observation of catastrophic inversion provided an opportunity to further study the ability of MWNTs to stabilize emulsions since they can cause significant changes in emulsion type and droplet size. Emulsion stability tests were conducted in the same manner as the previous stability tests. It was found that emulsion stability did not change regardless of the oil to water ratio as shown for sample 3.1MWNT, Figure 8. It was also found that even after emulsion inversion and a significant change in emulsion droplet size, the emulsion was still stable. Once catastrophic inversion takes place with silica, however, changing the oil to water ratio decreases emulsion stability[46]. With MWNTs, the oil to water ratio can be used to change the emulsion type and droplet size without affecting emulsion stability, which may prove useful for separating and recycling solid catalyst particles based on Pickering emulsion inversion[47].

This study found that the most hydrophilic MWNTs, sample 4.4MWNT, showed no change in emulsion type, Figure 7(d). As the oil fraction was decreased, emulsion droplet size decreased and the interfacial area increased. A similar trend is seen in emulsion droplet size when using hydrophilic titanium dioxide particles[45]. With less oil in a system and the amount of MWNTs held constant, the number of emulsion droplets increased. The increase in the number of emulsion droplets and the decrease in droplet size increased the interfacial area.

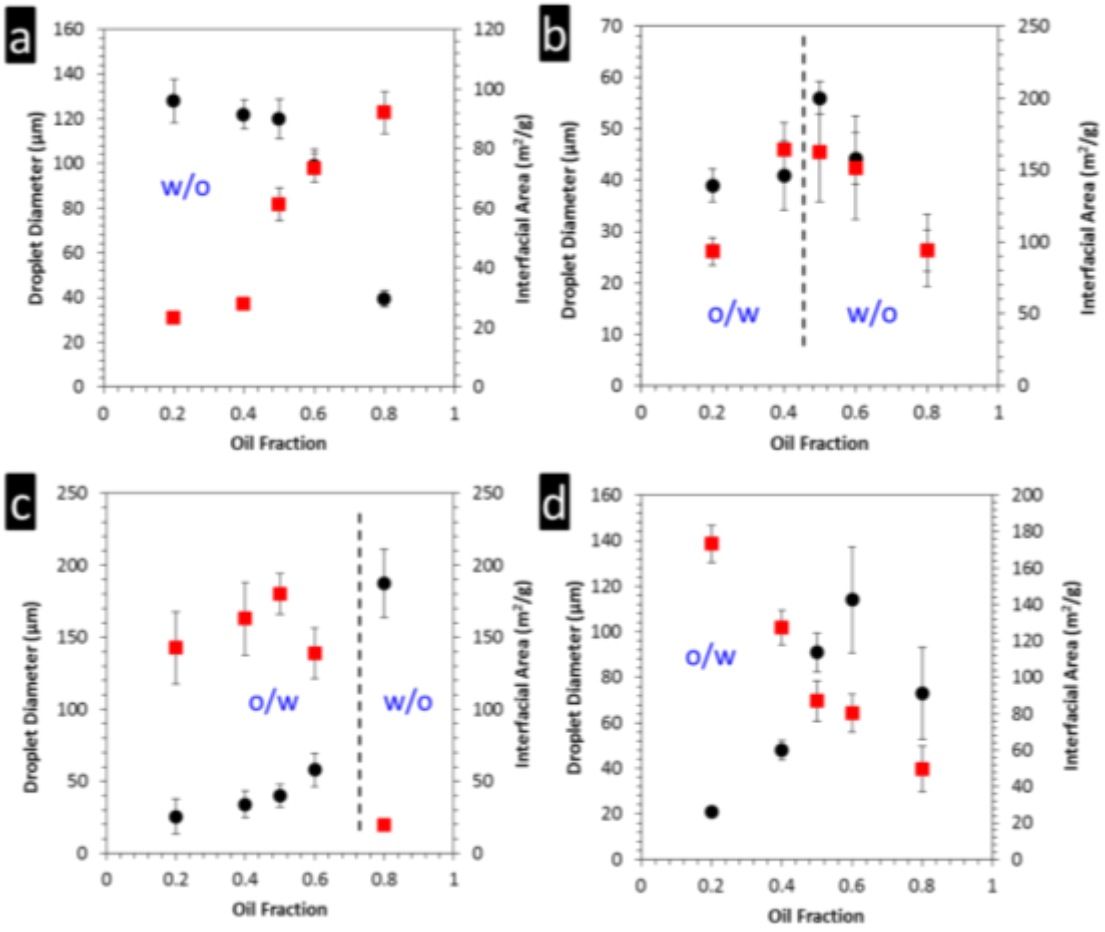

Figure 7: Effect of changing the oil (dodecane) to water ratio on droplet diameter. Sample (a) 0.8MWNT, (b) 2.3MWNT, (c) 3.1MWNT, & (d) 4.4MWNT. Circles represent droplet diameter and squares represent interfacial area divided by the amount of MWNTs used.

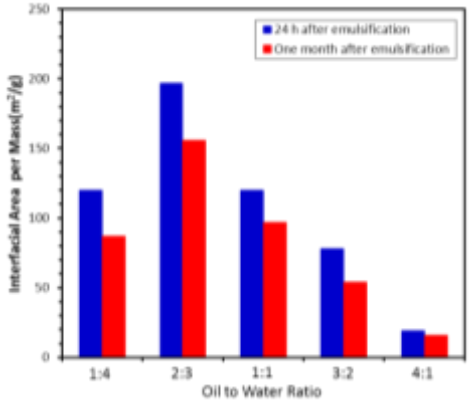

Figure 8: Change in interfacial areas per mass of MWNTS for different oil to water ratios over a one month period for sample 3.1MWNT.

Mixture of MWNTs of Different Wettability

While the ability to change emulsion properties by tuning MWNT wettability characteristics offers interesting possibilities, doing so has proven to be difficult. The ability to mix two MWNT particles with different wettability characteristics to create an emulsion with the desired properties is easier and possibly a faster approach. To test if emulsion properties could be tuned with a mixture of hydrophobic MWNTs, sample 0.8MWNT, and amphiphilic MWNTs, sample 3.1MWNT, were mixed together at different fractions while keeping the total MWNT concentration constant. Both types of MWNTs were initially dispersed in water, and as stated previously, no significant change was initially observed when dispersing the MWNTs in oil or water.

Increasing the ratio of sample 0.8MWNT to sample 3.1MWNT produced increases in emulsion droplet size that occurs slowly at first as the ratio increases, but rapidly accelerates after the mixture of the two sample types of MWNTs become equal, Figure 9. The emulsion type does not change until the ratio of sample 0.8MWNT to sample 3.1MWNT reaches 0.97. This trend agrees with what has been seen by others when silica particles of different hydrophobicity are mixed together to make emulsions[48]. The hydrophobic silica used in their study stabilized smaller droplets than hydrophilic silica did, and only at a high ratio of hydrophilic to hydrophobic silica did the emulsion droplet size increase significantly and the emulsion type change. It could be concluded that the emulsion inversion point and when the emulsion droplet size changes significantly may depend on how well one particle stabilizes an emulsion compared to another.

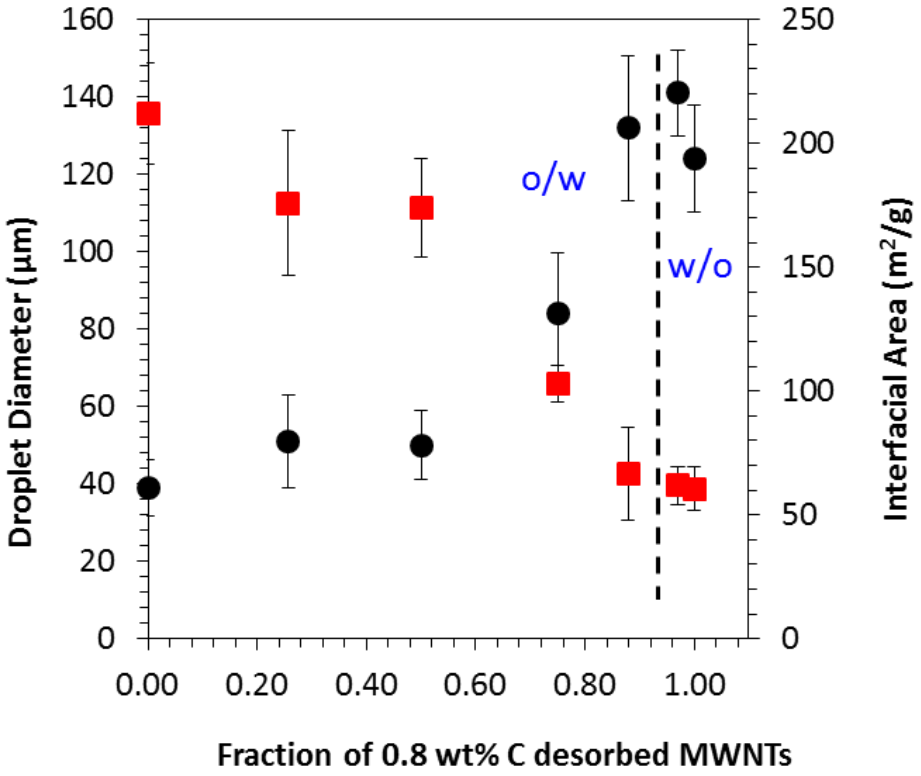

Figure 9: Effect of changing the ratio of MWNTs with different wettability. 0.7 wt% of MWNTs used, varied fraction of 0.8MWNT to 3.1MWNT. Change in emulsion droplet size (a) and change in interfacial area per mass (b). Circles represent droplet diameter and squares represent interfacial area divided by the amount of MWNTs used.

Conclusion

Pickering emulsions stabilized with MWNTs are highly stable. The MWNTs used to stabilize emulsions can also be tuned to have different wettability characteristics to change emulsion properties. Through controlled functionalization of MWNTs, the properties of Pickering emulsions can be controlled along with changes in emulsion droplet size and emulsion inversion points consistent with different oils. Changing the oil to water ratio allows for emulsion droplet size to be changed, and for amphiphilic MWNTs, the emulsion type to be changed. Mixing MWNTs of different wettability characteristics in different ratios can be used to control emulsion droplet size and type,

which creates the prospect of achieving the same results as tuning MWNTs to specific wettability characteristics. Most important, MWNT wettability characteristics can be tuned to change emulsion properties while inhibiting emulsion droplet coalescence, which has not been achieved with silica. MWNTs may allow for a wider range of possibilities with Pickering emulsions due to their high stability over other solid particle emulsion stabilizers.

Chapter 3: Multi-Walled Carbon Nanotubes at the Interface of Pickering Emulsions

The following chapter is based on a publication which can be found in Langmuir using the citation: Briggs, Nicholas M., et al. "Multiwalled Carbon Nanotubes at the Interface of Pickering Emulsions" *Langmuir* 31.48 (2015): 13077-13084.

Introduction

Pickering emulsions have found uses in a wide range of applications, including catalysis[49,] oil recovery,[50] food applications,[51] drug delivery,[52] and templates[53]. This has led to significant research efforts investigating the influence of the hydrophilic/hydrophobic properties of the solid particles[54,55,56,57,58] to the addition of polymers[59,60] and surfactants[61,62] on the stability of Pickering emulsions. However, these publications all deal with spherical metal oxide particles or fumed metal oxide particles. Cylindrical carbon nanotubes exhibit very unique properties upon stabilizing Pickering emulsions. Carbon nanotubes can reside at an oil−water interface while also displaying attractive forces between the tubes at the interface. A recent report by Wu et al. has shown a promising decrease in emulsion coalescence rates with nanotube-stabilized emulsions when compared with spherical particles[63]. While it is known that cylindrical carbon nanotubes can form Pickering emulsions, very little is known about these systems[62]. The promising evidence of enhanced emulsion stability in nanotube stabilized emulsions warrants further investigation.

Carbon nanotubes have found numerous applications as catalyst supports, with notable enhancements in activity and selectivity to target products when used at the oil−water interface of biphasic systems[49,64]. Carbon nanotubes have also shown promise in oil−water systems in the area of enhanced oil recovery[65]. The wide range of applications where carbon nanotubes are used, including drug delivery capsules,[66,67] batteries,[68] sensors,[69] field effect transistors,[70] coatings,[71] hydrogen storage,[72,73] yarns,[74,75] thermal management,[76] and compressible foams,[77] is a testament to their promising properties and potential to impact even more fields as emulsion stabilizers.

The first emulsion stabilized by carbon nanotubes was reported by Wang et al., who used single-walled carbon nanotubes to stabilize water-in-oil (W/O) emulsions in a toluene and water system[62]. In 2005, Hobbie et al. showed that DNA-coated single-walled carbon nanotubes can also stabilize emulsions[78]. Single-walled carbon nanotube bundles have also been shown to preferentially locate at an oil−water interface[79]. Carbon nanotubes fused to silica support particles from which they were grown, or nanohybrids, can also be used to stabilize emulsions[80]. A shift in the type of emulsion stabilized (W/O vs O/W) has been observed upon oxidation of both nanohybrids[80] and carbon nanotubes[81].

While it has been shown that carbon nanotubes are capable of stabilizing Pickering emulsions, very little is known about the nature of these resulting emulsions and how the nanotubes arrange at an oil−water interface. Single-walled carbon nanotubes have been suggested to bend with the curvature of the interface in emulsions to form nanorings based on analysis of nanotube curvature after solvent removal[82,83]. Even less is known about the behavior of nanotubes in biphasic systems where the

hydrophilicity of the surface has been modified, either covalently by introducing carboxylic groups or noncovalently through the use of polymers or surfactants. Only very recent work has shown that the attractive forces between carbon nanotubes help inhibit droplet coalescence, unlike silica or latex particles where electrostatic repulsive forces promote droplet coalescence[63]. The impact of surface functionalization on the orientation of nanotubes at an interface and the resulting impact on droplet coalescence remains unknown. Here we investigate carbon nanotube stabilized Pickering emulsions by using both paraffin wax/water and dodecane/water systems to study multiwalled carbon nanotube (MWNT) orientation at the interface of an O/W Pickering emulsion and the resulting emulsion stability. A similar technique has been used to study the location of particles in polymer blends[84]. Paraffin wax/water systems have been used to capture silica nanoparticles at an O/W interface for the preparation of Janus silica particles[85,86,87,88,89,90] and to study emulsions under shear and gelation[92]. MWNTs were functionalized through covalent and noncovalent methods and compared with unmodified MWNTs. The MWNT location and thickness at the interface were then characterized through a combination of microscopy techniques. The droplet diameter, volume of each phase, and interfacial area were all obtained for each system. This relationship between the hydrophilicity of the MWNTs modified through various methods and the location and orientation of MWNTs at the interface are discussed. The relationship between emulsion stability and interfacial thickness is also investigated for the first time. The critical role of a continuous carbon nanotube network provides further insight into the stability of carbon nanotube stabilized Pickering emulsions.

Experimental Details

The MWNTs used in this study were SWeNT SMW100 type nanotubes obtained from SouthWest Nanotechnologies. The MWNTs have reported diameters of 6−9 nm, 3−6 walls, and an average length of less than 1 μm per the manufacturer. Alkyl glucoside, AG 6202, was purchased from Akzo Nobel. 2-Hydroxyethyl cellulose with a Mw ∼1 300 000 and paraffin wax, with a melting point between 53 and 57 °C, were both purchased from Sigma-Aldrich. 18 MΩ water was obtained from an in house filtration system.

Oxidation of the MWNTs was completed by adding 1 g of MWNTs to a round-bottom flask with 50 mL of 70% nitric acid. The solution was refluxed for 3 h at 120 °C. The MWNTs were filtered using a vacuum filtration setup and a 0.22 μm PTFE filter. The filtered material was then rinsed with 18 MΩ water to remove residual nitric acid until a neutral pH was reached.

Pickering emulsions stabilized by oxidized MWNTs were prepared by adding a specific amount of carbon nanotubes to 50 mL of 18 MΩ water in a beaker, between 0.033 and 0.20 wt % with respect to H2O. This was then horn sonicated with a Fisher Scientific Model 505 Sonic Dismembrator for 3 h at 50% amplitude using a 1/2 in. tip to disperse the nanotubes. The beaker was then placed in an oil bath at 80 °C. A quantity of 6.6 g of paraffin wax was added to the beaker and allowed to melt. Once the paraffin wax had melted, the solution was horn sonicated for 1 h at 50% amplitude using a 1/2 in. tip to form the Pickering emulsion. This sample is labeled Ox-MWNT.

Pickering emulsions stabilized with pristine MWNTs were prepared with the same procedure as the Ox-MWNT, except with unmodified SWeNT SMW100 carbon

nanotubes. The weight percent of unmodified MWNTs with respect to water used was 0.165. This sample is identified as p-MWNT.

Emulsions with 2-hydroxyethyl cellulose dispersed nanotubes (labeled HEC-MWNT) were prepared with a high-viscosity aqueous solution of the polymer. A 1 wt % solution of 2-hydroxyethyl cellulose, with respect to water, was mixed overnight to solubilize and exfoliate the 2-hydroxyethyl cellulose. 50 mL of water was used in this experiment. The same procedure used to make sample Ox-MWNT was used; 0.165 wt % of MWNTs with respect to water was used.

For preparation of Pickering emulsions with alkyl glucoside dispersed MWNTs, a procedure similar to the one used for making sample Ox-MWNT was used. First, 0.165 wt % of MWNTs with respect to water was added to 50 mL of water. The solution was then horn sonicated for 1.5 h at 50% amplitude using a 1/2 in. tip. After this, alkyl glucoside was added to give a weight percent of 1.1, 6.4, or 12 of alkyl glucoside with respect to water. The solution was further horn sonicated for 1.5 h at 50% amplitude using a 1/2 in. tip. Paraffin wax (6.6 g) was subsequently added and melted, and the mixture was horn sonicated using the same conditions as described earlier for the Ox-MWNT sample. For sample AG-MWNT, 0.165 wt % of MWNTs and 6.4 wt % of alkyl glucoside were used. A control experiment using 6.4 wt % of alkyl glucoside with no MWNTs is labeled AG.

Emulsion stability tests were conducted by replacing the paraffin wax with dodecane. The same volumetric amount of dodecane was used as paraffin wax at room temperature. The procedure for making the emulsions was the same as described above.

The droplet size and volume of oil, emulsion, and water fractions were measured 24 h and 2 weeks after making the emulsion.

Electron microscope images of the MWNTs on the surface of the wax droplets were obtained with a Zeis NEON 40 EsB scanning electron microscope using an accelerating voltage of 2 kV. Samples were prepared by placing a drop of the emulsion on a Si wafer and allowing the water to evaporate. Only the paraffin wax droplets remained after evaporation of the water.

To determine the location of MWNTs at the interface, wax droplets resulting from Pickering emulsions stabilized with oxidized MWNTs, pristine MWNTs with alkyl glucoside, or pristine MWNTs with 2-hydroxyethyl cellulose were filtered using a Whatman 1 filter and rinsed with water to remove any unattached particles. After this, 3.5 wt% of the wax droplets covered with MWNTs was mixed with LR White resin, a hydrophilic resin. The solution was then shaken by hand for several minutes to disperse the wax droplets in the resin. After mixing, the solution was placed in a gel capsule and then placed in an oven at 40 °C (below the melting point of the wax) to allow the LR White Resin to polymerize. The gel capsule was then removed, and the polymerized LR White was then thin sectioned using an ultramicrotome, making 100 nm thick sections. These sections were then placed on a TEM gird. TEM of the samples was performed to see the location of the MWNTs at the interface using a JEOL 2000-FX with an acceleration voltage of 200 kV. Interfacial thickness measurements and angles of MWNTs at the interface were obtained from the TEM images. Differences in interfacial thickness and angles between each sample were determined using a paired t test with unequal variances.

Acoustic spectrometry measurements were conducted on 200 mL of paraffin wax-in-water emulsion stabilized with MWNTs and hexyl glucoside, sample AG-MWNTs with a Dispersion Technology Inc. DT 1201 acoustic spectrometer. The sample was analyzed after emulsification, and the wax had solidified.

Results and Discussion

MWNT Pickering Emulsions Characteristics

The characteristics of MWNT stabilized Pickering emulsions are investigated by analyzing droplet distributions resulting from cooled wax droplets produced in the paraffin wax/water system. After emulsification using molten paraffin wax at 80 °C, the Pickering emulsion is cooled to room temperature yielding a dispersion of solid wax particles with the MWNTs remaining trapped at the interface. While the unmodified carbon nanotubes are capable of stabilizing Pickering emulsions, their hydrophobic nature stabilizes water-in-oil (W/O) emulsions. The oxidation of MWNTs with nitric acid creates hydrophilic functional groups such as carboxylic acids on the surface of the MWNTs, thereby improving their dispersion in water. This increased hydrophilicity modifies the contact angle of the carbon nanotube. As Binks et al. have demonstrated, increasing or decreasing the number of hydroxyl groups on silica nanoparticles can influence the stabilized emulsion droplet size, resulting in emulsion inversion[56]. Silica particles hydrophobized by silanation yield W/O emulsions while hydrophilic silica particles stabilize O/W emulsions. A similar trend is observed when comparing the p-MWNTs with Ox-MWNTs, with the increasing hydrophilicity of the nanotubes upon functionalization leading to the formation of O/W emulsions.

By varying the concentration of Ox-MWNT in the mixture, the impact on the size and the resulting interfacial area stabilized can be determined. The weight of the wax layer formed on the top of the emulsion after cooling is used to calculate the volume of the excess oil phase. As the amount of oxidized MWNTs increases, the continuous oil and water phase volumes decrease while the emulsion volume increases as shown in Figure 10. This demonstrates the clear increase in interfacial area that can be stabilized by the addition of more carbon nanotubes to the mixture.

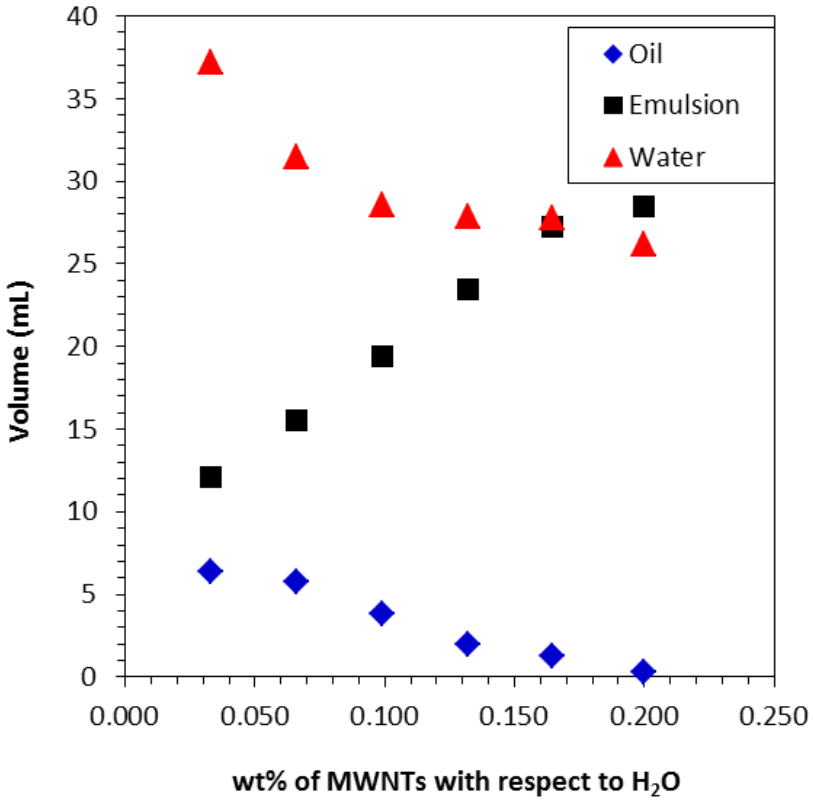

Figure 10: Trends of oil, emulsion, and water volumes of Pickering emulsions made with oxidized carbon nanotubes (Ox-MWNT).

The hydrophilicity of the nanotubes can be modified by noncovalent means as well. The polymer 2-hydroxyethyl cellulose can wrap around the MWNTs and increase their hydrophilicity, a strategy that has been used to improve the hydrophilicity of drug

capsules[93]. A second noncovalent dispersant, alkyl glucoside (AG), is a hydrophilic linker that likely increases the interaction of the MWNTs with the water, just as hydrophilic linkers are used to increase a surfactant's interaction with water[94]. A similar approach has been employed with silica particles and cetyltrimethylammonium bromide (CTAB)[85,86,87,88,89,90,92]. It is important to note that the AG influences the hydrophilicity of the nanotubes and is not responsible for the lone stabilization of emulsion droplets as evidenced by Figure 11. In the absence of MWNTs, Figure 11a shows that the addition 6.4 wt % AG results in large wax particle agglomerates with an average size of 88.5 μm. Additionally, a significant wax layer was formed on top of the mixture once the emulsion was brought to room temperature, indicating inadequate emulsion stabilization. In contrast, the combined use of 6.4 wt % AG and 0.165 wt % carbon nanotubes creates smaller emulsion droplets with no observed agglomerates as shown in Figure 11b. Similar results have been reported in the literature with CTAB and silica systems[92].

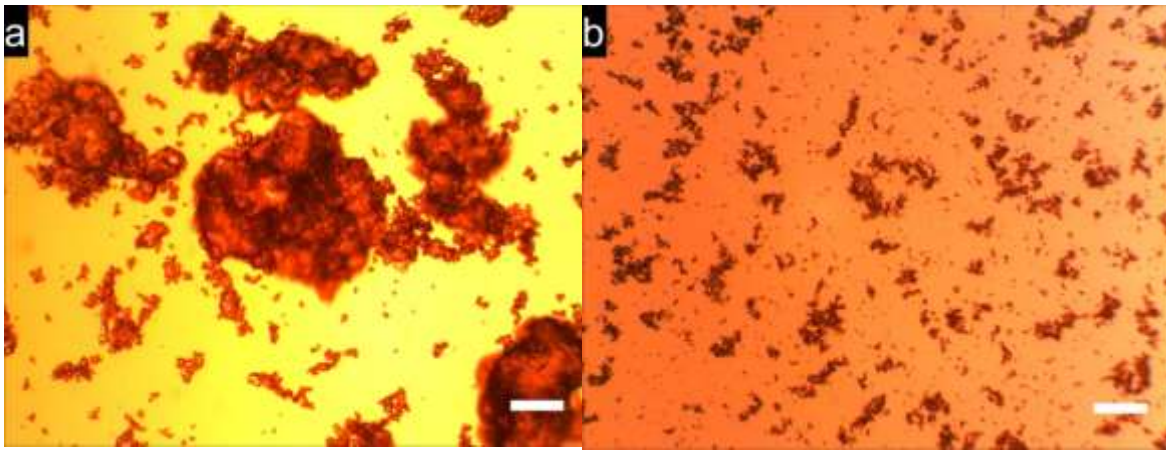

Figure 11: (a) Wax particles stabilized by 6.4 wt% alkyl glucoside, sample AG-MWNTs. (b) Wax particles stabilized by 6.4 wt% of alkyl glucoside and 0.165 wt% MWNTs, sample AG-MWNTs. Weight percent's are with respect to water. Images were taken at 40°C after cooling of the molten wax/water system. Each scale bar is 100 μm.

The amount of AG necessary to hydrophilize the MWNTs necessary for the stabilization of O/W emulsions was determined by varying the AG content. Previous work has shown that if the concentration of surfactant used to wet the particles is above the critical micelle concentration, an unstable emulsion is obtained[92]. The concentration of alkyl glucoside was increased until the emulsion type changed from W/O to O/W. Using 1.1 wt % AG created a W/O emulsion, while 6.4 wt % of AG created an O/W emulsion, which was also the case when using 12 wt % of alkyl glucoside, with emulsion droplet sizes of 4.9 and 6.9 μm, respectively. A 6.4 wt % concentration of alkyl glucoside was selected for subsequent experiments to minimize excess surfactant in the system while stabilizing a O/W emulsion.

As can be seen in Figure 10 and Figure 12, as the concentration of oxidized carbon nanotubes increases, the increase in volume of the emulsion fraction is accompanied by a decrease in the emulsion droplet size. This is consistent with numerous publications that show this behavior of decreased particle size with increasing concentrations of silica particles,[57,58] singlewalled carbon nanotubes,[62] oxidized carbon nanotubes,[81] and carbon nanotube−silica nanohybrids[80].

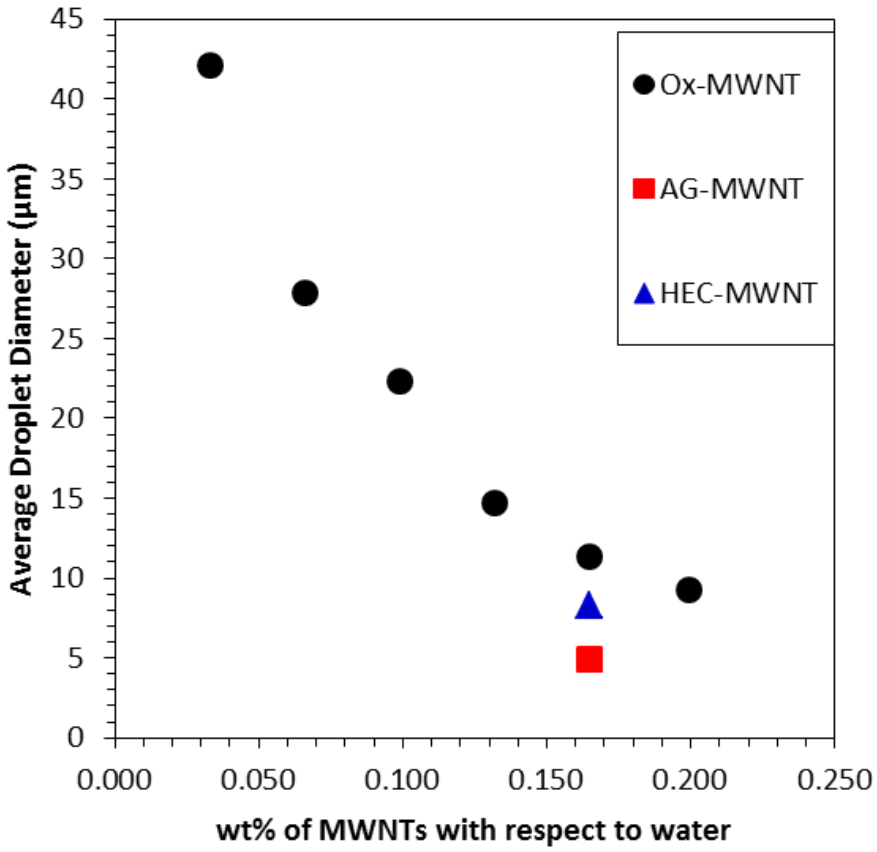

Figure 12: Emulsion droplet diameter as a function of MWNT wt% with respect to water. Samples used were oxidized MWNTs (Ox-MWNT), MWNTs with 6.4 wt% of alkyl glucoside (AG-MWNT), MWNTs with 1 wt% of 2-hydroxylethyl cellulose (HEC-MWNT).

In order to further confirm the accuracy of the experimental technique for droplet size measurements, acoustic spectrometry was used to determine the droplet size distribution of the AGMWNT sample. The acoustic spectrometer allowed for the diameter of the emulsion droplets to be measured in liquid after emulsion formation and solidification of the wax. Results from acoustic spectroscopy showed the average paraffin wax droplet diameter and distribution were similar to that obtained with measuring wax particle diameters from optical microscope images as shown in Figure 13. The mean size of the paraffin wax particles calculated using acoustic spectroscopy

and optical microscopy were 5.2 and 4.9 μm, respectively, further confirming the accuracy of the droplet size measurements.

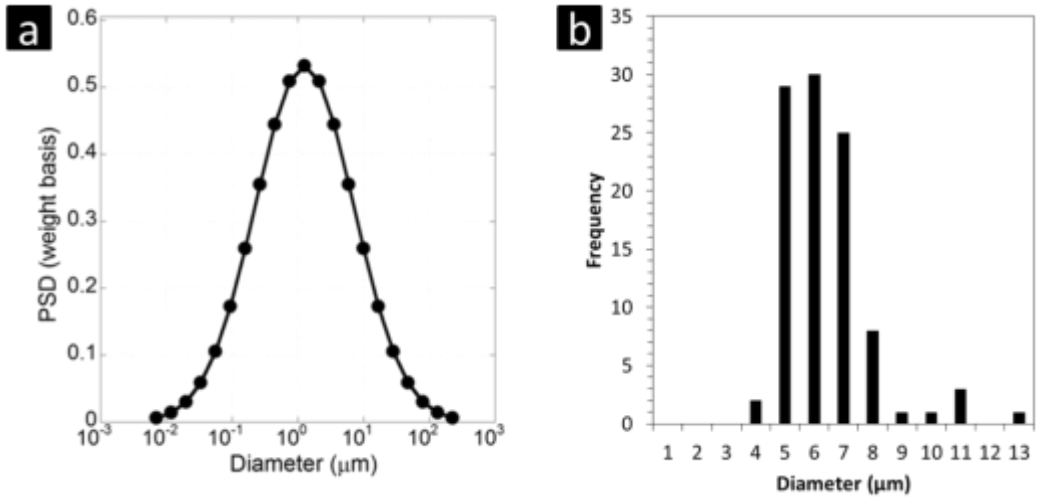

Figure 13: Distribution of droplet diameters for paraffin wax droplets stabilized with pristine carbon nanotubes and alkyl glucoside. (a) Distribution obtained with acoustic spectroscopy and (b) optical microscopy.

The oil−water interfacial area of the emulsions follows an increasing trend with decreasing emulsion droplet size and increasing emulsion volume as shown in Figure 14. It should be noted that when using MWNTs and 6.4 wt % of alkyl glucoside, a significantly higher interfacial area is obtained for a given weight percent of nanotubes. The different interfacial areas stabilized imply that the amount of nanotubes located at the oil−water interface may be different, which could result in important differences in emulsion stability. The thickness of nanotubes at the interface and resulting emulsion stability are discussed in more detail in the following sections.

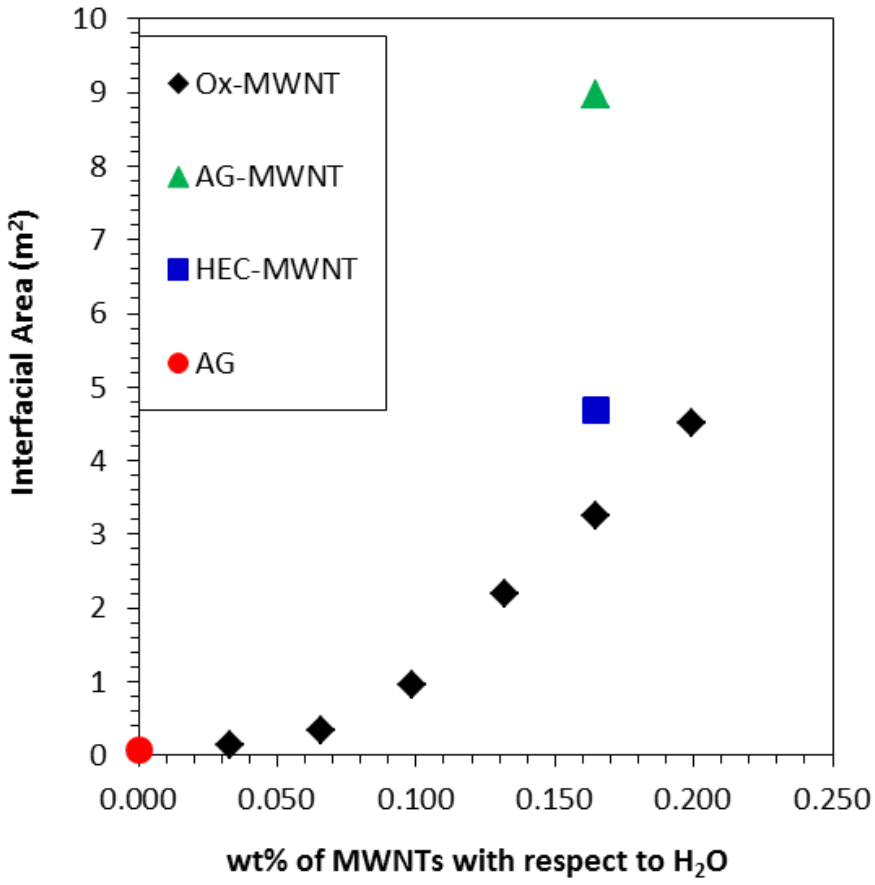

Figure 14: Change in interfacial area with respect to change in MWNT concentration for oxidized MWNTs (Ox-MWNT). Included are emulsions made with MWNTs with 1wt% hydroxyethyl cellulose (HEC-MWNT), MWNTs with 6.4 wt% alkyl glucoside, and 6.4 wt% alkyl glucoside (AG).

MWNT at the Interface of a Pickering Emulsion

Further information regarding the behavior of nanotubes at the oil−water interface can be found via electron microscopy of the produced Pickering emulsions. After emulsification using molten paraffin wax at 80 °C, the Pickering emulsion is cooled to room temperature and analyzed via SEM,Figure 15. The pristine nanotubes (p-MWNTs) alone under these conditions stabilize a water-in-oil emulsion, resulting in a solid oil continuous phase as shown in Figure 15e,f. By breaking open the cooled wax emulsion (Figure 15e), holes are observed where the water droplets once resided with

MWNTs lining their perimeter as shown near a cross section of one of these holes in Figure 15f. The majority of the emulsion droplets formed for samples p-MWNT, Ox-MWNT, HEC-MWNT, and AGMWNTs as shown in Figure 15a−h are roughly spherical in shape.

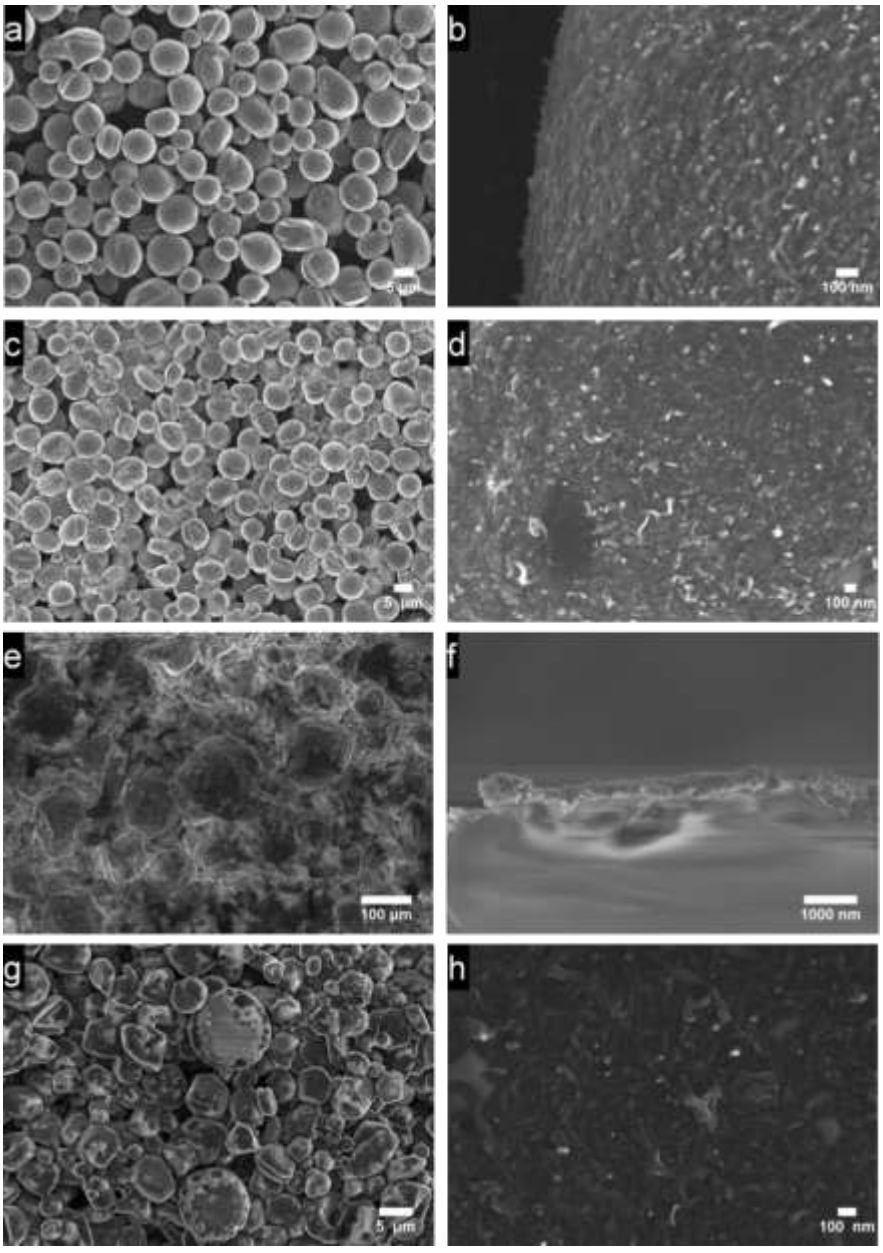

Figure 15: SEM images of wax particles formed on cooling of Pickering emulsions using 0.2wt% of oxidized MWNTs (a & b), HEC-MWNTs (c & d), p-MWNTs (e & f), and AG-MWNTs (g & h).

In order to better illustrate the interfacial behavior of nanotubes at the interface, samples Ox-MWNTs, AG-MWNTs, and HEC-MWNTs were embedded in LR white resin after cooling of the emulsions, thin sectioned, and then characterized with TEM. It is important to point out that for all samples shown in Figure 16 the MWNTs appear to be located at the interface of the wax droplets and not dispersed in the individual phases.

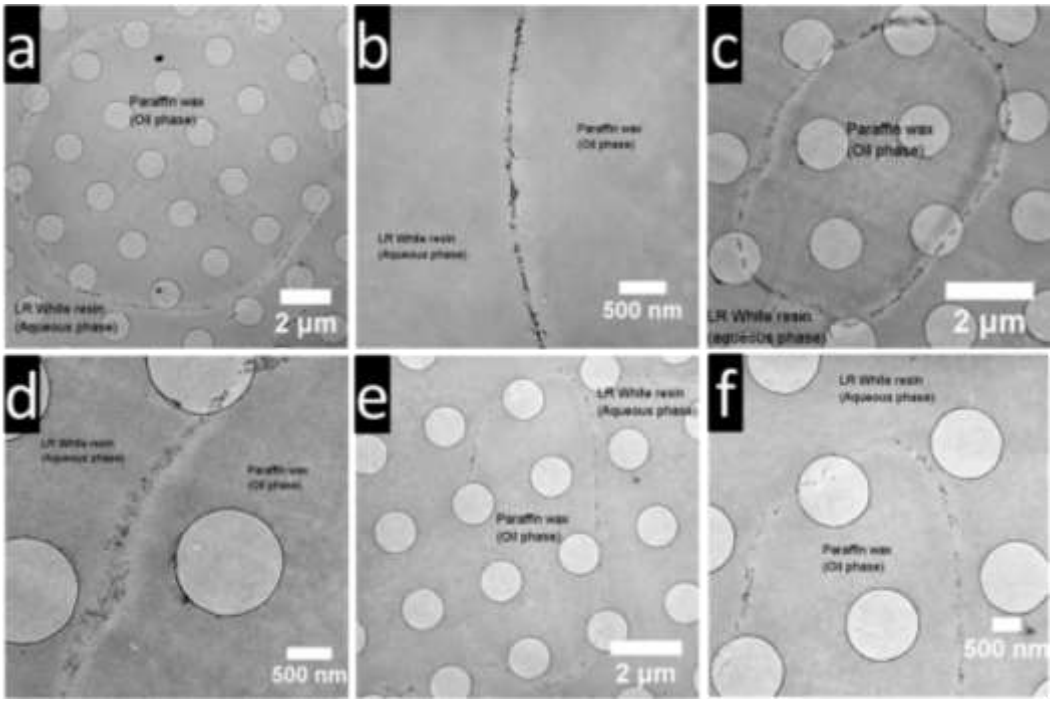

Figure 16: Images of thin sectioned wax droplets with MWNTs at the interface. Ox-MWNTs at the interface (a) (b). HEC-MWNTs at the interface (c) (d). AG-MWNTs at the interface (e) (f). All samples were made with 0.165 wt% MWNTs with respect to water.

The thickness of nanotubes at the interface, hereafter referred to as interfacial thickness, is significantly different for the three samples shown in Figure 16. By measuring the interfacial thickness at 350 different positions from TEM images, an average was obtained. Results indicate an average interfacial thickness of 75 nm for Ox-MWNT, 54 nm for AGMWNT, and 107 nm for HEC-MWNTs. A statistically

significant difference between each sample is confirmed by the t test as discussed in more detail in the Appendix. The AG-MWNTs sample has the lowest interfacial thickness while the HEC-MWNTs display the highest interfacial thickness.

The vast majority of the MWNTs for samples p-MWNT, Ox-MWNT, HEC-MWNT, and AG-MWNT appear to orient close to the interface. This is in agreement with calculations that show a lower adsorption energy required for a cylinder to orient parallel to an oil−water interface rather than perpendicular[95,96]. Analysis of the angle of 100 nanotubes with respect to the interface reveals that the majority of nanotubes in all samples lie along the interface. Average angles from the interface, with errors representing one standard deviation, were 18 ± 14° for the Ox-MWNT sample, 15 ± 9° for the AG-MWNT sample, and 30 ± 21° for the HECMWNT sample. While the angles of all samples fall within one standard deviation of one another, the broadest distribution of angles was found with the HEC-MWNT sample. This is also the sample that contained the greatest interfacial thickness, where the attractive forces among the nanotubes could lead to random agglomeration near the region of the interface. More details on the statistical distribution of angles with respect to the oil−water interface can be found in the Appendix.

The use of surfactants to disperse carbon nanotubes is well known[97]. A better dispersion of MWNTs leads to more MWNTs covering the interface of emulsion droplets, stabilizing a greater interfacial surface area. In addition, the emulsion droplets in the AG-MWNTs emulsions appear to have bare spots that can be observed in the SEM images in Figure 15g of places where MWNTs are missing from the droplet surface Figure 15e. The HEC-MWNT sample appears to have the largest interfacial

thickness, which could be due to polymer flocculating the MWNTs together. Previous work has shown the homopolymer hydroxypropyl cellulose can be used to flocculate Ludox silica particles[60].

Emulsion Stability

Perhaps the most important implication of the interfacial thickness of nanotubes at an interface is the resulting impact that the nanotube−nanotube attractive forces have on emulsion stability. While coalescence rates cease when the paraffin wax is solidified, this is not true in a liquid oil−water system. A dodecane/water mixture enables the investigation of interfacial thickness on emulsion stability. The emulsion stability is measured by comparing the emulsions 24 h and 2 weeks after preparation.

The first important observation is that the same trend in droplet size and interfacial area is observed 24 h after preparation in the dodecane/water system as was reported earlier for the paraffin wax/water system as shown in Figure 17. The AG-MWNTs results in the highest interfacial area stabilized after 24 h followed by the HEC-MWNTs and finally the Ox-MWNTs. The fact that the increase in interfacial area upon the introduction of AG is not as pronounced as was observed when using paraffin wax is likely due to coalescence that has already occurred in this system after 24 h.

Samples HEC-MWNTs and Ox-MWNTs exhibit the best stability as the emulsion droplet size and interfacial area change a small amount. The largest change in droplet size and interfacial area occurs for sample AG-MWNTs indicating much faster rates of droplet coalescence. It should be kept in mind that this sample also has a very thin interfacial thickness of nanotubes accompanied by interfacial regions devoid of

nanotubes as shown in Figure 16e,f. This is the first evidence demonstrating that a thick and continuous interface of carbon nanotubes results in enhanced emulsion stability.

Previous work has shown carbon nanotubes inhibit droplet coalescence more effectively than silica or latex particles[63]. This has been proposed to result from the attractive forces between the nanotubes being greater than their electrostatic repulsive forces. Silica and latex particles exhibit primarily electrostatic repulsive forces, whereas the attractive forces among carbon nanotubes form a network that is difficult to break when emulsion droplets come into contact with one another. A comparison of samples Ox-MWNT and HEC-MWNT to AGMWNT in Figure 17 further supports the importance of this interaction.

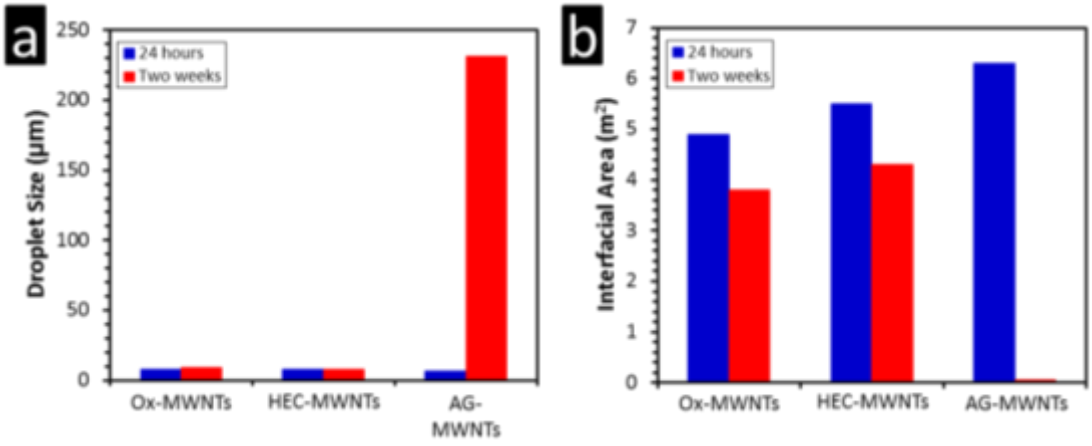

Figure 17: Emulsions stability test comparing emulsion (a) droplet size and (b) interfacial area. Comparison is 24 hours and two weeks after emulsion formation. Amount of MWNTs was kept constant for all emulsions made.

Surfactants are commonly used to disperse carbon nanotubes individually and provide a repulsive force between individual carbon nanotubes, inhibiting agglomeration of the tubes[97]. Only upon addition of a surfactant, AG-MWNT, does the emulsion droplet size and interfacial area change drastically which is due in large part to the surfactant creating a repulsive force between carbon nanotubes. While there is a

possibility that the surfactant cooperatively stabilizes the emulsions, a blank run with the AG in the absence of MWNTs yielded very little interfacial area as shown previously in Figure 14. With the carbon nanotube network disrupted, droplet coalescence can occur at a much faster rate. For sample HEC-MWNTs, the polymer likely wraps around the carbon nanotubes linking them together, which has shown to be the case with a mixture of silica and polymer,[60] thus maintaining the carbon nanotube network. Oxidation of carbon nanotubes introduces hydrophilic groups that can cause repulsion between carbon nanotubes. However, the extent of oxidation for the carbon nanotubes used in sample Ox-MWNTs appears to be enough to change emulsion type, but not enough to hinder the formation of a stable carbon nanotube network. This is evidenced by the multiple layers of nanotubes at the interface as well as the corresponding emulsion stability that is significantly greater than AG-MWNTs and comparable to HEC-MWNTs.

Sonication Intensity

Varying the amount of energy used for dispersion of oxidized MWNTs in water and the energy for emulsification resulted in differences in emulsion droplet diameter. Using 0.2 wt% oxidized MWNTs and a horn sonication setting of 25% amplitude for dispersion and emulsification formed large agglomerates of oxidized MWNTs with paraffin wax droplets inside are shown in Figure 18 (a) and (b). The agglomerates of MWNTs are 67 μm in diameter, while the average emulsion droplet diameter is 13.9 μm, which is slightly larger than the 9.2 μm droplets observed when using a horn sonication setting of 50% amplitude for dispersion and emulsification steps. It is important to note that no MWNT agglomerates were observed at the higher sonication

intensity. Changes in the MWNT concentration when using horn sonication settings of 25% amplitude for dispersion and emulsification is reported the Figure S4 of the appendix.

Increasing horn sonication amplitude to 50% during the dispersion of the MWNTs results in emulsion droplets that do not appear collected in large oxidized MWNT agglomerates, Figure 18 (c), however the oxidized MWNTs due appear to connect the emulsion droplets together Figure 18 (d). The attachment of emulsion droplets with oxidized MWNTs is further confirmed with optical microscopy where the emulsion droplets appear together in clumps rather than individual emulsion droplets, the average diameter of these clumps of droplets is 59 μm. Alternatively when using a low energy dispersion and high energy emulsification, no oxidized MWNT agglomerates are observed, Figure 18 (e), and the emulsion droplets are not connected to one another, Figure 18 (f). The results after a high energy emulsification step are similar to those obtained after using both a high energy dispersion and high energy emulsification step as shown in Figure 18 (a).

The energy used in pre-dispersing the MWNTs and the amount of energy used to make an emulsion from the MWNT dispersion both have a significant impact on the emulsion. One possible reason for the emulsion droplets embedded in MWNT agglomerates when using horn sonication setting of 25% or 50% amplitude for dispersion and 25% amplitude for emulsification is that any MWNT agglomerates present in the system are capable of capturing oil droplets or having oil droplets forced into them. This phenomenon is more like capillary imbibition than a true emulsification

process. Capillary imbibition occurs in oil recovery when water is used to displace oil in porous rock[90].

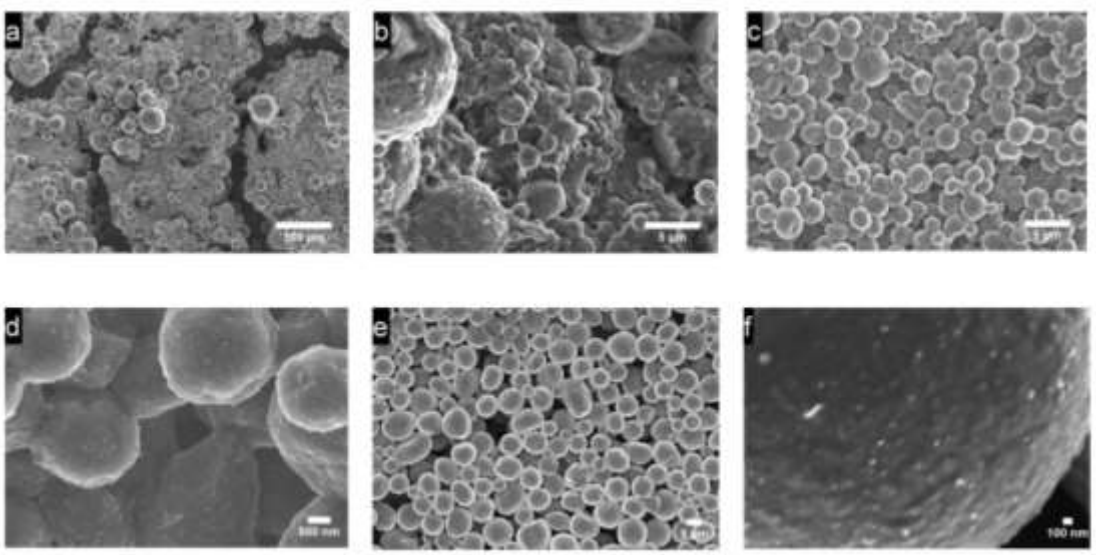

Figure 18: SEM images. Using 25% amplitude for dispersion of MWNTs and 25% amplitude for emulsification of MWNTs (a & b), 50% amplitude for dispersion of MWNTs and 25% amplitude for emulsification (c & d), 25% amplitude for dispersion of MWNTs and 50% amplitude for emulsification (e & f).

Conclusion

MWNTs are found to lie at the interface of paraffin wax emulsion droplets both when the wax is a liquid above its melting point and after the wax has solidified below its melting point. The majority of the MWNTs lie parallel to the O/W interface, which is consistent with calculations showing this to be the favorable position. The emulsion type can be changed from W/O to O/W by using either covalent or noncovalent methods to modify the hydrophilicity of the MWNTs. A cooperative effect between the introduction of alkyl glucosides and MWNTs was observed, stabilizing interfacial areas much higher than could be achieved by using the surfactant or oxidized MWNT's alone. The thickness of the interface was measured through TEM of thin sections, indicating a reduction in the thickness of MWNTs at the O/W interface for alkyl glucoside modified

nanotubes when compared with oxidized MWNTs or MWNTs dispersed with hydroxyethyl cellulose. Patches of oil−water interfacial area lacking nanotubes were observed when alkyl glucoside was used with the MWNTs. The introduction of a cellulose polymer appears to flocculate the nanotubes at the interface, resulting in both increased interfacial areas and a thicker layer of MWNTs at the oil−water interface.

Chapter 4: Controlling Reaction Selectivity in Emulsions Using Particles of Different Wettability

Introduction

Since the first discovery of the benefits of performing catalysis with solid stabilized emulsions[98] there has been a large effort to study heterogeneous catalysis in these systems[126,99,117,100,101,102]. A few of the benefits of performing heterogeneous catalysis reactions in emulsions is an increase in mass transfer of molecules between the oil and water phases, increase in oil-water interfacial area, easy recovery of products due to solid particles stabilizing the emulsion instead of a surfactant, separation of the products from the reaction mixture due to differences in oil-water solubility, and the opportunity to control reaction selectivity when operating under mass transfer limitations due to the presence of two different liquid phases. One particular application which benefits from these advantages is catalytic upgrading of bio-oil produced from pyrolysis of biomass.

Due to bio-oil having a highly oxygenated structure and after thermochemical conversion results in liquid products of high water solubility, high reactivity, and low vapor pressure biomass becomes difficult to upgrade in the vapor phase[103] making the catalytic upgrading in the liquid-phase more appealing[117]. Water is often a solvent of choice due to its relatively low cost, low environmental impact, and ability to solubilize oxygenated biomass molecules. Yet the presence of water can cause undesired side reactions and harm certain catalysts[100,117,104]. By having an oil and aqueous phase a catalyst can be functionalized to be in the oil phase and the impact of water mitigated,

such is the case when using zeolites at high enough temperature in water[117]. Another benefit of having two phases is in catalytic upgrading biofuel when it is desirable to acid-base catalysts with metal catalyst[126]. The acid-base catalyst can be used to dehydrate the reactant and the metal to hydrogenate the dehydrated product. If the hydrogenation catalyst were not in one specific phase then there will be competition with the acid-base catalyst, resulting in a decrease in yield of desired product. Due to the importance of controlling selectivity and mitigating catalyst deactivation in biomass upgrading conducting reactions in emulsions is advantageous.

Since solid stabilized emulsions provide many key advantages there is a strong need to understand how solid stabilized emulsions can be tuned and controlled. Fortunately there has been a large amount of work to understand how solid stabilized emulsions behave and the solid particles modified to control the emulsions properties. The wettability of the solid particle stabilizing an emulsion can be used to control emulsion type, emulsion droplet size, and emulsion stability[105]. By changing the wettability of the particle it is believed this changes the location of the particle at the oil-water interface, Figure 19. The addition of salts, change in pH, or surfactants has been found to control emulsion stability[106,107,108,109]. Mixing solid particles of different wettability at different ratios can be used to control emulsion type and emulsion droplet size[110] and changing the oil to water ratio can be used to change the emulsion droplet size and type[111]. With the vast array of tools for controlling a solid stabilized emulsion properties there are many opportunities to apply these tools for conducting reactions in emulsions and to control reaction selectivity.

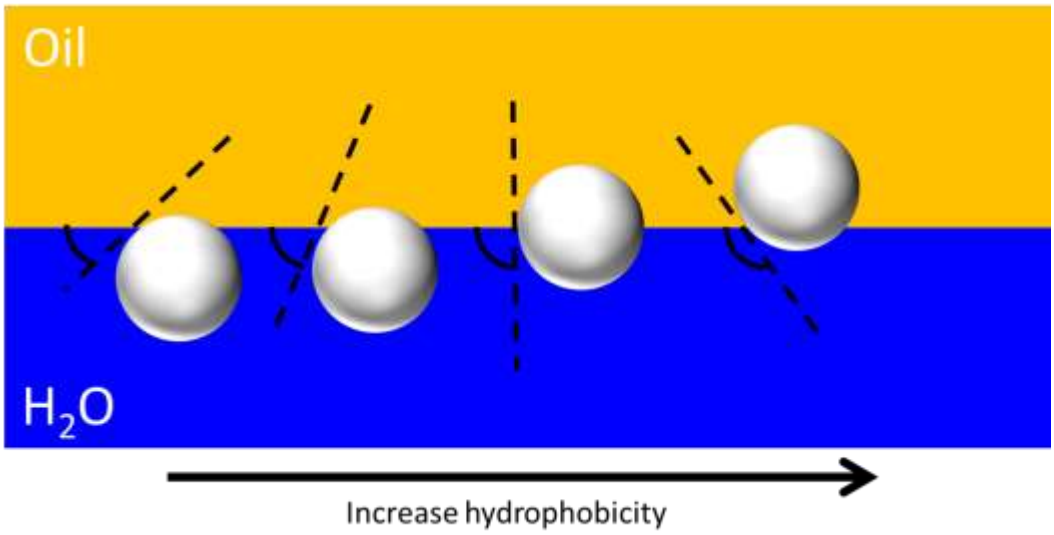

Figure 19: Location of the particle at the oil water interface as a function of the particles wettability.

In this work we combine knowledge from the emulsion and catalysis community to understand how reaction selectivity can be controlled in biphasic systems. Two reactants are used and were chosen such that one has a high oil solubility and the other a high water solubility to study how reaction selectivity of the reaction in the oil or water can be controlled by tuning spherical silica nanoparticles to be either hydrophobic, amphiphilic, or hydrophilic. Using this knowledge particles of different wettability are mixed together to create a "Janus effect", the same idea as a Janus particle, where in the reaction in the oil phase is catalyzed by hydrophobic silica nanoparticles and the reaction in the aqueous phase by hydrophilic silica nanoparticles, Figure 20. To study if not only silica nanoparticles of different wettability can be mixed together multi-walled carbon nanotubes (MWNTs) are mixed with silica. The approach of mixing MWNTs and silica nanoparticles allows for further control of the rates of reaction in the oil and aqueous phases.

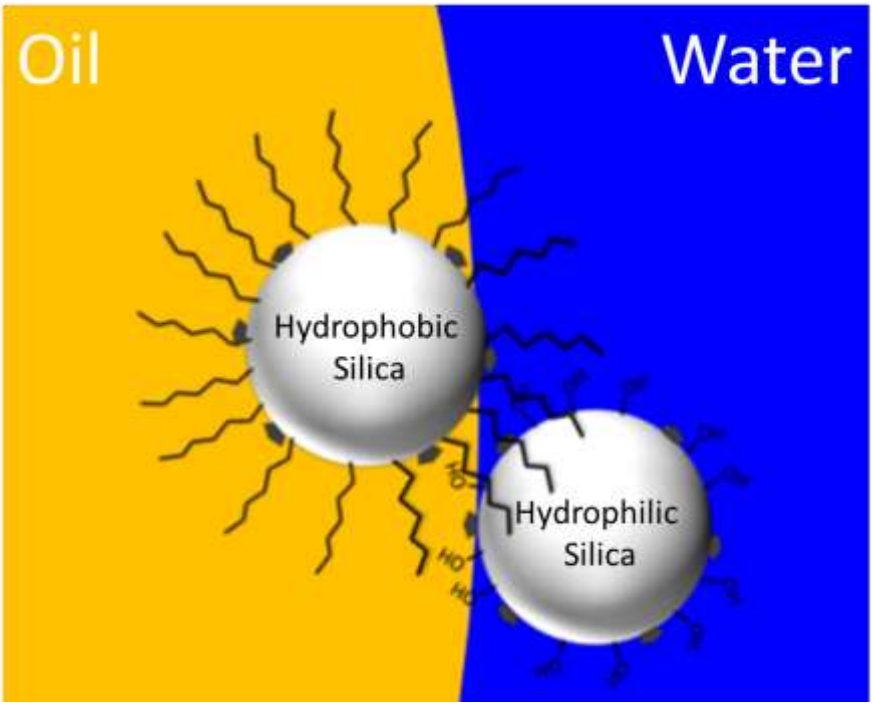

Figure 20: Hydrophobic and hydrophilic silica at the oil-water interface creating the same effect as a Janus particle.

Experimental Details

Ludox TM-50 colloidal silica was used as one of the catalyst supports and was purchased from Sigma Aldrich. The Ludox particles are 32 nm in diameter, have a specific surface area of 110-150 m^2/g. The silica particles come as a 50 wt% aqueous dispersion with a solution pH of 8.5-9.5. The other catalyst supports used in this study were MWNTs donated by SouthWest Nanotechnologies and designated by the company as SWeNT SMW100. The MWNTs have a reported outer diameter of six to nine nanometers, three to six walls, and an average length of less than one μm according to the manufacturer. Palladium nitrate dihydrate, octadecyltrichlorosilane (OTS), cis-2-butene-1,4-diol, decane, 1-dodecene, and 70% nitric acid were both purchased from Sigma Aldrich for functionalization of catalyst supports.

A detailed description of the process to functionalize Ludox TM-50 can be found in previous work[112]. The Ludox TM-50 colloidal silica nanoparticles were removed from aqueous solution for functionalization since octadecyltrichlorosilane reacts violently with water. Once removed the particles were repeatedly dispersed in water by vortex mixing and centrifuged at 7000 rpm. These steps were repeated until the supernatant solution conductivity was ≤ 75 µS/cm. Next the silica nanoparticles were washed two times with a 70/30 (v/v) mixture of isopropyl alcohol and deionized water and dried for 24 h in a vacuum oven at 120°C. Silanization of the silica nanoparticles was carried out by dispersing the one gram of silica particles in 50 mL of toluene with a ½" tip at 70% amplitude for 15 minutes. Once the silica particles were dispersed 37.5 µL of octadecyltrichlorosilane was added to functionalize 50% of the silanol groups on the silica surface. To functionalize 100% of the silanol groups on the silica surface 75 µL of octadecyltrichlorosilane was added to the mixture. The number of silanols on the silica surface was based on literature values of two to three surface hydroxyls per nm^2,[113,114]. The sample with 50% OTS coverage is labelled Ludox-50%OTS and the sample with 100% coverage is labelled Ludox-100%OTS. After functionalization with OTS the samples were removed from toluene by centrifugation and washed three times with toluene and two times with isopropyl alcohol to remove excess silane.

MWNTs were oxidized by adding one gram of MWNTs to a round-bottom flask and then adding 50 mL of six molarity nitric acid. The flask was connected to a condenser column and refluxed for 24 hours at 120°C. The MWNTs were removed

from solution using a vacuum filtration setup using a 0.22 μm PTFE filter. 18 MΩ water was used to wash the oxidized MWNTs until the pH was neutral.

Wet impregnation was used to deposit Pd precursors on the catalyst supports. Pd nitrate dihydrate was dissolved in water and impregnated dropwise onto a specified support. All catalysts were made to be one weight percent Pd with respect to the catalyst support material. After impregnation catalyst were placed in an alumina boat and loaded into a one inch diameter quartz tube. The quartz tube was placed in a furnace for heating and inlet and outlet of the gas tube connected to gas lines. Hydrogen at a rate of 200 sccm was flown through the gas tube while the furnace was heated. The furnace ramped to 100°C at 2°C/min, held at 100°C for four hours, ramped to 400°C at 2°C/min, and held at 400°C for four hours. This process decomposes the catalyst precursor and reduces the Pd.

Pd nanoparticles sizes were measured from TEM images and used to calculate the Pd dispersion on the catalyst supports. A JEOL 2000 FX equipped with a LaB_6 filament operating with an accelerating voltage of 200 kV was used to take the images. Measurements of the Pd nanoparticle sizes were determined by using ImageJ software. With the particle sizes a dispersion and turn over frequency (TOF) was calculated for each catalyst allowing for comparison between the different catalysts. TEM images can be found in the appendix section.

Reactions were conducted in a custom made glass reactor unit. The unit contains a three-neck round bottom flask with one neck connected to a condenser column. One of the other necks is used to bubble hydrogen into the flask and the other neck has a rubber cap which can be punctured to inject reactants. A hot plate with stirring

capabilities holds the round bottom flask to provide temperature control. For reactions with either oil or water 16 mg of catalyst was added and 50 mL of oil or water used. When using a single oil or water phase particles were dispersed with horn sonication using a ¼" tip at 45% amplitude for three minutes. For reactions with emulsions 8 mg of catalyst was added to a round bottom flask and 25 mL of decalin or water were used. The particles were dispersed with horn sonication using a ¼" tip at 35% amplitude for three minutes. Following this 25 mL of water or oil, opposite of what was added the first time, was added to the flask and horn sonicated using a ¼" tip at 45% amplitude for three minutes to create an emulsion. The round bottom flask with a single phase or emulsion was then connected to the reactor and hydrogen bubbled into the system at a rate of 125 sccm. The temperature of the reactor was set to 70°C and the stir speed at 60 rpm both temperature and stir speed were held constant for both reduction and reaction steps. The catalyst was reduced for 90 minutes with hydrogen flowing. After reduction reactants were injected into the reactor using a syringe. For a single aqueous phase a 10 mL mixture of cis-2-butene-1,4-diol and water was injected which made the concentration in the reactor after injection 0.2 M cis-2-butene-1,4-diol. For a single oil phase a 10 mL mixture of 1-dodecene and decalin was injected which made the concentration in the reactor after 0.2 M 1-dodecene. For a emulsion a five mL mixture of cis-2-butene-1,4-diol in water and 5 mL mixture of 1-dodecene and decalin was injected which made the concentration of 1-dodecene in oil 0.2 M and concentration of cis-2-butene-1,4-diol in water 0.2 M. Reactant cis-2-butene-1,4-diol has very low solubility in decalin and 1-dodecene very low solubility in water. After injection the reaction was allowed to proceed for one hour. To stop the reaction the flow of hydrogen

was stopped and nitrogen was bubbled into the reactor system at a rate of 125 sccm and the heating element of the hot plate turned off.

An Agilent 7890B GC-FID equipped with a capillary column, low-polarity column (Phenomen ZB-6) of 60.0m x 0.25 mm x 0.25 μm was used for quantification of products and reactants in the oil phase. For the water phase the same model GC-FID was used expect equipped with a polar column, Phenomen ZB-WaxPlus. For GC-FID analysis external standards decane was used for the oil phase and 1-butanol for the aqueous phase. All carbon balances were better than 90%.

Results and Discussion

Catalyst Supports of Different Wettability for Reactions in Emulsions

To investigate the ability of controlling selectivity in biphasic systems with silica nanoparticles of different wettability two reactants were chosen, cis-2-butene-1,4-diol (water soluble reactant) and 1-dodecene (oil soluble reactant) because these reactants provide two major advantages. The first advantage is the hydrogenation of cis-2-butene-1,4-diol[115] and alkenes[116] have been shown to be structure insensitive, which rules out changes in TOF between two different catalyst being due to the dispersion of the Pd particles. The second advantage is the solubility of the two reactants in decalin and water. The water soluble reactant has a high solubility in water and makes a separate phase in decalin. When mixing the water soluble reactant and decalin together, taking a sample of the decalin phase, and injecting in the GC-FID and GC-MS results in no discernable peaks of the water soluble reactant which is indicative of the low solubility in decalin. The same result is obtained when mixing 1-dodecene and water.

Thus, both reactants have almost exclusive solubility and allows for tracking of the hydrogenation activity in the organic and aqueous phases at the same time.

Three types of silica nanoparticles with different wettability are used with the water and oil soluble reactants. Pd/Ludox is the most hydrophilic due to the surface being entirely hydroxyls which interact strongly with the water. Pd/Ludox-50%OTS is amphiphilic due to having both hydroxyls and OTS groups and likely interacts with the aqueous and oil phase of the emulsion. Pd/Ludox-100%OTS is the most hydrophobic due to the entire surface being covered with OTS groups which strongly repel water. Multiple publications have shown particles functionalize with OTS become hydrophobic[112,117,100]. Each of these three silica nanoparticles has been found to have different water contact angles and create emulsions with different properties[112]. Therefore, each of these three catalysts will interact differently at the oil-water interface of an emulsion and can be used to study how selectivity can be controlled in emulsion systems. The catalyst dispersion was calculated using the particle size measurements from TEM[118]. The dispersions for the three catalysts were 25% for Pd/Ludox, 26% for Pd/Ludox-50%OTS, and 19% for Pd/Ludox-100%OTS, TEM images of the catalyst used in this study can be found in the appendix information. With the dispersions calculated the turn over frequency for each catalyst was calculated allowing for a fair comparison between the three catalysts.

Hydrogenation reactions with Pd on silica nanoparticles of different wettability show vast differences in selectivity when in an emulsion and operating with mass transfer limitations, Figure 21 (a). Hydrophilic silica nanoparticles, Pd/Ludox, have a high selectivity for the water soluble reactant and low selectivity for the oil soluble

reactant. This strong favoritism for the water soluble reactant is likely due to the hydroxyl groups of the silica Pd/Ludox bringing the catalyst into a aqueous environment at the oil-water interface. Amphiphilic silica nanoparticles Pd/Ludox-50%OTS has a roughly equal TOF for the oil soluble reactant and water soluble reactant. The hydroxyl groups and OTS groups expose the catalyst to the oil and aqueous environments at the same time at the oil-water interface. Hydrophobic silica, Pd/Ludox-100%OTS has a high TOF for the oil soluble reactant and low TOF for the water soluble reactant. This is a similar but opposite case of what occurs with the hydrophilic silica. With the hydrophobic silica the OTS groups expose the catalyst to an oil environment at the oil-water interface. The three catalysts were tested in a single phase of oil and water to compare with the emulsions, Figure 21 (b). TOF of the three catalyst of the oil soluble reactant in a single oil phase is roughly the same and the TOF of the three catalyst of the water soluble reactant in a single aqueous phase is the same.

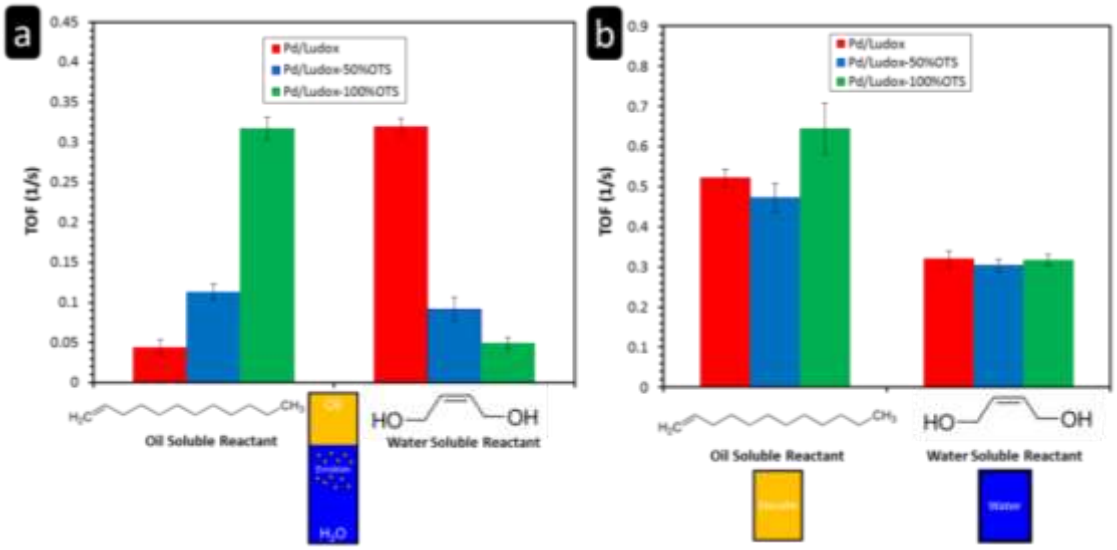

Figure 21: TOF for silica nanoparticles of different wettability in (a) emulsions and (b) single phase systems.

Controlled selectivity with particles of different wettability when under operating under mass transfer limitations is due to the oil and aqueous phases not being in thermodynamic equilibrium. When the two phases are not in thermodynamic the chemical potential for the oil soluble reactant and water soluble reactants are not the same. With the chemical potentials unequal the low solubility of the oil soluble reactant in the aqueous phase can be used to limit the reaction with catalyst particles in an aqueous environment at the oil-water interface, while the low solubility of the water soluble reactant in the oil phase is used to limit the reaction with catalyst particles in an oil environment at the oil-water interface. In addition to the low solubility the molecules must also diffuse through the oil or water film covering the particles surface, which is controlled by the stir speed.

If the oil and aqueous phases were in thermodynamic equilibrium the chemical potentials for the oil and water soluble reactants would be the same[119]. With the chemical potentials for the reactants the same the environment the catalyst particle is in would not control selectivity and the dramatic differences in selectivity would be unachievable. In such a case chemical potential controlled-kinetics can be applied.

Solvents present during reactions in liquid phase can also play a role in the reaction and if the rate limiting step then chemical potential controlled-kinetics cannot be applied[120,121,122,123,124]. Solvents, such as water, can compete for active sites with the reactants or play a part in the reaction mechanism. To rule out the role of water in causing the drastic change in selectivity with particle wettability a reaction was run in a single oil phase and small amounts of water injected.

Small amounts of water were injected by bubbling hydrogen through water before entering the reactor with a single oil phase and catalyst. Bubbling hydrogen through water exposes the catalyst to small amounts of water, but does not put the catalyst at the oil-water interface. This test allows for water to be present in the system and a comparison made between when a single oil phase with no water present is used. If a change in conversion occurs when hydrogen is bubbled through water then water is competing for sites on the catalyst surface with the oil soluble reactant or playing a role in the reaction. Testing catalysts Pd/Ludox and Pd/Ludox-100%OTS results in little to no change in conversion due to the presence of water, Figure 22, indicating there are no solvent effects or competition for sites due to the presence of water.

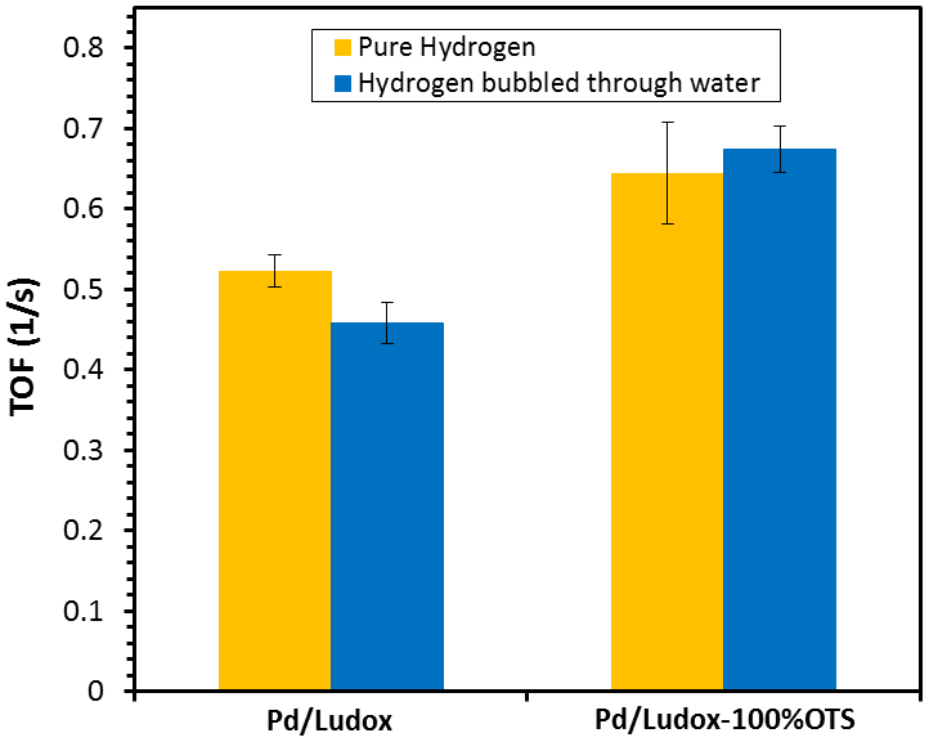

Figure 22: Reaction with Pd/Ludox and Pd/Ludox-100%OTS in a single oil phase and hydrogen bubbled into the system and bubbled through water before being bubbled into the system.

To rule out competition between reactants is not playing a part in controlling reaction selectivity reactions with an emulsion were run with one reactant at a time. For all three catalysts the TOF does not change significantly when the two reactants are present, Figure 23. This result rules out the oil soluble reactant and water soluble reactant are competing for active sites and gives further proof that the change in selectivity as a function of the particles wettability is controlled by mass transfer limitations and not competition between reactants or solvents.

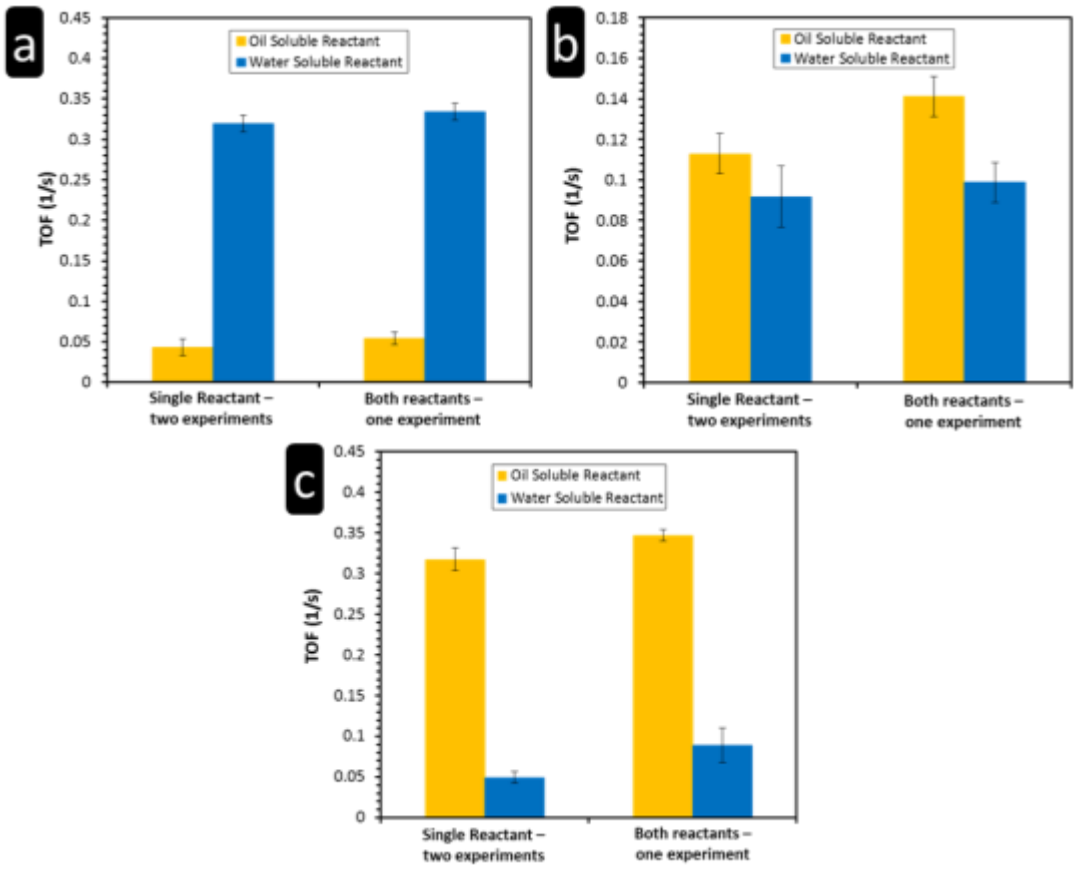

Figure 23: Reactions run with one reactant at a time in a emulsion and both reactants at the same time for the three catalyst (a) Pd/Ludox, (b) Pd/Ludox-50%OTS, (c) and Pd/Ludox-100%OTS.

Pickering emulsions made with particles wetted equally by oil and water can cause the type of emulsion to change depending on which phase the particles are dispersed in before forming an emulsion[125]. None of the three catalysts tested here change emulsion type when dispersed in a different phase before emulsification. However, we were interested in determining if dispersing the particles in the opposite phase created a different film over the surface of the particle and could change selectivity. For the reactions carried out with Pd/Ludox is dispersed in the water since it is hydrophilic. Reactions with Pd/Ludox-100%OTS catalyst were dispersed in the oil due to the silica nanoparticles floating on water. The majority of Pd/Ludox-50%OTS floats on the surface of the water and therefore was dispersed in the oil. When dispersing the three catalysts in the opposite phase normally dispersed in there is no significant difference in selectivity, Figure 24. Indicating the catalyst particles keep the same amount of oil and water films over the surface of the particle which keeps the reaction selectivity constant.

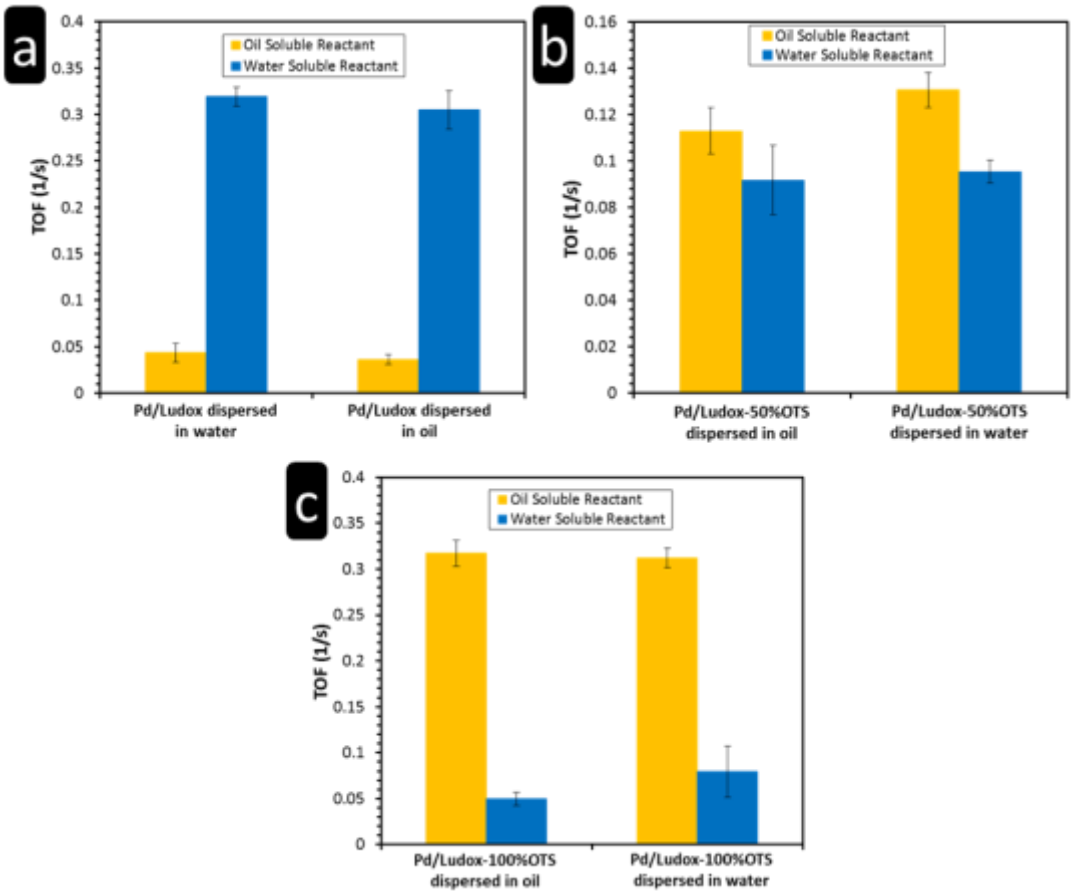

Figure 24: TOF for (a) Pd/Ludox, (b) Pd/Ludox-50%OTS, and (c) Pd/Ludox-100%OTS when dispersing the particles in oil or water before emulsification.

Mixture of Particles for Reactions in Emulsions

An advantage of conducting reactions in emulsions is to be able to put different catalyst in different phases. Therefore molecules can be reacted in a particular phase with one type of catalyst and then phase transferred to another phase for a reaction with a different catalyst. As described above one advantage of this process is in biofuels refining[126]. One method to conduct such a reaction is to make a Janus particle, where one side of the particle is made hydrophobic and the other hydrophilic. With the two sides of different wettability one type of catalyst can be placed on the hydrophobic side and a different type of catalyst on the hydrophilic side. Then operating under mass

transfer limitations reactant molecules in one phase will have quick access to one type of catalyst and starved from the other catalyst in the other phase. Janus particles have yielded the ability to control selectivity in an emulsion system as shown by Resasco's group[126]. When depositing Pd catalyst on the hydrophobic side of the Janus particle a high selectivity for the reaction in the oil phase was achieved when compared to when the Pd was on both sides of the Janus particle.

Janus particles prove promising for the possibility to have two different catalyst in a emulsion system, however, Janus particles are difficult to synthesize and the synthesis procedures for Janus particles may limit the type of catalyst which can be deposited on the Janus particles[127,128,129,130,131]. Binks et al. has shown Pickering emulsions can be stabilized with a mix of hydrophobic and hydrophilic particles and by controlling the ratio of hydrophobic to hydrophilic particles the emulsion droplet size and type can be tuned.[132] Since Pickering emulsions can be stabilized with a mix of particles of different wettability there is potential to deposit one type of catalyst on hydrophilic particles and a different catalyst on hydrophobic particles and create a system which behaves the same as with Janus particles.

To test the potential of this idea we have made emulsions with a one to one ratio of hydrophilic catalyst, Pd/Ludox, and hydrophobic catalyst, Pd/Ludox-100%OTS and keeping the total amount of Pd between the two catalyst the same as when one of the catalyst is used. With this mix system both Pd/Ludox and Pd/Ludox-100%OTS work together in the reaction, Figure 25. Comparing Pd/Ludox to the mix of Pd/Ludox and Pd/Ludox-100%OTS the conversion of the oil soluble reactant increased and conversion of the water soluble reactant decreased. Comparing the Pd/Ludox-100%OTS to the mix

of Pd/Ludox and Pd/Ludox-100%OTS the conversion of the oil soluble reactant decreased the water soluble reactant has increased. Thus, indicating in the mix system the Pd/Ludox is mainly responsible for the conversion of the water soluble reactant and the Pd/Ludox-100%OTS is responsible for the conversion of the oil soluble reactant. By conducting reactions with a mix of hydrophobic and hydrophilic particles the same effect can be achieved as when using Janus particles.

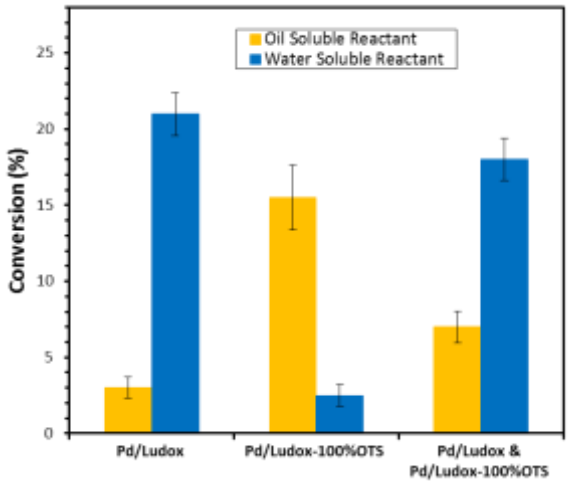

Figure 25: Reaction when mixing Pd/Ludox and Pd/Ludox-100%OTS in a emulsion.

In this mix system half of the Pd is on the hydrophobic Ludox and the other half is on the hydrophilic Ludox. Therefore, one can check the results of the mix system as the conversion of the oil soluble reactant in the mix system should be the sum of half of the conversion of the oil soluble reactant with Pd/Ludox and Pd/Ludox-100%OTS. The same should also be true for the water soluble reactant. The expected conversions for the oil soluble reactant are 8.5% and the water soluble reactant 11.5%. Comparing with the results for the mix system in Figure 25 the oil soluble reactant is slightly lower at 7% and the water soluble reactant higher at 18%. These changes in conversion may be

due to how the particles interact at the oil-water interface. Dissipative particle dynamics simulations have shown two particles with different wettability can get closer to one another at the oil-water interface due to the differences in contact angles of the two particles than particles with the same contact angle.[133] With the two different particles closer together there is a possibility one of the particles environment dominates the other which influences the film on the other particle which influences mass transfer limitations which controls the rate of reaction under these mass transfer limitation conditions. To test this idea MWNTs were mixed with the two silica nanoparticles of different wettability. As can be seen in Figure 26 the MWNTs decrease the conversion of the water soluble reactant and the conversion value is close to what is expected.

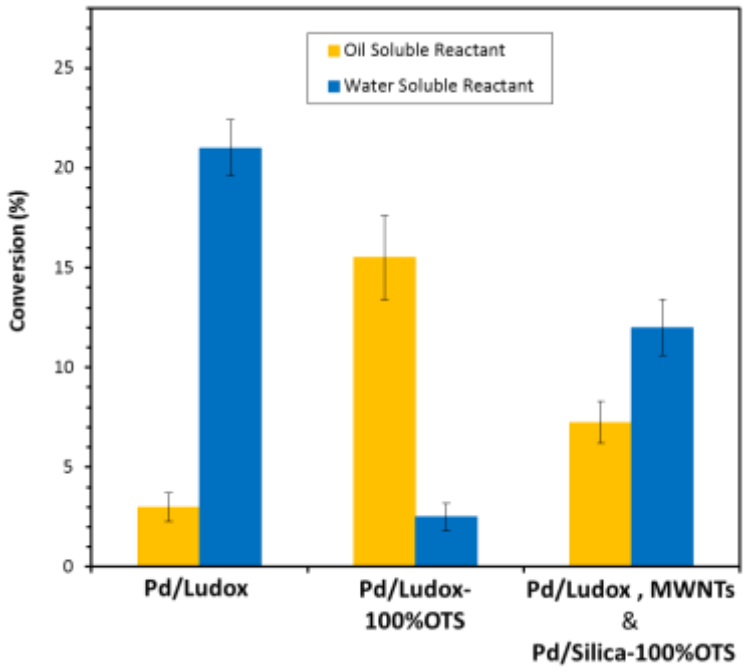

Figure 26: Pd/Ludox and Pd/Ludox-100%OTS mixed with MWNTs to act as a separator between the two silica nanoparticles.

To further test the flexibility of this system a different type of particle was chosen to mix with the functionalized silica nanoparticles. We recently showed

MWNTs have high emulsion stability and multiple carbon nanotubes are present at the oil-water interface of an emulsion.[134] This high emulsion stability has been attributed to the van der Waals forces creating strong attraction between MWNTs and helping to decrease droplet coalescence[135]. With the benefit of using MWNTs in emulsions we deposited Pd catalyst on MWNTs and mixed with silica nanoparticles with the intent of seeing how having the Pd on the MWNTs effects conversion of the oil and water soluble reactants. For reactions in emulsions stabilized by MWNTs the catalyst Pd/CNT gives a roughly equal conversion for the oil and water soluble reactant, Figure 27. This may be attributed to there being multiple MWNTs at the oil-water interface[134], whereas with spherical particles, such as silica used in our study, there tends to be a monolayer of particles at the oil-water interface[129]. Combining the two catalyst Pd/CNT and Pd/Ludox-100%OTS yields in a higher conversion of the oil soluble reactant than the water soluble reactant, Figure 27 (a). Additionally, the expected conversions when combining these two catalysts matches well with the results obtained experimentally. By using a different type of catalyst support the interaction between the two particles has been changed and for this reaction has shifted selectivity to the oil soluble reactant. Mixing Pd/CNT with Pd/Ludox results in a higher conversion of the water soluble reactant, Figure 27 (b), and unlike with the mix of Pd/Ludox and Pd/Ludox-100%OTS the expected conversions match well with the results obtained experimentally. Here we show MWNTs and silica nanoparticles can be mixed together to favor a reaction in the water or oil by using silica nanoparticles that are either hydrophilic or hydrophobic.

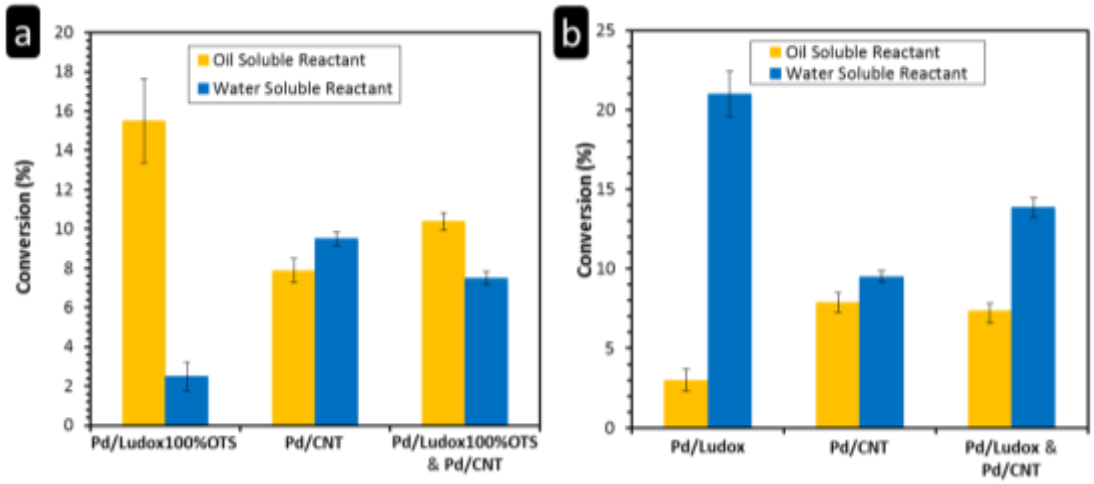

Figure 27: Reactions with (a) Pd/Ludox and Pd/CNT mixed together in an emulsion. Reactions with (b) Pd/Ludox-100%OTS and Pd/CNT mixed together in an emulsion.

To further test the boundaries of how reaction selectivity can be controlled in mixed particles systems MWNTs were oxidized to be more hydrophilic. We have observed MWNTs create w/o emulsions due to their inherent hydrophobicity while oxidized MWNTs create o/w emulsions due to the oxygen containing functional groups formed on the surface of the MWNTs.[134] Using oxidized MWNTs as a support for Pd, catalyst Pd/o-CNT, in a emulsion system alone results in an increase in conversion of both oil and water soluble reactants, Figure 28, compared to the catalyst with MWNTs as the support, Pd/CNT, Figure 27. We believe this increase in conversion with the Pd/o-CNT compared to the Pd/CNT may be due to there being two to three times less oxidized MWNTs at the oil-water interface than with the MWNTs[134]. With less MWNTs at the oil-water interface there is less of a barrier, internal mass transfer limitations, the reactants must pass through, however, due to the presence of multiple MWNTs at the interface there is roughly equal conversion of the oil and water soluble reactants.

Mixing Pd/Ludox-100%OTS and Pd/o-CNT results in roughly equal conversion of the oil and water soluble reactants, just as when Pd/Ludox-100%OTS and Pd/CNT are used, Figure 28 (a). The conversion of the oil and water soluble reactants is higher than when using Pd/Ludox-100%OTS and Pd/CNT, which is possibly due to there being fewer oxidized MWNTs at the oil-water interface creating less internal mass transfer limitations for the reactants to reach the Pd on the oxidized MWNTs. Mixing the catalyst Pd/o-CNT and Pd/Ludox results in a higher conversion of the water soluble reactant compared to the oil soluble reactant, Figure 28 (b), which is the same trend as with Pd/CNT and Pd/Ludox, Figure 27 (b), but the conversions are higher which again is possibly due to fewer oxidized MWNTs being at the oil-water interface creating less internal mass transfer limitations. If the environment the MWNTs and oxidized MWNTs create around the silica nanoparticles influences the rates of reaction then this may also be what is occurring with the Pd/Silica and Pd/Silica-OTS. The Pd/Silica may be creating an environment which is also influencing the Pd/Silica-OTS as suggested earlier.

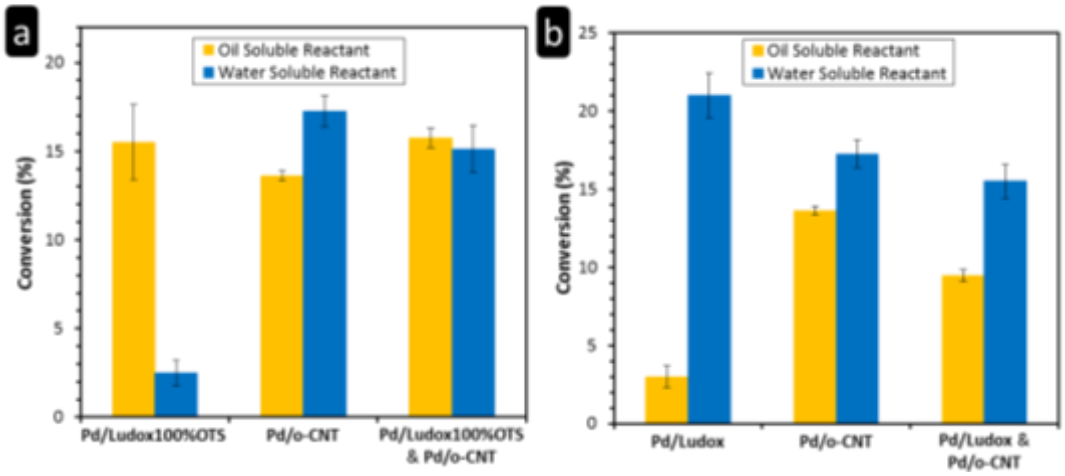

Figure 28: Reactions with (a) Pd/Ludox and Pd/o-CNT mixed together in an emulsion. Reactions with (b) Pd/Ludox-100%OTS and Pd/o-CNT mixed together in an emulsion.

Conclusion

Reaction selectivity can be tuned to favor the reaction in either phase of an emulsion system by tuning the particles wettability to be the same as the desired phase. Additional experiments rule out the control in selectivity being due to solvent effects or competition between reactants. Dispersing particles in the oil or water phase before emulsification does not result in a change in selectivity for the catalyst tested. Implying the catalyst particles after emulsification are in the same environment regardless of what phase the catalyst particles are dispersed initially. Mixing particles of different wettability allows for the creation of a "Janus effect", the same effect as when using Janus particles. Not only can the same type of materials with different wettability be mixed together, but different materials, which can be used to favor a reaction in one phase of the emulsion more than another. Mixing particles of different wettability to create this Janus effect is a simpler method than making Janus particles and opens the doorway for creating systems with different catalyst in different phases a emulsions for new reaction schemes. Additionally, the mixtures of particles at the oil-water interface may not retain their original environment with one particle being influenced by another environment causing changes in rates of reactions.

Chapter 5: Responsive System for Tuning Reaction Selectivity in Biphasic Systems

Introduction

Heterogeneous catalysis reactions gain many benefits when performed in a oil-water emulsion where the catalyst participates in the reaction and stabilizes the emulsion[136,137,138,139,140,141,142,143,144]. The benefits of conducting reactions in emulsions allows for easy recovery of products since solid particles stabilize are responsible for stabilizing the emulsion rather than a surfactant, separation of the products from the reaction mixture by using the differences in oil-water solubility, the possibility to control reaction selectivity when operating under mass transfer limitations due two different liquid phases, and an increase in oil-water interfacial area which increases the mass transfer of molecules between the oil and water phases. These advantages have proven particularly advantageous for those working in biomass upgrading due to biomass being composed of a sizable portion of water and the ability to control selectivity in these systems[136,138,142] and in Fischer-Tropsch where having two solvents can help prolong catalyst life[143,144].

A goal currently being worked on with these systems is to recycle the solid catalyst by breaking the emulsion allowing for products to be extracted from the catalyst and then fresh reactant added and the emulsion reformed so the process can be repeated. This is advantageous over the current method where filtration is used to remove the solid particles from the liquid, which interrupts the reaction process and is time consuming[139,140,141,148,145,146,147]. Several different routes to recycle catalyst by

breaking the emulsions have been taken. One approach is to use magnetic particles to stabilize an emulsion and then use a magnet to pull the magnetic particles from the oil-water interface breaking the emulsion droplet.[141,148,149] A second approach is to change the solid particle stabilizing the emulsions wettability by making the particle more hydrophobic or hydrophilic which can be used to break the emulsion or transfers the particles between the oil and water phases. Solid particles have been functionalized with thermos-responsive functional groups[150,147,151], light-responsive functional groups[152,153], pH responsive functional groups[141,154], and mixed with surfactants in attempts to change the particles wettability[155,156]. In addition, particles have been made to respond to more than one type of stimuli, such as particles which are sensitive to magnetic fields and temperature variations.[157]

Another use for these responsive systems is to move the solid particles into different phases as the reaction proceeds for cleaning of the catalyst or to change the rate of reaction in the oil or water phase of the emulsion. The ability to move solid particles into different phases is useful if during the reaction a polymer forms on the catalyst. By moving the catalyst into the phase the polymer is soluble in the catalyst can be cleaned. A similar concept is used for Fischer-Tropsch reactions in emulsions.[143,144] The reaction is accelerated in the presence of water, but quickly deactivates the catalyst due to the growth of the carbon chains. Combining an oil and aqueous phase the catalyst is at the interface of the emulsion and the oil can clean the catalyst of the growing carbon chains on the catalyst allowing for the growth of more carbon chains. Controllably moving the catalyst between the oil and aqueous phase of the emulsion can prove useful for taking advantage of solvent effects to control reaction selectivity. A

molecule can be partially reacted in one solvent and then phase transfer to another phase where the catalyst can move with the molecule and continue the reaction where in this different solvent effects take place creating different reaction pathways. Without the ability to move the catalyst the reaction would continue to proceed in both phases and could not increase in the opposite phase giving a low yield of desired product.

Herein we report the creation of a responsive system where the particles wettability is tuned to increase the rate of reaction in the oil or aqueous phases of the emulsion. Cationic surfactant is used to change the silica nanoparticles wettability changing the environment of the catalyst which changes reaction selectivity for the reactants in the oil or aqueous phase. Using ionic surfactants is advantageous since an oppositely charged surfactant can be added to the system causing the cationic and anionic surfactants to form ion pairs. Once ion pairs are formed the silica nanoparticles return to their original environment and reaction selectivity returns to the state before surfactant was added to the system. To change the selectivity again additional cationic surfactant can be added to the system. This process of adding cationic and anionic surfactant to change the rate of reaction of the reactants in the oil or aqueous phase of the emulsion can be repeated. Silica nanoparticle wettability and surfactant hydrophilic-lipophilic characteristics control if reaction selectivity can be tuned. To the best of our knowledge this is the first report of a responsive system used to change reaction selectivity during the reaction process.

Experimental Details

The chemicals octadecyltrichlorosilane (OTS), dodecane, 1-dodecene, cis-2-butene-1,4-diol, butane-1,4-diol, decane, sodium dodecyl sulfate, cetyltrimethylammonium bromide, and decalin were all purchased from Sigma Aldrich. The catalyst precursor Pd nitrate dehydrate was purchased from Sigma Aldrich. Silica nanoparticles, with diameters between 10 – 20 nm, and Ludox TM-50 colloidal silica nanoparticles, with average diameter of 32 nm, were both purchased from Sigma Aldrich. Ludox TM-50 colloidal silica from the manufacturer comes as a 50 wt% aqueous dispersion of silica with a solution pH of 8.5 – 9.5. Silica nanoparticles were removed from the aqueous solution by filtering and washing as previously described[158].

Wet impregnation was used to deposit Pd on the silica nanoparticles. The catalyst precursor Pd nitrate dihydrate was dissolved in water and impregnated dropwise onto silica nanoparticles. Catalysts were made have one weight percent Pd with respect to the silica support. After impregnation of the Pd on the silica nanoparticles the silica nanoparticles were placed in an alumina boat and loaded into a one inch diameter quartz tube. Next the outlet and inlet of the quartz tube was connected to gas lines and the quartz tube placed in a furnace. Hydrogen at a flow rate of 200 sccm was flowed through the quartz tube while the furnace heated the catalyst. The furnace was set to ramp at 2°C/min to 100°C, held at 100°C for four hours, ramp at 2°C/min to 200°C, and hold at 200°C for four hours. This process decomposes the catalyst precursor and reduces the Pd.

Functionalization of the of the silica nanoparticles with OTS was carried out by dispersing the one gram of the dried and washed Ludox TM-50 silica particles in 50 mL

of toluene with a ½" tip at 70% amplitude for 15 minutes. Once the silica particles were dispersed 75 µL of OTS was added to functionalize 100% of the silanol groups on the silica surface. The number of silanols on the silica surface was based on literature values of two to three surface hydroxyls per nm^2.[159,160] After functionalization with OTS the samples were removed from toluene by centrifugation and washed three times with toluene and two times with isopropyl alcohol to remove excess silane. The sample functionalized with OTS is labelled Pd/Silica-OTS. Silica purchased from Sigma Aldrich was not functionalized with OTS to remain hydrophilic and is labelled Pd/Silica.

The Pd nanoparticles on the silica particles were measured from TEM images taken using a JEOL 2000 FX equipped with a LaB_6 filament and operating at an accelerating voltage of 200 kV. From the TEM images Image J software was used to measure the Pd nanoparticle sizes. With the Pd particle sizes a dispersion of Pd over the silica nanoparticles surface was calculated and for the reactions a turn over frequency (TOF) was calculated allowing for comparison between different catalysts.

Reactions were conducted in a custom made glass reactor unit. The unit contains a three-neck round bottom flask with one neck connected to a condenser column. One of the other necks has a rubber cap which can be punctured with a syringe needle to inject reactants and the other neck is used to bubble hydrogen into the flask. A hot plate with stirring capabilities holds the round bottom flask to provide temperature control. For reactions eight milligrams of catalyst was added to a round bottom flask and 25 mL of water added or 25 mL of an aqueous solution with the desired amount of surfactant. The silica nanoparticles were dispersed with horn sonication using a ¼" tip at 35%

amplitude for three minutes. Following this 25 mL of decalin was added to the flask and horn sonicated using a ¼" tip at 45% amplitude for three minutes to create an emulsion. Next the round bottom flask was connected to the reactor and hydrogen bubbled into the system at a rate of 125 sccm. The temperature of the reactor was set to 70°C and the stir speed at 60 rpm. Both temperature and stir speed were held constant for both reduction and reaction steps. The catalyst was reduced for 90 minutes with hydrogen flowing. After reduction reactants were injected into the reactor using a syringe. Five millimeter mixture of cis-2-butene-1,4-diol in water and a five millimeter mixture of 1-dodecene and decalin was injected which made the concentration of 1-dodecene in oil 0.2 M and concentration of cis-2-butene-1,4-diol in water 0.2 M. Reactant cis-2-butene-1,4-diol has very low solubility in decalin and 1-dodecene very low solubility in water. After injection the reaction was allowed to proceed for one hour. To stop the reaction the flow of hydrogen was stopped and nitrogen was bubbled into the reactor system at a rate of 125 sccm and the heating element of the hot plate turned off.

An Agilent 7890B GC-FID equipped with a capillary column, low-polarity column (Phenomen ZB-6) of 60.0m x 0.25 mm x 0.25 μm was used for quantification of products and reactants in the oil phase. For the water phase the same model GC-FID was used expect equipped with a polar column, Phenomen ZB-WaxPlus. For GC-FID analysis external standards decane was used for the oil phase and 1-butanol for the aqueous phase. All carbon balances were better than 90%.

Results and Discussion

Particle Wettability and Switchable Emulsion Stability

Before testing the responsiveness of the catalyst the particles wettability and ability to stabilize emulsions was tested. To test the catalyst particles wettability particles were placed in water. As can be seen in, Figure 29, the hydrophilic silica used in this study sinks in water due to its inherent hydrophilic nature, while hydrophobic silica made for this study floats on the surface of the water due to the functionalization with OTS making the silica hydrophobic.

Figure 29: Hydrophilic silica in the vial on the left and hydrophobic silica in the vial on the right.

Making emulsions with the hydrophobic and hydrophilic silica nanoparticles used in this study results in an unstable emulsion when using hydrophilic silica nanoparticles, Figure 30 (a), and little to no emulsion when using hydrophobic silica, Figure 30 (b). This has been observed in other studies where silica nanoparticles have been functionalized to have a completely hydrophilic or hydrophobic surface.[161,162] From these studies it is believed if the silica nanoparticles are at the extreme of being

hydrophilic or hydrophobic then the silica nanoparticles are not rigidly held at the oil-water interface or can be desorbed from the oil-water interface. If the particles are not held rigidly at the oil-water interface or desorb from the oil-water interface then droplet coalescence occurs rapidly and the emulsion becomes unstable.

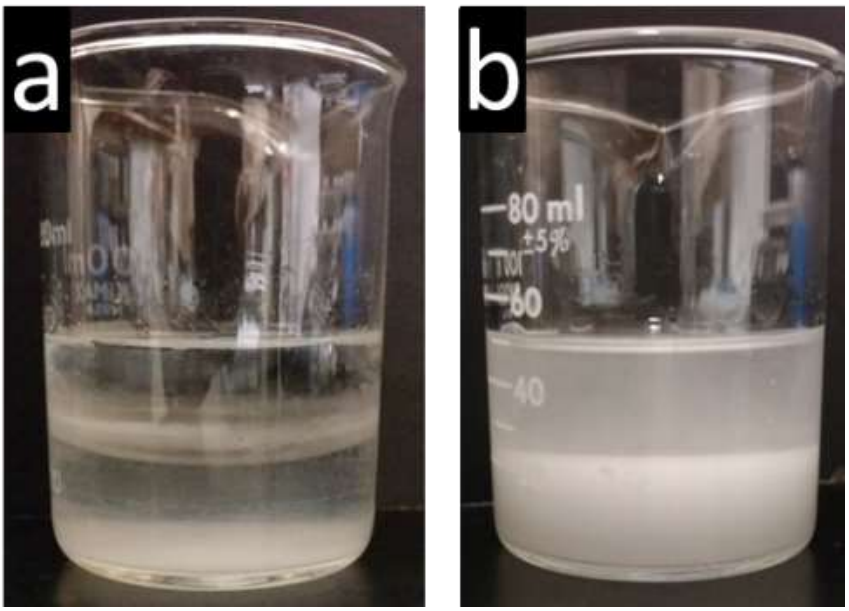

Figure 30: Emulsions made with hydrophilic silica (a) and hydrophobic silica (b).

Hydrophilic silica which cannot stabilize an emulsion can be mixed with a cationic surfactant to form stable emulsions due to the surfactant changing the wettability of the silica to be more amphiphilic[163]. Recently it has been shown when mixing hydrophilic silica and CTAB, a cationic surfactant, a stable emulsion is formed when SDS, an anionic surfactant, is added the emulsion becomes unstable and breaks,[164] Figure 31. The instability is due the CTAB and SDS forming ion pairs, which changes the wettability of the silica. A stable emulsion can be formed again if additional CTAB is added to the system.

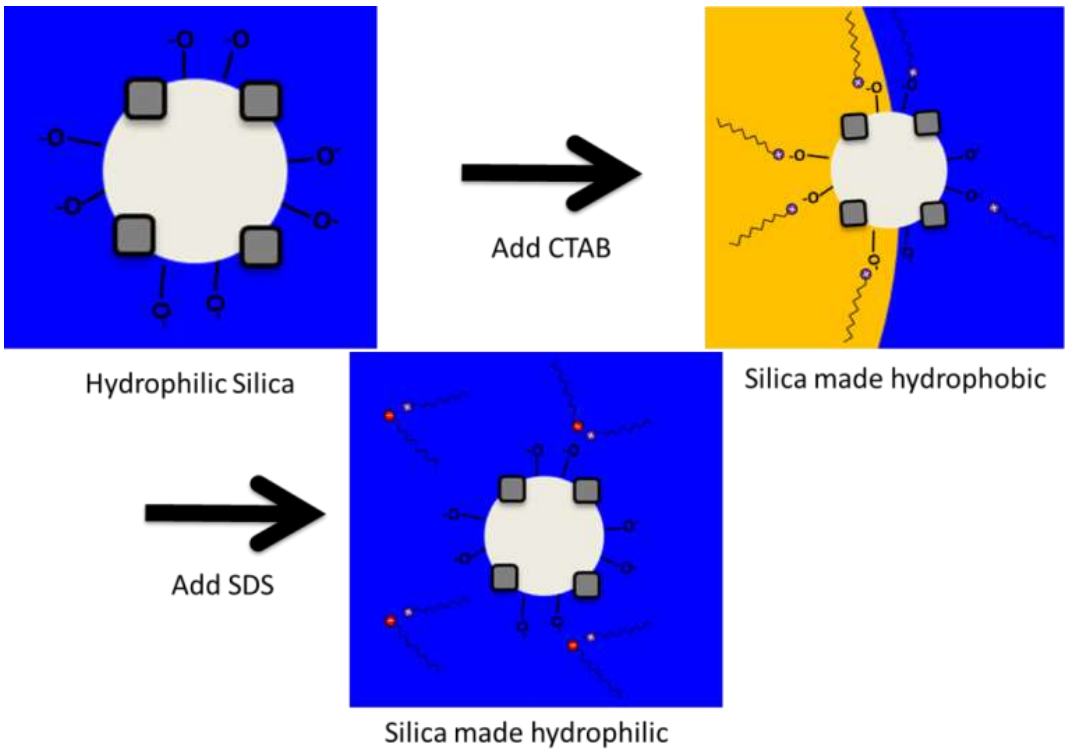

Figure 31: Hydrophobization of hydrophilic silica with cationic surfactant and then formation of ion pairs by addition of anionic surfactant to make the silica hydrophilic.

This switching in emulsion stability is due to the CTAB, which has a positive charge, having a strong attraction for the silica, due to the negative surface charge. Due to the opposite charge the CTAB is attracted to the silica surface and reduces the hydrophilicity of the silica due to the presence of the surfactants hydrophobic tail. This change in wettability of the silica nanoparticles due to the presence of surfactant has been measured by Granick's group, where they show the hydrophilic silica particles contact angle increases with increasing surfactant concentration[165]. Addition of an equimolar amount of SDS to CTAB surfactant causes the CTAB to form ion pairs with the added SDS making the surface of the silica hydrophilic and unable to stabilize an emulsion. A stable emulsion can be reformed by adding a surplus of CTAB to the

system which hydrophobizes the silica once again. This process of stabilization and destabilization of the emulsion can be accomplished by changing the ratio of CTAB to SDS in the system. Using the hydrophilic silica in our study we are able to reproduce these results, Figure 32.

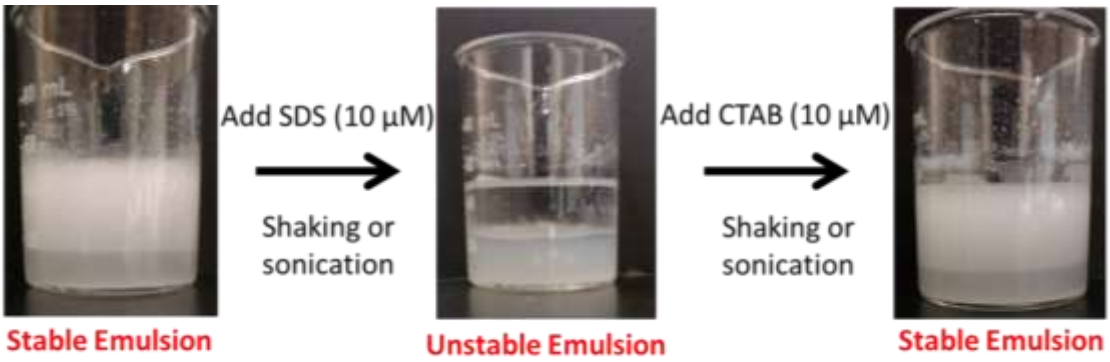

Figure 32: Stable emulsion made with 0.5 wt% hydrophilic silica nanoparticles and 10 µM CTAB. Addition of equimolar amount of CTAB to SDS results in emulsion destabilization. After adding a surplus of CTAB the emulsion can be stabilized again.

Since surfactants have a hydrophobic tail and hydrophilic head the idea of mixing cationic and anionic surfactants to stabilize and destabilize an emulsion stabilized by hydrophobic silica nanoparticles was tested. Our test show mixing CTAB and hydrophobic silica results in a stable emulsion and addition of equimolar amount of SDS to CTAB results in an unstable emulsion, Figure 33. Once a surplus of CTAB is added to the system then a stable emulsion can be reformed. We believe mixing the hydrophobic silica nanoparticles with CTAB results in hydrophobic tail of the surfactant interacting with the OTS groups on the silica surface instead of the hydrophilic head, Figure 34.

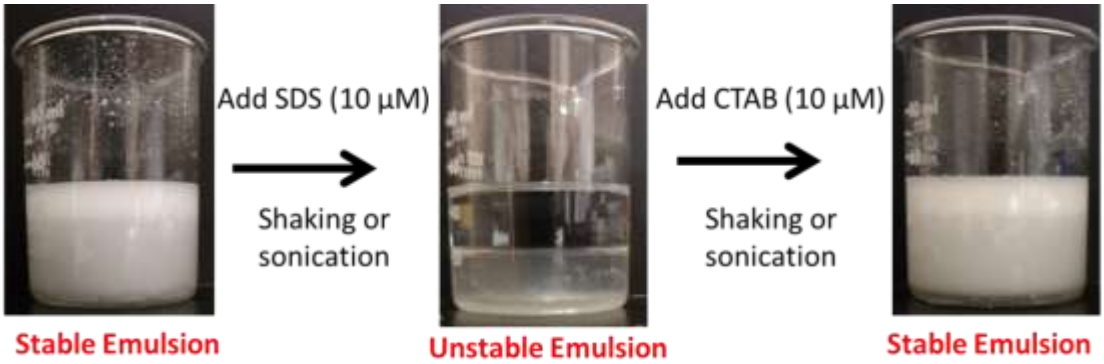

Figure 33: Stable emulsion made with 0.5 wt% hydrophobic silica nanoparticles and 10 µM CTAB. Addition of equimolar amount of CTAB to SDS results in emulsion destabilization. After adding a surplus of CTAB the emulsion can be stabilized again.

The exposure of the hydrophilic head decreases the hydrophobicity of the hydrophobic silica nanoparticles making them more hydrophilic and capable of stabilizing an emulsion. Adding an equimolar amount of SDS to CTAB causes the two surfactants to form ion pairs making the silica hydrophobic again and unable to stabilize an emulsion. A stable emulsion can be reformed if a surplus of CTAB is added to the system due to the hydrophobic silica nanoparticles becoming more hydrophilic.

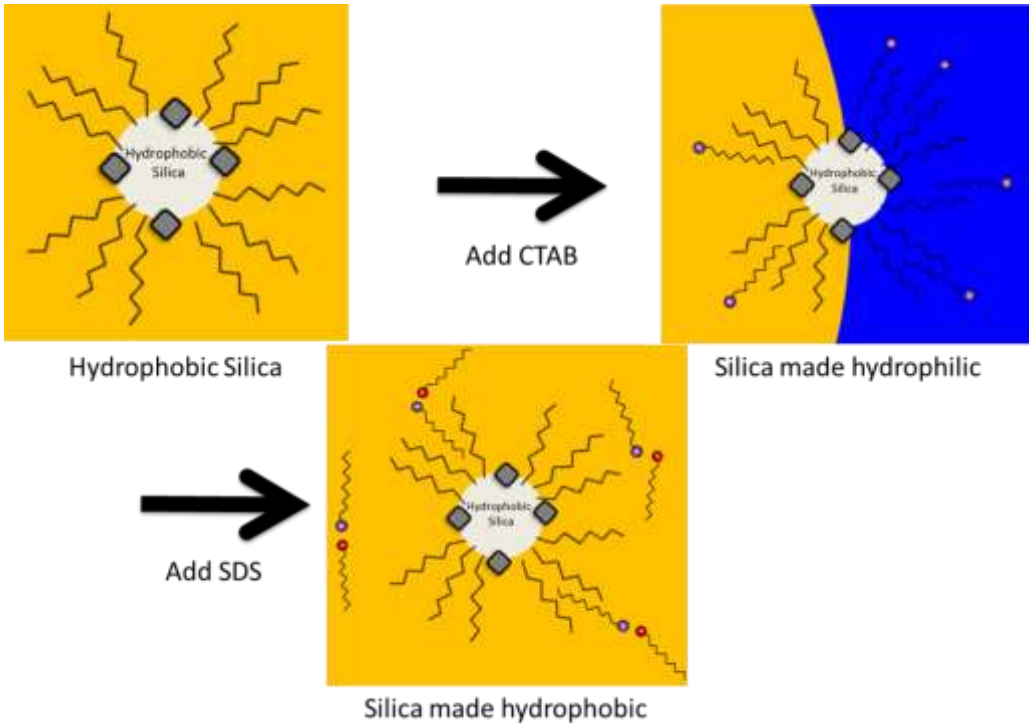

Figure 34: Hydrophilization of hydrophobic silica with cationic surfactant and then formation of ion pairs by addition of anionic surfactant to make the silica hydrophobic.

Reactions with Responsive System

This change in emulsion stability and location of the particle in the system seen when using surfactants and hydrophilic or hydrophobic silica nanoparticles offers the opportunity to tune reaction selectivity as the reaction proceeds. To test the feasibility of using surfactants to tune the silica nanoparticles wettability for controlling reaction selectivity reactions were performed. Two probe molecules one for the oil phase and the one for the aqueous phase were chosen to test if the reaction selectivity can be tuned during the reaction period. For the aqueous phase cis-2-butene-1,4-diol (water soluble reactant), was chosen for its high water solubility and low solubility in decalin and for the oil phase 1-dodecene (oil soluble reactant) was chosen which has a high solubility in

decalin and low solubility in water. The hydrogenation of cis-2-butene-1,4-diol[166] and alkenes[167] have been shown to be structure insensitive which allows for comparison of different catalysts using the TOF.

The hydrophobic catalyst, Pd/Silica-OTS, yields a higher TOF for the oil soluble reactant than the water soluble reactant and the hydrophilic catalyst Pd/Silica yields the opposite result, a higher TOF for the water soluble reactant than the oil soluble reactant, Figure 35. This drastic change in selectivity depending on the silica nanoparticles wettability occurs when operating under mass transfer limitations in a biphasic system. The Pd/Silica-OTS catalyst particles at the oil-water interface favor the oil phase and the Pd/Silica catalyst particles at the oil-water interface favor the aqueous phase. Due to the particles at the interface favoring one phase more than another the reaction selectivity is changed. This drastic change in selectivity depending on the wettability of the particle means these two catalysts are ideal for mixing with a surfactant to see if the selectivity can be changed.

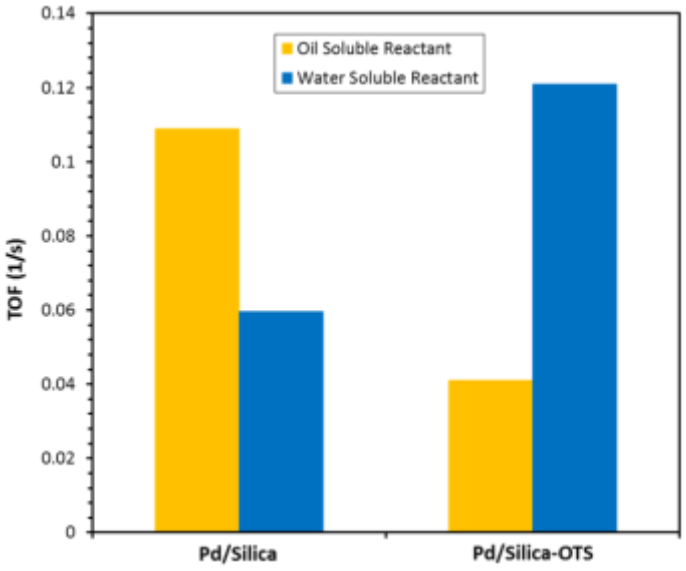

Figure 35: TOFs for the oil and water soluble reactants for the catalysts Pd/Silica-OTS and Pd/Silica in an emulsion.

Hydrophobic silica Pd/Silica-OTS mixed with a small amount of CTAB at the beginning of a reaction results in an increase in conversion of the water soluble reactant and a decrease in conversion of the oil soluble reactant, Figure 36. In this case the hydrophobic tails of CTAB interact with the OTS groups of the Pd/Silica-OTS catalyst and the hydrophilic head groups of the CTAB decrease the hydrophobicity of the Pd/Silica-OTS catalyst. This decrease in hydrophobicity of the Pd/Silica-OTS catalyst causes the increase in TOF of the water soluble reactant and decrease in the oil soluble reactant.

Addition of a trace amount of SDS and CTAB with Pd/Silica-OTS at the beginning of the reaction results in a favorable conversion for the oil soluble reactant and low conversion for the water soluble reactant, Figure 36. The SDS in the system forms ion pairs with the CTAB which increase the hydrophobicity of the Pd/Silica-OTS catalyst. Increasing the amounts and ratio of SDS and CTAB added at the beginning of the reaction shows the same trend. If there is a surplus of CTAB then the water soluble reactant conversion increases and with an equimolar amount of SDS and CTAB the conversion of the oil soluble reactant increases. While the selectivity changes the conversion of the water and oil soluble reactants decrease as the amount of surfactant in the system increases. The surfactant may be adsorbing to the Pd metal and taking up active sites or acting as poison for the Pd catalyst.

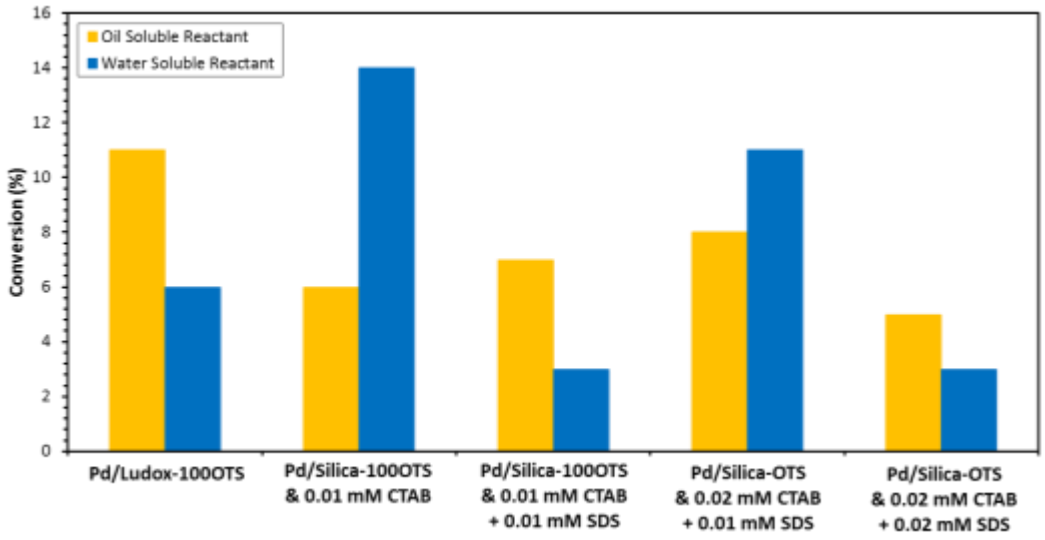

Figure 36: Pd/Silica-OTS catalyst mixed with different amounts of surfactant, showing the change in selectivity.

Depending on the ratio of CTAB and SDS in the system the reaction selectivity can be controlled by changing the wettability of the hydrophobic catalyst, Pd/Silica-OTS. Next the ability to control selectivity over a reaction period of five hours was tested. Starting with Pd/Silica-OTS in an emulsion there is a higher conversion of the oil soluble reactant than the water soluble reactant due to the hydrophobic nature of the catalyst, Figure 37. After bringing the CTAB concentration in the system to 10 µM and after one hour of reaction there is a shift from in rates of reaction with the water soluble reactant being converted faster than the oil soluble reactant. As can be seen in Figure 37 the conversion of the water soluble reactant increase is greater than the conversion of the oil soluble reactant, indicating the rate of reaction for the water soluble reactant is increased. Adding enough SDS to bring the ratio of CTAB to SDS equal and allowing the reaction to proceed for one hour results in an increase in rate of reaction for the oil soluble reactant and decrease in rate of reaction for the water soluble reactant. No

further change in conversion of the water or oil soluble reactants is observed when adding additional CTAB or SDS over the next two hours, Figure 37. This is possibly due to the surfactant blocking Pd active sites or the surfactant is poisoning the catalyst.

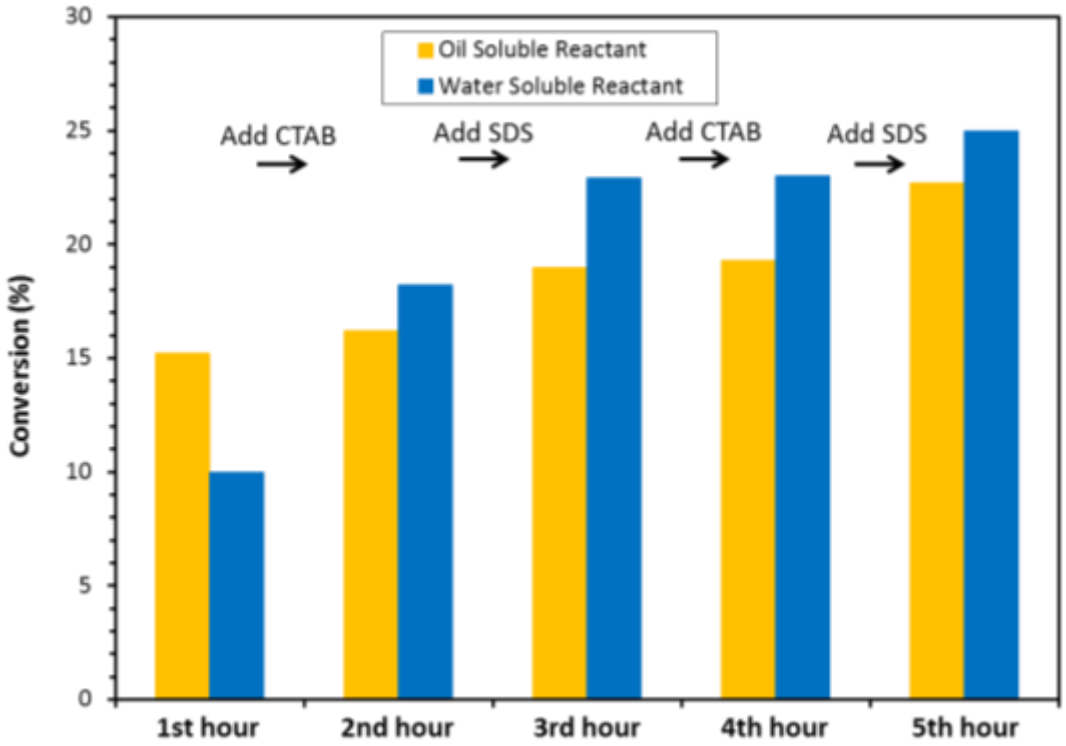

Figure 37: Addition of CTAB and SDS as the reaction proceeds over a 4 hour time period.

With evidence showing the hydrophobic catalyst Pd/Silica-OTS and surfactants can be used to control the reaction selectivity we tested the hydrophilic catalyst, Pd/Silica, with surfactants to see how selectivity could be tuned. Mixing Pd/Silica with CTAB does not change the selectivity as in the case with the hydrophobic catalyst Pd/Silica-OTS, Figure 38. Instead the water soluble reaction is still the dominant compared to the oil soluble reaction. The only change seen is the rates of both the oil and water soluble reactions drop. Previous work has shown the concentration of CTAB can change the wettability of the silica changing the particles contact angle[163,165].

Investigating this further we increased the CTAB concentration to the point where the entire surface of the silica should have been covered by a monolayer of CTAB. The amount of CTAB required for monolayer coverage was based on an adsorption isotherm from another study,[164] from this adsorption isotherm the required concentration for monolayer coverage was 141 μM of CTAB. However, at all CTAB concentrations tested above and below this value no change in selectivity was observed.

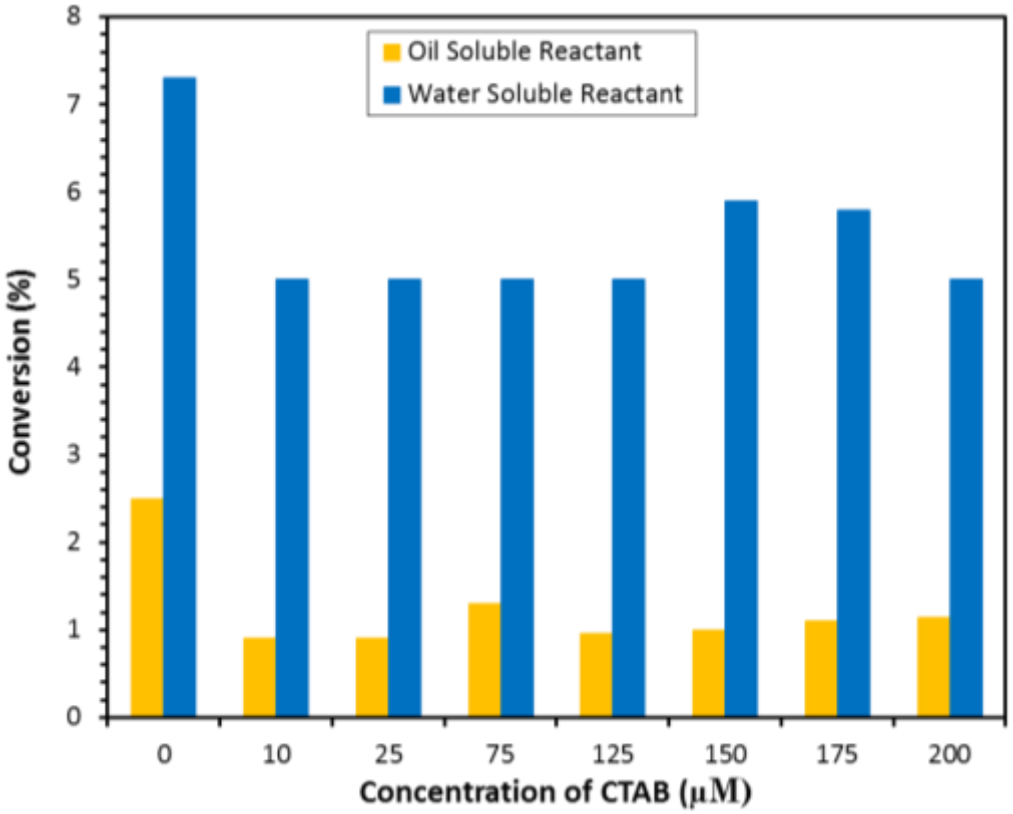

Figure 38: Reactions in emulsions with different concentrations CTAB using the hydrophilic Pd/Silica catalyst.

We noticed when making the emulsions for the reactions at these different CTAB concentrations the emulsion type was consistently o/w and the emulsion droplet size initially decreases, but eventually becomes constant, Figure 39. Changing silica nanoparticles wettability by covalent functionalization with a hydrophobic group

follows the trend of the emulsion droplet size being large for hydrophilic silica nanoparticles, then decreasing as the silica nanoparticles are made more hydrophobic, and when the silica nanoparticles are amphiphilic the emulsion type flips from o/w to w/o and as the particles become more hydrophobic the emulsion droplet size increases[161,162]. Since the CTAB, regardless of concentration, when mixed with the hydrophilic silica nanoparticles does not change the emulsion type this leads us to believe the CTAB does not sufficiently change the hydrophobicity of the silica nanoparticles to see a change in reaction selectivity. However, the CTAB can sufficiently lower the hydrophobicity of the hydrophobic silica to change the reaction selectivity.

A surfactants hydrophilic-lipophilic character can be determined from its hydrophilic-lipophilic balance (HLB) value[168,169]. The HLB value is based on the type and number of hydrophobic and hydrophilic groups the surfactant consist from. CTAB has a HLB value of 12.3 and this value makes it suitable for forming o/w emulsions. Since CTAB is suitable for making o/w emulsions when it is mixed with hydrophilic silica nanoparticles the emulsion type stays the same even though the emulsion becomes stable and the droplet size changes. This limit to how much the CTAB can change the wettability of hydrophilic silica nanoparticles is what causes there to be no change in reaction selectivity when using the hydrophilic catalyst Pd/Silica. However, mixing CTAB with hydrophobic silica nanoparticles results in the CTAB being able to sufficiently decrease the hydrophobicity of the hydrophobic silica nanoparticles and change emulsion type. This decrease in hydrophobicity of the hydrophobic catalyst, Pd/Silica-OTS, results in a change in selectivity of the oil and water soluble reactants.

Thereofre, the wettability of the particle and surfactants HLB may play a vital role in determining how and if reaction selectivity can be tuned.

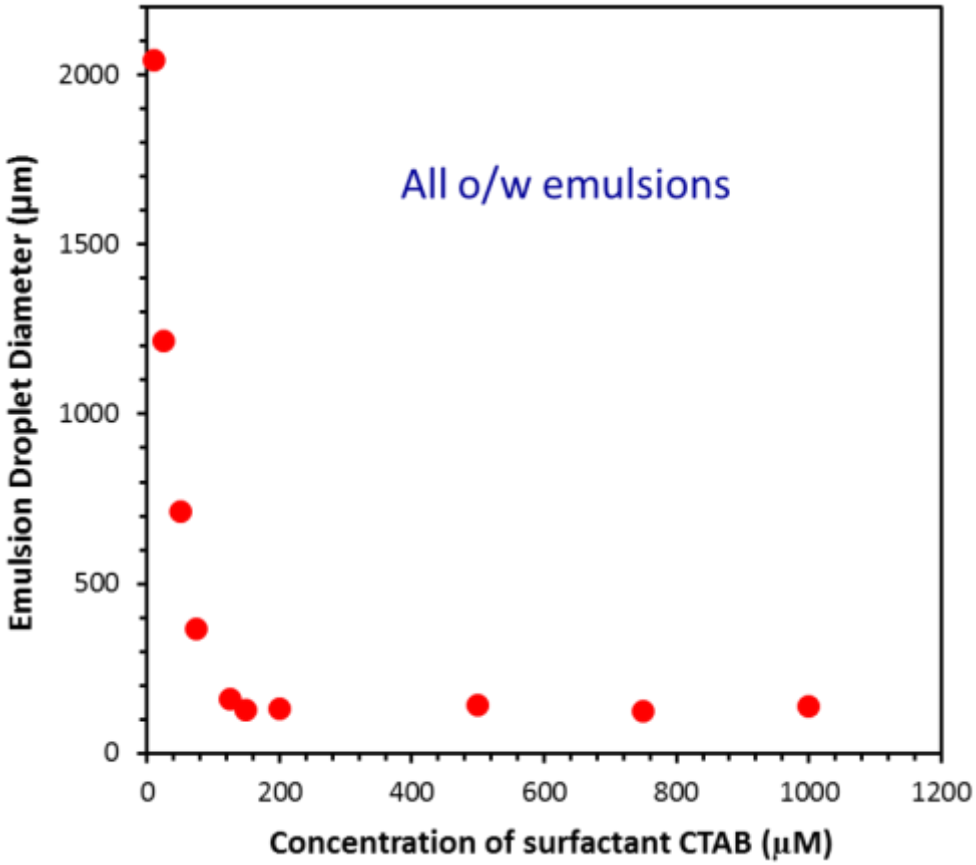

Figure 39: Emulsion droplet diameter as a function of CTAB concentration mixed with a constant amount of hydrophilic silica nanoparticles.

Results of mixing multi-walled carbon nanotubes with CTAB and SDS along with reactions using palladium supported on multi-walled carbon nanotubes and CTAB can be found in the appendix section.

Conclusion

Reaction selectivity in a emulsion system can be tuned by changing a silica nanoparticles wettability by using surfactants. By changing the ratio of CTAB to SDS

surfactants the silica nanoparticles wettability can be tuned and this tuning is responsible for changes in the reaction selectivity. The rate of reactions can be tuned to be higher in the oil or aqueous phase of the emulsion system and can be done reversibly. During our study we found this this control in selectivity is dependent on the hydrophilic-lipophilic characteristics of the surfactant and the wettability of the silica nanoparticles. The particles wettability and the surfactants ability to change the wettability of the particle are critical in achieving changes in reaction selectivity.

Chapter 6: Rapid Growth of Vertically Aligned Multi-Walled Carbon Nanotubes on a Lamellar Support

The following chapter is based on a publication which can be found in RSC Advances using the citation: Briggs, N. M., and S. P. Crossley. "Rapid growth of vertically aligned multi-walled carbon nanotube on a lamellar support" *RSC Advance*s 5. 102 (2015): 83945-83952.

Introduction

Carbon nanotubes have found uses in a variety of applications ranging from catalyst supports[170] to electronic devices[176]. The vertical alignment of carbon nanotube forests exhibit several advantages over non-aligned carbon nanotubes that tend to agglomerate. The unique orientation of the carbon nanotubes makes them useful because of their field emission properties[177] and their self-cleaning capabilities resulting from the super hydrophobicity created by the lotus leaf effect of their arrays[178]. Vertically aligned carbon nanotubes have also shown promise for use in thermal management,[179] hydrogen storage,[180,181] sensors,[182] yarns,[183,184] energy adsorbing hybrid composites,[185] compressible foams,[186] lithium-ion batteries,[174] hydrophobic coatings,[171] oil adsorption,[187] and applications that require strong adhesive forces[188].

An additional key benefit of vertically aligned carbon nanotubes is the reduced catalyst weight required to produce a given amount of nanotubes as a result of longer lengths. The reduced catalyst requirement could enable the use of carbon nanotubes in applications that would otherwise be cost prohibitive.[189] In addition, due to the

unconfined growth in a vertical array, Hata *et al.* reported that the addition of small amounts of water during the synthesis can result in ultra-long (up to 2.5 mm) vertically aligned nanotubes in ten minutes.[190] Due to the increased length, a carbon purity of 99.98% was achieved and the carbon nanotubes could more easily be removed from the substrate.[190] This easy separation from the substrate and high purity should eliminate the need for typical purification processes that may create defects[189] and change the point of zero charge of the carbon nanotubes.[191]

The synthesis of aligned carbon nanotubes was first reported on mesoporous silica in 1996[192] and on glass in 1998.[193] Two approaches to further increase the yield of vertical carbon nanotube arrays that have been proposed are by moving flat substrates on a conveyor belt[194,195] and by using lamellar clay as supports in fluidized beds.[185,196,197,198,199] By synthesizing the nanotubes within the layers of the lamellar support, the vertical growth of the tubes is enabled while avoiding cleavage of the nanotubes from attrition during fluidization. While vertical carbon nanotubes have been grown on substrates with different geometries, including flakes[200], spheres[201,202,203,204], and fibers[204], lamellar supports[185,196,197,198,199] have shown the best potential to produce the highest ratio of nanotube weight per gram of catalyst.[196] The longest reported vertical carbon nanotubes arrays produced over lamellar supports are 50 μm with a growth rate a rate of 20 μm/h. While these lengths are promising for fluidized bed growth and indicate there is potential to grow longer vertically aligned carbon nanotubes in large quantities, there is significant room for improvement to approach the nanotube lengths obtained on single flat substrates.

In this article, the growth of vertically aligned multi-walled carbon nanotubes (V-MWNTs) is investigated in a fluidized bed using lamellar supports while incorporating alumina within the catalyst to inhibit metal particle sintering. We report V-MWNT growth rates of 160 μm/h with lengths over 80 microns, which is 8 times faster than the highest rate reported over lamellar supports with unprecedented lengths.[185,196,197,198,199] Only a small handful of literature reports[185,196,197,198,199] investigate V-MWNTs growth with lamellar clay supports. Most literature on lamellar supports reports growth of randomly oriented carbon nanotubes.[206,207,208,209,210] The limited work on this subject only emphasizes the need to further understand these systems to maximize length and production of vertically aligned carbon nanotube arrays. This article, therefore, reports on the role of varying amounts of Al, Fe, and Co, the method by which the catalyst is deposited, and the effect of reduction and reaction temperatures. The role of elevated catalyst impregnation temperature is also discussed. A typical approach for increasing carbon nanotube length is to increase the reaction temperature, however, this typically results in larger diameter carbon nanotubes.[211,212] This article shows that by modifying the catalyst loading, alumina concentration, reduction temperature, and partial pressure of the carbon source, the length of the V-MWNTs grown between layers of a lamellar catalyst support can be increased with a minimal increase in nanotube diameter. The critical role of an aluminum precursor is also discussed, which inhibits sintering and enables the use of higher temperatures where longer carbon nanotubes and more rapid growth rates are achieved.

Experimental Section

Mica grade V-5 muscovite with a lateral size of 75 mm by 50 mm and thickness of 0.15 mm was purchased from SPI Supplies/Structure Probe, Inc. The mica sheets were then cut into small rectangular pieces roughly 2 mm by 2 mm and placed in a beaker of water. A T25 Digital Ultra Turrax with dispersant element IKA S 25 N – 18 GA was then used to break the mica sheets into small mica flakes by homogenizing them in water for three minutes at 10,000 rpm. The flakes were then sieved to sort out sizes between 150 and 355 μm using Cole Parmer mesh screens.

For wet impregnation of the mica flakes, Iron (III) nitrate nonahydrate, Cobalt (II) nitrate hexahydrate, and Aluminium nitrate nonahydrate were added to a beaker to obtain the desired metal concentrations. Fifty millilitres of either 18 MΩ water or isopropanol (IPA) was then added to the beaker as a solvent and the solution was mixed to dissolve the catalyst precursors. Two grams of the mica flakes were then placed in a mesh boat with a sieve size of 66 μm. The mesh boat was then placed in a glass petri dish and the catalyst solution was poured into the petri dish. The mica flakes were then soaked in the solution for two hours, after which the mesh boat was slowly removed from the solution and hung for two days to allow for excess catalyst solution to drip off and for the catalyst solution to dry.

The mica flakes were then calcined in air in a Thermolyne 48000 furnace for two hours at 450°C. To grow the V-MWNTs, 100 mg of the catalyst was placed on top of a quartz frit in the center of a 1 inch diameter quartz tube. The quartz tube was oriented vertically, so that fluidization of the mica flakes could take place. The catalyst was reduced by increasing the temperature to either 560°C or 650°C at a rate of 10°C per minute under a hydrogen flow rate of 300 sccm. The temperature was then held at the

desired reduction temperature for 30 minutes with a hydrogen flow rate of 300 sccm. After reduction, the temperature was increased to the desired reaction temperature at a rate of 10°C per minute at a nitrogen flow rate of 300 sccm. The temperature was then held at the reaction temperature for 10 minutes under nitrogen flow to bring the reactor temperature to a steady state. Ethylene or a mixture of ethylene and nitrogen was then introduced for 30 minutes with a total flow rate of 400 sccm. After the reaction, the reactor was allowed to cool to room temperature under a flow rate of 300 sccm nitrogen.

Table 2 contains the sample labels, precursor concentrations, solvent used to dissolve the catalyst, temperature of reduction and reaction, and flow rates of ethylene and hydrogen used during reaction.

Samples	Metal precursor concentration (mM)			Solvent	Temperature of:		Flow rate (sccm)	
	Fe	Co	Al		Reduction (°C)	Reaction (°C)	C_2H_4	N_2
NoAlRx760	2.6	0.7	0	Isopropanol	560	760	400	0
WRx760	2.6	0.7	5.3	Water	560	760	400	0
HWRx760	2.6	0.7	5.3	Water (Heated)	560	760	400	0
Rx760	2.6	0.7	5.3	Isopropanol	560	760	400	0
HRRx760	2.6	0.7	5.3	Isopropanol	650	760	400	0
HRRx650	2.6	0.7	5.3	Isopropanol	650	650	400	0
HRRx650D	2.6	0.7	5.3	Isopropanol	650	650	200	200
HRRx650D-A	2.2	1.1	5.3	Isopropanol	650	650	200	200
HRRx650D-B	2.6	0.7	2.6	Isopropanol	650	650	200	200
HRRx650D-C	2.2	1.1	2.6	Isopropanol	650	650	200	200
HRRx650D-D	2.2	1.1	2.6	Isopropanol	650	700	200	200

Table 2: Sample names, catalyst loading, solvent used, reduction, reaction temperature, and partial pressure of ethylene. NoAl = No alumina layer made, HW = hot water was used a solvent, W = Water was used as a solvent, D = ethylene was diluted with nitrogen, and HR = reduction temperature of 650°C

For SEM characterization, a Zeis NEON 40 EsB SEM was used to determine vertical alignment of the V-MWNTs and take images for measurement of their lengths using ImageJ software. For TEM characterization, a JEOL 2010F high resolution TEM, equipped with a field emission gun, was used to take images that were used to measure the diameter distribution of the carbon nanotubes. Measurement of the inner and outer diameters was determined by using ImageJ software. The average inner and outer diameter measurements of 100 randomly selected nanotubes were used to obtain an estimate of the average number of walls assuming an average nanotube wall thickness of 0.344 nm.[213] To test the validity of this method the number of walls for 100 carbon nanotubes were also counted for three samples. The three samples were HRRx760, HRRx650D, and HRRx650D-D, which span a range from an average of 4 to 32 walls. Both methods for determining the number of carbon nanotube walls gave comparable results as can be seen in the Appendix. The validity of this approach is further supported by Chiodarelli *et al.* who came to the same conclusion upon correlating the number of walls of multiwalled carbon nanotubes to their diameters.[214] Carbon yields were determined by oxidizing the carbon nanotubes and catalyst in air to 800°C in the previously described calcination system and measuring the resulting weight loss using a Metler Toledo AL204 analytical balance.

Temperature Programmed Reduction (TPR) experiments were conducted by flowing 5% H_2 in Ar at a rate of 30 sccm over a packed bed of 60 mg of mica flakes with catalyst. A temperature increase of 10°C per minute starting at room temperature and ending at 900°C was used. Analysis of effluent gas was detected with an SRI 110

thermal conductivity detector (TCD). The effluent gas was dried by passing through a packed bed filled with Drierite before introduction into the TCD detector.

Results and Discussion

Relationship between volume of nanotube arrays and nanotube length

A noticeable change in the volume of the mica flakes can be observed during the nanotube growth. This can be attributed to the expansion of the mica via V-MWNT growth between the layers. An average length of the V-MWNTs is measured for each sample by estimating the lengths of over 50 arrays via SEM imaging. The volume of the recovered catalyst and nanotubes post reaction are plotted against the average lengths of the V-MWNTs as shown in Figure 40. All reaction data obtained with pure ethylene used during the reaction step is plotted in Figure 40 (a) while the results obtained with an ethylene stream diluted with N_2 during the reaction step are shown in Figure 40 (b). The role of reactant dilution is discussed in following sections of this article. Carbon yield is also plotted versus average V-MWNT length as shown by Figure S1 & S2 of the Appendix. These figures show a linear correlation in both cases but the slope is not as pronounced as the volume expansion of the material. As will be discussed in the following sections, a small fraction of the ethylene decomposes during the reaction to form an amorphous carbon layer under certain conditions. This leads to a more direct and pronounced correlation between the catalyst volume expansion and nanotube length when compared to the relationship between volume expansion and carbon yield.

To demonstrate the important role of Al in the growth of V-MWNTs on mica flakes, Fe and Co catalysts were tested without any additional Al precursor. This

approach does not create a V-MWNT forest upon reaction at 760°C as shown for sample NoAlRx760 in Figure 41(a) with only small fragments of non aligned carbon nanotubes observed.

Precursors that decompose to form alumina have been shown to play a critical role in the synthesis of V-MWNTs by Fe catalysts supported on silicon wafers.[190,215,216] The incorporation of an Al precursor during catalyst synthesis results in a similar positive influence resulting in the production VMWNT arrays on lamellar supports as shown in Figure 40(a) and 2(b). The increase in both length and volume, shown by comparison of samples NoAlRx760 and Rx760, is significant since the only change is the incorporation of an Al precursor with the Fe and Co catalyst. The average V-MWNT length increased from 1 to 50 μm and the volume increased from one cm^3 to almost four cm^3, as can be seen in Figure 40(a). As observed on non-lamellar supports, alumina likely hinders the sintering of the catalyst particles responsible for growth of the carbon nanotubes, as has been shown by Mattevi *et al.*[215] and Kaneko *et al.*[216] Both groups showed reduced sintering of the iron by using alumina resulting in a narrower carbon nanotube diameter because of the narrower catalyst size distribution when compared to silica supported catalysts. This reduction in the rate of sintering is likely responsible for the longer growth of V-MWNTs in a shorter time frame than was achieved by other groups that previously synthesized vertically aligned carbon nanotubes between lamellar supports.[185,196,197,198,199]

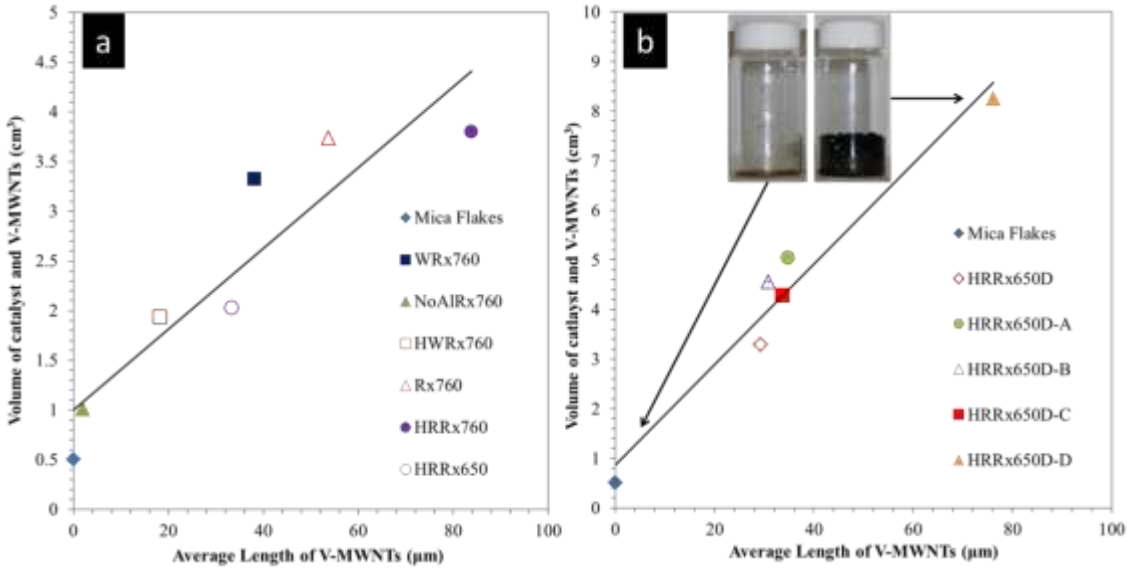

Figure 40 (a) Correlation between volume of catalyst and V-MWNTs and average length of V-MWNTs when only ethylene is used during the reaction step. (b) Correlation between volume of catalyst and V-MWNTs and average length of V-MWNTs when ethylene is diluted with nitrogen during the reaction step

Mattevi *et al.* showed the existence of Fe^{2+} and Fe^{3+} and their strong interaction with the surface oxygen atoms of the alumina support by using in-situ X-ray photoelectron spectroscopy and annealing under H_2 and Ar at 580°C.[215] This group found, however, that only metallic Fe existed on a silica surface, when annealed under the same conditions. Interface states formed between the Fe and surface oxygen atoms of the alumina were proposed to help reduce the surface mobility, which are not present when Fe is supported on silica. Because no interfacial states formed between Fe and silica, the Fe coalesces into large islands. It can, therefore, be concluded that the Al precursor is likely forming interface states with the Fe, which is reducing the sintering of Fe and promoting growth of the V-MWNTs. An Al precursor is therefore incorporated in all samples discussed hereafter.

The role of heating the catalyst and mica flakes during impregnation at 80°C in reflux for 24 hours was investigated by preparing a sample, HWRx760, in a similar

manner to literature reports.[196,197,199] Other studies report catalyst impregnation in lamellar supports at ambient temperatures,[185] with no clear rationale for either impregnation technique. Samples HWRx760, WRx760 and Rx760 serve to elucidate the role of heating solvent choice during wet impregnation of the catalyst within layers of mica flakes. An Al precursor was incorporated in each case.

Previous reports demonstrated growth of V-MWNT arrays between layers of lamellar clay supports of approximately 10 μm in nanotube length in half an hour,[185,196,197,198,199] while sample HWRx760 shows growth of 20 μm over the same period of time. As can be seen in Figure 40(a) for sample HWRx760, the volume expands to approximately two cm^3 post reaction. SEM and TEM results are shown in Figure S3 of the Appendix along with outer and inner diameters of the V-MWNTs. During preparation of sample HWRx760, the heating turned the catalyst solution from a transparent orange to a dark red color. The darker color of the heated solution could be due to the formation of insoluble iron hydroxide particulates, in agreement with literature observations.[217]

By maintaining the catalyst solution at ambient temperature the formation of the precipitate is avoided, with the resulting catalyst sample designated as WRx760. V-MWNT length significantly increased over the heated precursor impregnation sample, HWRx760, as can be seen in Figure 40(a). This result implies that insoluble iron hydroxide particulates hinder V-MWNT growth. SEM and TEM images can be seen in Figure S4 of the Appendix, along with inner and outer diameter measurements of the V-MWNTs.

To test the impact of the solvent during catalyst impregnation, isopropanol was used as a solvent in place of water, sample Rx760. Replacing isopropanol with water as a solvent yielded an increase in V-MWNT length as shown in Figure 41(b), and volume of material as shown in Figure 40(a). Measurements of the V-MWNTs from TEM images, such as Figure 41(c), indicate their average outer and inner diameters to be 19.2±6.9 nm and 6.7±2.3 nm, respectively, and with an average wall number of 18. The variance in growth resulting from the two different solvents during catalyst deposition may be due to (i) hindered amounts of iron hydroxide formation in isopropanol or (ii) isopropanol, having a lower surface tension than water, may have created a more uniform coating of catalyst upon evaporation of the solvent. The lower surface tension may have resulted in the catalyst being left behind as the evaporated whereas with water a higher surface tension will pull the catalyst particles to the remaining liquid as evaporation occurs. Isopropanol appears to be a superior catalyst deposition solvent, and as will be discussed in the following sections, further optimization of reaction conditions using this deposition technique results in V-MWNT lengths over 80 μm and a volume expansion of almost four cm^3.

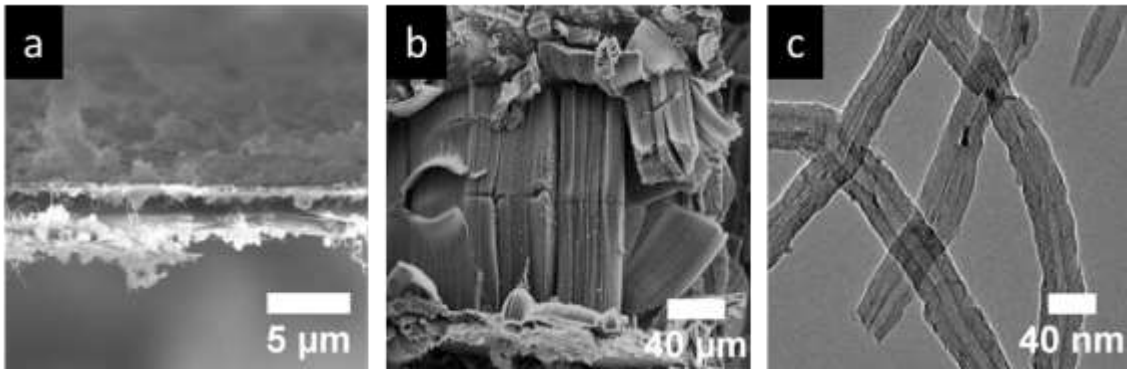

Figure 41 (a) SEM image of sample NoAlRx760 without incorporation of alumina, (b) SEM image of sample Rx760, incorporation of alumina, and (c) TEM image of sample Rx760.

During the reaction step when pure ethylene was flowed above 700°C, an orange-yellow colored gas was produced due to pyrolysis of ethylene. The quartz glass tube after reaction was coated with a black opaque layer of carbon. Similar observations have been reported during V-MWNT growth with ethylene in the literature.[203] It is possible this pyrolysis of ethylene is producing carbon that is coking and deactivating catalyst particles or possibly fusing layers of the mica.

To overcome the problem of fast coking or fusing layers of mica together, ethylene was diluted with nitrogen during the reaction step. The dilution of the ethylene resulted in a large increase in V-MWNTs volume and a decrease in diameter as shown in Figure 40(b), which will be discussed in later sections. This indicates there is more growth of V-MWNT arrays since the detrimental impact of high ethylene concentrations is minimized. Regardless of whether nitrogen was or was not used to dilute the ethylene during the reaction step, a linear relationship was found between the average length of the V-MWNTs and the volume of the samples post reaction as shown in Figure 40(b).

Role of Reduction Temperature

V-MWNTs with lengths over 80 μm were obtained for sample HRRx760 by increasing the reduction temperature to 650°C. Inner and outer diameters of the V-MWNTs of sample HRRx760 were 8.3±1.9 nm and 32±3.5 nm respectively, resulting in an average number of 36 walls per nanotube. SEM and TEM images of sample HRRx760 can be seen in the appendix, Figure S5. A reasonable explanation for the increased length of the V-MWNTs is that the Fe and Co have been reduced to a greater extent at 650°C, as shown by the TPR in Figure 42. When the Fe and Co is not fully

reduced, the ethylene serves as the reducing agent, potentially at the expense of excessive carbon deposition, that may deactivate the catalyst for V-MWNTs growth.

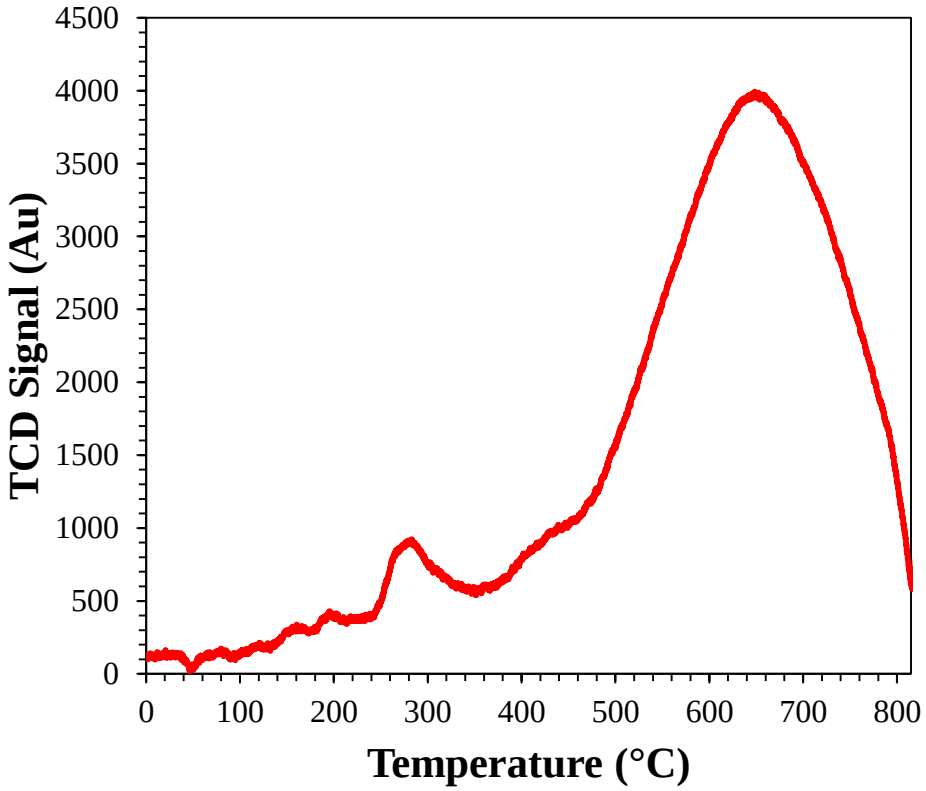

Figure 42 Temperature programmed reduction of catalyst used for samples RX760, HRRX760, HRRX650, and HRRX650D.

Consistent with Brown *et al.* the major reduction of bulk Fe and Co is around 650°C, see Figure 42.[218] The peak at 300°C shown on Figure 42 was observed by this group for both Fe and Co. Brown *et al.* attributed this peak to well dispersed Fe and Co on the alumina. The maximum hydrogen uptake was found to be greater at lower temperatures as the Co to Fe ratio increased, which is observed in the TPR profile shown in Figure S6 of the Appendix. Mossbauer spectroscopy revealed as the Co to Fe ratio increased Fe and Co spinels formed because of the depletion of Fe_2O_3 by Co.[219]

The role of the Co to Fe ratio on V-MWNT growth will be discussed in the following sections.

Growth of few walled V-MWNTs

Due to the assumption that excessive pyrolysis occurs when flowing pure ethylene, the ethylene was diluted with nitrogen and the reaction temperature lowered for this research in an attempt to decrease the diameter of the V-MWNTs and to produce few-walled V-MWNTs, defined as two to five layers of side walls and diameters between three to eight nm.[220] To study the effect of diluting the ethylene and lowering the reaction temperatures both cases were studied, using increased reduction temperature of 650°C instead of 560°C. Sample HRRx650 is the result of lowering the reaction temperature, which resulted in no observable pyrolysis or oil coating the glass reactor vessel during the reaction step. Based on SEM and TEM images Figure S7 of the Appendix, V-MWNT lengths up to 30 μm were produced with average outer and inner diameters of 6.9±2.4 nm and 3.7±1.3 nm, respectively. From this information, the average number of V-MWNT walls was determined to be five, with some double and triple walled V-MWNTs present.

Carbon nanotube yield can be increased by changing the partial pressure of the carbon source.[221] To increase the yield of V-MWNTs, the partial pressure of ethylene was modified while keeping all other parameters the same as for sample HRRx650. To change the partial pressure of ethylene, an equal volume of nitrogen and ethylene were flown, sample HRRx650D. This ratio of ethylene to nitrogen results in an increase in volume expansion with the same catalyst, Figure 40 (a & b). The V-MWNTs produced are up to 30 μm in length as shown in Figure 43 (a).

An explanation for the increase in volume of the collected material is the change in partial pressure, which decreased the amount of catalyst particles that were deactivated or inaccessible due to the excessive ethylene partial pressures. TEM results for sample HRRx650D are similar to results shown for sample HRRx650. Sample HRRx650 shows an average V-MWNT outer diameter of 6.8±2.4 nm and inner diameter of 3.9±2.4 nm, and an average of 4 walls with some double and triple walls being present as shown in Figure 43 (b). The use of the proper reduction temperature allows for a lower reaction temperature to be used and still grow longer V-MWNTs with few walls. Dilution of the ethylene during the reaction step increased the yield of V-MWNTs.

Role of Catalyst Ratios and Temperatures

The role of the Co to Fe ratio was modified in an attempt to increase the length of the V-MWNTs without increasing the V-MWNTs' diameters, which is usually the case when increasing temperature.[211,212] The synergistic effect of Fe and Co has been shown to give a higher yield of carbon nanotubes than either Fe or Co alone.[222] Increasing the Co to Fe ratio for sample HRRx650D-A, resulted in an increase in V-MWNT length and volume compared to using a lower Co to Fe ratio as used for sample HRRx650D. TEM results show that the average diameter and number of walls for sample HRRx650D-A are comparable to HRRx650D. SEM and TEM images for sample HRRx650D-A are in Figure S8 of the Appendix. Two possible reasons for the increased length and volume expansion of material are, (i), the Co helps to reduce the Fe further[217] and, (ii) the formation of Fe and Co spinels may hinder particle sintering.[218]

Excessive amounts of the Al precursor could possibly coat the Fe and Co and render them inactive. The role of Al precursor concentration was explored by decreasing the concentration by half as shown for sample HRRx650D-B. With the reaction conditions kept the same as for sample HRRx650D, there was an increase in the volume of V-MWNTs and the mica. TEM results indicate that the average diameters and the number of walls were similar to samples HRRx650D-A and HRRx650D. SEM and TEM images can be found in the Figure S9 of the Appendix. By decreasing the amount of Al precursor, more Fe and Co may be exposed for growing V-MWNTs, which is a likely reason for the increased volume expansion.

While improvements in the volume expansion and length of the V-MWNTs are observed by either increasing the amount of Co or decreasing the amount of Al in the sample, further improvements are not obtained by combining both strategies. HRRx650D-C was prepared with both a higher Co and lower Al loading. This resulted in an effect similar to both samples HRRx650D-B and HRRx650D-C, in which neither a significant volume expansion or length change of the V-MWNTs occurred. TEM results for sample HRRx650D-C show no significant change in average diameter or number of walls. The appendix has SEM and TEM images of sample HRRx650D-C as shown by Figure S10.

The reaction temperature has a significant influence on the final nanotube length and diameter. This is illustrated by sample HRRx650D-D, which was prepared using the same catalyst as in sample HRRx650D-C at a higher reaction temperature of 700°C. The results of these changes are quite dramatic showing a significant increase in the length of the V-MWNTs, over 80 μm, and a significant volume expansion in material as

shown in Figure 43(c). The V-MWNTs grew at a rate of 160 μm/h, which is eight times faster than previously reported.[185,196,197,198,199] In addition to the length and significant volume expansion, the diameter of the V-MWNTs doubled to an average outer diameter of 11.5±3.5 nm, average inner diameter of 5.6±1.8 nm, and average wall number of 9, as shown in Figure 43(d). Increased nanotube diameters as a function of temperature have also been reported in the literature using vermiculite clay supports.[199] The increase in growth of the V-MWNT arrays results in the separation of layers within the mica sheets, as can be seen in Figure 43(c). This finding is in agreement with those reported by Zhang *et al.* who observed unequal rates of nanotube growth along the mica surfaces resulting in fracturing of the mica sheets.[196]

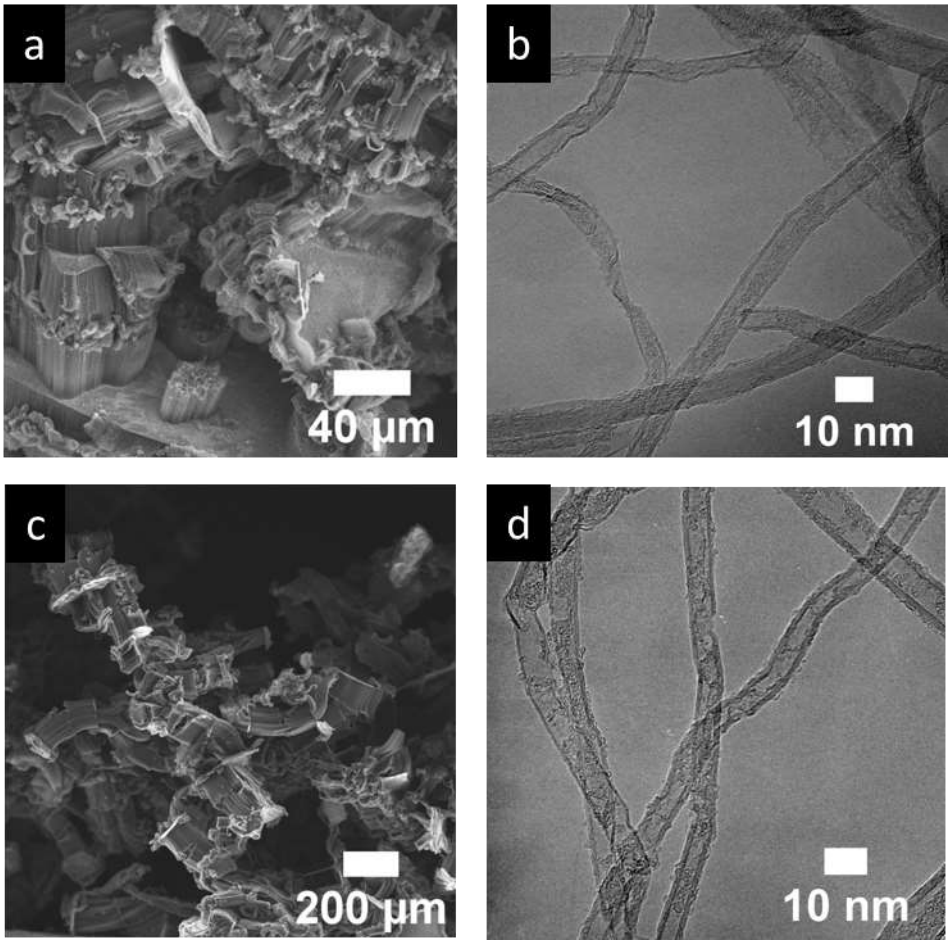

Figure 43 (a) SEM image of sample HRRx650D, decrease in partial pressure of ethylene and reduction temperature of 650°C (b) TEM image of sample HRRx650D, (c) SEM image of sample HRRx650D-D, reaction temperature of 700°C and catalyst precursor of Al decreased and Co increased, and (d) TEM image of sample HRRx650D-D.

Conclusions

The synthesis of V-MWNTs in a scalable fashion over lamellar supports at lengths greater than those reported in the literature is achieved. This is accomplished through the incorporation of Co and Al within the Fe catalyst to promote metal reduction and reduce sintering. Few walled V-MWNTs with lengths of up to 40 μm are synthesized via this approach. The incorporation of Al enables increased growth temperatures, resulting in V-MWNTs over 80 μm in length. The height of the expanded mica flakes post reaction shows a linear correlation with the average MWNT length. Modifications in precursor concentration, catalyst deposition method, and reaction temperature allow for control of both nanotube length and diameter in lamellar supports.

Chapter 7: Method for Determination of Catalytic Active Sites for Bifunctional Catalysts

Introduction

Bifunctional Catalysts

Bifunctional catalysts have found use in a variety of fields and industries due to their ability to open the doorway for the production of new products. One common type of bifunctional catalyst is a metal catalyst supported on an oxide or solid-acid catalyst. These types of bifunctional catalysts create a synergistic benefit because of the presence of two different catalysts each with their own set of abilities to react with molecules. Molecules can react with the two catalysts in a variety of ways one way is the molecule reacts with one catalyst and then the other[223], another way is the two catalysts work together when reacting with the molecule,[247,248,224,225,226] and lastly one of the two catalysts creates active sites on the other.[227,228] Since there are many different ways bifunctional catalysts can provide this synergy there has been a large effort to determine which way the molecule reacts with the two catalysts. To do this it is important to understand how each catalyst works alone.

The most important metals for catalysis are transition metals, specifically, from groups VIII and I-B of the periodic table. Catalytic activity for metals are controlled by electronic, geometric, or an interplay of electronic and geometric effects.[229],[230],[231],[232] There has been great debate as to whether a reactions activity is controlled by geometric or electronic effects for reactions.[233,234,235,236] The electronic effect is the role of the bond strength and can be explained by the d-band model.[230,231,232] The d-band model

takes into account the interaction between the s and d states of the transition metal and the adsorbates valence states. The coupling of the adsorbate to the metal s states is approximately the same for each metal, but differs for the coupling of the adsorbate to the metal d states. Therefore, transition metals reactivity can be determined by looking at the density of states and locating the position of the center of the d-band relative to the Fermi level. As the d-band center approaches the Fermi level the number of antibonding states above the Fermi level increase which increases the reactivity of the metal due to the antibonding states becoming depopulated. The geometric effect is the arrangement of the surface atoms near the adsorption site. Important contributions to the geometric effect are the ensemble effect which is the required number of adjacent surface atoms required to form an adsorption site, the template effect where a molecule requires a adsorption site of a certain shape and size, and the coordination effect where a reactant or reactants requires a minimum number of adjacent adsorption sites.[229,237] Norskov has shown how alloying of metals, different planes, and other factors can change the electronic binding energy of metals by changing the location of the d-band center.[232] Showing there can be interplay of geometric and electronic effects which control the reactivity of metal catalyst.

Oxides offer a variety of different active sites.[238] The metal cations act as Lewis acids since they can accept electrons, with metal cations of lower oxidation states typically being more reactive. Oxygen ions behave as Bronsted bases because they can accept protons. Due to the definition of Lewis and Bronsted acids and bases the oxygen ion can also be considered a Lewis base. With the presence of both acid and bases acid-base chemistry can be performed on the surface of oxides.[239]

Much debate exists in the literature as to the location of the catalytic active site for bifunctional catalysts. Catalytic active sites are typically thought to be at the metal oxide interface or on the oxide created by hydrogen spillover from the metal. The interface of the metal oxide is one type of catalytic active site because the metal catalyst and oxide catalyst can work together creating a synergistic effect. The metal oxide interface can be changed if there is a strong metal support interaction (SMSI) where a thin metal-oxide coating begins to form over the surface of the metal[224,240,241,242], Figure 44. Hydrogen spillover can create surface defects, subsurface defects, or Bronsted acids or bases on the oxide which serve as catalytic active sites,[243,244,245,246] Figure 44. Surface and subsurface defects are missing oxygen anions or metal cations, usually missing oxygen anions. Due to the importance of knowing where the catalytic active site is there is a great effort to determine the location of the catalytic active site to maximize production. In this quest to determine the active site conflicting viewpoints arise as to the location of the catalytic active site.

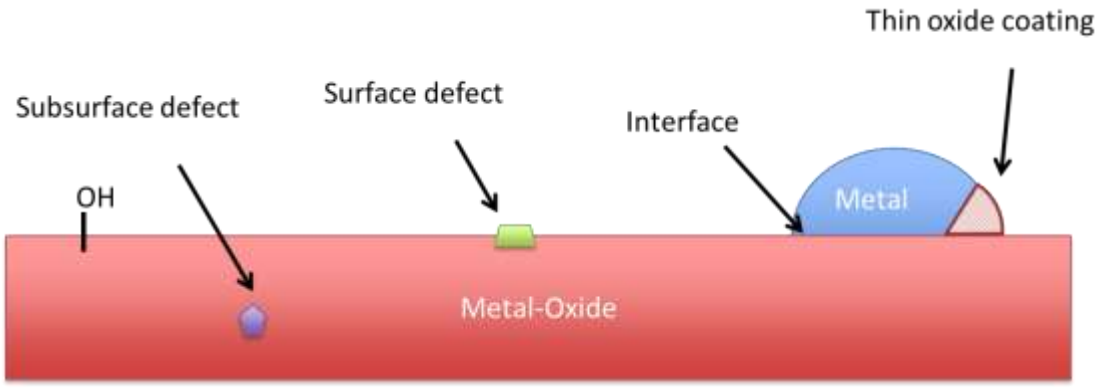

Figure 44: Type of catalytic active sites for bifunctional catalysts of metals and oxides.

One example of debate about the location of the catalytic active site is the Fischer-Tropsch reaction where carbon monoxide and hydrogen are converted to liquid

hydrocarbons. Several groups have proposed carbon monoxide bonds at the metal oxide interface with the carbon end of the molecule bonded to the metal while the oxygen interacts with exposed metal cations of the oxide creating a Lewis acid-base interaction[247,248]. Others groups have suggested the metal serves to facilitate hydrogen spillover onto the oxide and the intermediate formed on the metal will spillover onto the oxide, where the intermediate undergoes hydrogenation to methane more rapidly than on the metal[249,250]. The location of the active site has been studied for metals supported on oxides for furfural hydrogenation,[227] catalytic reforming of n-hexane,[226] enhanced CO oxidation,[225] and selective hydrogenation of C=O.[228] With the large number of studies to determine the location of the active site several experimental methods have been developed to find the active site.

Methods to Determine the Catalytic Active Site

A variety of methods have been applied to determine the active sites responsible for the synergistic benefit with bifunctional catalyst. One method is to change the particle size of the metal supported on the oxide which changes the perimeter of the metal oxide interface[224,247]. As the perimeter is increased or decreased then the rate of reaction should increase or decrease, respectively. If the rate reaction does not change with change in metal oxide perimeter then the active site is considered to be located on the oxide. However, this method has its complications which can cause difficulty in ascertaining the location of the active site. The metal oxide interface can change solely if there is SMSI where the metal becomes encapsulated by the oxide.[224,240,241,242] Additionally, density functional theory (DFT) calculations have shown the distance

which spilled over hydrogen from the metal travels on the oxide varies depending on the oxide[259]. With smaller particles more hydrogen will spillover onto the oxide creating active sites. A second method is to use reaction kinetics; however, there is a limit to this approach because as the kinetics become more complex the difficulty increases to ascertain the location of the active site. A third method is to use spectroscopy however, this technique suffers from limitations of equipment and what is observed on the surface of the catalyst may be a spectator and not the intermediate in the reaction leading to the wrong conclusion. There is a still a need for improving how the location of the active site is determined.

A New Method to Determine the Catalytic Active Site

In this work carbon nanotubes are used to create a novel catalyst to answer the question of where the catalytic active site is when using a metal catalyst supported on a oxide catalyst. This is accomplished by separating metal and oxide catalysts on carbon nanotubes breaking the metal oxide interface that is normally formed when the metal is supported on the oxide. By separating the two catalysts on carbon nanotubes the only catalytic active sites on the oxide can be formed allowing for one to determine if the catalytic active site is on the oxide or at the metal oxide interface. By comparing results of the catalysts with the metal and oxide catalysts separate and together and seeing which reactions occur and which do not the active site can be found. With the metal and oxide catalysts separated on the carbon nanotubes reactions which do not take place occur at the metal oxide interface, while reactions which do occur take place on the metal or oxide. To determine if the reaction takes place on the metal or oxide the metal

alone can be tested. A critical part to the success of this approach is two abilities of carbon nanotubes.

The first set of abilities is the one dimensional nature of carbon nanotubes, the rod like structure, the ability to grow them in a vertical orientation parallel to one another, and to different lengths.[251],[252],[253],[254],[255] The second ability is carbon nanotubes can facilitate hydrogen spillover.[73,272,274,276] Using the first set of abilities carbon nanotubes can be grown vertically allowing for selective deposition of nanoparticles along the length of the carbon nanotube.[256,257,258] It has been shown that by partially coating the carbon nanotubes in polymer one end of the carbon nanotubes is exposed and platinum nanocubes are deposited on this end of the carbon nanotubes. After which the exposed end is coated in a polymer with a different solubility than the first and the first polymer washed away. Platinum nanospheres were then deposited on this now exposed end and the second polymer removed, creating carbon nanotubes with a portion of the length with platinum nanospheres and the other platinum nanocubes. This can be taken advantage of to deposit along one half of the length of the carbon nanotube a metal catalyst and the other half an oxide catalyst. Therefore, the two catalysts are on the same carbon nanotube which can facilitate hydrogen spillover.

The facilitation of hydrogen spillover on carbon nanotubes is a second critical ability as it serves as a bridge between the metal and oxide for the creation of catalytic active sites on the oxide. The metal catalyst can dissociate hydrogen and the dissociated hydrogen can then travel along the carbon nanotube to the oxide to create catalytic active sites on the oxide. Carbon nanotubes have been shown to be capable of transporting hydrogen along the surface and are currently studied for use as hydrogen

storage materials.[73,272,274,276] The process for hydrogen spillover with a metal supported on a carbon nanotube is as follows: (1) hydrogen is chemisorbed on the metal and dissociated (2) dissociated hydrogen spills over from the metal to the carbon support and (3) hydrogen diffuses over the carbon surface to the oxide.

Hydrogen Spillover Mechanism

Before discussing the hydrogen spillover mechanism on carbon the hydrogen spillover mechanism on oxides will be discussed. Since the discovery of hydrogen spillover there has been significant interest in understanding the mechanism and is covered in several review articles.[259,260,261] The first discovery of hydrogen spillover was by Khoobiar who found Pt/A_2O_3 was capable of reducing WO_3 at a temperature below which WO_3 reduced[262]. This was then followed up by Boudart *et al.* who found a significant uptake when Pt was supported on the WO_3 which was attributed to the hydrogen spilling over from the Pt to the WO_3. In addition, it was found the rate of hydrogen spillover increases with the addition of water and was reduced when water was replaced by molecules of higher proton affinity.[263] With the apparent role of water the hydrogen spillover mechanism proposed was the dissociated hydrogen on the metal would move to the WO_3 by using the electron to reduce the tungsten cation from W^{6+} to W^{5+} and the proton of the hydrogen atom would create a hydronium ion with the water, Figure 45. The proton and electron would then move across the WO_3 surface with the electron reducing tungsten cations and proton hoping to the next water molecule, thereby maintaining charge balance.

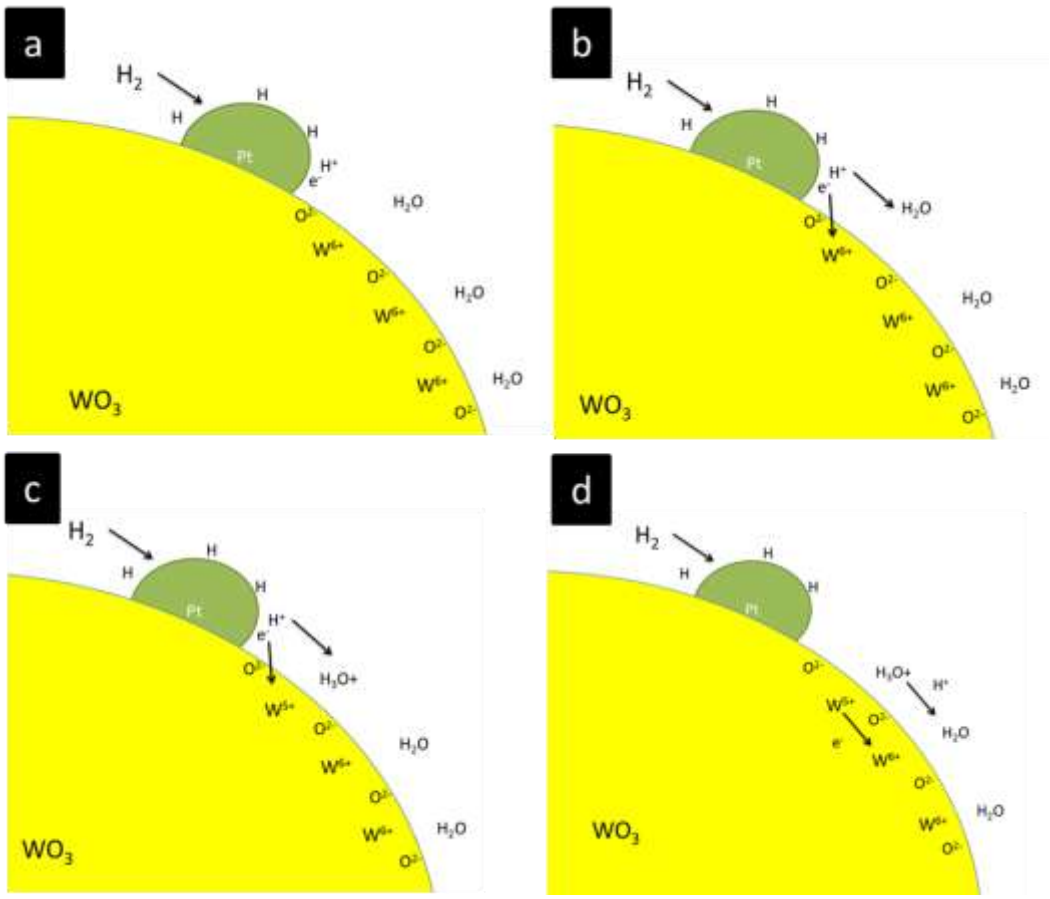

Figure 45: (a) Hydrogen dissociated on platinum. (b) Electron reduces W6+ to W5+ and the proton moves to the water. (c) Charge balance is maintained. (d) Process is repeated allowing for the hydrogen to diffuse across the WO3 surface.

This was followed up with DFT calculations which found for platinum on molybdenum oxide the hydrogen migrates from the metal to the oxide as a proton and electron[264]. A hydrogen atom on the platinum gains 0.05-0.15 electrons from the Pt-5d bands and the terminal oxygen on MoO_3 are 0.8-1.2 electrons negatively charged. Therefore, hydrogen atoms are unable to migrate onto the MoO_3 due to repulsive interactions. However, if the H atoms electron is used to reduce the Mo^{6+} to Mo^{5+} then the hydrogen proton can migrate to the terminal oxygen and this creates an attractive interaction between the hydrogen proton and reduced molybdenum cation, Figure 46.

This process can be repeated allowing the hydrogen to migrate over the surface of MoO_3. Both studies state the hydrogen atom moves as a proton and electron the only difference is how the proton moves over the surface. In one case the proton moves using water and the other the proton moves using the terminal oxygens of the oxide. Xi *et al.* performed a DFT study with platinum on WO_3 found hydrogen migration occurs by reducing the tungsten cation and moving to the terminal oxygen, but found water can serve as a bridge for the hydrogen proton to hop to the next terminal oxygen[265]. Therefore, the hydrogen proton may be using water and terminal oxygens to travel across the surface.

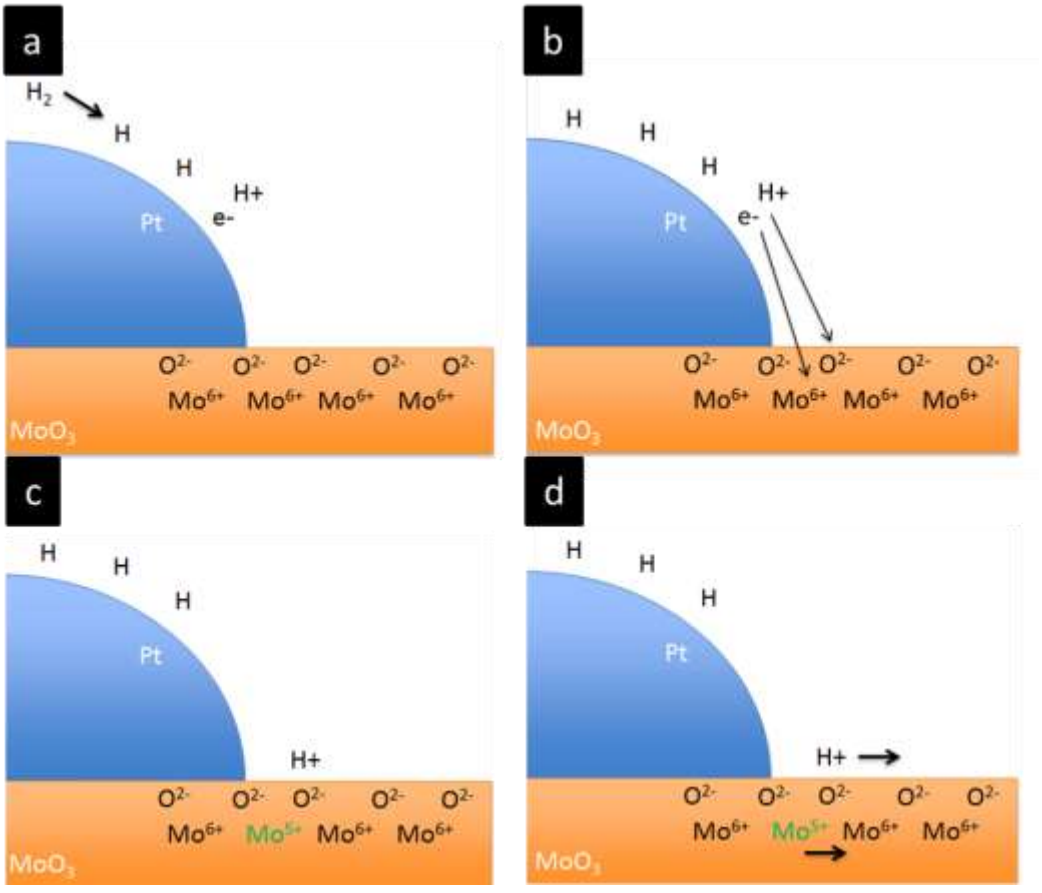

Figure 46: (a) Hydrogen dissociated on platinum. (b) Electron reduces Mo6+ to Mo5+ and the proton moves to the water. (c) Charge balance is maintained. (d) Process is repeated allowing for the hydrogen to diffuse across the MoO3 surface.

Hydrogen spillover has been shown to occur on reducible oxides. Examples of reducible oxides are: TiO_2, CeO_2, MoO_3, WO_3, V_2O_5, and Fe_2O_3. However, DFT calculations have shown hydrogen spillover cannot occur on a non-reducible oxide support[266]. Examples of non-reducible oxides are: Al_2O_3, SiO_2, and MgO. This is due to the electron of the hydrogen atom being unable to reduce the metal cation and stopping the hydrogen proton from migrating to a water molecule or terminal oxygen of the oxide, Figure 47. As was already discussed there is a repulsive interaction if the hydrogen atom tries to move to the oxide due to the electrons it gains from the platinum metal and the terminal oxygens of the oxide.

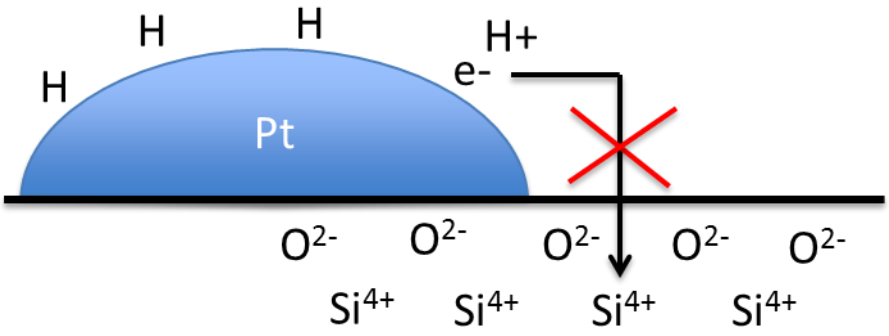

Figure 47: Electron of hydrogen unable to reduce the silicon cation which stops hydrogen spillover.

Hydrogen spillover can occur in the presence of non-reducible supports if there are carbon contaminants on the non-reducible oxide which act as a bridge for hydrogen to spill over from the metal[266,267]. While a large amount of evidence suggests hydrogen spillover does not occur on non-reducible supports a recent report by Somorjai *et al.* showed a substantial increase in the reaction rate when platinum and cobalt particles are together supported on silica for CO_2 methanation. However, when mixing platinum

supported on silica with cobalt supported on silica a roughly 50% drop in apparent activation energy is observed which is attributed to hydrogen spillover on silica.[268] The authors counter the argument that the spillover could be done on carbon deposits since the drop in activation energies are above what would be expected for a diffusion limited process. Therefore, while most studies suggest non-reducible supports cannot facilitate hydrogen spillover there is obviously a need for further investigation.

Since the discovery of the possibility for using carbon nanotubes as hydrogen storage materials there has been a great effort to understand the hydrogen spillover mechanism on carbon nanotubes and other carbon materials.[269,270,271,272,273,274,275] Hydrogen spillover from the metal to the carbon support has been proposed to occur by either physisorption[269,270,271] or chemisorption[272,273,274,275]. Hydrogen spillover by physisorption occurs with the hydrogen atom just above the carbon surface and the hydrogen atom migrating over the carbon surface, but these physisorbed H atoms can recombine to form molecular hydrogen and leave the surface[270]. Chemisorption occurs by C-H bond formation and on carbon nanotubes this occurs by breaking one of the carbon double bonds changing the carbon atoms hybridization from sp^2 to sp^3, this breaking of bonds and formation of C-H bonds is how the hydrogen diffuses across the carbon surface[272]. Several studies have found the migration of hydrogen from the metal to carbon and diffusion over the carbon surface occurs at a low rate, by solely C-H bond formation, but can be significantly enhanced by the presence of oxygen functional groups on the surface of the carbon[276,277] or the presence of water[278,279,280]. With strong evidence that hydrogen spillover can occur on carbon nanotubes a reactant must be

selected which has been previously shown to interact at the metal oxide interface or on catalytic active sites created on the oxide.

Probe Reaction - Furfural

Furfurals are a major component produced during pyrolysis of biomass[281,282]. Furfural itself can be upgraded to more valuable molecules which are typically produced using fossil fuels.[283,284,285,286] Therefore, the catalytic upgrading of furfural has gained much attention as an renewable and environmentally friendly replacement for fossil fuels. Furfural can be upgraded to a variety of molecules with different uses. Hydrogenation of the aldehyde group of furfural produces furfuryl alcohol which can be used for synthesis of solvent and resins for ceramic processing.[283] Hydrogenolysis of furfural yields 2-methylfuran which can be used to produce fine chemicals, perfumes, and medicines.[284,285] Recently it has been shown cyclopentanone can be produced from furfural.[286] Cylcopentanone can be used for rubber and pharmaceutical applications or can undergo self-aldol condensation and further hydrodeoxygenation to form hydrocarbons in the jet fuel range.[287,288,289] With the wide range of applications there has been a large effort to study the catalytic upgrading and determine which catalytic active sites are responsible for producing the desired product. The end goal is more of the desired active sites can be made to maximize the yield of the desired product.

Work has been done with metals supported on non-reducible and reducible oxide supports. Copper, palladium, and nickel supported on silica each can be used to hydrodeoxygenate furfural and give different product distributions.[290,291] This difference in product distributions with different metals was attributed to the type of surface

intermediate that each metal is able to stabilize and the strength of the interaction of the furan ring with the metal surface. Studies have also been conducted with the combinations of metals Pd-Cu on silica[292] and Ni-Fe on silica.[293] With reducible oxides platinum supported on titania furfural hydrogenation to furufuryl alcohol can be favored due to active sites created on the titania by spillover of hydrogen from the platinum.[227] On the reducible oxide titania there has been shown to be a favor for hydrogenation of furfural to furfuryl aclochol with $Pt/TiO_{2.}$ This selectivity to furfuryl alcohol over furan is attributed to the hydrogen dissociated on platinum spilling over onto the titania to create active sites on the titania. These active sites allow for the carbonyl oxygen atom of the furfural intermediate to bond to the titania and be hydrogenated producing furfuryl aclochol. With the large number of studies available and differences in selectivity seen with metals and metals supported on oxides furfural is an acceptable choice for testing this novel catalyst.

By growing VMWNTs and depositing palladium and titania on opposite ends of the VMWNTs a catalyst is tested as a way to determine the location of active sites for bifunctional catalysts. With the metal and oxide catalysts separated on VMWNTs reactions occurring at the metal oxide interface will not occur, but reactions requiring the active sites created from hydrogen spillover onto the oxide can occur. Therefore, with the ability to remove one type of active site it can be determined if the catalytic active site for specific reactions using bifunctional catalysts occurs at the metal oxide interface or on active sites created on the oxide from hydrogen spillover.

Experimental Details

Valeria Herrera Araque performed the reactions with the furfural in the flow reactor.

Chemicals used for multi-walled carbon nanotube growth were isopropanol, iron nitrate nonahydrate, cobalt nitrate hexahydrate, aluminum nitrate nonahydrate, and 2-hydroxyethyl cellulose (M_w ~ 1,300,000). All of the chemicals used were purchased from Sigma Aldrich. Silicon wafers of n-type were purchased from Silicon were purchased from Wafer World, Inc. (SKU: 1186). 18 MΩ water was obtained from an in house filtration system and used in this study.

Vertical multi-walled carbon nanotubes (VMWNTs) were grown by spin coating a catalyst solution on silicon wafers. First silicon wafers were cut using a diamond scribe into 20 mm x 20 mm square pieces. A catalyst solution was made containing 1.11 wt% iron nitrate nonahydrate, 0.39 wt% cobalt nitrate hexahydrate, 1.23 wt% aluminum nitrate nonahydrate, and 0.74 wt% 2-hydroxyethyl cellulose all with respect to water. The solution was spin coated on the silicon wafers by putting one millimeter of solution on the silicon wafer and spin coating using two stages which followed one another. The silicon wafer was first spin coated at 500 rpm for 10 seconds and then at 2000 rpm for 30 seconds. The silicon wafers with the solution were then allowed to dry overnight and calcined the next day.

The silicon wafer with spin coated catalyst solution was calcined the next day by placing the sample in a one inch quartz diameter tube and connecting one end to an inlet and the other an outlet airline. The one inch quartz diameter tube was placed in a furnace oriented horizontally. With a continuous flow of 150 sccm of air through the quartz tube the furnace was ramped to 450°C at 10°C per minute and then held at 450°C

for two hours. After heating at 450°C the reactor was allowed to cool to room temperature and the sample removed from the quartz tube.

For the growth of vertically aligned MWNTs the silicon wafer with catalyst was placed in a one inch quartz diameter tube and connected to inlet and outlet gas lines. The quartz tube was placed in a furnace oriented horizontally for heating. With a flow of 300 sccm of hydrogen passing through the quartz tube the furnace was heated to 650°C at a rate of 10°C per minute and then held at 650°C for 30 minutes. The flow of hydrogen was stopped and a flow of 300 sccm of argon was flowed through the quartz tube and the quartz tube ramped to a reaction temperature of 675°C or 700°C at a rate of 10°C per minute. Once the temperature stabilized at the desired temperature, the flow of argon was changed to 200 sccm and flowed with ethylene at 200 sccm for 30 seconds, 1 minute, 5 minutes, or 20 minutes, depending on the desired length of VMWNTs. After the reaction the flow of ethylene was stopped and argon continued to flow through the quartz tube as the temperature decreased to room temperature.

To facilitate the removal of the VMWNTs from the silicon wafer the sample was heated in air to help weaken the interaction between the VMWNTs and catalyst particles on the silicon wafer. The sample was loaded into an inch diameter quartz tube and the quartz tube connected to inlet and outlet airlines. Next the quartz tube was loaded into a furnace oriented horizontally. Air was flowed through the quartz tube at 150 sccm while the furnace was heated to 480°C at 10°C per minute and then held at 480°C for two hours. After this step the sample was removed from the quartz tube once the temperature of the furnace reached room temperature.

Physical vapor deposition of palladium and titanium onto VMWNTs was completed by using a JEOL vacuum evaporator type JEE-4C. To evaporate metal onto the VMWNTs the VMWNTs were placed in the vacuum evaporator sample area. Next a tungsten wire, 0.030 inches, was connected to two electrodes which held the tungsten wire 3.8 cm above the sample. The tungsten wire was wrapped either titanium, 0.020" inches, or palladium wire, 0.010. When evaporating titanium 8 cm of titanium wire was wrapped around the tungsten wire and when using palladium 4 cm was used. During each evaporation step a silicon wafer was placed in the chamber to determine how much titanium or palladium was deposited on the VMWNTs. Titanium was first evaporated on the VMWNTs by heating the tungsten wire wrapped with titanium wire up to 25 amps. After evaporation of the titanium the side of the VMWNTs with titanium was attached to carbon tape, with an adhesive layer, to remove the VMWNTs from the silicon wafer. Following this the carbon tape with VMWNTs was placed back into the vacuum evaporator sample area with the end of the VMWNTs without titanium face up. Palladium was then evaporated by heating the tungsten wire wrapped with palladium wire up to 20 amps. After evaporation of the palladium onto the VMWNTs on the carbon tape the VMWNTs on carbon tape were removed from the vacuum evaporator and the edges of the VMWNTs on the carbon tape were cut off using a razor blade. This removal of the edges was performed to ensure that any palladium which came into contact with titanium was removed. Next the VMWNTs on carbon tape were placed in a petri dish filled with isopropanol and soaked for one hour to solubilize the acrylic adhesive holding the VMWNTs to the carbon tape. After soaking for one hour the carbon tape was shaken to help dislodge the VMWNTs from the carbon tape. The

VMWNTs were then recovered from the isopropanol by filtering with vacuum filtration using and a Whatman 1 filter. By measuring the thickness of metal deposited on the silicon wafers the weight percent of metal deposited on the VMWNTs was calculated and measuring the amount of VMWNTs grown on a silicon wafer which yielded 0.018 mg/cm^2. Three weight percent of palladium was deposited on the VMWNTs and 2 weight percent of titania deposited on the VMWNTs. Exposure of the titanium to air was responsible for producing titania.

Reactions with the VMWNTs with palladium on one end and titania on the other were performed using a flow reactor connected to a Hewlett Packard 6890 GC/ FID. Ten milligrams of catalyst were mixed with 190 mg of glass beads and placed into a ¼" diameter quartz tube. The catalyst and glass beads were held in place in the quartz tube by packing quartz wool around the catalyst and glass beads. The quartz tube was placed in a furnace oriented vertically and connected to an inlet gas line at the top and an outlet gas line at the bottom. The catalyst was reduced by flowing 50 sccm of hydrogen through the quartz tube and heating the furnace up to 400°C at 5°C/minute and then holding at 400°C for four hours. After reduction the hydrogen flow rate was set at 20 sccm of hydrogen for the reaction step. Furfural was introduced using a syringe pump at a rate of 0.1 mL/h and carried by the hydrogen flowing at 20 sccm. The gases exiting the reactor passed through a sample loop which is used to inject a sample of the gas into the GC-FID for analysis.

Scanning electron microscopy of the catalyst was performed using a Zeis Neon 40 EsB scanning electron microscope operating at an accelerating voltage of 5 kV for imaging and 10 kV when performing energy-dispersive x-ray spectroscopy.

Transmission electron microscopy was performed by using a JEOL 200 FX equipped with a LaB_6 filament and operating at 200 kV. Temperature programmed reduction (TPR) was performed using the same procedure and apparatus as in Chapter 7, except 30 mg of catalyst was used.

Results and Discussion

Vertical Multi-Walled Carbon Nanotube Growth

VMWNTs were grown with different heights and diameters depending on the temperature of the reaction. Different lengths of VMWNTs with a constant diameter can be grown by changing the length of the reaction time. This flexibility offers potential to maximize hydrogen spillover as diffusion of the hydrogen may become a rate limiting step if the dissociated hydrogen has to travel over the length of the carbon nanotube to reach the oxide. Reports have also suggested hydrogen spillover may be dependent on the diameter of the VMWNTs[294]. VMWNTs can be grown between five and one hundred microns depending on the temperature or reaction time, Figure 48.

The diameter of the VMWNTs can be controlled by the reaction temperature due to higher temperatures creating larger particles which in turns creates larger diameter carbon nanotubes[295]. The average diameter of the VMWNTs grown at 650°C, 665°C, 675°C, and 700°C were 7.9 nm, 8.7 nm, 10.3nm, and 12 nm, respectively. VMWNTs grown at 650°C had an average of five walls, while VMWNTs grown at 700°C had an average of nine walls. Diameters and numbers of walls were measured from TEM images. The flexibility to grow VMWNTs of different diameters and lengths offers the ability to maximize hydrogen spillover from the metal to the oxide for the creation of catalytic active sites on the oxide.

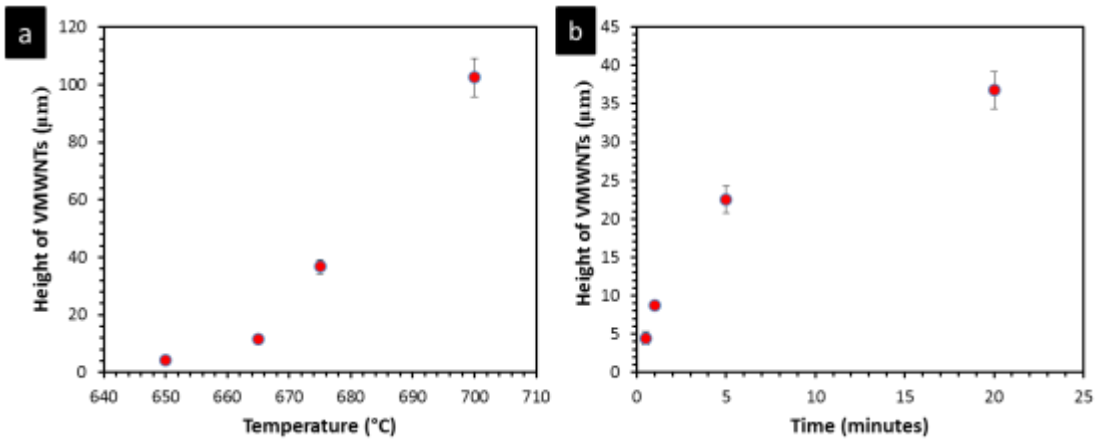

Figure 48: VMWNTs height dependence on the (a) reaction temperature and (b) reaction time.

Deposition of Palladium and Titania on VMWNTs

Palladium and titania was deposited on VMWNTs and separated by using metal evaporation. To ensure separation of the palladium and titania SEM and EDS were used for characterization of the catalyst. As can be seen in the SEM image, Figure 49, there is a coating of palladium on the top portion of the VMWNTs and a titania coating on the bottom portion of the VMWNTs.

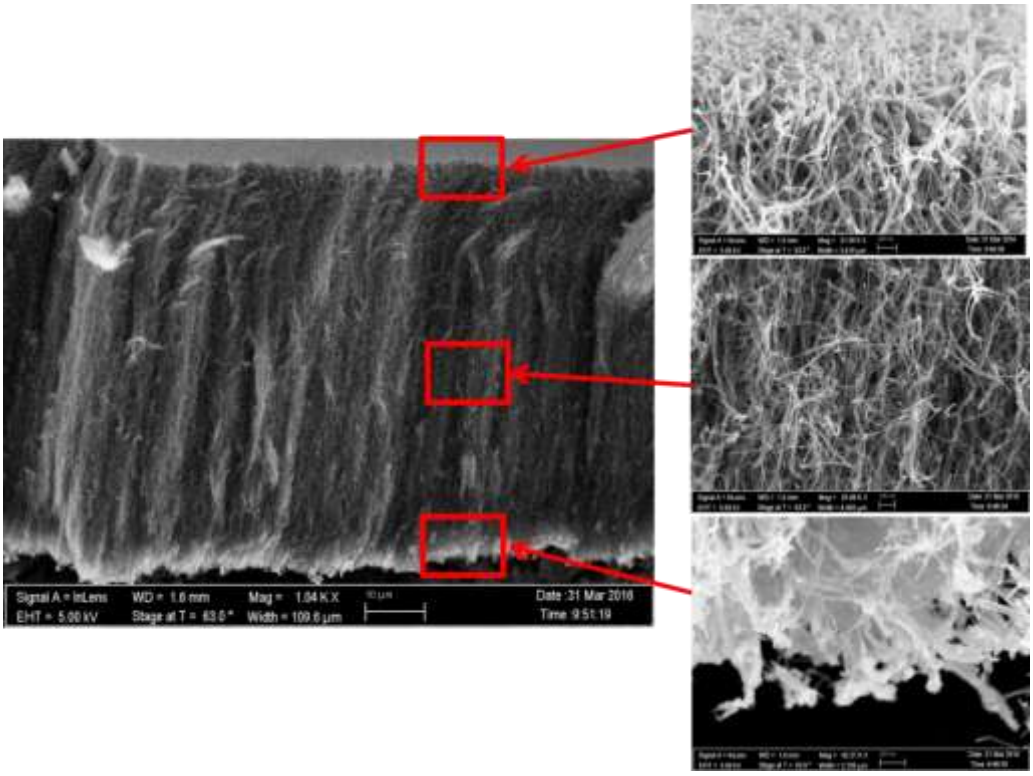

Figure 49: Visible coating of palladium at the top of the VMWNTs and coating of titania on the bottom. No visible coating in the middle of the VMWNTs.

EDS was used to confirm the presence palladium and titanium on the VMWNTs and to ensure both metals were at opposite ends of the VMWNTs. Viewing the EDS maps there is palladium at the top and titanium at the bottom of the VMWNTs, Figure 53. The presence of the few dots in the EDS map of palladium and titanium in the middle of the VMWNTs is due to noise from Bremsstrahlung scattering. The EDS spectra also show peaks present above the noise for palladium and titanium. To ensure no palladium or titanium was deposited in the middle of the VMWNTs or on top of the other metal EDS spectra and maps were collected at the top, middle, and bottom of the VMWNTs. At the top of the VMWNTs there is only palladium present as can be seen in the map and EDS spectra, Figure 51. In the middle of the VMWNTs there is neither palladium nor titanium, Figure 52. At the bottom of the VMWNTs only titanium is present, Figure

53. Thus, the deposition allows for palladium and titanium to be deposited on opposite ends of the VMWNTs without either catalyst coming into contact.

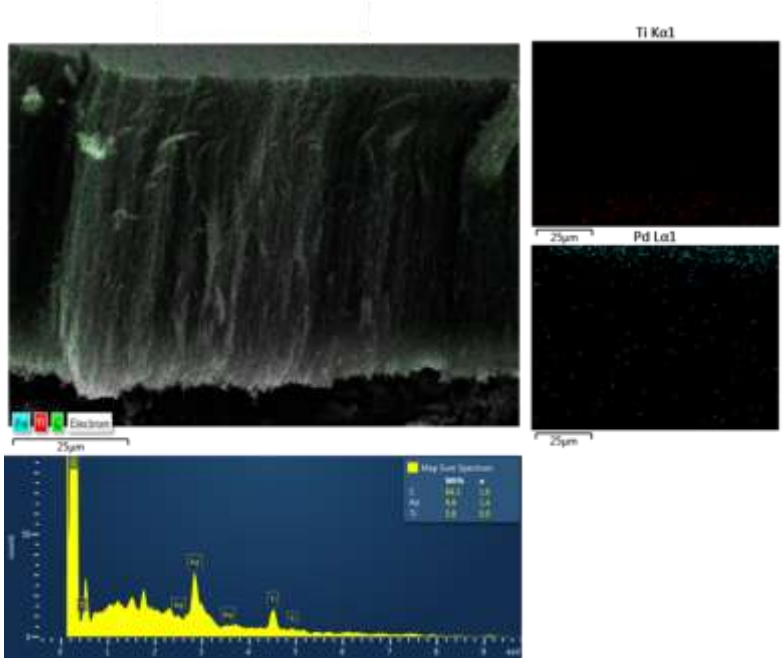

Figure 50: EDS spectra and map of entire catalyst with palladium and titanium separated on VMWNTs.

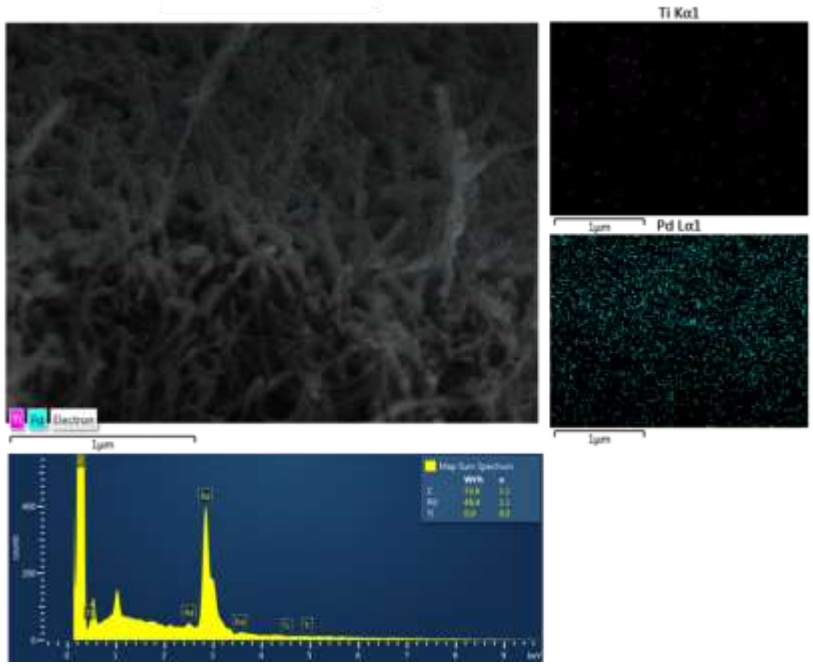

Figure 51: EDS spectra and map of the top of the catalyst with palladium and titanium separated on VMWNTs.

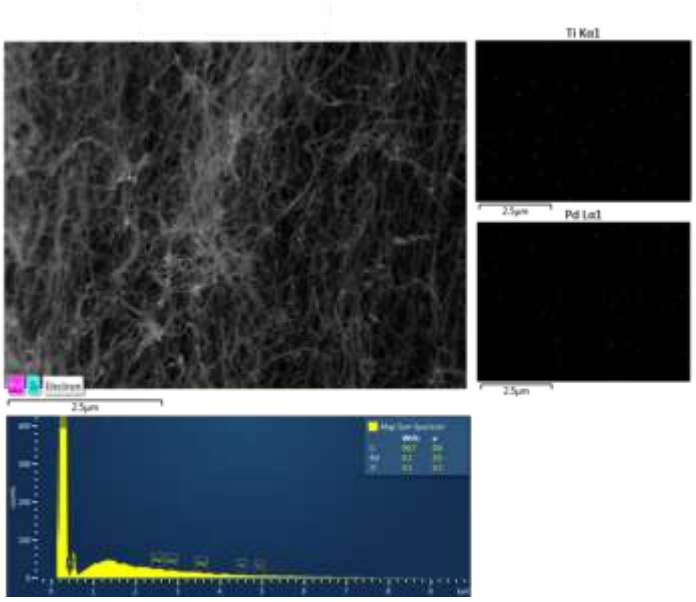

Figure 52: EDS spectra and map of the middle of the catalyst with palladium and titanium separated on VMWNTs.

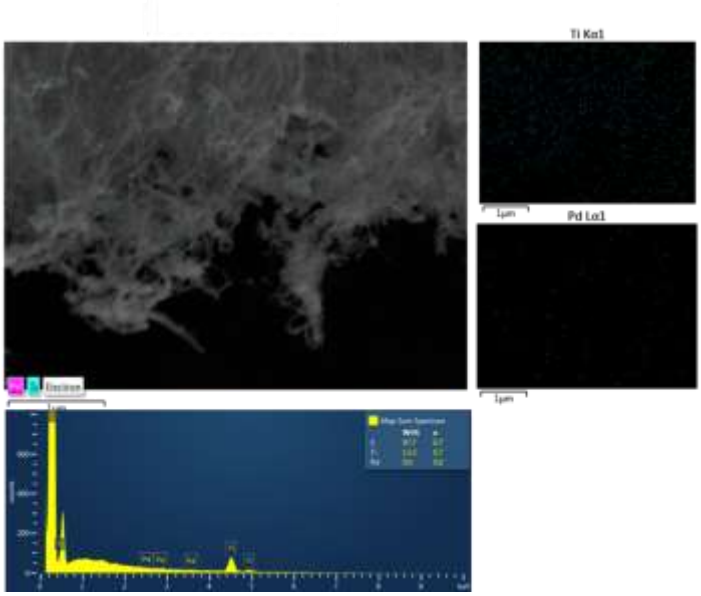

Figure 53: EDS spectra and map of bottom of the of the catalyst with palladium and titanium separated on VMWNTs.

With the successful deposition palladium and titanium on separate ends of the VMWNTs the catalyst had to be tested under reaction conditions to ensure the palladium or titania would not sinter on the carbon nanotubes and come in contact with

one another. Palladium and other metals have been shown to sinter on carbon supports.[296,297] Sintering is an important consideration for chemical reactions and efforts have been made to mix different oxides to reduce metal sintering.[298,299,300] To ensure the palladium and titania did not sinter the catalyst was reduced at 400°C for four hours with a flow of hydrogen. After this treatment the catalyst was again characterized with SEM and EDS. With EDS characterization the palladium and titania did not sinter over a great length of the VMWNTs. A strong presence of palladium can be seen at the top of the VMWNTs and a strong presence of titanium at the bottom of the VMWNTs and EDS spectra shows peaks for palladium and titanium, Figure 54. Focusing on the top of the VMWNTs only palladium is present and there is no titanium peak in the spectra, Figure 55. In the middle of the VMWNTs there is neither palladium nor titanium present, Figure 56. At the bottom of the VMWNTs only titanium is present no palladium, Figure 57.

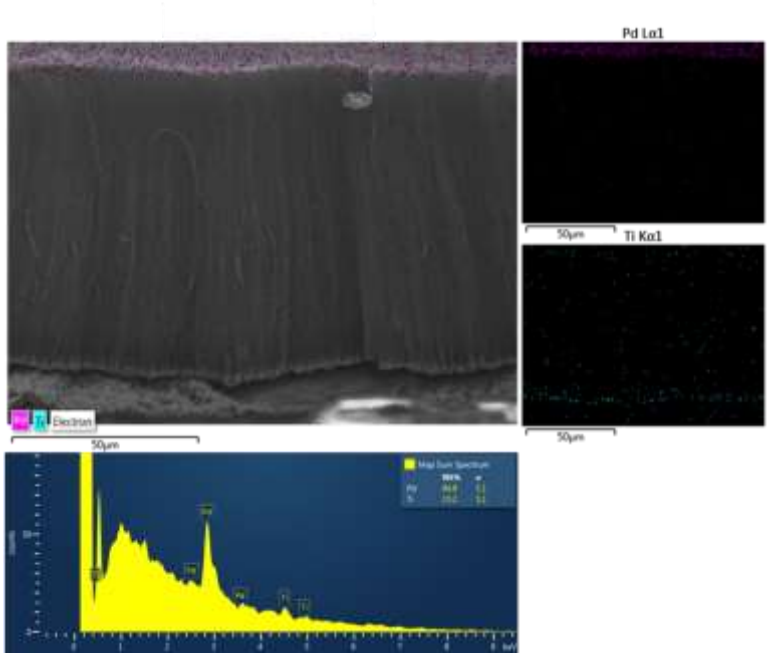

Figure 54: EDS spectra and map of entire catalyst with palladium and titanium separated on VMWNTs after heating in hydrogen at 400°C.

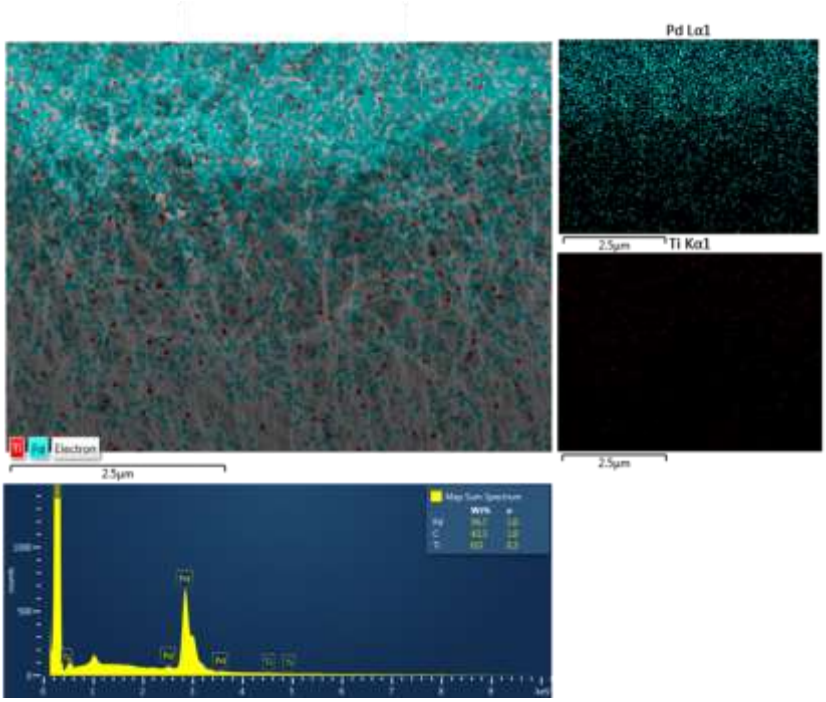

Figure 55: EDS spectra and map of the top of the catalyst with palladium and titanium separated on VMWNTs after heating in hydrogen at 400°C.

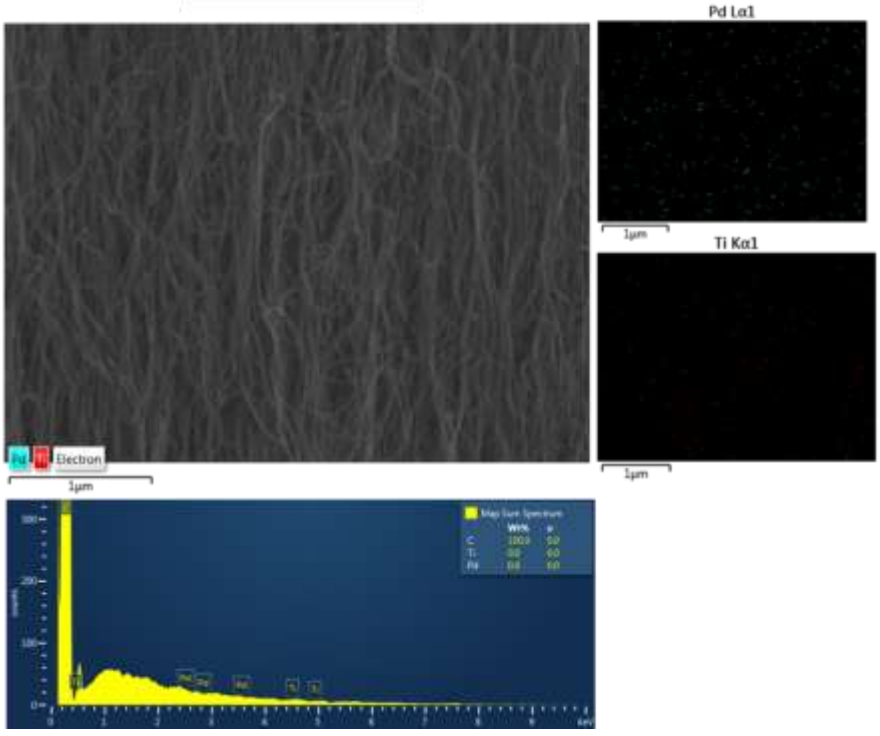

Figure 56: EDS spectra and map of the middle of the catalyst with palladium and titanium separated on VMWNTs after heating in hydrogen at 400°C.

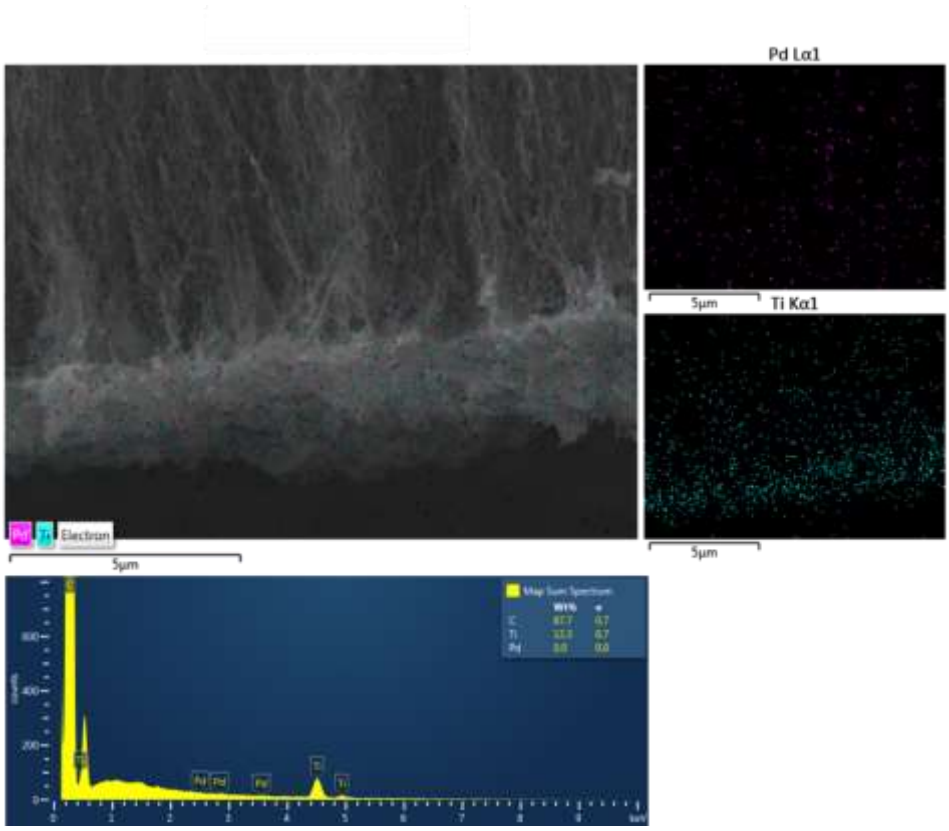

Figure 57: EDS spectra and map of the bottom of the catalyst with palladium and titanium separated on VMWNTs after heating in hydrogen at 400°C.

The EDS maps and spectra give strong evidence that the palladium and titania have not sintered significantly enough for the two catalysts to come in contact on the carbon nanotubes. While sintering is likely to occur along the length of the VMWNTs the VMWNTs is greater than the distance the catalyst particles can sinter, thus no palladium titania interface is formed. Since it appears the VMWNTs used for this study are more than sufficient in length to reduce the palladium and titania coming into contact shorter VMWNTs can be tested in the future which may provide better hydrogen spillover since the distance the hydrogen must diffuse across to reach the oxide is shorter.

Iron and cobalt are used to grow VMWNTs and depending on the growth mechanism the catalyst can be at the tip or root of the VMWNTs.[301] To ensure no residual iron are present at either ends of the VMWNTs the EDS spectra at both ends of the VMWNTs were analyzed for the presence of iron and cobalt, Figure 58. As can be seen in there are no discernable peaks for iron and cobalt. The catalyst likely stays on the silicon wafer or becomes entrapped in the carbon nanotubes and does not play any catalytic role.

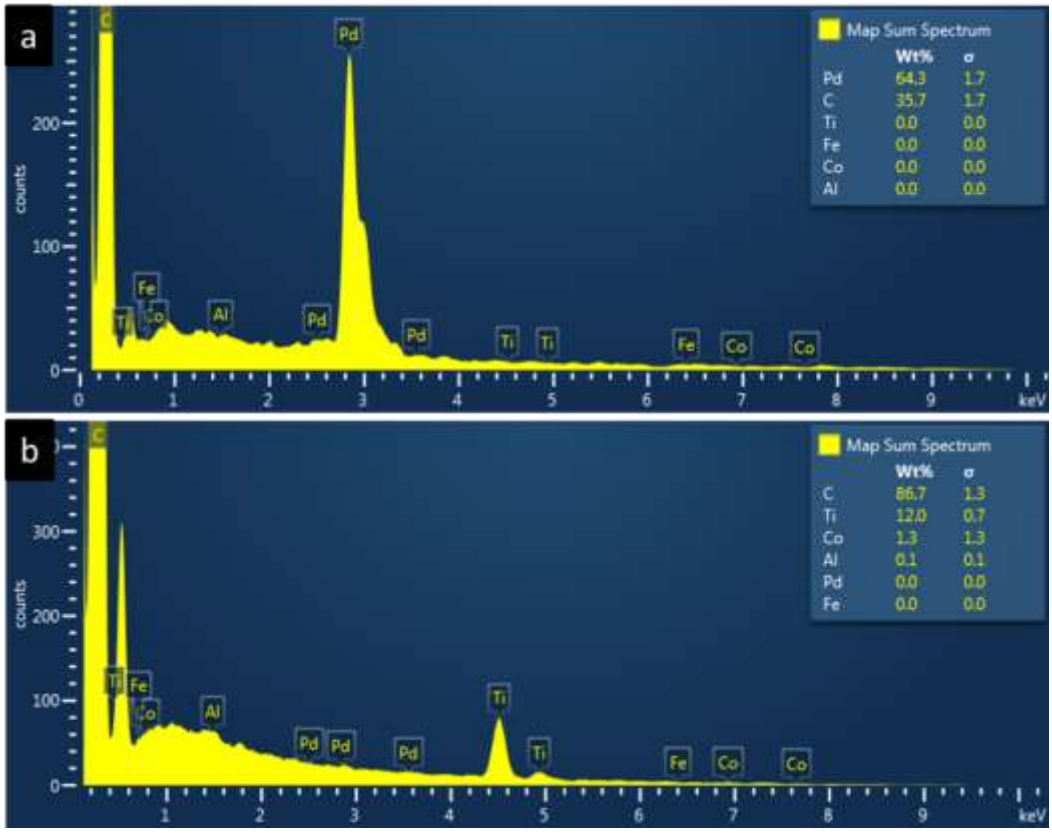

Figure 58: EDS spectra of the (a) top of the VMWNTs, end with palladium, and (b) bottom of the VMWNTs, end with titania.

Reactions with Furfural

Due to the importance of furfurals in biofuels, furfural was chosen as a probe molecule to test this novel catalyst and see if the catalytic active site responsible for a

specific reaction pathway or for enhancing a reaction pathway when using a bifunctional catalyst is located at the palladium titania interface or on the titania. A significant difference can be found when comparing palladium and titania separated and supported on VMWNTs to palladium supported on titania supported on VMWNTs, Table 3. Additional reaction data can be found in the Appendix.

For all three catalysts furan, tetrahydrofuran, methylfuran, cyclopentanone, 2-cyclopenten-1-one, furfuryl alcohol and methane were produced from furfural. However, furan, 2-methylfuran, and methane were produced in significant amounts and vary between the three catalysts under the reaction conditions tested. Testing the catalyst with palladium supported on VMWNTs results in furan being produced in the highest yield. Introducing the palladium titania interface by using the catalyst with palladium supported on titania supported on VMWNTs results in equal yields of 2-methylfuran and furan. Indicating the presence of titania is playing a role in increasing the yield of 2-methylfuran. To elucidate if the active site responsible for the increase in yield of 2-methylfuran the catalyst with the palladium and titania separated on VMWNTs was tested. In this case the yield of furan increases and the results are similar to when using solely palladium supported on VMWNTs. With the palladium and titania interface no longer present the yield of furan increases and 2-methylfuran drops. Thus, indicating the increase in yield of 2-methylfuran seen with palladium and titania is due to the palladium titania interface.

Catalysts	Conversion (%)	Yields (%)						
		Furan	2MF	FOH	THF	2COP	COP	Me
Pd on VMWNTs	98.1	77.9	12.9	0.3	0.1	0.2	0.1	6.5
Pd on TiO_2 on VMWNTs	51	20.5	25.2	0.1	0.2	0.6	0	4.5
Pd and TiO_2 separated on VMWNTs	87	59.6	16.0	0.3	0.1	0.2	0.3	11.3

Table 3: Conversion and yields for furfural on the three different catalyst at a time on stream of 33 minutes. 2MF = 2-methylfuran, FOH = furfuryl alcohol, THF = tetrahydrofuran, 2COP = 2-cyclopeten-1-one, COP = cyclopentanone, and Me = methane.

Production of 2-methylfuran occurs first with hydrogenation of furfural to furfuryl alcohol and then hydrogenolysis of furfuryl alcohol.[290] Hydrogenation of furfural and hydrogenolysis of furfuryl alcohol occurs on the metal catalysts Cu, Pd, and Ni.[290,291,292,293,302] However, the sites formed between the palladium and titania may be able to enhance hydrogenolysis of furfuryl alcohol to 2-methylfuran. This enhancement may be similar to how the metal oxide interface can enhance CO bond activation[247] and carbon-carbon bond activation in alkane hydrogenolysis.[224] An enhancement for furfuryl alcohol hydrgeonolysis to methyl furan has been seen with Pd/TiO_2 catalyst with the palladium titania interface proposed as responsible for the increase in yield of methyl furan.[303] Therefore, the hydrogenolysis may be enhanced by the presence of the palladium titania interface.

Furan is formed from decarbonylation of furfural. On palladium furfurals carbon and oxygen atoms of the carbonyl group interact with the metal. If the reaction temperature is low then hydrogenation of the aldehyde takes place producing furfuryl alcohol. If the temperature is high the bonding of solely the carbon atom to the metal

surface is more stable forming an acyl species.[290] At high temperatures the acyl species increases in stability and the C atom strongly binds to the metal surface, thus forming the intermediate for decarbonylation and production of furan.

The results indicate the palladium titania interface, the palladium and titania catalysts working together, is responsible for enhancing the production of 2-methylfuran and not active sites created on titania. To prove the existence of active sites on the titania by hydrogen spillover on the carbon nanotube a TPR of the catalyst with palladium and titania separated on VMWNTs was performed. As can be seen in Figure 59 the titania on the catalyst with palladium and titania separated on VMWNTs begins to reduce at 300°C. There is no palladium reduction peak present since the catalyst had to be pre-flushed at room temperature with hydrogen which reduced the palladium and the palladium was deposited in metal form on the VMWNTs and it is likely that little to palladium oxide exists. In the literature titania alone without a metal begins to reduce around 500°C.[304] Therefore, since the reduction occurs at a lower temperature the palladium is dissociating hydrogen which can travel along the carbon nanotube to the titania to create active sites on the titania below the temperature titania normally reduces. Thus, the same active sites on this catalyst are created when palladium is supported on titania. Combining this result with the reaction results, Table 3, indicates the active sites on the titania are not responsible for the enhanced production of 2-methylfuran, even though active sites are on the titania. Instead the synergistic effect which increases production of 2-methylfuran is caused by the palladium titania interface. The palladium and titania work together to perform hydrogenolysis of the furfuryl alcohol.

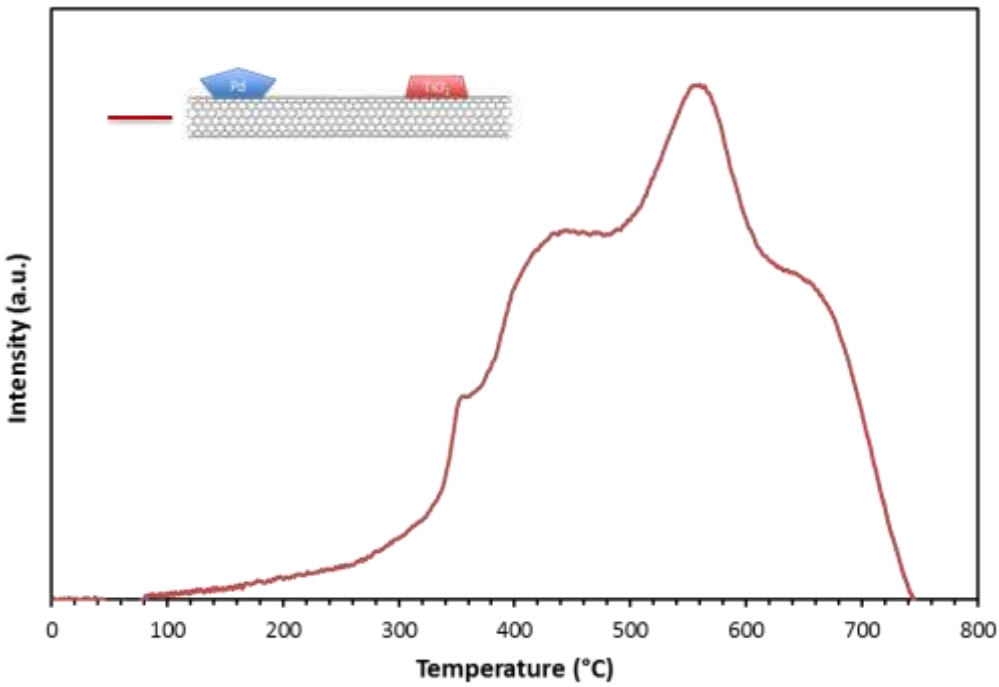

Figure 59: Temperature programmed reduction of a catalyst with palladium and titania separated on VMWNTs.

Conclusions

Palladium and titania have been deposited on opposite ends of the VMWNTs using physical vapor deposition. Due to length of the VMWNTs and spacing between the two catalysts the palladium and titania remain separated and at the ends of the VMWNTs. The palladium and titania do not sinter enough to come in contact with one another on the VMWNTs and this is likely due to the length of the VMWNTs being sufficient enough to keep the two catalysts apart. TPR indicates hydrogen can spillover on the VMWNTs occurs after being dissociated on the palladium since titania is reduced below the normal reduction temperature of titania. Indicating active sites on the titania can still be produced with the palladium and titania separated on VMWNTs. The VMWNTs act as a conductive bridge for hydrogen spillover. Using furfural as a probe

molecule there is a significant difference in selectivity. Palladium alone on VMWNTs yields the highest production of furan. When palladium is supported on titania on VMWNTs the presence of titania increases production of 2-methylfuran and decreases production of furan. To determine if the palladium titania interface or active sites solely on the titania are responsible for the enhancement of 2-mehtlyfuran the palladium and titania are separated on VMWNTs. With the palladium and titania separated on the VMWNTs the production of furan increases and 2-methylfuran decreases. This indicates the enhancement of 2-methlyfuran is due to the synergistic benefit of the palladium titania interface, having two different catalysts in close proximity, and not the active sites created on titania.

This novel catalyst provides the opportunity to determine the location of the active site in bifunctional catalysts and measure hydrogen spillover rates on carbon nanotubes. Other reactions requiring bifunctional catalysts can be tested and knowledge gained to help improve catalyst design. The length and diameter of the VMWNTs can be tuned to measure the rate of hydrogen spillover on carbon nanotubes which may have important implications for hydrogen storage. This novel catalyst warrants further investigation as a tool for studying bifunctional catalysts and understanding hydrogen spillover for hydrogen storage materials.

Chapter 8: Concluding Remarks

Carbon nanotubes have been studied as catalyst supports in biphasic systems. Changing carbon nanotubes wettability by either covalent or non-covalent means has an impact on the emulsions properties, yet emulsion stability is maintained unlike other nanoparticles since the tendency of carbon nanotubes to agglomerate is not significantly hindered by the functionalization. Multiple carbon nanotubes were found to reside at the oil-water interface of an emulsion and the carbon nanotubes wettability as well as the and way in which the carbon nanotubes wettability is modified has an effect on the quantity of carbon nanotubes at the oil-water interface. Carbon nanotubes can stabilize emulsions with a wide variety of different properties and the amount of carbon nanotubes at the oil-water interface controlled. Controlling the amount of carbon nanotubes at the oil-water interface may have future applications as a mass transfer barrier. The understanding of particles properties on emulsion characteristics may have use in the fields of enhanced oil recovery and increasing the strength of polymer blends. Since carbon nanotubes are highly suitable for applications with emulsions they may also be suitable for forming bicontinuous interfacially jammed emulsion gels (BIJEL). A BIJEL will allow for the oil and water to be flowed continuously over the catalyst particles, like a gas flow reactor, allowing for continuous operation.

Utilizing this knowledge of how carbon nanotubes of different wettability change an emulsions characteristics and existing literature on silica nanoparticles reactions were used to further understand the environment of the particle at the oil-water interface. Silica nanoparticles were functionalized to have different wettability to change their environment at the oil-water interface which in turn changes the reaction

selectivity. The environment of the particle at the oil-water interface can be changed by controlling the ratio of cationic to anionic surfactants which influences the silica nanoparticles wettability in the system. By changing the nanoparticles environment at the oil-water interface the reaction selectivity can be tuned, while the reaction proceeds. Evidence that a responsive system can be created in a biphasic system opens the doorway to using other stimuli's and other types of biphasic systems such as foams.

Carbon nanotubes of different wettability did not change the selectivity as silica nanoparticles did. However, the rates of reaction for reactants in the oil and aqueous phases increased when fewer carbon nanotubes resided at the oil-water interface, possibly due to the thinner barrier the molecules were forced to diffuse through to reach the catalyst. If a mass transfer barrier is being formed this may have uses for delaying the release of chemicals or as a separation tool.

An area which needs further exploration is what the environment of the particle at the oil-water interface looks like which is responsible for controlling selectivity. Two possible scenarios for how selectivity is controlled (1) is the particles position at the interface, which controls the number of active sites in each phase or (2) are the patches of oil and water on the particles surface where in the number and size of these patches are dependent on the number and type of functional groups. Catalyst particles in the oil patches favor reactions in the oil phase and catalyst particles in water patches favor reactions in the aqueous phase.

Utilizing the ability to synthesize carbon nanotubes with different properties, carbon nanotubes were used to create a novel catalyst. This novel catalyst can be used to determine the location of the catalytic active site for bifunctional catalysts and

understand hydrogen spillover on carbon nanotubes. Bifunctional catalysts can be designed to optimize the desired reaction pathway with the improved understanding of these catalysts.

References

[1] Diamond, A. D., and J. T. Hsu. "Aqueous two-phase systems for biomolecule separation." *Bioseparation*. Springer Berlin Heidelberg, 1992. 89-135.

[2] Rito-Palomares, Marco. "Practical application of aqueous two-phase partition to process development for the recovery of biological products." *Journal of Chromatography B* 807.1 (2004): 3-11.

[3] Fagan, Jeffrey A., et al. "Isolation of Specific Small-Diameter Single-Wall Carbon Nanotube Species via Aqueous Two-Phase Extraction." *Advanced Materials* 26.18 (2014): 2800-2804.

[4] Dunphy, Patrick J., Alan J. Meyers, and Richard T. Rigg. "Cosmetic water-in-oil emulsion lipstick comprising a phospholipid and glycerol fatty acid esters emulsifying system." U.S. Patent No. 5,085,856. 4 Feb. 1992.

[5] Friberg, Stig, Kare Larsson, and Johan Sjoblom, eds. *Food emulsions*. CRC Press, 2003.

[6] Cole-Hamilton, David J. "Homogeneous catalysis--new approaches to catalyst separation, recovery, and recycling." *Science* 299.5613 (2003): 1702-1706.

[7] Crossley, Steven, et al. "Solid nanoparticles that catalyze biofuel upgrade reactions at the water/oil interface." *Science* 327.5961 (2010): 68-72.

[8] Faria, Jimmy, M. Pilar Ruiz, and Daniel E. Resasco. "Phase-Selective Catalysis in Emulsions Stabilized by Janus Silica-Nanoparticles." *Advanced Synthesis & Catalysis* 352.14-15 (2010): 2359-2364.

[9] Drexler, Santiago, et al. "Amphiphilic nanohybrid catalysts for reactions at the water/oil interface in subsurface reservoirs." *Energy & Fuels* 26.4 (2012): 2231-2241.

[10] Giermanska-Kahn, J., et al. "Particle-stabilized emulsions comprised of solid droplets." *Langmuir* 21.10 (2005): 4316-4323.

[11] Perro, Adeline, et al. "Design and synthesis of Janus micro-and nanoparticles." *Journal of materials chemistry* 15.35-36 (2005): 3745-3760.

[12] Hong, Liang, Shan Jiang, and Steve Granick. "Simple method to produce Janus colloidal particles in large quantity." *Langmuir* 22.23 (2006): 9495-9499.

[13] Perro, Adeline, et al. "Production of large quantities of “Janus” nanoparticles using wax-in-water emulsions." *Colloids and Surfaces A: Physicochemical and Engineering Aspects* 332.1 (2009): 57-62.

[14] Jiang, Shan, and Steve Granick. "Controlling the geometry (Janus Balance) of amphiphilic colloidal particles." *Langmuir* 24.6 (2008): 2438-2445.

[15] Jiang, Shan, et al. "Solvent-free synthesis of Janus colloidal particles." *Langmuir* 24.18 (2008): 10073-10077.

[16] Bragg, James R. *Oil recovery method using an emulsion. 5,855,243* January 5, 1999.

[17] *Food emulsions and foams: Stabilization by particles.* Dickinson, Eric. 1-2, 2010, Current Opinion in Colloid & Interface Science, Vol. 15, pp. 40-49.

[18] *Silica-lipid hybrid (SLH) microcapsules: A novel oral delivery system for poorly soluble drugs.* Tan, Angel, et al., et al. 1, 2009, Journal of Controlled Release, Vol. 134, pp. 62-70.

[19] *Particle-Stabilized Surfactant-Free Medium Internal Phase Emulsions as Templates for Porous Nanocomposite Materials: poly-Pickering-Foams.* Menner, Angelika, et al., et al. 5, 2007, Langmuir, Vol. 23, pp. 2398-2403.

[20] Binks, B. P., and S. O. Lumsdon. "Influence of particle wettability on the type and stability of surfactant-free emulsions." *Langmuir* 16.23 (2000): 8622-8631.

[21] Shen, Min, and Daniel E. Resasco. "Emulsions Stabilized by Carbon Nanotube− Silica Nanohybrids." *Langmuir* 25, no. 18 (2009): 10843-10851.

[22] Levine, Samuel, Bruce D. Bowen, and Susan J. Partridge. "Stabilization of emulsions by fine particles I. Partitioning of particles between continuous phase and oil/water interface." *Colloids and Surfaces* 38.2 (1989): 325-343.

[23] Binks, B. P., and P. D. I. Fletcher. "Particles adsorbed at the oil-water interface: A theoretical comparison between spheres of uniform wettability and “Janus” particles." *Langmuir* 17.16 (2001): 4708-4710.

[24] Dong, Lichun, and Duane T. Johnson. "Adsorption of acicular particles at liquid-fluid interfaces and the influence of the line tension." *Langmuir* 21.9 (2005): 3838-3849.

[25] He, Jinbo, et al. "Drying droplets: a window into the behavior of nanorods at interfaces." *Small* 3.7 (2007): 1214-1217.

[26] Wang, Randy K., et al. "Improving the effectiveness of interfacial trapping in removing single-walled carbon nanotube bundles." *Journal of the American Chemical Society* 130.44 (2008): 14721-14728.

[27] Briggs, Nicholas M., et al. "Multi-Walled Carbon Nanotubes at the Interface of Pickering Emulsions." *Langmuir* (2015).

[28] Wang, Howard, and Erik K. Hobbie. "Amphiphobic carbon nanotubes as macroemulsion surfactants." *Langmuir* 19, no. 8 (2003): 3091-3093.

[29] Hobbie, Erik K., Barry J. Bauer, J. Stephens, M. L. Becker, P. McGuiggan, S. D. Hudson, and H. Wang. "Colloidal particles coated and stabilized by DNA-wrapped carbon nanotubes." *Langmuir* 21, no. 23 (2005): 10284-10287.

[30] Wang, Randy K., Ryan D. Reeves, and Kirk J. Ziegler. "Interfacial trapping of single-walled carbon nanotube bundles." *Journal of the American Chemical Society* 129, no. 49 (2007): 15124-15125.

[31] Wang, Randy K., Hyun-Ok Park, Wei-Chiang Chen, Carlos Silvera-Batista, Ryan D. Reeves, Jason E. Butler, and Kirk J. Ziegler. "Improving the effectiveness of interfacial trapping in removing single-walled carbon nanotube bundles." *Journal of the American Chemical Society* 130, no. 44 (2008): 14721-14728.

[32] Chen, Wenbao, Xuyan Liu, Yangshuo Liu, and Hyung-Il Kim. "Novel synthesis of self-assembled CNT microcapsules by O/W Pickering emulsions." *Materials Letters* 64, no. 23 (2010): 2589-2592.

[33] Chen, Wenbao, Xuyan Liu, Yangshuo Liu, Youngkil Bang, and Hyung-Il Kim. "Preparation of O/W Pickering emulsion with oxygen plasma treated carbon nanotubes as surfactants." *Journal of Industrial and Engineering Chemistry* 17, no. 3 (2011): 455-460.

[34] Wu, T.; Wang, H.; Jing, B.; Liu, F.; Burns, P.C.; & Na Chongzheng. Multi-body coalescence in Pickering emulsions. *Nature Communications.* **2015**, 6, 5929, 1-9.

[35] Esumi, K., et al. "Chemical treatment of carbon nanotubes." *Carbon* 34.2 (1996): 279-281.

[36] Bower, C., et al. "Intercalation and partial exfoliation of single-walled carbon nanotubes by nitric acid." *Chemical Physics Letters* 288.2 (1998): 481-486.

[37] Shaffer, Milo SP, X. Fan, and A. H. Windle. "Dispersion and packing of carbon nanotubes." *Carbon* 36.11 (1998): 1603-1612.

[38] Binks, B. P., and S. O. Lumsdon. "Effects of oil type and aqueous phase composition on oil–water mixtures containing particles of intermediate hydrophobicity." *Physical Chemistry Chemical Physics* 2.13 (2000): 2959-2967.

[39] Luu, Xuan-Cuong, Jing Yu, and Alberto Striolo. "Ellipsoidal Janus nanoparticles adsorbed at the water–oil interface: some evidence of emergent behavior." *The Journal of Physical Chemistry B* 117.44 (2013): 13922-13929.

[40] Luu, Xuan-Cuong, and Alberto Striolo. "Ellipsoidal Janus nanoparticles assembled at spherical oil/water interfaces." *The Journal of Physical Chemistry B* 118.47 (2014): 13737-13743.

[41] Binks, Bernard P., and Catherine P. Whitby. "Silica particle-stabilized emulsions of silicone oil and water: aspects of emulsification." *Langmuir* 20.4 (2004): 1130-1137.

[42] Binks, Bernard P., and John H. Clint. "Solid wettability from surface energy components: relevance to Pickering emulsions." *Langmuir* 18.4 (2002): 1270-1273.

[43] Binks, Bernard P., et al. "Drop sizes and particle coverage in emulsions stabilised solely by silica nanoparticles of irregular shape." *Physical Chemistry Chemical Physics* 12.38 (2010): 11967-11974.

[44] Wu, Tong, Haitao Wang, Benxin Jing, Fang Liu, Peter C. Burns, and Chongzheng Na. "Multi-body coalescence in Pickering emulsions." *Nature communications* 6 (2015).

[45] Stiller, S., et al. "Investigation of the stability in emulsions stabilized with different surface modified titanium dioxides." *Colloids and Surfaces A: Physicochemical and Engineering Aspects* 232.2 (2004): 261-267.

[46] Binks, B. P., and S. O. Lumsdon. "Catastrophic phase inversion of water-in-oil emulsions stabilized by hydrophobic silica." *Langmuir* 16.6 (2000): 2539-2547.

[47] Yang, Hengquan, Ting Zhou, and Wenjuan Zhang. "A Strategy for Separating and Recycling Solid Catalysts Based on the pH-Triggered Pickering-Emulsion Inversion." *Angewandte Chemie* 125.29 (2013): 7603-7607.

[48] Binks, B. P., and S. O. Lumsdon. "Transitional phase inversion of solid-stabilized emulsions using particle mixtures." *Langmuir* 16.8 (2000): 3748-3756.

[49] Crossley, Steven, et al. "Solid nanoparticles that catalyze biofuel upgrade reactions at the water/oil interface." *Science* 327.5961 (2010): 68-72.

[50] Bragg, James R. "Oil recovery method using an emulsion." U.S. Patent No. 5,855,243. 5 Jan. 1999.

[51] Dickinson, Eric. "Food emulsions and foams: stabilization by particles." *Current Opinion in Colloid & Interface Science* 15.1 (2010): 40-49.

[52] Tan, Angel, et al. "Silica-lipid hybrid (SLH) microcapsules: a novel oral delivery system for poorly soluble drugs." *Journal of controlled release* 134.1 (2009): 62-70.

[53] Menner, Angelika, et al. "Particle-stabilized surfactant-free medium internal phase emulsions as templates for porous nanocomposite materials: poly-pickering-foams." *Langmuir* 23.5 (2007): 2398-2403.

[54] Binks, B. P., and S. O. Lumsdon. "Effects of oil type and aqueous phase composition on oil–water mixtures containing particles of intermediate hydrophobicity." *Physical Chemistry Chemical Physics* 2.13 (2000): 2959-2967.

[55] Binks, B. P., and S. O. Lumsdon. "Catastrophic phase inversion of water-in-oil emulsions stabilized by hydrophobic silica." *Langmuir* 16.6 (2000): 2539-2547.

[56] Binks, B. P., and S. O. Lumsdon. "Influence of particle wettability on the type and stability of surfactant-free emulsions." *Langmuir* 16.23 (2000): 8622-8631.

[57] Binks, Bernard P., and Catherine P. Whitby. "Silica particle-stabilized emulsions of silicone oil and water: aspects of emulsification." *Langmuir* 20.4 (2004): 1130-1137.

[58] Binks, Bernard P., John Philip, and Jhonny A. Rodrigues. "Inversion of silica-stabilized emulsions induced by particle concentration." *Langmuir* 21.8 (2005): 3296-3302.

[59] Hassander, Helen, Beatrice Johansson, and Bertil Törnell. "The mechanism of emulsion stabilization by small silica (Ludox) particles." *Colloids and surfaces* 40 (1989): 93-105.

[60] Midmore, B. R. "Preparation of a novel silica-stabilized oil/water emulsion." *Colloids and Surfaces A: Physicochemical and Engineering Aspects* 132.2 (1998): 257-265.

[61] Binks, Bernard P., Jhonny A. Rodrigues, and William J. Frith. "Synergistic interaction in emulsions stabilized by a mixture of silica nanoparticles and cationic surfactant." *Langmuir* 23.7 (2007): 3626-3636.

[62] Wang, Howard, and Erik K. Hobbie. "Amphiphobic carbon nanotubes as macroemulsion surfactants." *Langmuir* 19.8 (2003): 3091-3093.

[63] Wu, Tong, et al. "Multi-body coalescence in Pickering emulsions." *Nature communications* 6 (2015).

[64] Shi, Dachuan, et al. "Enhanced Activity and Selectivity of Fischer–Tropsch Synthesis Catalysts in Water/Oil Emulsions." *ACS Catalysis* 4.6 (2014): 1944-1952.

[65] Kadhum, Mohannad J., et al. "Propagation of interfacially active carbon nanohybrids in porous media." *Energy & Fuels* 27.11 (2013): 6518-6527.

[66] Chen, Wenbao, et al. "Novel synthesis of self-assembled CNT microcapsules by O/W Pickering emulsions." *Materials Letters* 64.23 (2010): 2589-2592.

[67] Yi, Haixia, Huaihe Song, and Xiaohong Chen. "Carbon nanotube capsules self-assembled by W/O emulsion technique." *Langmuir* 23.6 (2007): 3199-3204.

[68] Welna, Daniel T., et al. "Vertically aligned carbon nanotube electrodes for lithium-ion batteries." *Journal of Power Sources* 196.3 (2011): 1455-1460.

[69] Star, Alexander, et al. "Gas sensor array based on metal-decorated carbon nanotubes." *The Journal of Physical Chemistry B* 110.42 (2006): 21014-21020.

[70] Javey, Ali, et al. "Carbon nanotube field-effect transistors with integrated ohmic contacts and high-κ gate dielectrics." *Nano Letters* 4.3 (2004): 447-450.

[71] Lau, Kenneth KS, et al. "Superhydrophobic carbon nanotube forests." *Nano letters* 3.12 (2003): 1701-1705.

[72] Zhu, Hongwei, et al. "Hydrogen adsorption in bundles of well-aligned carbon nanotubes at room temperature." *Applied surface science* 178.1 (2001): 50-55.

[73] Cao, Anyuan, et al. "Hydrogen storage of dense-aligned carbon nanotubes." *Chemical physics letters* 342.5 (2001): 510-514.

[74] Jiang, Kaili, Qunqing Li, and Shoushan Fan. "Nanotechnology: spinning continuous carbon nanotube yarns." *Nature* 419.6909 (2002): 801-801.

[75] Zhang, Mei, Ken R. Atkinson, and Ray H. Baughman. "Multifunctional carbon nanotube yarns by downsizing an ancient technology." *Science* 306.5700 (2004): 1358-1361.

[76] Lin, Wei, et al. "Synthesis of high-quality vertically aligned carbon nanotubes on bulk copper substrate for thermal management." *Advanced Packaging, IEEE Transactions on* 33.2 (2010): 370-376.

[77] Cao, Anyuan, et al. "Super-compressible foamlike carbon nanotube films." *Science* 310.5752 (2005): 1307-1310.

[78] Hobbie, Erik K., et al. "Colloidal particles coated and stabilized by DNA-wrapped carbon nanotubes." *Langmuir* 21.23 (2005): 10284-10287.

[79] Wang, Randy K., Ryan D. Reeves, and Kirk J. Ziegler. "Interfacial trapping of single-walled carbon nanotube bundles." *Journal of the American Chemical Society* 129.49 (2007): 15124-15125.

[80] Shen, Min, and Daniel E. Resasco. "Emulsions stabilized by carbon nanotube− silica nanohybrids." *Langmuir* 25.18 (2009): 10843-10851.

[81] Chen, Wenbao, et al. "Preparation of O/W Pickering emulsion with oxygen plasma treated carbon nanotubes as surfactants." *Journal of Industrial and Engineering Chemistry* 17.3 (2011): 455-460.

[82] Wang, Wenda, et al. "Bending single-walled carbon nanotubes into nanorings using a Pickering emulsion-based process." *Carbon* 50.5 (2012): 1769-1775.

[83] Chen, Liyong, et al. "General methodology of using oil-in-water and water-in-oil emulsions for coiling nanofilaments." *Journal of the American Chemical Society* 135.2 (2013): 835-843.

[84] Baudouin, Anne-Christine, et al. "Polymer blend emulsion stabilization using carbon nanotubes interfacial confinement." *Polymer* 52.1 (2011): 149-156.

[85] Perro, Adeline, et al. "Design and synthesis of Janus micro-and nanoparticles." *Journal of Materials Chemistry* 15.35-36 (2005): 3745-3760.

[86] Perro, Adeline, et al. "Production of large quantities of “Janus” nanoparticles using wax-in-water emulsions." *Colloids and Surfaces A: Physicochemical and Engineering Aspects* 332.1 (2009): 57-62.

[87] Hong, Liang, Shan Jiang, and Steve Granick. "Simple method to produce Janus colloidal particles in large quantity." *Langmuir* 22.23 (2006): 9495-9499.

[88] Jiang, Shan, and Steve Granick. "Controlling the geometry (Janus balance) of amphiphilic colloidal particles." *Langmuir* 24.6 (2008): 2438-2445.

[89] Jiang, Shan, et al. "Solvent-free synthesis of Janus colloidal particles." *Langmuir* 24.18 (2008): 10073-10077.

[90] Graham, J. W., and J. G. Richardson. "Theory and application of imbibition phenomena in recovery of oil." *Journal of Petroleum Technology* 11.02 (1959): 65-69.

[91] Drexler, Santiago, et al. "Amphiphilic nanohybrid catalysts for reactions at the water/oil interface in subsurface reservoirs." *Energy & Fuels* 26.4 (2012): 2231-2241.

[92] Giermanska-Kahn, J., et al. "Particle-stabilized emulsions comprised of solid droplets." *Langmuir* 21.10 (2005): 4316-4323.

[93] Lerk, C. F., et al. "Effect of hydrophilization of hydrophobic drugs on release rate from capsules." *Journal of pharmaceutical sciences* 67.7 (1978): 935-939.

[94] Sabatini, David A., Edgar Acosta, and Jeffrey H. Harwell. "Linker molecules in surfactant mixtures." *Current opinion in colloid & interface science* 8.4 (2003): 316-326.

[95] Dong, Lichun, and Duane T. Johnson. "Adsorption of acicular particles at liquid-fluid interfaces and the influence of the line tension." *Langmuir* 21.9 (2005): 3838-3849.

[96] He, Jinbo, et al. "Drying droplets: a window into the behavior of nanorods at interfaces." *Small* 3.7 (2007): 1214-1217.

[97] Matarredona, Olga, et al. "Dispersion of single-walled carbon nanotubes in aqueous solutions of the anionic surfactant NaDDBS." *The Journal of Physical Chemistry B* 107.48 (2003): 13357-13367.

[98] Crossley, Steven, et al. "Solid nanoparticles that catalyze biofuel upgrade reactions at the water/oil interface." *Science* 327.5961 (2010): 68-72.

[99] Yu, Chang, et al. "Phase-Reversal Emulsion Catalysis with CNT–TiO2 Nanohybrids for the Selective Oxidation of Benzyl Alcohol." *Chemistry–A European Journal* 19.48 (2013): 16192-16195.

[100] Zapata, Paula A., et al. "Silylated hydrophobic zeolites with enhanced tolerance to hot liquid water." *Journal of Catalysis* 308 (2013): 82-97.

[101] Yu, Yuhong, et al. "Pickering-Emulsion Inversion Strategy for Separating and Recycling Nanoparticle Catalysts." *ChemPhysChem* 15.5 (2014): 841-848.

[102] Wang, Haixia, et al. "A mesoporous silica nanocomposite shuttle: pH-triggered phase transfer between oil and water." *Langmuir* 29.22 (2013): 6687-6696.

[103] Huber, George W., Sara Iborra, and Avelino Corma. "Synthesis of transportation fuels from biomass: chemistry, catalysts, and engineering." *Chemical reviews* 106.9 (2006): 4044-4098.

[104] Zhang, Lu, et al. "Factors that Determine Zeolite Stability in Hot Liquid Water." *Journal of the American Chemical Society* 137.36 (2015): 11810-11819.

[105] Binks, B. P., and S. O. Lumsdon. "Influence of particle wettability on the type and stability of surfactant-free emulsions." *Langmuir* 16.23 (2000): 8622-8631.

[106] Binks, B. P., and S. O. Lumsdon. "Stability of oil-in-water emulsions stabilised by silica particles." *Physical Chemistry Chemical Physics* 1.12 (1999): 3007-3016.

[107] Binks, Bernard P., and Jhonny A. Rodrigues. "Enhanced stabilization of emulsions due to surfactant-induced nanoparticle flocculation." *Langmuir* 23.14 (2007): 7436-7439.

[108] Binks, Bernard P., Jhonny A. Rodrigues, and William J. Frith. "Synergistic interaction in emulsions stabilized by a mixture of silica nanoparticles and cationic surfactant." *Langmuir* 23.7 (2007): 3626-3636.

[109] Zhu, Yue, et al. "Switchable Pickering Emulsions Stabilized by Silica Nanoparticles Hydrophobized in Situ with a Conventional Cationic Surfactant." *Langmuir* 31.11 (2015): 3301-3307.

[110] Binks, B. P., and S. O. Lumsdon. "Transitional phase inversion of solid-stabilized emulsions using particle mixtures." *Langmuir* 16.8 (2000): 3748-3756.

[111] Binks, B. P., and S. O. Lumsdon. "Catastrophic phase inversion of water-in-oil emulsions stabilized by hydrophobic silica." *Langmuir* 16.6 (2000): 2539-2547.

[112] Weston, J. S., et al. "Silica Nanoparticle Wettability: Characterization and Effects on the Emulsion Properties." *Industrial & Engineering Chemistry Research* 54.16 (2015): 4274-4284.

[113] Binks, B. P.; Whitby, C. P. Nanoparticle silica-stabilised oil-inwater emulsions, improving emulsion stability. Colloids Surf., A 2005, 253, 105−115.

[114] Tombacz, E.; Szekeres, M.; Kertesz, I.; Turi, L. pH-dependent aggregation state of highly dispersed alumina, titania, and silica particles in aqueous medium. Prog. Colloid Polym. Sci. 1995, 98, 160−168.

[115] Musolino, Maria Grazia, et al. "Supported palladium catalysts for the selective conversion of cis-2-butene-1, 4-diol to 2-hydroxytetrahydrofuran: Effect of metal particle size and support." *Applied Catalysis A: General* 325.1 (2007): 112-120.

[116] Cremer, Paul S., and Gabor A. Somorjai. "Surface science and catalysis of ethylene hydrogenation." *Journal of the Chemical Society, Faraday Transactions* 91.20 (1995): 3671-3677.

[117] Zapata, Paula A., et al. "Hydrophobic zeolites for biofuel upgrading reactions at the liquid–liquid interface in water/oil emulsions." *Journal of the American Chemical Society* 134.20 (2012): 8570-8578.

[118] Bergeret, G. and Gallezot, P. 2008. Particle Size and Dispersion Measurements. Handbook of Heterogeneous Catalysis. 3:3.1:3.1.2:738–765.

[119] Madon, R. J., J. P. O'connell, and Michel Boudart. "Catalytic hydrogenation of cyclohexene: Part II. Liquid phase reaction on supported platinum in a gradientless slurry reactor." *AIChE Journal* 24.5 (1978): 904-911.

[120] Madon, Rostam J., and Enrique Iglesia. "Catalytic reaction rates in thermodynamically non-ideal systems." *Journal of Molecular Catalysis A: Chemical* 163.1 (2000): 189-204.

[121] Madon, R. J., J. P. O'connell, and Michel Boudart. "Catalytic hydrogenation of cyclohexene: Part II. Liquid phase reaction on supported platinum in a gradientless slurry reactor." *AIChE Journal* 24.5 (1978): 904-911.

[122] Mukherjee, Samrat, and M. Albert Vannice. "Solvent effects in liquid-phase reactions: I. Activity and selectivity during citral hydrogenation on Pt/SiO2 and evaluation of mass transfer effects." *Journal of Catalysis* 243.1 (2006): 108-130.

[123] Mukherjee, Samrat, and M. Albert Vannice. "Solvent effects in liquid-phase reactions II. Kinetic modeling for citral hydrogenation." *Journal of Catalysis* 243.1 (2006): 131-148.

[124] Struijk, J., et al. "Partial liquid-phase hydrogenation of benzene to cyclohexene over ruthenium catalysts in the presence of an aqueous salt solution: II. Influence of various salts on the performance of the catalyst." *Applied Catalysis A: General* 89.1 (1992): 77-102.

[125] Binks, B. P., and S. O. Lumsdon. "Effects of oil type and aqueous phase composition on oil–water mixtures containing particles of intermediate hydrophobicity." *Physical Chemistry Chemical Physics* 2.13 (2000): 2959-2967

[126] Faria, Jimmy, M. Pilar Ruiz, and Daniel E. Resasco. "Phase-Selective Catalysis in Emulsions Stabilized by Janus Silica-Nanoparticles." *Advanced Synthesis & Catalysis* 352.14-15 (2010): 2359-2364.

[127] Perro, Adeline, et al. "Design and synthesis of Janus micro-and nanoparticles." *Journal of Materials Chemistry* 15.35-36 (2005): 3745-3760.

[128] Giermanska-Kahn, J., et al. "Particle-stabilized emulsions comprised of solid droplets." *Langmuir* 21.10 (2005): 4316-4323.

[129] Jiang, Shan, and Steve Granick. "Controlling the geometry (Janus balance) of amphiphilic colloidal particles." *Langmuir* 24.6 (2008): 2438-2445.

[130] Perro, Adeline, et al. "Production of large quantities of “Janus” nanoparticles using wax-in-water emulsions." *Colloids and Surfaces A: Physicochemical and Engineering Aspects* 332.1 (2009): 57-62.

[131] Jiang, Shan, et al. "Janus particle synthesis and assembly." *Advanced materials* 22.10 (2010): 1060-1071.

[132] Binks, B. P., and S. O. Lumsdon. "Transitional phase inversion of solid-stabilized emulsions using particle mixtures." *Langmuir* 16.8 (2000): 3748-3756.

[133] Luu, Xuan-Cuong, Jing Yu, and Alberto Striolo. "Nanoparticles adsorbed at the water/oil interface: coverage and composition effects on structure and diffusion." *Langmuir* 29.24 (2013): 7221-7228.

[134] Briggs, N. M., Weston, J. S., et al. . P. (2015). “Multiwalled Carbon Nanotubes at the Interface of Pickering Emulsions.” *Langmuir*, *31 (2015).*

[135] Wu, Tong, et al. "Multi-body coalescence in Pickering emulsions." *Nature communications* 6 (2015).

[136] Crossley, Steven, et al. "Solid nanoparticles that catalyze biofuel upgrade reactions at the water/oil interface." *Science* 327.5961 (2010): 68-72.

[137] Faria, Jimmy, M. Pilar Ruiz, and Daniel E. Resasco. "Phase-Selective Catalysis in Emulsions Stabilized by Janus Silica-Nanoparticles." *Advanced Synthesis & Catalysis* 352.14-15 (2010): 2359-2364.

[138] Zapata, Paula A., et al. "Hydrophobic zeolites for biofuel upgrading reactions at the liquid–liquid interface in water/oil emulsions." *Journal of the American Chemical Society* 134.20 (2012): 8570-8578.

[139] Yu, Yuhong, et al. "Pickering-Emulsion Inversion Strategy for Separating and Recycling Nanoparticle Catalysts." *ChemPhysChem* 15.5 (2014): 841-848.

[140] Wang, Haixia, et al. "A mesoporous silica nanocomposite shuttle: pH-triggered phase transfer between oil and water." *Langmuir* 29.22 (2013): 6687-6696.

[141] Tan, Hongyi, et al. "Multifunctional amphiphilic carbonaceous microcapsules catalyze water/oil biphasic reactions." *Chemical Communications* 47.43 (2011): 11903-11905.

[142] Zapata, Paula A., et al. "Silylated hydrophobic zeolites with enhanced tolerance to hot liquid water." *Journal of Catalysis* 308 (2013): 82-97.

[143] Shi, Dachuan, et al. "Enhanced Activity and Selectivity of Fischer–Tropsch Synthesis Catalysts in Water/Oil Emulsions." *ACS Catalysis* 4.6 (2014): 1944-1952.

[144] Shi, Dachuan, et al. "Fischer–Tropsch Synthesis Catalyzed by Solid Nanoparticles at the Water/Oil Interface in an Emulsion System." *Energy & Fuels* 27.10 (2013): 6118-6124.

[145] Wang, Dong, and Didier Astruc. "Fast-growing field of magnetically recyclable nanocatalysts." *Chemical Reviews* 114.14 (2014): 6949-6985.

[146] Liu, Huifang, et al. "Recycling nanoparticle catalysts without separation based on a Pickering emulsion/organic biphasic system." *ChemSusChem* 7.7 (2014): 1888-1900.

[147] Bao, Chunhui, et al. "Stimuli-triggered phase transfer of polymer-inorganic hybrid hairy particles between two immiscible liquid phases." *Journal of Polymer Science Part B: Polymer Physics* 52.24 (2014): 1600-1619.

[148] Zeltner, Martin, et al. "Magnetothermally responsive C/Co@ PNIPAM-nanoparticles enable preparation of self-separating phase-switching palladium catalysts." *Journal of Materials Chemistry* 21.9 (2011): 2991-2996.

[149] Karimi, Babak, Fariborz Mansouri, and Hojatollah Vali. "A highly water-dispersible/magnetically separable palladium catalyst based on a Fe 3 O 4@ SiO 2 anchored TEG-imidazolium ionic liquid for the Suzuki–Miyaura coupling reaction in water." *Green Chemistry* 16.5 (2014): 2587-2596.

[150] Gong, Zai-lin, and Dong-yan Tang. "The fabrication and self-flocculation effect of hybrid TiO 2 nanoparticles grafted with poly (N-isopropylacrylamide) at ambient temperature via surface-initiated atom transfer radical polymerization." *Journal of Materials Chemistry* 22.33 (2012): 16872-16879.

[151] Tsuji, Sakiko, and Haruma Kawaguchi. "Thermosensitive Pickering emulsion stabilized by poly (N-isopropylacrylamide)-carrying particles." *Langmuir* 24.7 (2008): 3300-3305.

[152] Wu, Ying, et al. "Light-triggered reversible phase transfer of composite colloids." *Langmuir* 26.12 (2010): 9442-9448.

[153] Peng, Lu, et al. "Reversible Phase Transfer of Nanoparticles Based on Photoswitchable Host–Guest Chemistry." *ACS nano* 8.3 (2014): 2555-2561.

[154] Wang, Haixia, et al. "A mesoporous silica nanocomposite shuttle: pH-triggered phase transfer between oil and water." *Langmuir* 29.22 (2013): 6687-6696.

[155] Jiang, Jianzhong, et al. "Switchable pickering emulsions stabilized by silica nanoparticles hydrophobized in situ with a switchable surfactant." *Angewandte Chemie International Edition* 52.47 (2013): 12373-12376.

[156] Zhu, Yue, et al. "Switchable Pickering Emulsions Stabilized by Silica Nanoparticles Hydrophobized in Situ with a Conventional Cationic Surfactant." *Langmuir* 31.11 (2015): 3301-3307.

[157] Zeltner, Martin, et al. "Magnetothermally responsive C/Co@ PNIPAM-nanoparticles enable preparation of self-separating phase-switching palladium catalysts." *Journal of Materials Chemistry* 21.9 (2011): 2991-2996.

[158] Weston, J. S., et al. "Silica Nanoparticle Wettability: Characterization and Effects on the Emulsion Properties." *Industrial & Engineering Chemistry Research* 54.16 (2015): 4274-4284.

[159] Binks, B. P.; Whitby, C. P. Nanoparticle silica-stabilised oil-inwater emulsions, improving emulsion stability. Colloids Surf., A 2005, 253, 105−115.

[160] Tombacz, E.; Szekeres, M.; Kertesz, I.; Turi, L. pH-dependent aggregation state of highly dispersed alumina, titania, and silica particles in aqueous medium. Prog. Colloid Polym. Sci. 1995, 98, 160−168.

[161] Binks, B. P., and S. O. Lumsdon. "Influence of particle wettability on the type and stability of surfactant-free emulsions." *Langmuir* 16.23 (2000): 8622-8631.

[162] Binks, Bernard P., et al. "Drop sizes and particle coverage in emulsions stabilised solely by silica nanoparticles of irregular shape." *Physical Chemistry Chemical Physics* 12.38 (2010): 11967-11974.

[163] Binks, Bernard P., Jhonny A. Rodrigues, and William J. Frith. "Synergistic interaction in emulsions stabilized by a mixture of silica nanoparticles and cationic surfactant." *Langmuir* 23.7 (2007): 3626-3636.

[164] Zhu, Yue, et al. "Switchable Pickering Emulsions Stabilized by Silica Nanoparticles Hydrophobized in Situ with a Conventional Cationic Surfactant." *Langmuir* 31.11 (2015): 3301-3307.

[165] Jiang, Shan, and Steve Granick. "Controlling the geometry (Janus balance) of amphiphilic colloidal particles." *Langmuir* 24.6 (2008): 2438-2445.

[166] Musolino, Maria Grazia, et al. "Supported palladium catalysts for the selective conversion of cis-2-butene-1, 4-diol to 2-hydroxytetrahydrofuran: Effect of metal particle size and support." *Applied Catalysis A: General* 325.1 (2007): 112-120.

[167] Cremer, Paul S., and Gabor A. Somorjai. "Surface science and catalysis of ethylene hydrogenation." *Journal of the Chemical Society, Faraday Transactions* 91.20 (1995): 3671-3677.

[168] Griffin, William C. "Classification of surface-active agents by" HLB"." *J Soc Cosmetic Chemists* 1 (1946): 311-326.

[169] Davies, J. T. *Gas/Liquid and Liquid/Liquid Interface. Proceedings of the International Congress of Surface Activity*. Vol. 1. 1957.

[170] Crossley, Steven, et al. "Solid nanoparticles that catalyze biofuel upgrade reactions at the water/oil interface." *Science* 327.5961 (2010): 68-72.

[171] Lau, Kenneth KS, et al. "Superhydrophobic carbon nanotube forests." *Nano letters* 3.12 (2003): 1701-1705.

[172] Wang, Howard, and Erik K. Hobbie. "Amphiphobic carbon nanotubes as macroemulsion surfactants." *Langmuir* 19.8 (2003): 3091-3093.

[173] Chen, Wenbao, et al. "Preparation of O/W Pickering emulsion with oxygen plasma treated carbon nanotubes as surfactants." *Journal of Industrial and Engineering Chemistry* 17.3 (2011): 455-460.

[174] Welna, Daniel T., et al. "Vertically aligned carbon nanotube electrodes for lithium-ion batteries." *Journal of Power Sources* 196.3 (2011): 1455-1460.

[175] Star, Alexander, et al. "Gas sensor array based on metal-decorated carbon nanotubes." *The Journal of Physical Chemistry B* 110.42 (2006): 21014-21020.

[176] Javey, Ali, et al. "Carbon nanotube field-effect transistors with integrated ohmic contacts and high-κ gate dielectrics." *Nano Letters* 4.3 (2004): 447-450.

[177] Fan, Shoushan, et al. "Self-oriented regular arrays of carbon nanotubes and their field emission properties." *Science* 283.5401 (1999): 512-514.

[178] Bu, Ian YY, and Shu Pei Oei. "Hydrophobic vertically aligned carbon nanotubes on Corning glass for self cleaning applications." *Applied surface science* 256.22 (2010): 6699-6704.

[179] Lin, Wei, et al. "Synthesis of high-quality vertically aligned carbon nanotubes on bulk copper substrate for thermal management." *Advanced Packaging, IEEE Transactions on* 33.2 (2010): 370-376.

[180] Cao, Anyuan, et al. "Hydrogen storage of dense-aligned carbon nanotubes." *Chemical physics letters* 342.5 (2001): 510-514.

[181] Zhu, Hongwei, et al. "Hydrogen adsorption in bundles of well-aligned carbon nanotubes at room temperature." *Applied surface science* 178.1 (2001): 50-55.

[182] Yang, Jing, et al. "Direct electrochemistry study of glucose oxidase on Pt nanoparticle-modified aligned carbon nanotubes electrode by the assistance of chitosan–CdS and its biosensoring for glucose." *Electrochemistry Communications* 10.12 (2008): 1889-1892.

[183] Jiang, Kaili, Qunqing Li, and Shoushan Fan. "Nanotechnology: spinning continuous carbon nanotube yarns." *Nature* 419.6909 (2002): 801-801.

[184] Zhang, Mei, Ken R. Atkinson, and Ray H. Baughman. "Multifunctional carbon nanotube yarns by downsizing an ancient technology." *Science* 306.5700 (2004): 1358-1361.

[185] Zhang, Qiang, et al. "Energy-absorbing hybrid composites based on alternate carbon-nanotube and inorganic layers." *Advanced Materials* 21.28 (2009): 2876-2880.

[186] Cao, Anyuan, et al. "Super-compressible foamlike carbon nanotube films." *Science* 310.5752 (2005): 1307-1310.

[187] Zhao, Meng-Qiang, et al. "Improvement of oil adsorption performance by a sponge-like natural vermiculite-carbon nanotube hybrid." *Applied Clay Science* 53.1 (2011): 1-7.

[188] Qu, Liangti, et al. "Carbon nanotube arrays with strong shear binding-on and easy normal lifting-off." *Science* 322.5899 (2008): 238-242.

[189] Seah, Choon-Ming, Siang-Piao Chai, and Abdul Rahman Mohamed. "Synthesis of aligned carbon nanotubes." *Carbon* 49.14 (2011): 4613-4635.

[190] Hata, Kenji, et al. "Water-assisted highly efficient synthesis of impurity-free single-walled carbon nanotubes." *Science* 306.5700 (2004): 1362-1364.

[191] Matarredona, Olga, et al. "Dispersion of single-walled carbon nanotubes in aqueous solutions of the anionic surfactant NaDDBS." *The Journal of Physical Chemistry B* 107.48 (2003): 13357-13367.

[192] Li, W. Z., et al. "Large-scale synthesis of aligned carbon nanotubes." *Science* 274.5293 (1996): 1701.

[193] Ren, Z. F., et al. "Synthesis of large arrays of well-aligned carbon nanotubes on glass." *Science* 282.5391 (1998): 1105-1107.

[194] de Villoria, R. Guzmán, et al. "High-yield growth of vertically aligned carbon nanotubes on a continuously moving substrate." *Nanotechnology* 20.40 (2009): 405611.

[195] Guzmán de Villoria, Roberto, A. John Hart, and Brian L. Wardle. "Continuous high-yield production of vertically aligned carbon nanotubes on 2D and 3D substrates." *ACS nano* 5.6 (2011): 4850-4857.

[196] Zhang, Qiang, et al. "Vertically aligned carbon nanotube arrays grown on a lamellar catalyst by fluidized bed catalytic chemical vapor deposition." *Carbon* 47.11 (2009): 2600-2610.

[197] Zhang, Qiang, et al. "Comparison of vertically aligned carbon nanotube array intercalated production among vermiculites in fixed and fluidized bed reactors." *Powder Technology* 198.2 (2010): 285-291.

[198] Zhao, Meng-Qiang, et al. "Large scale intercalated growth of short aligned carbon nanotubes among vermiculite layers in a fluidized bed reactor." *Journal of Physics and Chemistry of Solids* 71.4 (2010): 624-626.

[199] Zhang, Qiang, et al. "Mass production of aligned carbon nanotube arrays by fluidized bed catalytic chemical vapor deposition." *Carbon* 48.4 (2010): 1196-1209.

[200] Pint, Cary L., et al. "Synthesis of high aspect-ratio carbon nanotube “flying carpets” from nanostructured flake substrates." *Nano letters* 8.7 (2008): 1879-1883.

[201] Xiang, Rong, et al. "Large area growth of aligned CNT arrays on spheres: towards large scale and continuous production." *Chemical Vapor Deposition* 13.10 (2007): 533-536.

[202] Xiang, Rong, et al. "Large area growth of aligned CNT arrays on spheres: cost performance and product control." *Materials Letters* 63.1 (2009): 84-87.

[203] Zhang, Qiang, et al. "Radial growth of vertically aligned carbon nanotube arrays from ethylene on ceramic spheres." *Carbon* 46.8 (2008): 1152-1158.

[204] Philippe, Régis, et al. "An original growth mode of MWCNTs on alumina supported iron catalysts." *Journal of Catalysis* 263.2 (2009): 345-358.

[205] An, Feng, et al. "Preparation of vertically aligned carbon nanotube arrays grown onto carbon fiber fabric and evaluating its wettability on effect of composite." *Applied Surface Science* 258.3 (2011): 1069-1076.

[206] Bakandritsos, A., A. Simopoulos, and D. Petridis. "Carbon nanotube growth on a swellable clay matrix." *Chemistry of materials* 17.13 (2005): 3468-3474.

[207] Manikandan, Dhanagopal, et al. "Carbon nanotubes rooted montmorillonite (CNT-MM) reinforced nanocomposite membrane for PEM fuel cells." *Materials Science and Engineering: B* 177.8 (2012): 614-618.

[208] Manikandan, Dhanagopal, et al. "Montmorillonite–carbon nanotube nanofillers by acetylene decomposition using catalytic CVD." *Applied Clay Science* 71 (2013): 37-41.

[209] Moura, Flávia CC, and Rochel M. Lago. "Catalytic growth of carbon nanotubes and nanofibers on vermiculite to produce floatable hydrophobic “nanosponges” for oil spill remediation." *Applied Catalysis B: Environmental* 90.3 (2009): 436-440.

[210] Purceno, Aluir D., et al. "Carbon nanostructures-modified expanded vermiculites produced by chemical vapor deposition from ethanol." *Applied Clay Science* 54.1 (2011): 15-19.

[211] Huh, Yoon, et al. "Controlled growth of carbon nanotubes over cobalt nanoparticles by thermal chemical vapor deposition." *Journal of materials chemistry* 13.9 (2003): 2297-2300.

[212] Kim, Nam Seo, et al. "Vertically aligned carbon nanotubes grown by pyrolysis of iron, cobalt, and nickel phthalocyanines." *The Journal of Physical Chemistry B* 107.35 (2003): 9249-9255.

[213] Saito, Yahachi, et al. "Interlayer spacings in carbon nanotubes." *Physical Review B* 48.3 (1993): 1907.

[214] Chiodarelli, Nicolò, et al. "Correlation between number of walls and diameter in multiwall carbon nanotubes grown by chemical vapor deposition." *Carbon* 50.5 (2012): 1748-1752.

[215] Mattevi, Cecilia, et al. "In-situ X-ray photoelectron spectroscopy study of catalyst−support interactions and growth of carbon nanotube forests." *The Journal of Physical Chemistry C* 112.32 (2008): 12207-12213.

[216] Kaneko, Akira, et al. "Comparative study of catalytic activity of iron and cobalt for growing carbon nanotubes on alumina and silicon oxide." *The Journal of Physical Chemistry C* 116.49 (2012): 26060-26065.

[217] Barzegar, Hamid R., et al. "Simple Dip-Coating Process for the Synthesis of Small Diameter Single-Walled Carbon Nanotubes□ Effect of Catalyst Composition and Catalyst Particle Size on Chirality and Diameter." *The Journal of Physical Chemistry C* 116.22 (2012): 12232-12239.

[218] Brown, Ronald, Maureen E. Cooper, and David A. Whan. "Temperature programmed reduction of alumina-supported iron, cobalt and nickel bimetallic catalysts." *Applied Catalysis* 3.2 (1982): 177-186.

[219] Tricker, M. J., P. P. Vaishnava, and D. A. Whan. "57 Iron transmission and conversion electron mössbauer spectroscopic characterization of iron-cobalt ammonia synthesis catalysts." *Applied Catalysis* 3.3 (1982): 283-295.

[220] Hou, Ye, et al. "Functionalized few-walled carbon nanotubes for mechanical reinforcement of polymeric composites." *ACS nano* 3.5 (2009): 1057-1062.

[221] J. E. Brown, M.S. Dissertation, University of Oklahoma, 2011.

[222] Nagaraju, N., et al. "Alumina and silica supported metal catalysts for the production of carbon nanotubes." *Journal of molecular catalysis A: Chemical* 181.1 (2002): 57-62.

[223] Zecevic, Jovana, et al. "Nanoscale intimacy in bifunctional catalysts for selective conversion of hydrocarbons." *Nature* 528.7581 (2015): 245-248.

[224] Resasco, D. E., and G. L. Haller. "A model of metal-oxide support interaction for Rh on TiO 2." *Journal of Catalysis* 82.2 (1983): 279-288.

[225] An, Kwangjin, et al. "Enhanced CO oxidation rates at the interface of mesoporous oxides and Pt nanoparticles." *Journal of the American Chemical Society* 135.44 (2013): 16689-16696.

[226] An, Kwangjin, et al. "High-Temperature Catalytic Reforming of n-Hexane over Supported and Core–Shell Pt Nanoparticle Catalysts: Role of Oxide–Metal Interface and Thermal Stability." *Nano letters* 14.8 (2014): 4907-4912.

[227] Baker, L. Robert, et al. "Furfuraldehyde hydrogenation on titanium oxide-supported platinum nanoparticles studied by sum frequency generation vibrational spectroscopy: Acid–base catalysis explains the molecular origin of strong metal–support interactions." *Journal of the American Chemical Society* 134.34 (2012): 14208-14216.

[228] Kennedy, Griffin, L. Robert Baker, and Gabor A. Somorjai. "Selective Amplification of C□ O Bond Hydrogenation on Pt/TiO2: Catalytic Reaction and Sum-Frequency Generation Vibrational Spectroscopy Studies of Crotonaldehyde Hydrogenation." *Angewandte Chemie* 126.13 (2014): 3473-3476.

[229] Held, Georg. "The interplay between geometry, electronic structure, and reactivity of Cu-Ni bimetallic (111) surfaces." *Applied Physics A* 76.5 (2003): 689-700.

[230] Hammer, B., and J. K. Nørskov. "Electronic factors determining the reactivity of metal surfaces." *Surface Science* 343.3 (1995): 211-220.

[231] Nørskov, Jens K., et al. "Density functional theory in surface chemistry and catalysis." *Proceedings of the National Academy of Sciences* 108.3 (2011): 937-943.

[232] Hammer, Bjørk, and Jens Kehlet Nørskov. "Theoretical surface science and catalysis—calculations and concepts." *Advances in catalysis* 45 (2000): 71-129.

[233] Primet, M., M. V. Mathieu, and W. M. H. Sachtler. "Infrared spectra of carbon monoxide adsorbed on silica-supported PdAg alloys." *Journal of Catalysis* 44.2 (1976): 324-327.

[234] Toolenaar, F. J. C. M., F. Stoop, and V. Ponec. "On electronic and geometric effects of alloying: An infrared spectroscopic investigation of the adsorption of carbon monoxide on platinum-copper alloys." *Journal of Catalysis* 82.1 (1983): 1-12.

[235] Hendrickx, H. A. C. M., C. Des Bouvrie, and V. Ponec. "On the electronic competition effect upon CO adsorption on metals." *Journal of Catalysis* 109.1 (1988): 120-125.

[236] Primet, Michel. "Electronic transfer and ligand effects in the infrared spectra of adsorbed carbon monoxide." *Journal of Catalysis* 88.2 (1984): 273-282.

[237] Sachtler, Wolfgang MH. "The Second Rideal Lecture. What makes a catalyst selective?." *Faraday Discussions of the Chemical Society* 72 (1981): 7-31.

[238] Chorkendorff, Ib, and Johannes W. Niemantsverdriet. *Concepts of modern catalysis and kinetics*. John Wiley & Sons, 2006.

[239] Idriss, Hicham, and Mark A. Barteau. "Active sites on oxides: from single crystals to catalysts." *Advances in Catalysis* 45 (2000): 261-331.

[240] Haller, Gary L., and Daniel E. Resasco. "Metal-support interaction: group VIII metals and reducible oxides." *Adv. Catal* 36 (1989): 173-235.

[241] Tauster, S. J., S. C. Fung, and R. L. Garten. "Strong metal-support interactions. Group 8 noble metals supported on titanium dioxide." *Journal of the American Chemical Society* 100.1 (1978): 170-175.

[242] Tauster, S. J. "Strong metal-support interactions." *Accounts of Chemical Research* 20.11 (1987): 389-394.

[243] Haubrich, Jan, Efthimios Kaxiras, and Cynthia M. Friend. "The Role of Surface and Subsurface Point Defects for Chemical Model Studies on TiO2: A First-Principles Theoretical Study of Formaldehyde Bonding on Rutile TiO2 (110)." *Chemistry–A European Journal* 17.16 (2011): 4496-4506.

[244] Benz, Lauren, et al. "Acrolein coupling on reduced TiO 2 (110): The effect of surface oxidation and the role of subsurface defects." *Surface Science* 603.7 (2009): 1010-1017.

[245] Rekoske, James E., and Mark A. Barteau. "Isothermal reduction kinetics of titanium dioxide-based materials." *The Journal of Physical Chemistry B* 101.7 (1997): 1113-1124.

[246] Cheng, Hongzhi, and Annabella Selloni. "Surface and subsurface oxygen vacancies in anatase TiO 2 and differences with rutile." *Physical Review B* 79.9 (2009): 092101.

[247] Komaya, Takashi, et al. "Effects of Dispersion and Metal-Metal Oxide Interactions on Fischer-Tropsch Synthesis over Ru/TiO 2 and TiO 2-Promoted Ru/SiO 2." *Journal of Catalysis* 150.2 (1994): 400-406.

[248] Haller, Gary L., and Daniel E. Resasco. "Metal-support interaction: group VIII metals and reducible oxides." *Adv. Catal* 36 (1989): 173-235.

[249] Flesner, RAYMOND L., and JOHN L. Falconer. "The role of spillover in carbon monoxide hydrogenation over alumina-supported platinum." *Journal of Catalysis* 139.2 (1993): 421-434.

[250] Robbins, John L., and Elise Marucchi-Soos. "Evidence for multiple carbon monoxide hydrogenation pathways on platinum alumina." *The Journal of Physical Chemistry* 93.8 (1989): 2885-2888.

[251] Kitiyanan, B., et al. "Controlled production of single-wall carbon nanotubes by catalytic decomposition of CO on bimetallic Co–Mo catalysts." *Chemical Physics Letters* 317.3 (2000): 497-503.

[252] Herrera, Jose E., et al. "Relationship between the structure/composition of Co–Mo catalysts and their ability to produce single-walled carbon nanotubes by CO disproportionation." *Journal of Catalysis* 204.1 (2001): 129-145.

[253] Shi, Dachuan, et al. "Role of water on the surface-guided growth of horizontally aligned single-walled carbon nanotubes on quartz." *Chemical Physics Letters* 525 (2012): 82-86.

[254] Zhang, Liang, Yongqiang Tan, and Daniel E. Resasco. "Controlling the growth of vertically oriented single-walled carbon nanotubes by varying the density of Co Mo catalyst particles." *Chemical physics letters* 422.1 (2006): 198-203.

[255] Zhang, Liang, et al. "Influence of a top crust of entangled nanotubes on the structure of vertically aligned forests of single-walled carbon nanotubes." *Chemistry of materials* 18.23 (2006): 5624-5629.

[256] Qu, Liangti, and Liming Dai. "Polymer-masking for controlled functionalization of carbon nanotubes." *Chem. Commun.* 37 (2007): 3859-3861.

[257] Peng, Qiang, et al. "Asymmetrically charged carbon nanotubes by controlled functionalization." *ACS nano* 2.9 (2008): 1833-1840.

[258] Poenitzsch, Vasiliki Z., et al. "Freestanding foils of nanotube arrays fused with metals." *Journal of Materials Science* 49.20 (2014): 7080-7086.

[259] Prins, Roel. "Hydrogen spillover. Facts and fiction." *Chemical reviews* 112.5 (2012): 2714-2738.

[260] Conner Jr, W. Curtis, and John L. Falconer. "Spillover in heterogeneous catalysis." *Chemical Reviews* 95.3 (1995): 759-788.

[261] Rozanov, Valerii Vasil'evich, and Oleg Valentinovich Krylov. "Hydrogen spillover in heterogeneous catalysis." *Russian chemical reviews* 66.2 (1997): 107-119.

[262] Khoobiar, S. "Particle to particle migration of hydrogen atoms on platinum—alumina catalysts from particle to neighboring particles." *The Journal of Physical Chemistry* 68.2 (1964): 411-412.

[263] Levy, R. B., and M. Boudart. *Journal of Catalysis* 32.2 (1974): 304-314.

[264] Chen, Liang, et al. “On the mechanism of hydrogen spillover in MoO3.” *The Journal of Physical Chemsitry C* 112.6 (2008): 1755-1758.

[265] Xi, Yongjie, Qingfan Zhang, and Hansong Cheng. "Mechanism of Hydrogen Spillover on WO3 (001) and Formation of H x WO3 (x= 0.125, 0.25, 0.375, and 0.5)." *The Journal of Physical Chemistry C* 118.1 (2013): 494-501.

[266] Prins, R., V. K. Palfi, and M. Reiher. "Hydrogen spillover to nonreducible supports." *The Journal of Physical Chemistry C* 116.27 (2012): 14274-14283.

[267] Schlatter, J. C., and M. Boudart. "Hydrogenation of ethylene on supported platinum." *Journal of Catalysis* 24.3 (1972): 482-492.

[268] Beaumont, Simon K., et al. "A nanoscale demonstration of hydrogen atom spillover and surface diffusion across silica using the kinetics of CO2 methanation catalyzed on spatially separate Pt and Co nanoparticles." *Nano letters* 14.8 (2014): 4792-4796.

[269] Chen, Liang, et al. "Mechanistic study on hydrogen spillover onto graphitic carbon materials." *The Journal of Physical Chemistry C* 111.51 (2007): 18995-19000.

[270] Sha, Xianwei, et al. "Dynamics of hydrogen spillover on carbon-based materials." *The Journal of Physical Chemistry C* 112.44 (2008): 17465-17470.

[271] Chen, Liang, et al. "A mechanistic study of hydrogen spillover in MoO3 and carbon-based graphitic materials." *Journal of Physics: Condensed Matter* 20.6 (2008): 064223.

[272] Bhowmick, Ranadeep, et al. "Hydrogen spillover in Pt-single-walled carbon nanotube composites: formation of stable C− H bonds." *Journal of the American Chemical Society* 133.14 (2011): 5580-5586.

[273] Mitchell, Philip CH, et al. "Hydrogen spillover on carbon-supported metal catalysts studied by inelastic neutron scattering. Surface vibrational states and hydrogen riding modes." *The Journal of Physical Chemistry B* 107.28 (2003): 6838-6845.

[274] Nikitin, Anton, et al. "Hydrogen storage in carbon nanotubes through the formation of stable CH bonds." *Nano Letters* 8.1 (2008): 162-167.

[275] Psofogiannakis, George M., and George E. Froudakis. "DFT study of hydrogen storage by spillover on graphite with oxygen surface groups." *Journal of the American Chemical Society* 131.42 (2009): 15133-15135.

[276] Singh, Priyanka, et al. "Enhancing the hydrogen storage capacity of Pd-functionalized multi-walled carbon nanotubes." *Applied Surface Science* 258.8 (2012): 3405-3409.

[277] Wang, Lifeng, et al. "Effect of surface oxygen groups in carbons on hydrogen storage by spillover." *Industrial & Engineering Chemistry Research* 48.6 (2009): 2920-2926.

[278] Li, Qixiu, and Angela D. Lueking. "Effect of surface oxygen groups and water on hydrogen spillover in Pt-doped activated carbon." *The Journal of Physical Chemistry C* 115.10 (2011): 4273-4282.

[279] Achtyl, Jennifer L., et al. "Aqueous proton transfer across single-layer graphene." *Nature communications* 6 (2015).

[280] Han, Sang Soo, Hyungjun Kim, and Noejung Park. "Effect of shuttling catalyst on the migration of hydrogen adatoms: A strategy for the facile hydrogenation of graphene." *The Journal of Physical Chemistry C* 115.50 (2011): 24696-24701.

[281] Elliott, Douglas C., and Todd R. Hart. "Catalytic hydroprocessing of chemical models for bio-oil." *Energy & Fuels* 23.2 (2008): 631-637.

[282] He, Ronghai, et al. "Influence of pyrolysis condition on switchgrass bio-oil yield and physicochemical properties." *Bioresource technology* 100.21 (2009): 5305-5311.

[283] Montané, Daniel, et al. "High-temperature dilute-acid hydrolysis of olive stones for furfural production." *Biomass and Bioenergy* 22.4 (2002): 295-304.

[284] Zhu, Yu-Lei, et al. "A new strategy for the efficient synthesis of 2-methylfuran and γ-butyrolactone." *New Journal of Chemistry* 27.2 (2003): 208-210.

[285] Yang, Jun, et al. "Effects of calcination temperature on performance of Cu–Zn–Al catalyst for synthesizing γ-butyrolactone and 2-methylfuran through the coupling of dehydrogenation and hydrogenation." *Catalysis Communications* 5.9 (2004): 505-510.

[286] Omotoso, Taiwo. *Conversion of Model Bio-Oil Compounds Over Metal Oxides and Supported Metal Catalysts.* Diss. University of Oklahoma, 2015. Web. 19 April. 2016.

[287] Yang, Yanliang, et al. "Conversion of furfural into cyclopentanone over Ni–Cu bimetallic catalysts." *Green Chemistry* 15.7 (2013): 1932-1940.

[288] Chheda, Juben N., and James A. Dumesic. "An overview of dehydration, aldol-condensation and hydrogenation processes for production of liquid alkanes from biomass-derived carbohydrates." *Catalysis Today* 123.1 (2007): 59-70.

[289] West, Ryan M., et al. "Catalytic conversion of biomass-derived carbohydrates to fuels and chemicals by formation and upgrading of mono-functional hydrocarbon intermediates." *Catalysis Today* 147.2 (2009): 115-125.

[290] Sitthisa, Surapas, and Daniel E. Resasco. "Hydrodeoxygenation of furfural over supported metal catalysts: a comparative study of Cu, Pd and Ni." *Catalysis letters* 141.6 (2011): 784-791.

[291] Sitthisa, Surapas, et al. "Kinetics and mechanism of hydrogenation of furfural on Cu/SiO 2 catalysts." *Journal of catalysis* 277.1 (2011): 1-13.

[292] Sitthisa, Surapas, et al. "Conversion of furfural and 2-methylpentanal on Pd/SiO 2 and Pd–Cu/SiO 2 catalysts." *Journal of Catalysis* 280.1 (2011): 17-27.

[293] Sitthisa, Surapas, Wei An, and Daniel E. Resasco. "Selective conversion of furfural to methylfuran over silica-supported Ni Fe bimetallic catalysts." *Journal of Catalysis* 284.1 (2011): 90-101.

[294] Nikitin, Anton, Zhiyong Zhang, and Anders Nilsson. "Energetics of C− H Bonds Formed at Single-Walled Carbon Nanotubes." *Nano letters* 9.4 (2009): 1301-1306.

[295] Briggs, N. M., and S. P. Crossley. "Rapid growth of vertically aligned multi-walled carbon nanotubes on a lamellar support." *RSC Advances* 5.102 (2015): 83945-83952.

[296] Campbell, Charles T. "The energetics of supported metal nanoparticles: relationships to sintering rates and catalytic activity." *Accounts of chemical research* 46.8 (2013): 1712-1719.

[297] Campbell, Charles T., and Jason RV Sellers. "Anchored metal nanoparticles: Effects of support and size on their energy, sintering resistance and reactivity." *Faraday discussions* 162 (2013): 9-30.

[298] Lu, Ping, Charles T. Campbell, and Younan Xia. "A sinter-resistant catalytic system fabricated by maneuvering the selectivity of SiO2 deposition onto the TiO2 surface versus the Pt nanoparticle surface." *Nano letters* 13.10 (2013): 4957-4962.

[299] Campbell, Charles T. "The energetics of supported metal nanoparticles: relationships to sintering rates and catalytic activity." *Accounts of chemical research* 46.8 (2013): 1712-1719.

[300] Dai, Yunqian, et al. "A Sinter-Resistant Catalytic System Based on Platinum Nanoparticles Supported on TiO2 Nanofibers and Covered by Porous Silica." *Angewandte Chemie International Edition* 49.44 (2010): 8165-8168.

[301] Sinnott, S. B., et al. "Model of carbon nanotube growth through chemical vapor deposition." *Chemical Physics Letters* 315.1 (1999): 25-30.

[302] Scholz, David, Christof Aellig, and Ive Hermans. "Catalytic Transfer Hydrogenation/Hydrogenolysis for Reductive Upgrading of Furfural and 5-(Hydroxymethyl) furfural." *ChemSusChem* 7.1 (2014): 268-275.

[303] Sitthisa, Surapas. "Conversion of Oxygenates from Biomass-Derived Compounds Over Supported Metal Catalysts." Order No. 3507879 The University of Oklahoma, 2012. Ann Arbor: *ProQuest.* Web. 5 May 2016.

[304] Boonyasuwat, Sunya, et al. "Conversion of guaiacol over supported Ru catalysts." *Catalysis letters* 143.8 (2013): 783-791.

Appendix A1: Hierarchical Zeolites for Enhanced Reaction Selectivity

Introduction

Zeolites have become an important material in catalysis and have been used for a wide range of reactions. Zeolites are used in fluidized catalytic cracking where low value high molecular weight hydrocarbons are converted to high value olefinic gases, gasoline and diesel oil.[305,306] However, since zeolites are composed of solely microspores intracrystalline diffusion limitations can limit the applicability of zeolites unless micropores are added.[312] Hierarchical zeolites allow for the diffusion paths to be modified which can change reaction selectivity.[307,308,309,310,311,312] Modification of the diffusion path can be done to increase the ability of molecules to diffuse in and out of the zeolite so that the molecules do not become trapped.

Several approaches have been taken to create hierarchical zeolites by using templates and chemicals. One approach is to etch away portions of the zeolite with an alkaline solution. The alkaline solution attacks defects on the zeolite creating mesopores.[313,314,315,316] However, this method suffers from the inability to control where and how the alkaline solution etches the zeolites. A different approach Mesoporous zeolites have been synthesized using surfactants which create rod-like micelles creating the well-known MCM-41[317,318] and SBA 15.[319,320] However, these catalysts can have low acidity due to the synthesis. Another approach is to construct zeolites using a template, such as carbon nanotubes.[321,322,323,324,325,326] Carbon nanotubes have also been used to construct oxide nanotubes.[327,328,329,330,331,332] By building the zeolite around the carbon nanotube a pore is formed and then carbon can then be burned away leaving the

zeolite with a pores the size of the carbon nanotubes. This approach suffers from the form in which carbon nanotubes and carbon particulates are received. Particulates of carbon can agglomerate together and can become trapped if the zeolite grows entirely around the carbon wasting zeolite material. Carbon nanotubes are typically in a random orientation and agglomerated together. Therefore, it is difficult to control the position of the pores and pore spacing. Carbon nanotubes can be grown vertically, however, approaches taken so far have been with the carbon nanotubes grown on a silicon wafer, which offers low surface area and is difficult to scale up.[333],[334] Therefore, there is a necessity to create a process which is scalable and can finely control the pores properties.

In this report we have created a hierarchical zeolite using vertically aligned multi-walled carbon nanotubes (VMWNTs) in a scalable method. This is accomplished by growing VMWNTs between mica sheets which was initially proven by Wei's group[335] and then improved upon by our group.[336] Zeolite crystals are grown on the outside of VMWNTs and then the VMWNTs are removed by oxidation. The result is a hierarchical zeolite with large pores the diameter and width of the VMWNTs. The VMWNTs are grown between mica sheets and this keeps the ends of the VMWNTs open allowing for molecules to diffuse into the large pores. By varying the amount of VMWNTs added to the solution for zeolite growth the density of zeolite crystals around the VMWNTs can be changed. Zeolite rods can be made or a zeolite block with large pores can be made. This hierarchical zeolite has enhanced selectivity for cracking bulky molecules such as triisopropylbenzene. Zeolite with solely micropores results in molecules resulting from cracking of triisopropylbenzene becoming trapped in the

zeolite pores and carbon deposited on the outside of the catalyst resulting in catalyst deactivation. With the the hierarchical zeolite the triisopropylbenzene and the products formed from cracking can diffuse in and out of the zeolite due to the large pores. This prolongs catalyst life and enhances reaction selectivity.

Experimental Details

Zeolite synthesis, reactions, surface area measurements and x-ray diffraction were performed by Abhishek Gumidyala.

VMWNTs Synthesis

VMWNTs were grown between mica sheets by following the conditions to grown sample HRRx650D-D.

Zeolite Synthesis:

Zeolite precursor was prepared with a gel composition of 9TPAOH/0.16NaOH/Al/25Si/495H2O/100EtOH.[337] The reagents used for the synthesis are tetraethyl orthosilicate (98%, Sigma-Aldrich), tetrapropylammonium hydroxide (40% W/W, Alfa-Aesar), aluminum isopropoxide (98%, Sigma-Aldrich), sodium hydroxide (>98%, Sigma-Aldrich) and double distilled water. Precursor gel was stirred at 500 rpm for 24hrs for incubation. Several batches of this gel were prepared and for each batch 500 mg, 750 mg, 1000 mg or 2000 mg of CNT's were added and stirred for 1 hr. The samples made with 500 mg are labelled Z-CNT-1, 750 mg are labelled Z-CNT-2, 1000 mg Z-CNT-3, and 2000 mg Z-CNT-4. Each batch was transferred into a Parr vessel and left in the oven at 165 °C for 120 hrs. The obtained sample after

synthesis was washed with water several times. The obtained cake was dried for twelve hours at 85 ˚C in an oven. The dried sample is ion-exchanged from sodium form to ammonia form with 2M ammonium nitrate solution at 80˚C for three hours. The ion-exchange procedure was repeated five times to ensure complete exchange. This was followed by washing with double distilled water three times and drying for twelve hours at 85˚C. Obtained ammonium form zeolite was calcined at 600˚C (ramp rate 2 ˚C/min) for five hours to burn off the CNT's and to get proton form of zeolite.

Nitrogen Adsorption for Surface Area Measurements

A Micrometrics ASAP 2020 Surface Area and Porosity Analyzer (Micrometrics; Norcross, GA) was used to perform nitrogen adsorption experiments to determine the total pore volume, micropore volume, and by difference the mesopore volume of the catalysts.

IPA-TPD

Isopropyl amine (IPA) temperature-programmed desorption (TPD) is a proven technique for estimating the number of Brønsted acid sites in H-form zeolites.[338] IPA reacts on a Brønsted acid site of H-zeolite to produce propylene and ammonia. IPA-TPD experiments were done on all the H-Zeolite samples used in this study to investigate the amount of Brønsted acid sites. 50mg of catalyst was loaded into a quartz reactor (1/4" OD) and flushed at 300˚C for two hours with helium as carrier gas (20ml/min). After flushing the sample the temperature was reduced to 100˚C and 2 μL pulses of IPA were injected into the reactor through a septum via a syringe. Mass to charge ratio (m/e) of 44 and 58 were tracked at exit of the reactor with a MKS Cirrus 200 quadrupole mass spectrometer (MS), to ensure saturation of all the acid sites in the

catalyst bed with IPA. Pulses of IPA were continued until a constant signal m/e=44 and 58 was observed. After adsorption of IPA on to the catalyst bed, it was flushed with carrier gas (20ml/min) at 100˚C for 4hrs to remove all the physically absorbed IPA. Flushing was followed by a temperature ramp from 100˚C to 600˚C at a rate of 10˚C/min. The products desorbing from the reactor with temperature ramp were tracked by MS. Quantification of the products was done by injecting standards and propylene gas pulsed using a sample loop.

X-Ray Diffraction

For checking the crystallinity of the sample, X-ray diffraction studies using Rigaku automatic diffractor (Model D-MAX A) with a curved crystal monochromator were performed. A flat surface of the well ground samples was prepared on a plastic slide for the experiments. The instrument has Cu-Kα as a radiation source and was operated at 40kV and 35 mA between the angle range of 5-60˚.

Reaction Studies

Flow reaction studies are performed in a quartz tube reactor (1/4" OD) at 400 °C and at atmospheric pressure. The H-zeolite catalyst is diluted with acid washed glass beads packed in the reactor between plugs of quartz wool. The inlet of the reactor is heated to create a vaporization zone and the outlet stream of the reactor as well as the six port valve for injection to the gas chromatograph (GC) were heated to 250 °C to prevent condensation. The temperature of the catalyst bed was controlled by a thermocouple attached to the outer wall of the reactor. The catalyst was preheated and flushed with helium (125 mL/min) for one hour at 400 °C before introducing the reactant using a syringe pump. The products were analyzed using a HP-6890GC

equipped with a flame ionization detector and innowax column (30m and 0.25 μm). Reaction products were condensed in a sample bubbler using ice and water as a coolant medium for identification via GCMS.

Probe chemical reactions are used to confirm the activity and stability of CNT-HZSM-5 in comparison of commercial HZSM-5. Triisopropylbenzene (TIPB) is a bulky molecule with three reactive isopropyl groups and a kinetic diameter of 8.5 Å, which is larger than the pores of MFI (5.6 Å). This limits the reactivity of TIPB to the external surface of the zeolite. Commercial zeolite which does not have any mesoporisity is to have activity only due to external sites if any present. On an equivalent acid site basis, the activity on commercial zeolite is limited to the surface activity. In contrast CNT-HZSM-5 should have stable activity due to high mesoporisity reducing the diffusion limitations. Thus a dramatic reduction in the reactivity of TIPB over H-ZSM-5 is seen compared to CNT-HZSM-5

Electron Microscopy

Scanning electron microscopy (SEM) was performed with a Zeis Neon 40 EsB scanning electron miscrocpe operating at an accelerating voltage of 2 kV or 5 kV. The accelerating voltage was chosen to minimize charging of the sample due to its non-conductive nature. Transmission electorn microscopy was performed with a JEOL 2000 FX equipped with a LaB_6 filament operating at 2000 kV.

Results and Discussion

Catalyst

VMWNTs deposited in a solution for growth of zeolites results in a layer of zeolites on the outside of the VMWNTs, Figure 60. After growth of the zeolites the

VMWNTs can be removed by heating the sample to 600°C at which point carbon nanotubes decompose.[339]

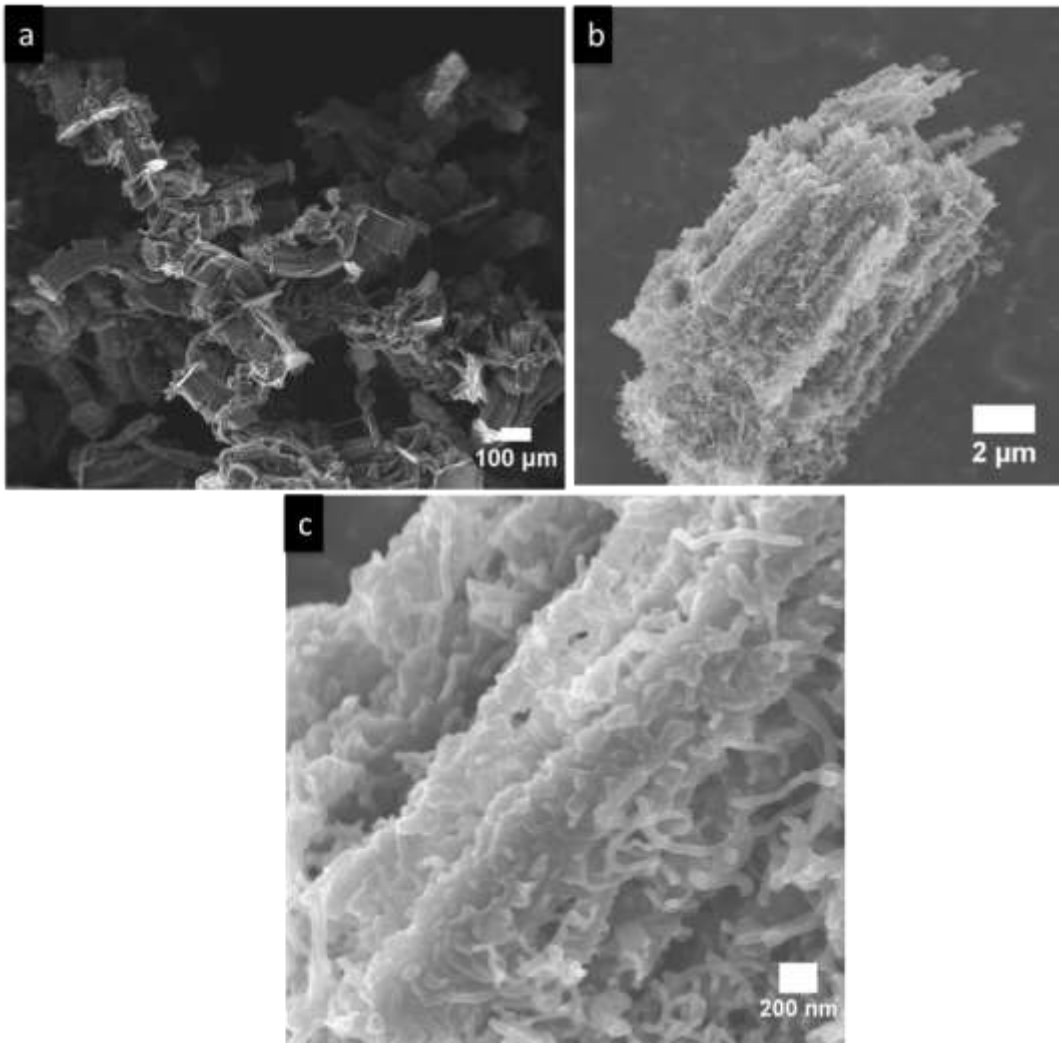

Figure 60: (a) VMWNTs grown between mica sheets and (b &c) after growth of zeolites on the VMWNTs.

The zeolites remain and the structure is maintained after the VMWNTs have been decomposed, Figure 61. As can be seen in the SEM images the zeolites maintain the shape of the VMWNTs and holes can be seen where possibly the ends of the carbon nanotubes protruded. This observation along with with TEM images, Figure 62, indicates after removal of the carbon nanotubes the zeolites do not collapse on

themselves and retain the spacing the VMWNTs once provided. This is evident since the diameter of the pores created after removal of the VMWNTs are comparable with the outer diameter of the VMWNTs.

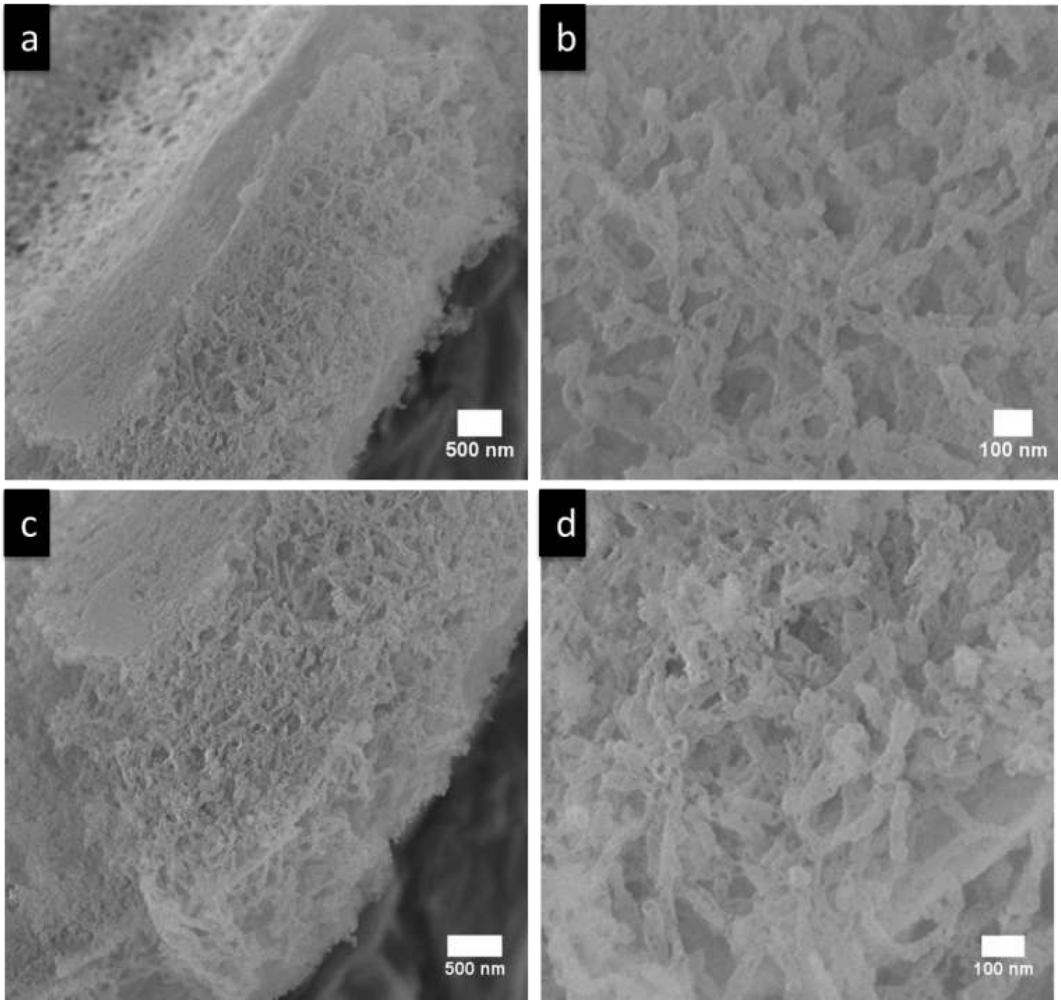

Figure 61: Images of zeolites after burning out the carbon nanotube template. (a) Low magnification image of the the middle of the VMWNT array (b) high magnification image of the middle of the VMWNT array, (c) low magnication image of the end of a VMWNT array, and (d) high magnification image of the end of the VMWNT array.

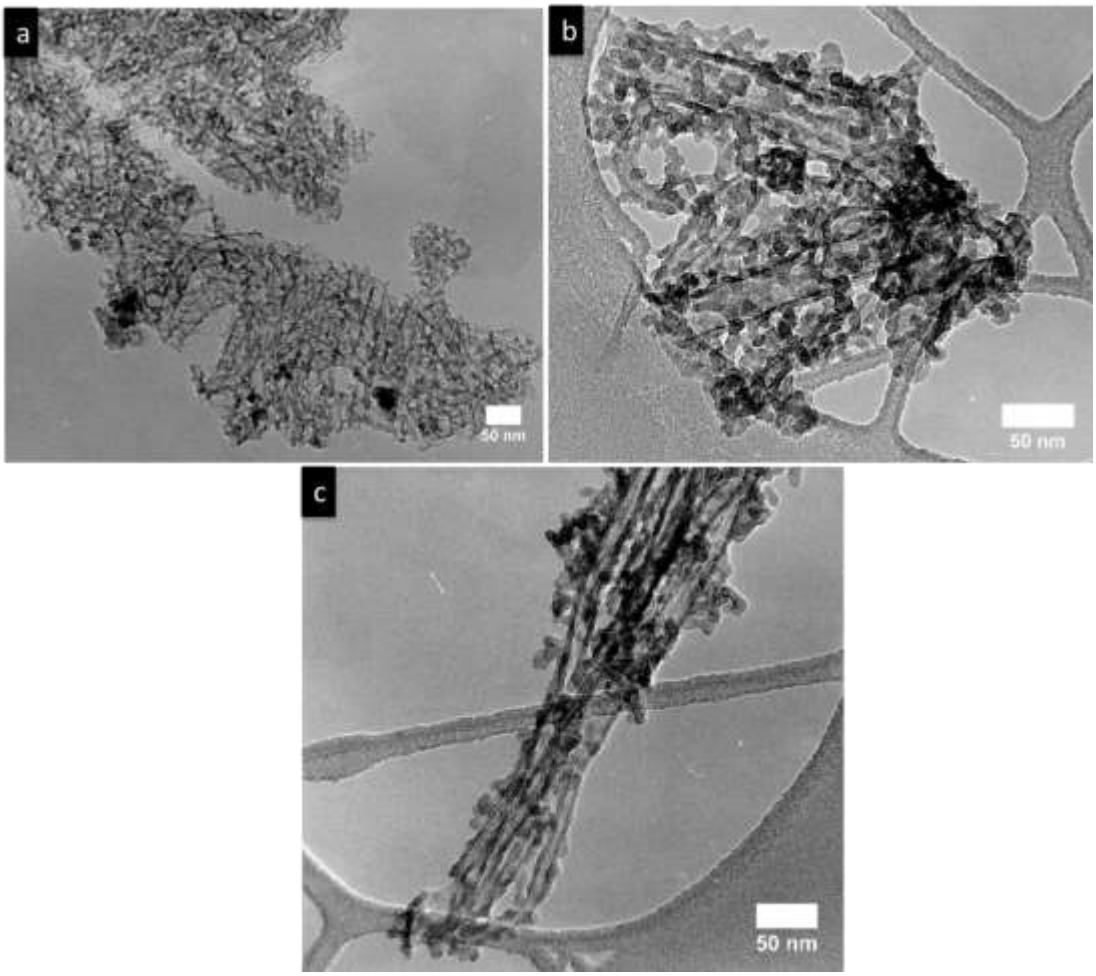

Figure 62: TEM images of sample Z-CNT-3 (a) low magnification showing arrays of zeolites and (b & c) high magniciation showing the channels created where the VMWNTs once resided.

From nitrogen adsorption experiments the surface area and presence of micropores and mesopores can be measured using the BET equation, Figure 63. From the nitrogen adsorption experiments the surface area was 309 m^2/g with a micropore volume of 0.0321 cm^2/g and a mesopore volume of 0.923 cm^2/g. The average pore diameter was 11.8 nm, which is an average of the mesoporous and microporous pores present, Figure 64.

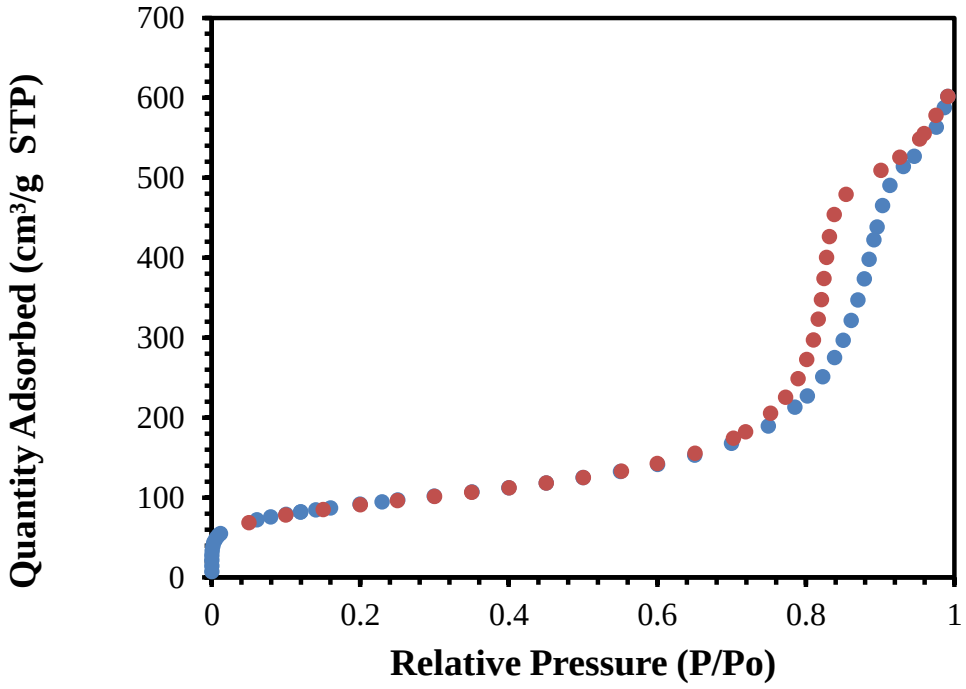

Figure 63: Nitrogen adsorption used to calculate the volume of the micropores and mesopores for sample Z-CNT-1.

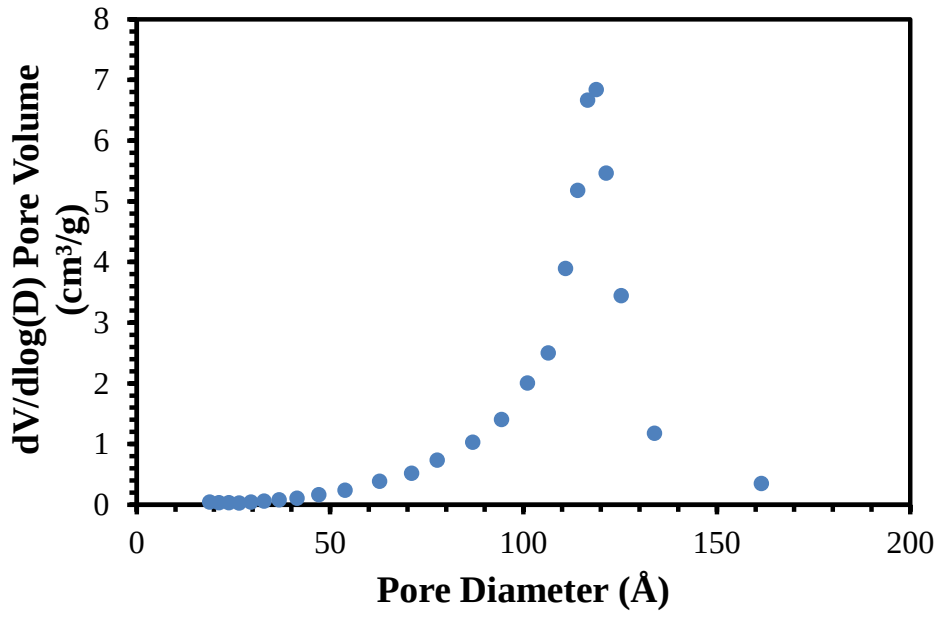

Figure 64: Average pore diameter of the Z-CNT-1 sample.

Reactions

To determine if our hierarchical zeolite changes the diffusion paths which allow for more selective cracking of bulky molecules compared to microporous zeolites triispropylbenzene (TIPB) was used as a probe molecule. Using HZSM5 with a Si/Al=40 the conversion of TIPB quickly drops off, Figure 65. In addition no cracking products are observed. This is likely due to the TIPB molecules and resulting products from the cracking becoming trapped in the micropores of the zeolite and coking up the catalyst due to poor diffusion. Using a HZSM5 with a Si/Al=11resutls in a slower deactivation. This is attributed to a few acid sites on the outside of the zeolite crystals which can crack the TIPB molecules before entering the pores. Active sites on the outside of the zeolite results in better conversion and propylene and benzene are observed, Figure 66. However, there is still not enough diffusion as the TIPB and resulting products from TIPB cracking become trapped in the zeolite. Thus, the zeolite catalyst deactivates from coking.

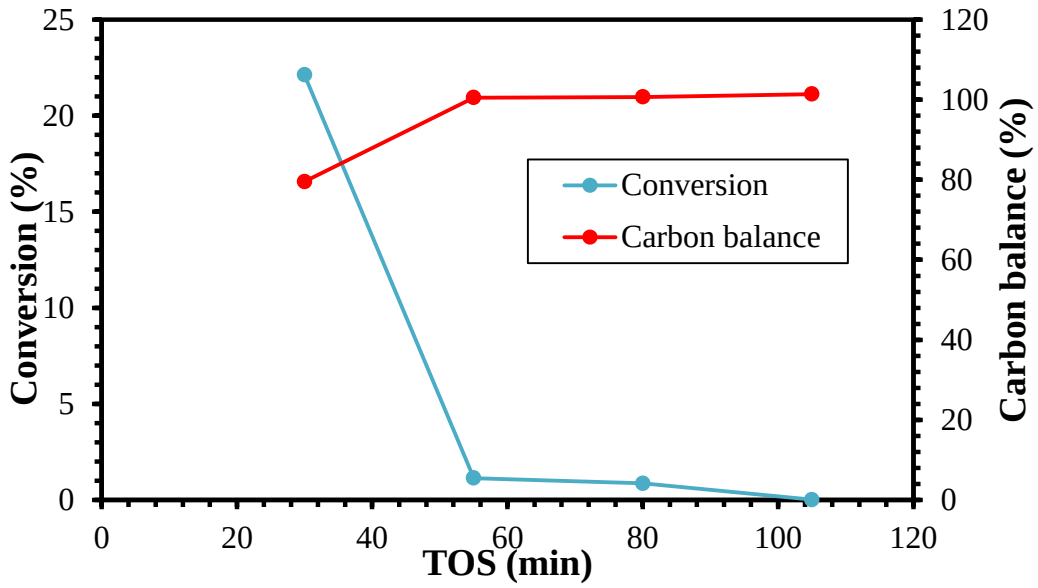

Figure 65: Conversion and carbon balance for HZSM5 with a Si/Al=40.

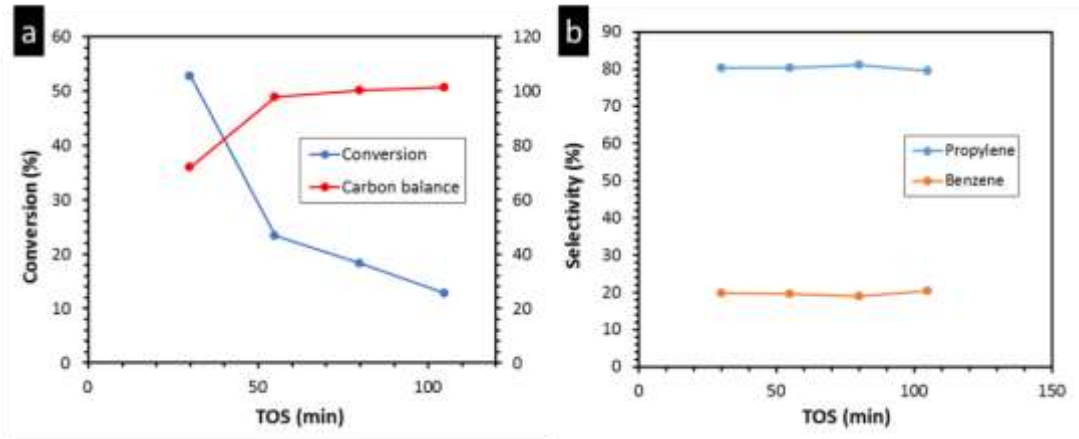

Figure 66: For HZSM5 with a Si/Al=11 the (a) conversion and carbon balance and (b) the selectivity for propylene and benzene.

The CNT-Zeolite-1 catalyst results in a stable conversion over the time tested and in a greater number of products, unlike the HZSM5 zeolites, Figure 67 (a). Benzene, cumene, diisopropylbezne, and propylene are all observed from the cracking of TIPB, Figure 67 (b). Due to the hierarchical zeolite structure there are more diffusion pathways for the TIPB molecules and the resulting products to enter and leave the micropores of the zeolite. Molecules can enter and leave from the outside of the zeolite nanotubes or can enter and leave from the pores created by the VMWNTs. The hierarchical structure created yields greater reaction selectivity and less catalyst deactivation than HZSM5.

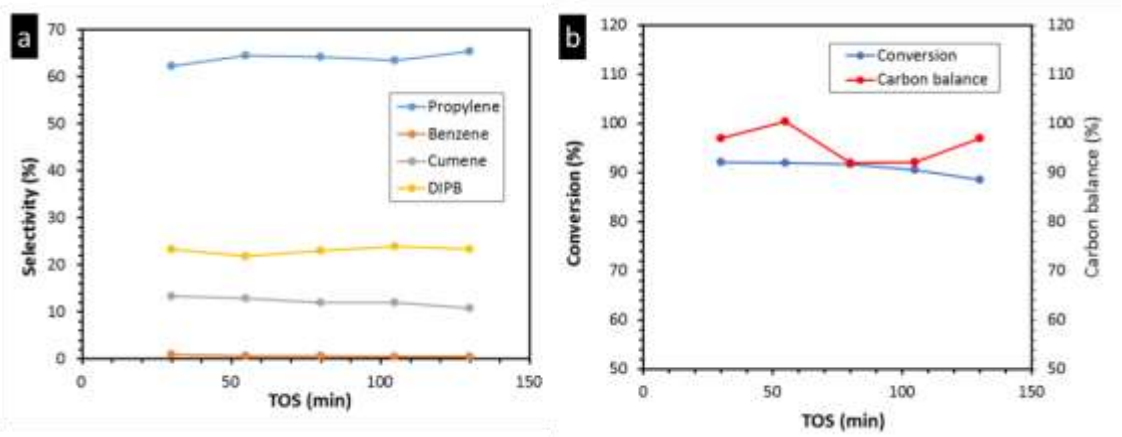

Figure 67: Reactions results for Z-CNT-1 (a) selectivity and (b) conversion and carbon balance.

Modification of the Zeolite Catalyst

By changing the amount of VMWNTs placed in the solution for zeolite growth the nucleation during the growth of the zeolites if changed, Figure 68. The higher the amount of VMWNTs in the solution the more surface area the zeolite has to nucleate over. With lower VMWNT surface area for the zeolite to nucleate over the zeolite grows outwards from the VMWNT forming a block. These differences can possibly be used to change the diffusion of molecules to the zeolites. Therefore, the reaction selectivity for the cracking of TIPB can be further tuned.

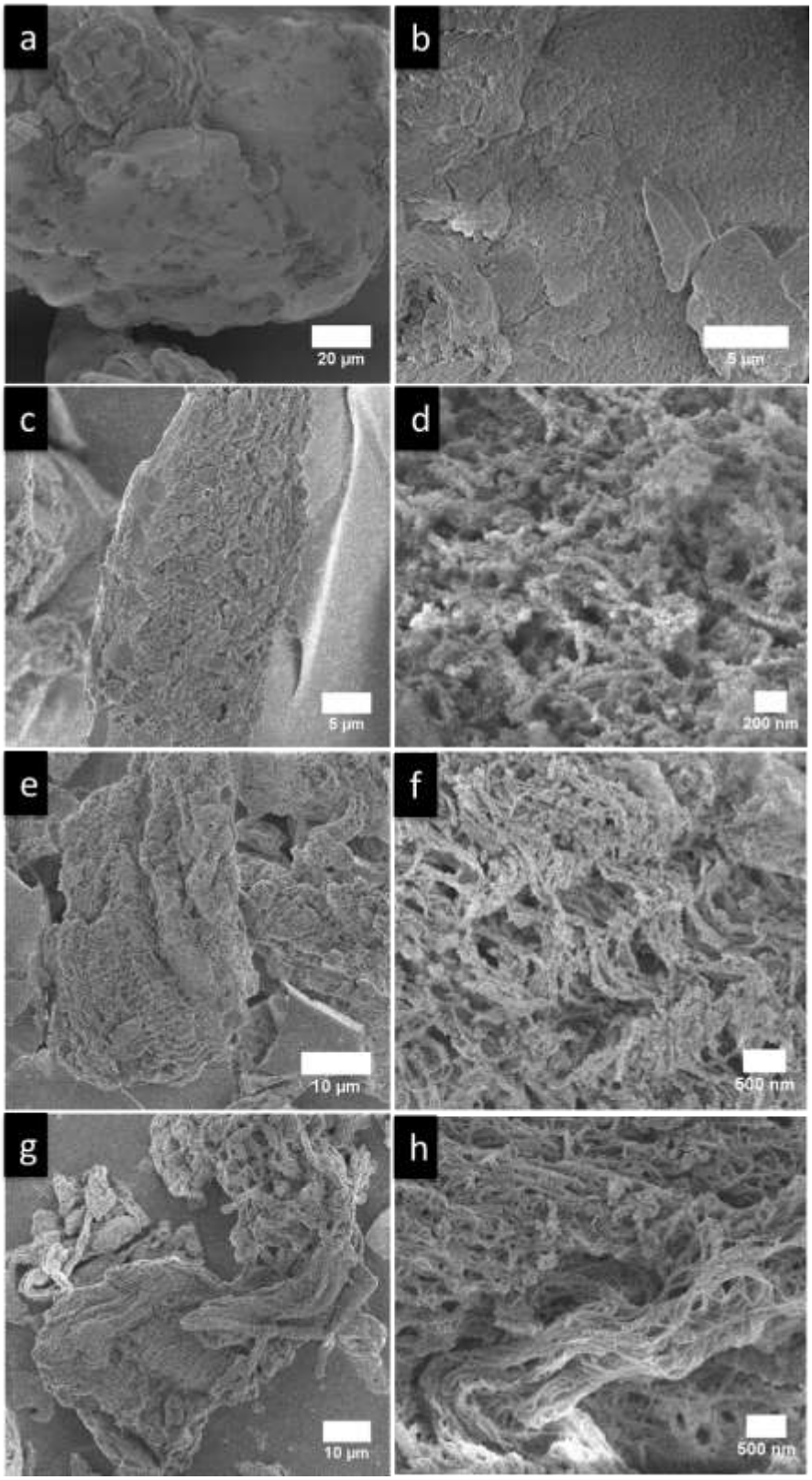

Figure 68: SEM images of samples (a & b) Z-CNT-1, (c & d) Z-CNT-2, (e & f) Z-CNT-3, (g & h) Z-CNT-4.

Conclusion

A hierarchical zeolite has been created which allows for bulky molecules such as triisopropyl benzene to diffuse in and out of the zeolite micropores because of the large pores. These large pores are formed by using VMWNTs for the zeolite crystals to grow around and then removing the VMWNTs through oxidation leaving a pore roughly the size of the VMWNT. With the large pores the hierarchical zeolites allow for molecules to diffuse in and out of the micropores, unlike the commercial zeolite with only micropores which can trap molecules and results in coking of the catalyst. The VMWNTs are grown between layers of mica sheets which allows for VMWNT growth in a fluidized bed, which allows for the manufacturing hierarchical zeolites to be scaled up. Additionally, the VMWNTs can be grown to different lengths and diameters offering further flexibility for tuning pore size which can change the molecules diffusion path. The diffusion path of the molecules can also be changed by varying the density of zeolite crystals surrounding the VMWNTs. These results in zeolite nanorods or a zeolite block with pores the size of the VMWNTs. Therefore, several routes are available to further enhance reaction selectivity by modification of the hierarchical zeolite which will be explored.

References

[305] Sadeghbeigi, Reza. *Fluid catalytic cracking handbook: An expert guide to the practical operation, design, and optimization of FCC units*. Elsevier, 2012.

[306] Biswas, J., and I. E. Maxwell. "Recent process-and catalyst-related developments in fluid catalytic cracking." *Applied Catalysis* 63.1 (1990): 197-258.

[307] Gobin, O. C., et al. "Comparison of the transport of aromatic compounds in small and large MFI particles." *The Journal of Physical Chemistry C* 113.47 (2009): 20435-20444.

[308] Reitmeier, S. J., et al. "Influence of Postsynthetic Surface Modification on Shape Selective Transport of Aromatic Molecules in HZSM-5." *The Journal of Physical Chemistry C* 113.34 (2009): 15355-15363.

[309] Christensen, Claus H., et al. "Crystals in Crystals Nanocrystals within Mesoporous Zeolite Single Crystals." *Journal of the American Chemical Society* 127.22 (2005): 8098-8102.

[310] Christensen, Christina Hviid, et al. "Catalytic benzene alkylation over mesoporous zeolite single crystals: improving activity and selectivity with a new family of porous materials." *Journal of the American Chemical Society* 125.44 (2003): 13370-13371.

[311] Christensen, Claus Hviid, Iver Schmidt, and Christina Hviid Christensen. "Improved performance of mesoporous zeolite single crystals in catalytic cracking and isomerization of n-hexadecane." *Catalysis Communications* 5.9 (2004): 543-546.

[312] Pérez-Ramírez, Javier, et al. "Hierarchical zeolites: enhanced utilisation of microporous crystals in catalysis by advances in materials design." *Chemical Society Reviews* 37.11 (2008): 2530-2542.

[313] Verboekend, Danny, and Javier Pérez-Ramírez. "Design of hierarchical zeolite catalysts by desilication." *Catalysis Science & Technology* 1.6 (2011): 879-890.

[314] Ogura, Masaru, et al. "Formation of Uniform Mesopores in ZSM-5 Zeolite through Treatment in Alkaline Solution." *Chemistry letters* 8 (2000): 882-883.

[315] Groen, J. C., et al. "Mesoporosity development in ZSM-5 zeolite upon optimized desilication conditions in alkaline medium." *Colloids and Surfaces A: Physicochemical and Engineering Aspects* 241.1 (2004): 53-58.

[316] Groen, J. C., J. Pérez-Ramírez, and L. A. A. Peffer. "Formation of uniform mesopores in ZSM-5 zeolite upon alkaline post-treatment?." *Chemistry Letters* 1 (2002): 94-95.

[317] Kresge, C. T., et al. "Ordered mesoporous molecular sieves synthesized by a liquid-crystal template mechanism." *nature* 359.6397 (1992): 710-712.

[318] Beck, J. S., et al. "A new family of mesoporous molecular sieves prepared with liquid crystal templates." *Journal of the American Chemical Society* 114.27 (1992): 10834-10843.

[319] Zhao, Dongyuan, et al. "Triblock copolymer syntheses of mesoporous silica with periodic 50 to 300 angstrom pores." *science* 279.5350 (1998): 548-552.

[320] Zhao, Dongyuan, et al. "Nonionic triblock and star diblock copolymer and oligomeric surfactant syntheses of highly ordered, hydrothermally stable, mesoporous silica structures." *Journal of the American Chemical Society* 120.24 (1998): 6024-6036.

[321] Pham-Huu, Cuong, et al. "BETA zeolite nanowire synthesis under non-hydrothermal conditions using carbon nanotubes as template." *Carbon* 42.10 (2004): 1941-1946.

[322] Schmidt, Iver, et al. "Carbon nanotube templated growth of mesoporous zeolite single crystals." *Chemistry of Materials* 13.12 (2001): 4416-4418.

[323] Egeblad, Kresten, et al. "Templating Mesoporous Zeolites†." *Chemistry of Materials* 20.3 (2007): 946-960.

[324] Gu, Lijun, et al. "Structured zeolites catalysts with hierarchical channel structure." *Chemical Communications* 46.10 (2010): 1733-1735.

[325] Tao, Yousheng, et al. "Mesopore-modified zeolites: preparation, characterization, and applications." *Chemical reviews* 106.3 (2006): 896-910.

[326] Tang, K., et al. "Carbon nanotube templated growth of nano-crystalline ZSM-5 and NaY zeolites." *Materials Letters* 60.17 (2006): 2158-2160.

[327] Ajayan, P. M., et al. "Carbon nanotubes as removable templates for metal-oxide nanocomposites and nanostructures." *Nature* 375.6532 (1995): 564-567.

[328] Satishkumar, B. C., et al. "Oxide nanotubes prepared using carbon nanotubes as templates." *Journal of materials research* 12.03 (1997): 604-606.

[329] Zhu, Kake, et al. "Carbon as a hard template for nano material catalysts." *Journal of Natural Gas Chemistry* 21.3 (2012): 215-232.

[330] Min, Y-S., et al. "Ruthenium oxide nanotube arrays fabricated by atomic layer deposition using a carbon nanotube template." *Advanced Materials* 15.12 (2003): 1019-1022.

[331] Sun, Xuemei, et al. "The synthesis of porous materials with macroscopically oriented mesopores interconnected by branched mesopores." *Journal of Materials Chemistry A* 1.15 (2013): 4693-4698.

[332] Ogihara, Hitoshi, et al. "Synthesis, characterization and formation process of transition metal oxide nanotubes using carbon nanofibers as templates." *Journal of Solid State Chemistry* 182.6 (2009): 1587-1592.

[333] Zhang, Liang, Yongqiang Tan, and Daniel E. Resasco. "Controlling the growth of vertically oriented single-walled carbon nanotubes by varying the density of Co Mo catalyst particles." *Chemical physics letters* 422.1 (2006): 198-203.

[334] Zhang, Liang, et al. "Influence of a top crust of entangled nanotubes on the structure of vertically aligned forests of single-walled carbon nanotubes." *Chemistry of materials* 18.23 (2006): 5624-5629.

[335] Q. Zhang, M. Zhao, Y. Liu, A. Cao, W. Qian, Y. Lu, and F. Wei, *Advanced Materials*, 2009, **21**, 2876-2880.

[336] Briggs, N. M., and S. P. Crossley. "Rapid growth of vertically aligned multi-walled carbon nanotubes on a lamellar support." *RSC Advances* 5.102 (2015): 83945-83952.

[337] Song, W., et al. "Synthesis, characterization, and adsorption properties of nanocrystalline ZSM-5." *Langmuir* 20.19 (2004): 8301-8306.

[338] Tittensor, J. G., R. J. Gorte, and D. M. Chapman. "Isopropylamine adsorption for the characterization of acid sites in silica-alumina catalysts." *Journal of Catalysis* 138.2 (1992): 714-720.

[339] Kitiyanan, B., et al. "Controlled production of single-wall carbon nanotubes by catalytic decomposition of CO on bimetallic Co–Mo catalysts." *Chemical Physics Letters* 317.3 (2000): 497-503.

Appendix A2: Oxidation of Oil for Enhanced Oil Recovery by Using Carbon Nanotubes as Transport Vessels of Hydrogen Peroxide

Introduction

Large oil field production is eventually stopped many times due to the extraction becoming uneconomical even though a significant fraction of oil still remains. Two approaches have been taken to enhance oil recovery.[340] The first is the introduction of chemicals into the oil well which has been investigated for several decades.[341] The second approach is the use of nanotechnology to help characterize the reservoir and recovery oil.[342,343,344] An example of this is the use of nanohybrids to modify the wettability of the porous media which alters the interaction between the rock and the fluids increasing oil recovery.[345,346] In addition a combination of nanoparticles and surfactant was found to decrease the interfacial tension about 70% more than when using surfactants alone.[347]

The mobility ratio and capillary number are two variables which may have an impact on the oil recovery process when using chemicals and particles. The capillary number is defined as $N_c = {\mu\nu}/{\sigma}$ where ν is the the Darcy velocity, ν is the viscosity of the mobilizing fluid, typically water, and σ is the interfacial tension between the oil and water. Surfactants have been injected into oil reservoirs to lower the interfacial tension and increase the interfacial area which decreases the capillary forces that act on the oil inside the pores.[348] The mobility ratio defined as $MR = \frac{{k_w}/{k_o}}{{\mu_w}/{\mu_o}}$ and is dependent on the relative permeatbility (k) of the porous media toward oil and water, and the viscosity

(μ) of the oil and the mobilizing fluid, typically water. For the water to displace the oil the mobility ratio must be less than one.[349] To achieve a mobility ratio less than one the viscosity of the sweeping fluid can be increased, typically by the addition of polymers.[350,351] Another approach is the creation of oil in water emulsions which can improve the mobility of the oil by increasing the sweep efficiently.[352]

Due to the drastic impact the interfacial tension can have on oil recovery and the need to improve oil recovery new methodologies are required. In this work we use carbon nanotubes loaded with hydrogen peroxide and tungsten oxide supported on carbon nanotubes to oxidize oil at the oil-water interface. The purpose of oxidation is to lower the interfacial tension of the oil by adding oxygen functional groups to the oil. Carbon nanotubes are used as a transport vessel due to residing preferentially at the oil-water interface and having hollow structure which can be filled with hydrogen peroxide.[353] By filling the carbon nanotubes with hydrogen peroxide the hydrogen peroxide is transported through the aqueous phase and released at the oil-water interface which helps reduce the amount of hydrogen peroxide required. Lastly, carbon nanotubes are loaded with hydrogen peroxide and then coated with paraffin wax to keep the hydrogen peroxide from leaking out of the carbon nanotubes during transport through the aqueous phase.

Experimental Details

Daniel Santhanaraj performed the reactions, loaded hydrogen peroxide on the carbon nanotubes, coated hydrogen peroxide loaded carbon nanotubes with paraffin wax, and deposited tungsten oxide on the oxidized carbon nanotubes.

MWNTs were donated by SouthWest Nanotechnologies and designated as SWeNT MW100. According the manufacturer the MWNTs had an outer diameter of six to nine nanometers, three to six walls, and an average length of less than one micron according to the manufacturer. Cyclohexene (99%), hydrogen peroxide (50%), methanol (99%), paraffin wax with a melting point between 53 and 57 °C, and hexadecane (99%) were all purchased from Sigma Aldrich.

The MWNTs were oxidized to increase their hydrophilicity. Oxidation of the MWNTs was performed using nitric acid in a reflux setup for 12 hours. To a round bottom flask two grams of carbon nanotubes and 100 mL of six molarity nitric acid were added. During reflux the solution temperature in the flask was held at 120°C and stirred at 750 rpm. After the reflux step the MWNTs were filtered using a 0.22 µm PTFE filter. With the MWNTs on the filter water was passed over the MWNTs to remove residual acid. The MWNTs were washed until the pH of the water was neutral.

Wet impregnation of WO_3 on oxidized MWNTs was performed by using ammonium metatungstate as the catalyst precursor and water as the solvent to create a one weight percent WO_3 loading on MWNTs. After impregnation the catalyst was calcined to decompose the catalyst precursor to WO_3. Calcination of the catalyst was performed in a custom built system. WO_3/MWNT catalyst was placed in an alumina boat which was then loaded into a one inch inner diameter quartz tube. With catalyst loaded the quartz tube was placed horizontally in a furnace and connected to the inlet and outlet lines. Air was flowed through the quartz tube at 100 sccm during the entire calcination procedure. The furnace was ramped to 350 °C at 10 °C/minute and then held at 350°C for four hours.

Hydrogen peroxide was loaded inside carbon nanotubes by using incipient wetness impregnation. One gram of oxidized MWNTs was placed in a mortar and then 0.6 mL of 50% hydrogen peroxide was added dropwise while mixing the oxidized MWNTs with a pestle. Once completed the MWNTs loaded with hydrogen peroxide were used in reaction or stored in a refrigerator was later use. Sealing hydrogen peroxide inside of MWNTs with wax was performed after incipient wetness impregnation of hydrogen peroxide inside MWNTs. MWNTs loaded with hydrogen peroxide were placed in a mortar and then 0.6 mL of paraffin wax added dropwise while mixing the MWNTs. After coating the MWNTs loaded with hydrogen peroxide with paraffin wax the material was placed in a refrigerator to quickly solidify the molten wax.

Characterization of the tungsten oxide on the MWNTs was completed by using transmission electron microscopy. A JEOL 2000FX transmission electron microscope was operated at 200 kV for taking images. The size of the tungsten oxide particles were measured by using the program ImageJ from the images taken.

Results and Discussion

The catalyst tungsten oxide supported on carbon nanotubes had an average tungsten oxide particle diameter of 1.8 nm. A representative TEM image can be seen in Figure 69. Tungsten oxide is used as an oxidation catalyst by reacting hydrogen peroxide and cyclohexene to form the cyclohexene diol, alcohol, epoxide, and ketone.

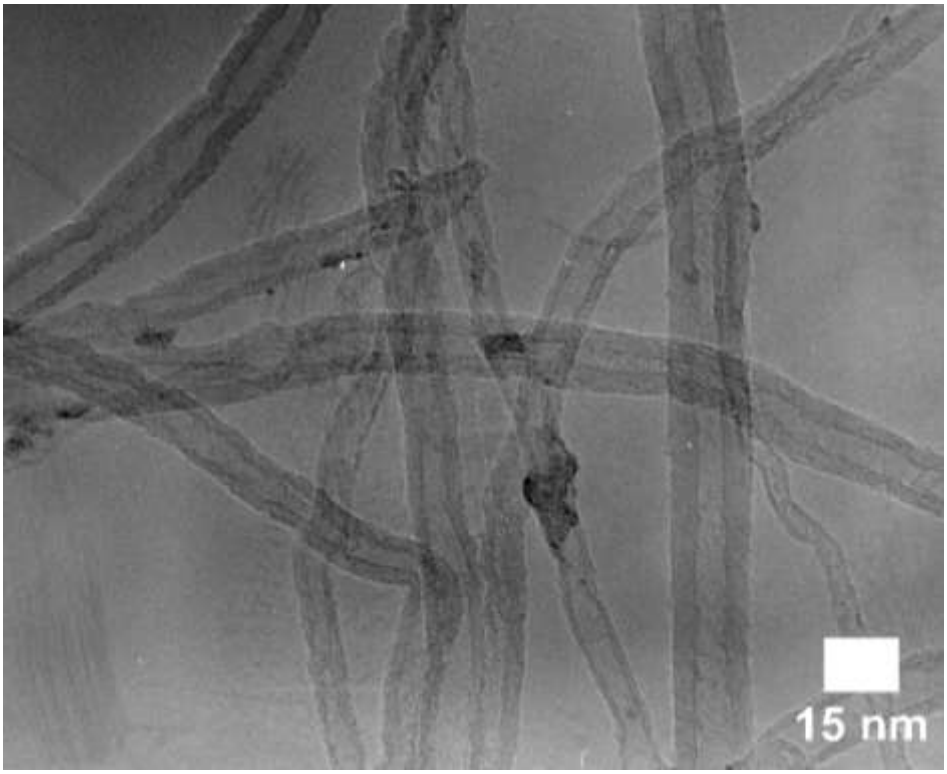

Figure 69: Representative TEM image of WO_3/Ox-MWNT catalyst

Tungsten oxide supported on carbon nanotubes reside at the oil-water interface and on the addition of hydrogen peroxide results in the oxidation of cyclohexene, Figure 70. By loading hydrogen peroxide in carbon nanotubes a conversion of cyclohexene is achieved due to the hydrogen peroxide being transported to the oil-water interface where the hydrogen peroxide is released. This is further confirmed when looking at the percentage of hydrogen peroxide decomposed during the reaction. As can be seen in Figure 71 there is a roughly 20% difference in the amount of hydrogen peroxide decomposed when carbon nanotubes are used as a transport vessel. By increasing the stir speed the reaction selectivity changes and the conversion of cyclohexene drops, Figure 70. This may be due to the hydrogen peroxide diffusing at a higher rate into the aqueous phase. The increase in stir speeds results in an increase in hydrogen peroxide

decomposition which may give warrant to the idea that the hydrogen peroxide is diffusing faster from the carbon nanotubes and into the aqueous phase, Figure 71.

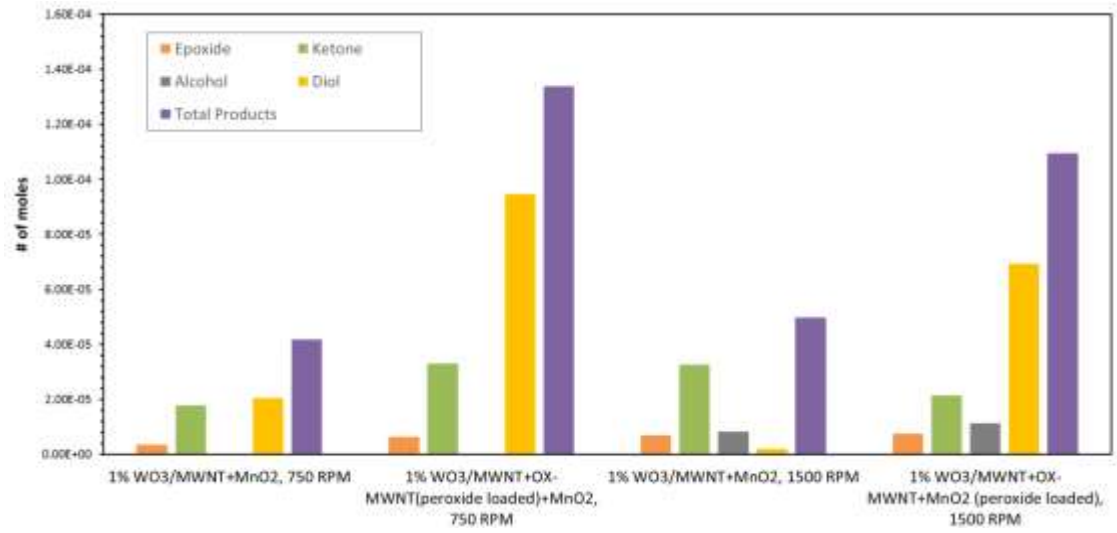

Figure 70: Amounts of oxidation products from cyclohexene oxidation with hydrogen peroxide catalyzed with tungsten oxide.

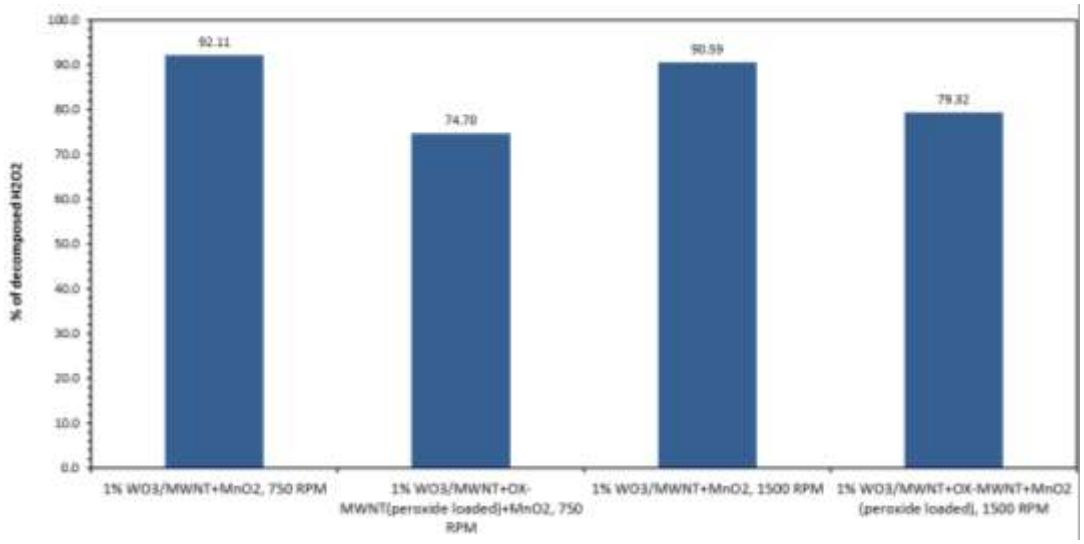

Figure 71: Decomposition of hydrogen peroxide after the reaction.

During oil recovery the carbon nanotubes may have to travel over a great distance to reach the oil-water interface. To overcome the problem of hydrogen

peroxide leaching out of the carbon nanotubes paraffin wax was used. Hydrogen peroxide was loaded into carbon nanotubes and then the carbon nanotubes coated with paraffin wax to seal in the hydrogen peroxide. The paraffin wax keeps the hydrogen peroxide from diffusing out the of carbon nanotubes and into the water since the paraffin wax is insoluble in water. Once the paraffin wax coated carbon nanotubes reach the oil-water interface the oil solubilizes the paraffin wax releasing the hydrogen peroxide at the oil-water interface. To test the feasibility of this idea we placed the carbon nanotubes loaded with hydrogen peroxide with and without a paraffin wax coating in the aqueous phase. The aqueous phase with the hydrogen peroxide loaded MWNTs was mixed for three hours. After which cyclohexene was added and the reaction started.

Coating the carbon nanotubes loaded with hydrogen peroxide proved to be beneficial in retaining conversion of cyclohexene. As can be seen in Figure 72 there is a significantly higher conversion of cyclohexene when the carbon nanotubes containing hydrogen peroxide were coated with paraffin wax. This is further confirmed by the percent of hydrogen peroxide decomposed. Almost all of the hydrogen peroxide is decomposed without a paraffin wax coating and with a paraffin wax coating roughly 30% of the hydrogen peroxide remains, Figure 73. Therefore, the paraffin wax coating of the hydrogen peroxide loaded carbon nanotubes delays the release time of the hydrogen peroxide to maximize oxidation of the oil. This can prove important since there is a significant distance the hydrogen peroxide loaded carbon nanotubes will have to travel through water to reach the oil-water interface in an oil reservoir.

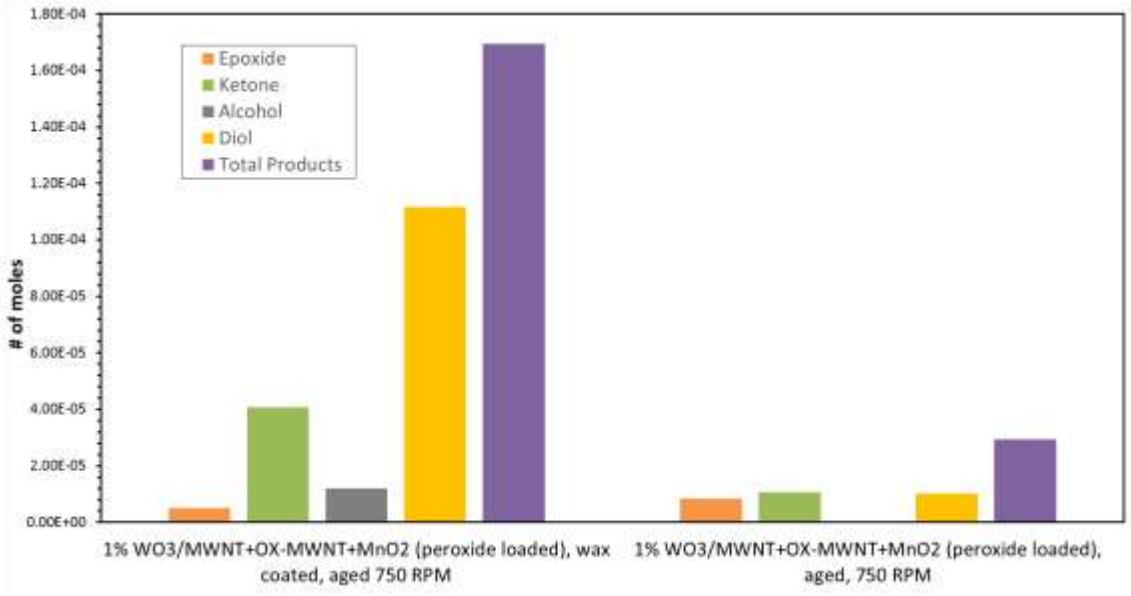

Figure 72: Amounts of oxidation products from cyclohexene oxidation with hydrogen peroxide catalyzed with tungsten oxide after allowing the catalyst to reside at the interface for a period of time.

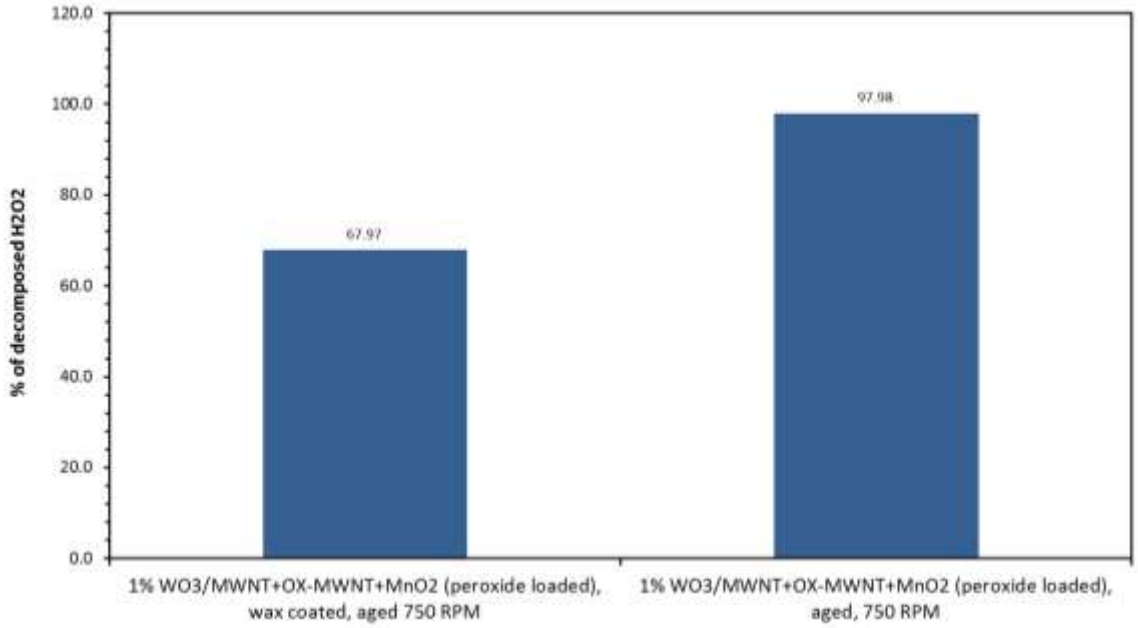

Figure 73: Decomposition of hydrogen peroxide after the reaction for catalyst when left to reside at the oil-water interface.

Conclusion

Carbon nanotubes can successfully transport hydrogen peroxide to the oil-water interface for catalytic oxidation of the oil. By oxidizing the oil the interfacial tension can be lowered which can help with oil recovery. Taking advantage of the porous nature of the carbon nanotubes allows for transport of the hydrogen peroxide directly to the oil-water interface, reducing the amount of hydrogen peroxide required to lower the interfacial tension. To further improve the process carbon nanotubes can be coated with a paraffin wax to keep the hydrogen peroxide from leaching out of the carbon nanotubes during transportation through the aqueous phase. By providing a protecting barrier more oil can be oxidized which can further help reduce the interfacial tension.

References

[340] Standnes, Dag C., and Tor Austad. "Wettability alteration in chalk: 2. Mechanism for wettability alteration from oil-wet to water-wet using surfactants." *Journal of Petroleum Science and Engineering* 28.3 (2000): 123-143.

[341] Iglauer, Stefan, et al. "New surfactant classes for enhanced oil recovery and their tertiary oil recovery potential." *Journal of Petroleum Science and Engineering* 71.1 (2010): 23-29.

[342] Ingram, D. R.; Kotsmar, C.; Yoon, K. Y.; Shao, S.; Huh, C.; Bryant, S. L.; Milner, T. E.; Johnston, K. P. J. Colloid Interface Sci. 2010, 351, 225−232.

[343] Yu, H.; Kotsmar, C.; Yoon, K. Y.; Ingram, D. R.; Johnston, K. P.; Bryant, S. L.; Huh, C. Presented at the 17th SPE Improved Oil Recovery Symposium, Tulsa, OK, 2010; SPE Paper No. 129887.

[344] Fletcher, A. J. P.; Davis, J. P. Presented at the 17th SPE Improved Oil Recovery Symposium, Tulsa, OK, 2010; SPE Paper No. 129531.

[345] Ju, B.; Fan, T.; Ma, M. China Particuol. 1996, 4, 41−46.

[346] Kadhum, Mohannad J., et al. "Propagation of interfacially active carbon nanohybrids in porous media." *Energy & Fuels* 27.11 (2013): 6518-6527.

[347] Suleimanov, B. A., F. S. Ismailov, and E. F. Veliyev. "Nanofluid for enhanced oil recovery." *Journal of Petroleum Science and Engineering* 78.2 (2011): 431-437.

[348] Thomas, Sara, and SM Farouq Ali. "Flow of emulsions in porous media, and potential for enhanced oil recovery." *Journal of Petroleum Science and Engineering* 3.1 (1989): 121-136.

[349] Satter, Abdus, Ghulam M. Iqbal, and James L. Buchwalter. *Practical enhanced reservoir engineering: assisted with simulation software*. Pennwell Books, 2008.

[350] Islam, M. R., and SM Farouq Ali. "Use of silica gel for improving waterflooding performance of bottom-water reservoirs." *Journal of Petroleum Science and Engineering* 8.4 (1993): 303-313.

[351] Cheremisinoff, Nicholas P. *Advances in Engineering Fluid Mechanics: Multiphase Reactor and Polymerization System Hydr: Multiphase Reactor and Polymerization System Hydr*. Gulf Professional Publishing, 1996.

[352] Kumar, R.; Dao, E.; Mohanty, K. K. Presented at the 17th SPE Improved Oil Recovery Symposium, Tulsa, OK 2010; SPE Paper No. 129914;

[353] Briggs, Nicholas M., et al. "Multiwalled Carbon Nanotubes at the Interface of Pickering Emulsions." *Langmuir* 31.48 (2015): 13077-13084.

Appendix A3: Morphology of Polystyrene/Poly(methyl methacrylate) Blends: Effects of Carbon Nanotubes Aspect Ratio and Surface Modification

This work was performed with Dr. Brian Grady and Dr. Jiaxi Guo. My contribution in this work was measuring the length of the mulit-walled carbon nanotubes before and after the polymer blends were made. The goal was to determine the breakage of the multi-walled carbon nanotubes when polymer blends were made. The length of the multi-walled carbon nanotubes was found to have an impact on the properties of the polymer blends. This work was published in the AIChE journal.

The citation is: Guo, Jiaxi, et al. "Morphology of polystyrene/poly (methyl methacrylate) blends: Effects of carbon nanotubes aspect ratio and surface modification." *AIChE Journal* 61.10 (2015): 3500-3510.

Appendix A4: Vertically Aligned Multi-walled Carbon Nanotube Growth of Unique Structures and on Different Supports

The following chapter is growth of vertically aligned multi-walled carbon nanotubes on various other substrates and of unique structures formed during the growth.

Mushroom Growth

Experimental Details

The substrate for growing vertically aligned multi-walled carbon nanotubes (V-MWNTs) was a three-inch diameter n-typesilicon wafer with orientation (100). The wafer was cut into 21mm x 21mm squares using a diamond scribe. The silicon wafer was bath sonicated in first acetone, then methanol and finally isopropanol. The silicon wafers where then blown dry with air.

A solution of aluminum isopropoxide in isopropanol with a concentration of 0.00489 M was made. 100μL of this solution was deposited with a micropipette onto a square 21 mm x 21 mm silicon wafer. The solution was allowed to dry overnight on the silicon wafer. The sample was then calcined in an oven at 450°C for two hours. Another solution was made by using isopropanol as a solvent with catalyst precursors iron nitrate nonahydrate and cobalt nitrate hexahydrate withconcentrations of 0.0111 M and 0.0028 M, respectively, which yielded a Fe:Co molar ratio of 4:1. 30 μL this solution was deposited on the silicon wafer with a micropipette. Again the solution was allowed to dry overnight on the silicon wafer. The sample was then calcined again in an oven at 450°C for two hours.

The sample was then placed in a vertical quartz tube reactor. The first step consisted of reduction. The reactor was ramped to 560°C in 50 minutes with a flow of 150 sccm of hydrogen. Then the temperature was held at 560°C for 30 minutes with a flow of 150 sccm of hydrogen. Following was a ramp to 760°C in 20 minutes under a flow of 300 sccm of nitrogen. The reaction took place at 760°C for 30 minutes under a flow of 200 sccm of ethylene. Finally, 300 sccm of nitrogen was flowed for five minutes to cool the reactor and remove any harmful gas. The sample was then removed from the reactor and had a V-MWNT forest over the entire silicon wafer.

Results and Discussion

VMWNTs were found to grow into mushroom structures, Figure 74. These structures are believed to be caused by the amount of catalyst solution containing iron and cobalt catalyst not being sufficient enough to cover the entire surface of the silicon wafer and small islands of catalyst particles were created. The nature of the alumina film formed on the silicon wafer surface may play a part in the formation of these unique structures. This may be also be due to the catalyst particles sintering as the reaction proceeds. Once the particles sinter and become close enough to one another then the VMWNTs grow vertically.

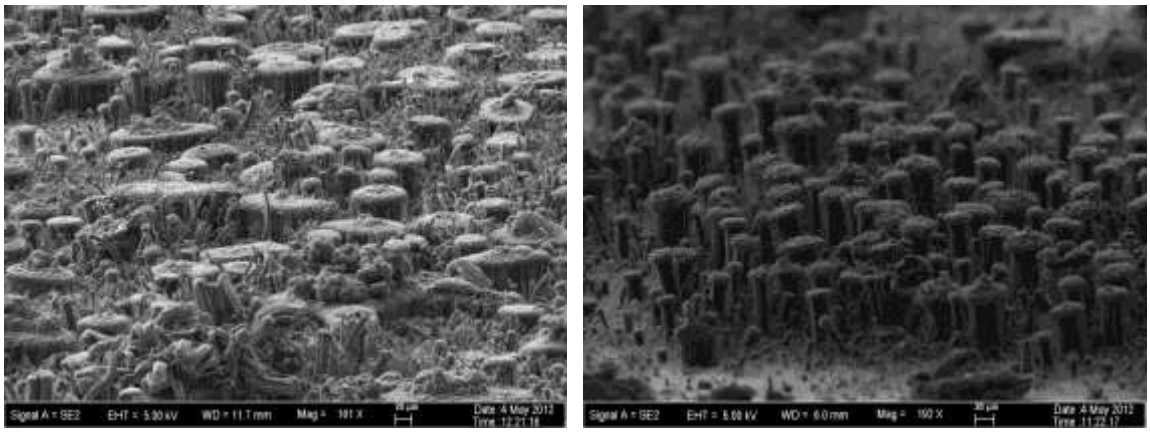

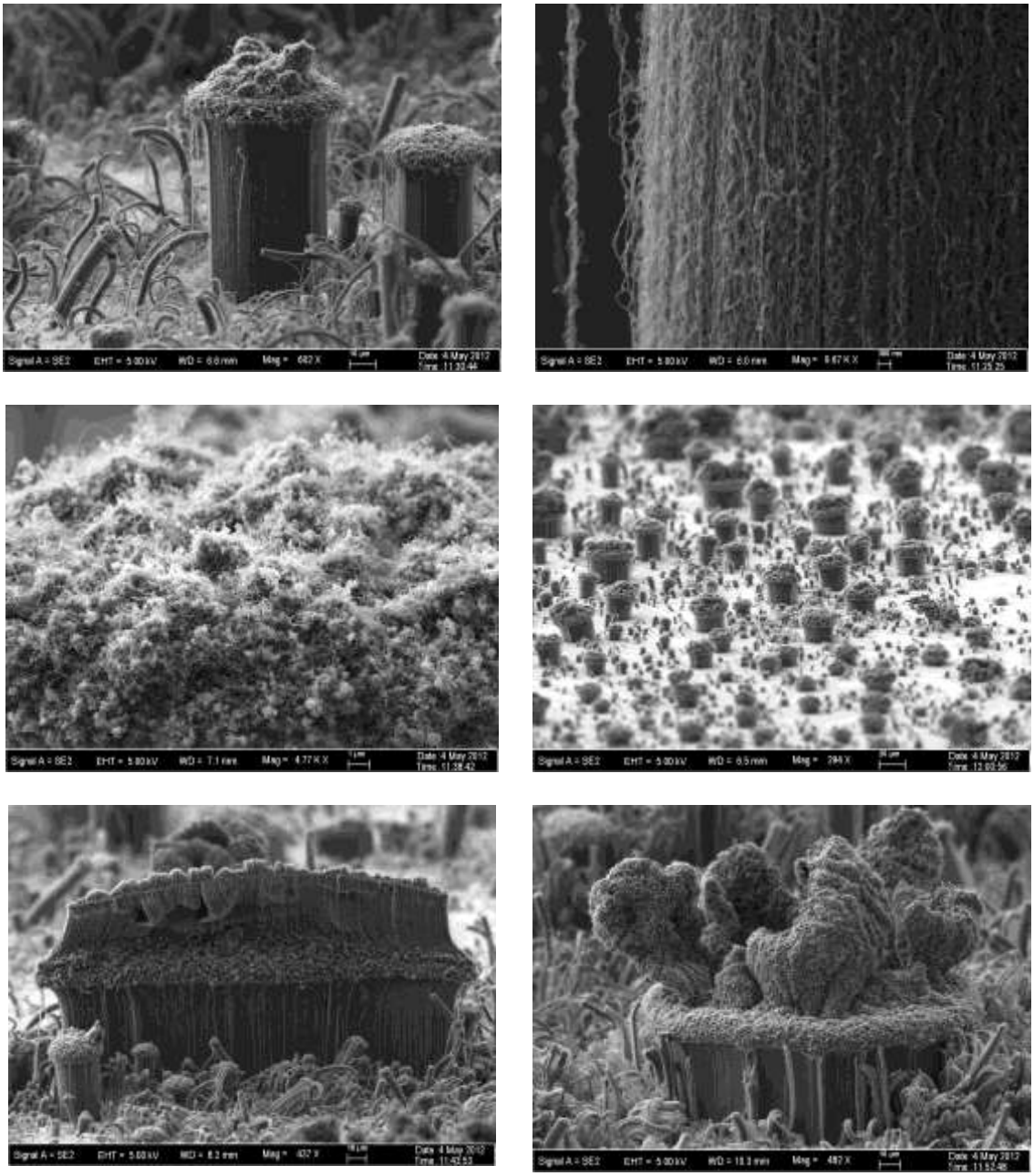

Figure 74: VMWNTs grown into a mushroom type structure.

During this process other unique and random structures have been observed.

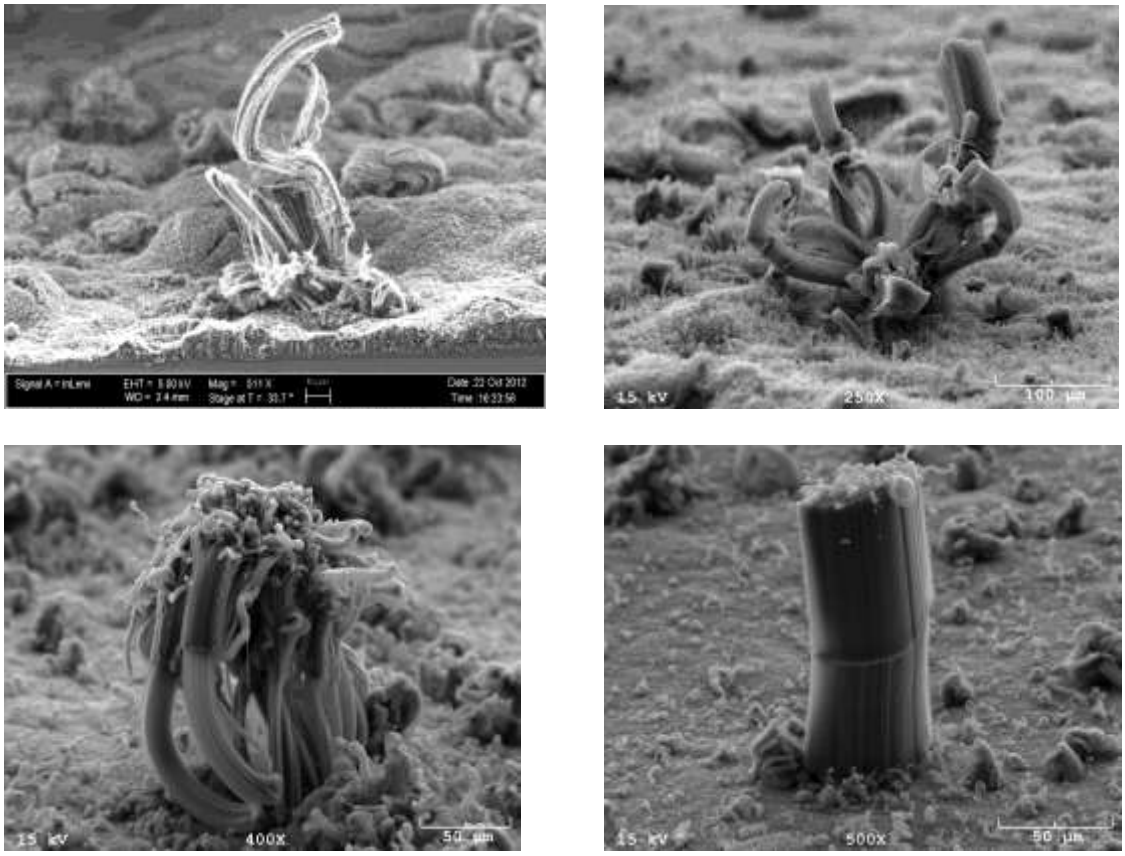

Figure 75: VMWNTs grown in random structures.

VMWNTs Grown on Alumina Spheres

Experimental Details

VMWNTs were grown on alumina spheres at 0.3 mm, 0.5 mm, and 1 mm in diameter, by following the same produces as in Chapter 7 for growing VMWNTs on mica sheets. The only differences alumina spheres are dipped in the catalyst solution instead of mica sheets. The same weight is used.

Results and Discussion

SEM images of the VMWNTs grown on alumina spheres can be seen in Figure 76.

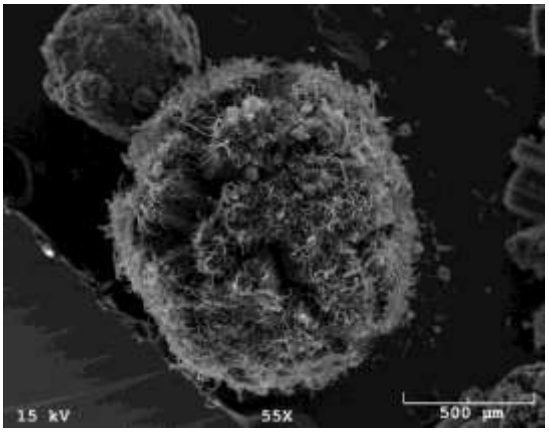
15 kV
55X
500 µm

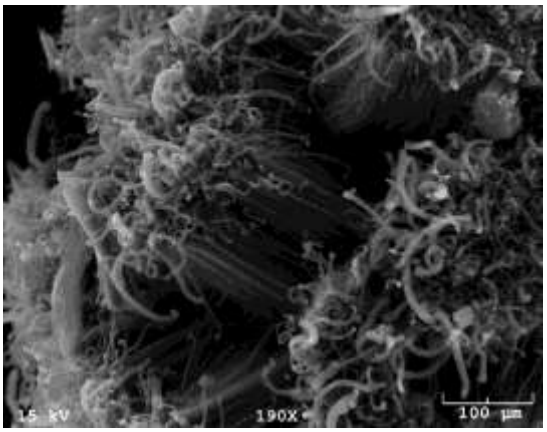
15 kV
190X
100 µm


15 kV
90X
200 µm

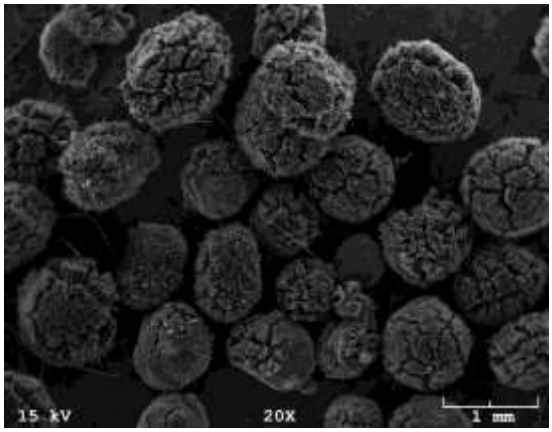
15 kV
20X
1 mm

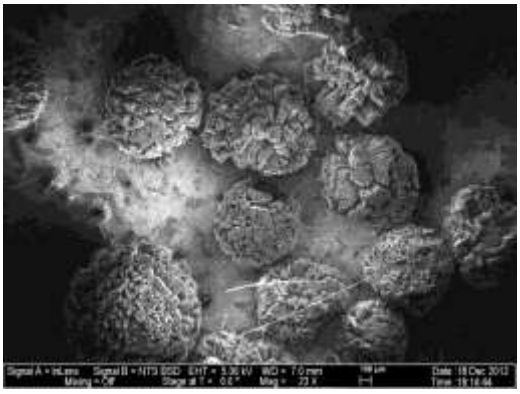

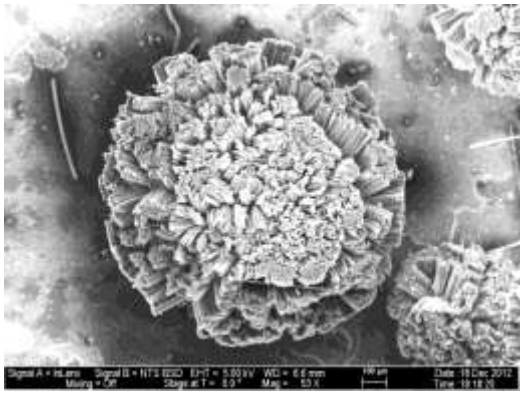

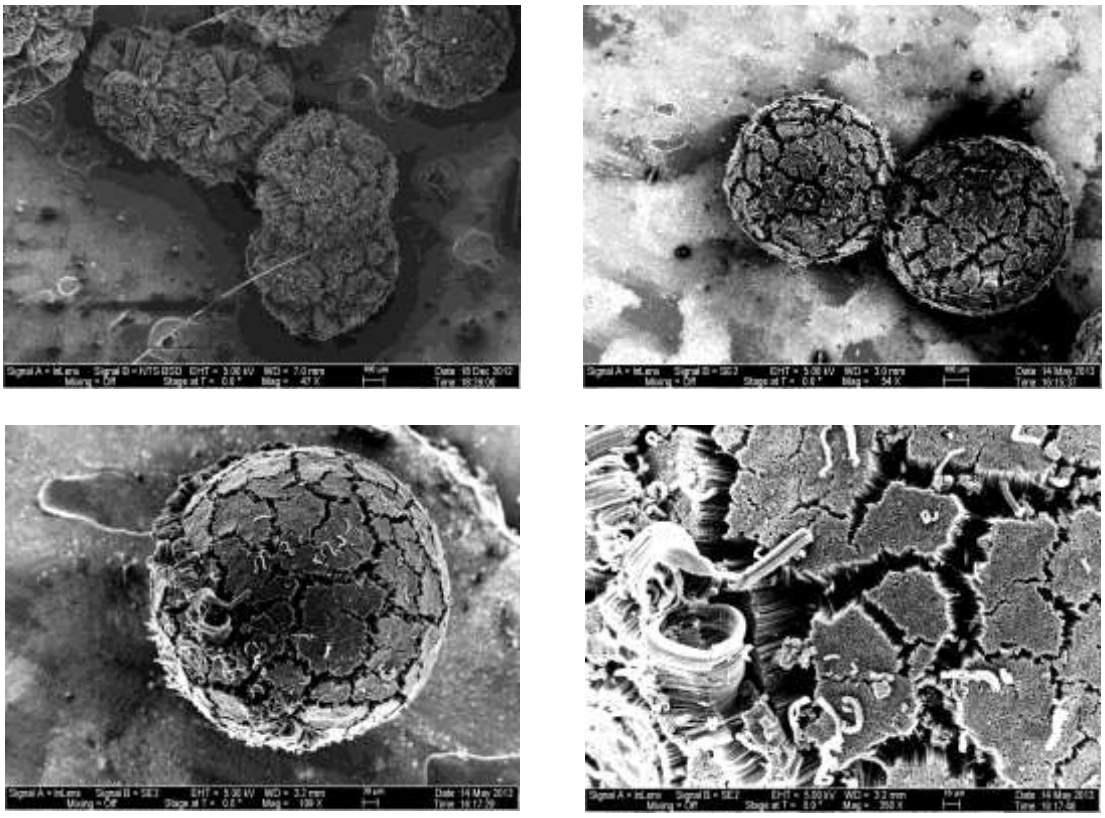

Figure 76: SEM images of VMWNTs grown on a variety of different size alumina spheres.

Nitrogen doped VMWNTs

Experimental Details

Nitrogen doped VMWNTs on mica were grown the same way as in Chapter 7 except ethylene was replaced with a flow of 0.1 mL/h of acetonitrile. Acetonitrile is responsible for incorporation of nitrogen into the VMWNTs. All samples were grown with the conditions use to make sample HRRx650D-D.

Results and Discussion

Raman data from of samples made with and without nitrogen doping.

Suppression of the G' at about 2600 cm^{-1} has been shown to be indicative of nitrogen doping.[354] The D peak at about 1350 cm^{-1} and G peak at about 1580 cm^{-1} do not change appreciably only the G' peak, Figure 77.

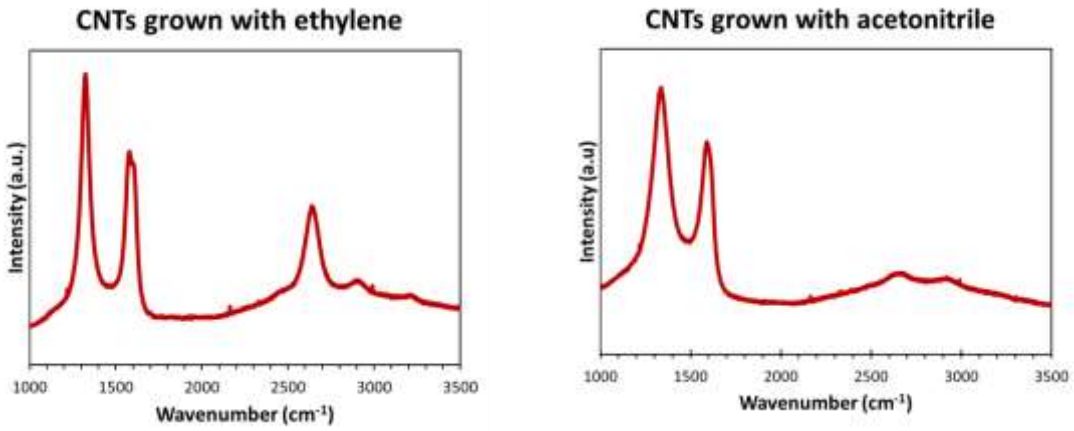

Figure 77: Raman data for VMWNTs grown with ethylene as a carbon source and with acetonitrile as a carbon and nitrogen source.

SEM and TEM images of the VMWNTs grown with acetonitrile can be seen in Figure 78. The effect of nitrogen doping causes the bamboo effect seen in the TEM images.[355] The outer and inner diameters of the VMWNTs grown with acetonitrile were 13.2 nm and 7.6 nm, respectively. Outer and inner diameters of the VMWNTs grown with ethylene diamine were 13.4 nm and 6.8 nm.

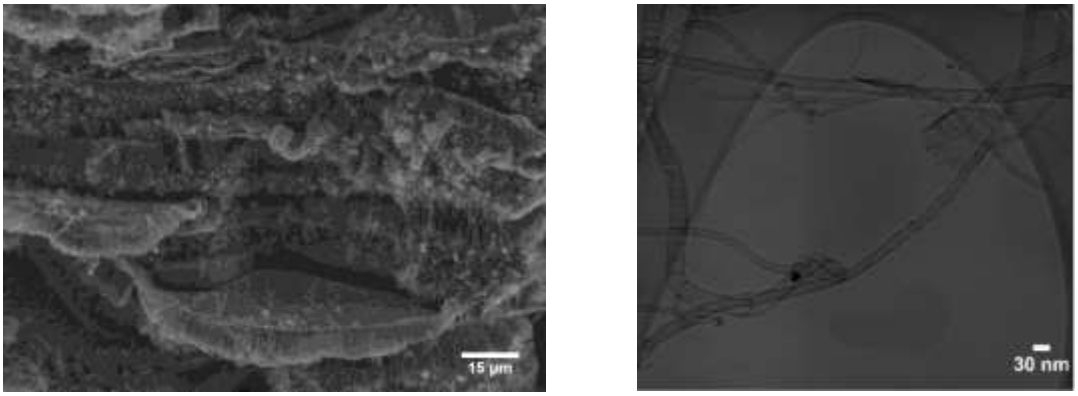

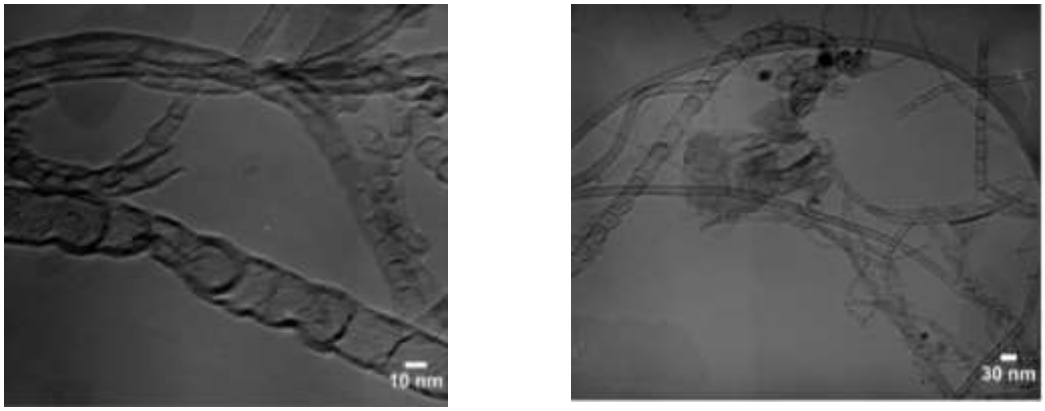

Figure 78: From left to right and down. SEM image of VMWNTs grown on mica and doped with nitrogen. The TEM images in the top right corner and bottom left corner are of VMWNTs grown with acetonitrile. The TEM image in the bottom right corner is grown with ethylene diamine.

References

[354] Bulusheva, L. G., Okotrub, A. V., Kinloch, I. A., Asanov, I. P., Kurenya, A. G., Kudashov, A. G., ... & Song, H. (2008). Effect of nitrogen doping on Raman spectra of multi-walled carbon nanotubes. *physica status solidi (b), 245*(10), 1971-1974.

[355] Trasobares, S., et al. "Compartmentalized CN nanotubes: Chemistry, morphology, and growth." *The Journal of chemical physics* 116 (2002): 8966.

Appendix A5: Supporting Information for Chapter 2

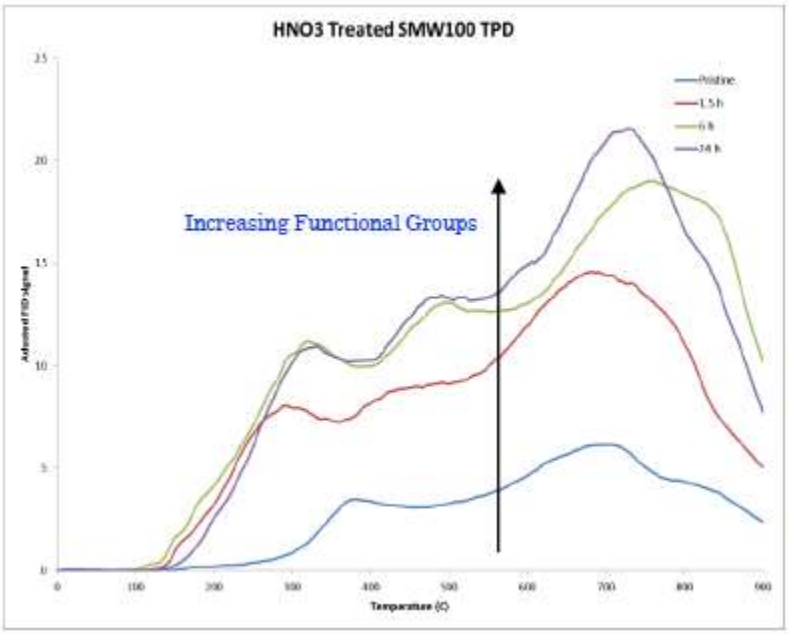

Figure 79: TPD profiles for MWNT samples as a function of temperature.

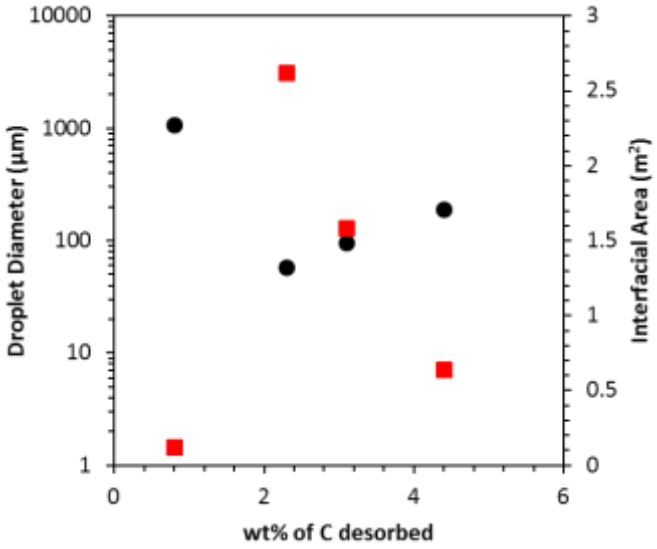

Figure 80: Emulsion droplet diameter and interfacial area when toluene is used as oil. Axis for emulsion droplet diameter is logarithmic scale to help better see the changes in emulsion droplet diameter. Circles are for droplet diameter and squares are for interfacial area.

Appendix A6: Supporting Information for Chapter 3

Supporting information for this chapter can be found on the Langmuir journal website where the article was published.

The publication and supporting information can be found using the citation: Briggs, Nicholas M., et al. "Multiwalled Carbon Nanotubes at the Interface of Pickering Emulsions." *Langmuir* 31.48 (2015): 13077-13084.

Appendix A7: Supporting Information for Chapter 5

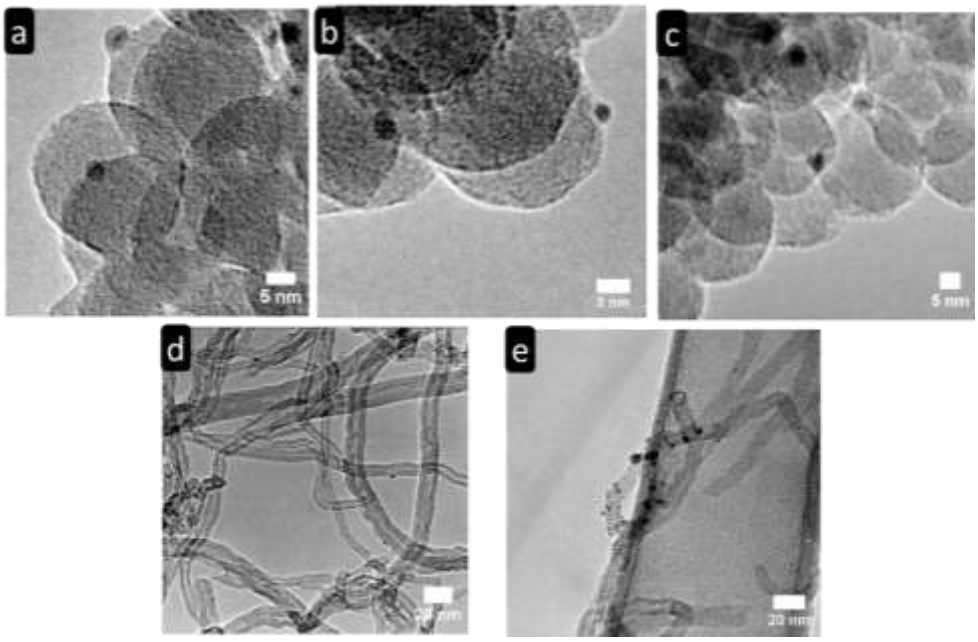

Figure 81: TEM images of catalysts (a) Pd/Ludox (b) Pd/Ludox-50%OTS, (c) Pd/Ludox-100%OTS, (d) Pd/CNT, and Pd/o-CNT.

Appendix A8: Supporting Information for Chapter 6

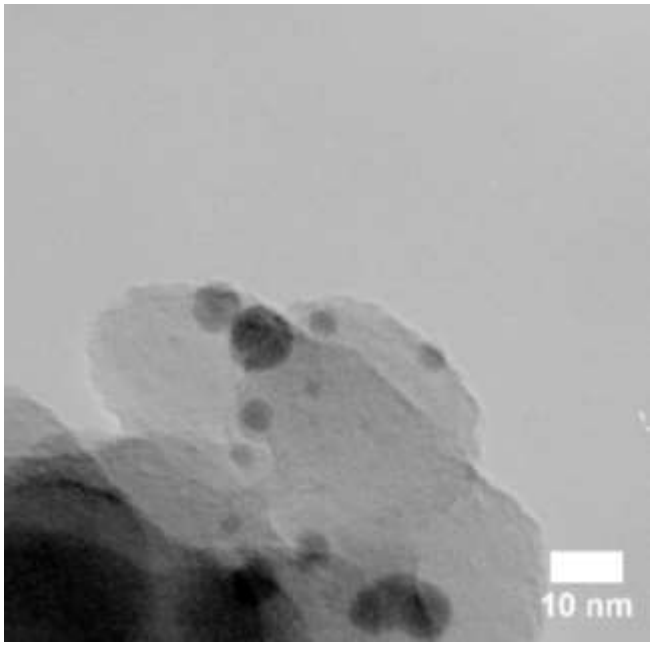

Figure 82: TEM image of Pd/Silica catalyst

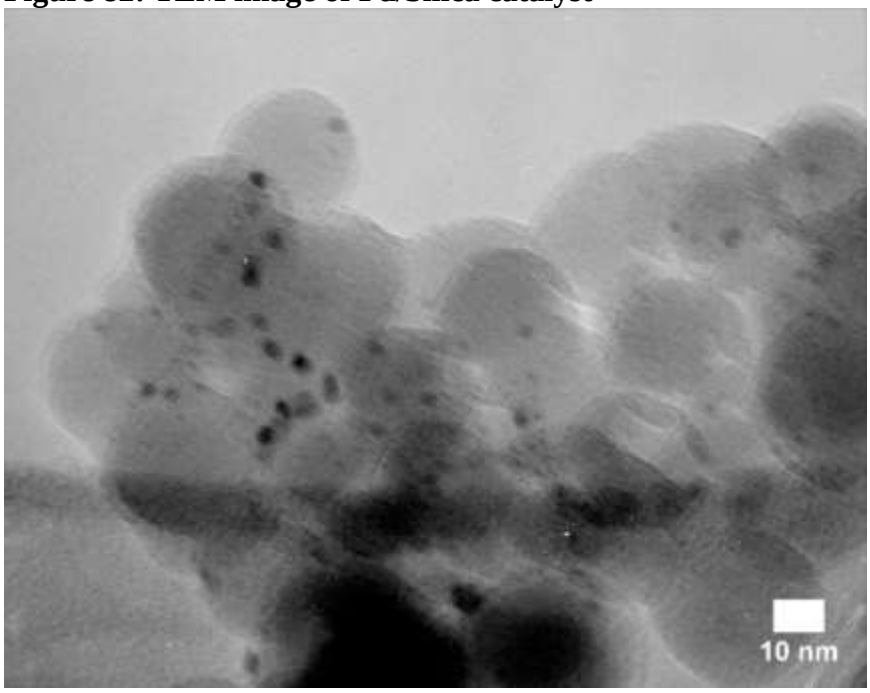

Figure 83: TEM image of Pd/Silica-OTS catalyst

Emulsions made with MWNTs and CTAB were made the same way as in Chapter 2 using 0.03 wt% of MWNTs with respect to water. The oil to water ratio was

kept at one to one. CTAB concentrations are with respect to the water. Decalin was used as an oil. The emulsions did not appear to break when varying the CTAB concentration. However, the emulsion droplet diameters did change, Figure 84.

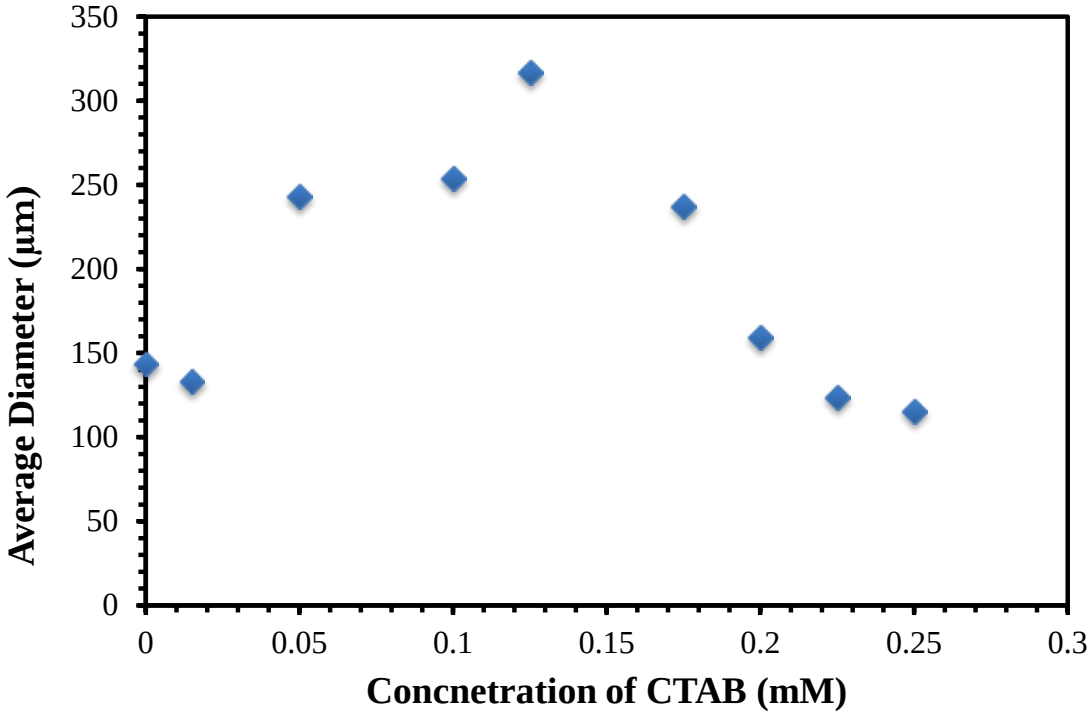

Figure 84: Dependence of emulsion droplet diameter with CTAB concentration when using MWNTs.

Since the most drastic change in droplet size is seen between CTAB concentrations of 50 µM and 175 µM CTAB an equimolar amount of SDS was added to samples with 50 µM, 125 µM, and 175 µM of CTAB. The solutions were then sonicated and droplet size measured again. After this a equimolar amount of CTAB was added and the solutions sonicated and the droplet size measured. As can be seen in Figure 85, Figure 86, and Figure 87 the emulsion droplet size initially increases due to the CTAB changing the wettability of the MWNTs. Then upon addition of SDS the CTAB and SDS form ion pairs and the MWNTs return to their original wettability,

indicated by the emulsion droplet size decreasing. Addition of additional CTAB results in the emulsion droplet size increasing due to the MWNTs wettability changing once again.

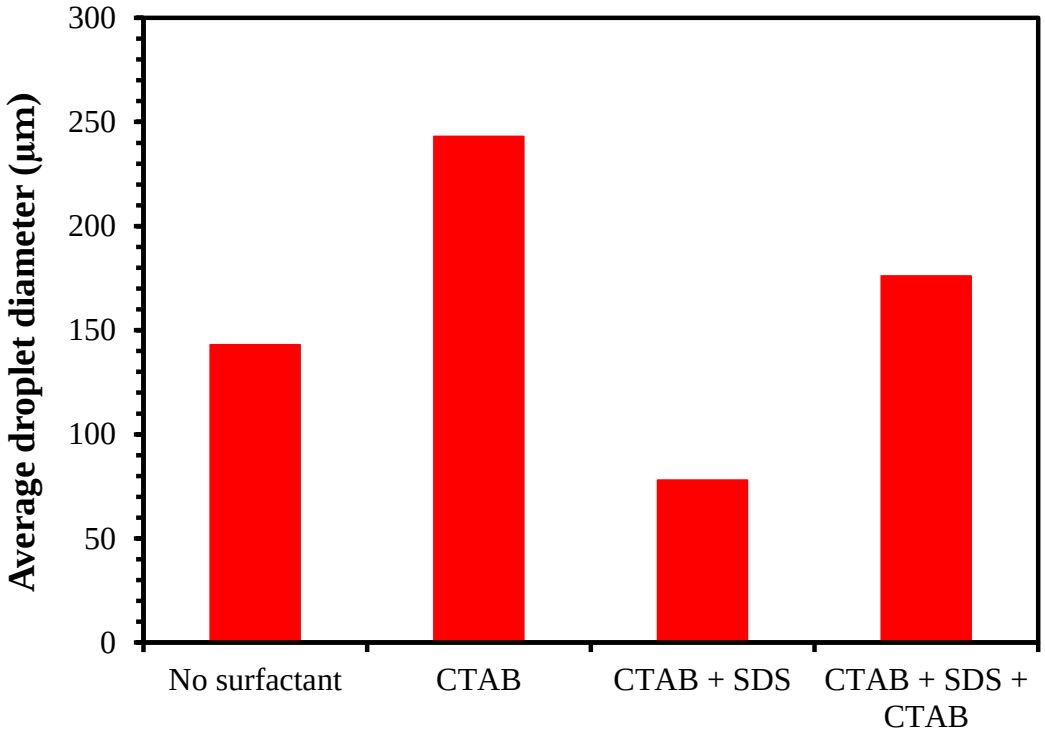

Figure 85: Comparison of emulsion droplet size when adding 50 µM CTAB, then 50 µM SDS, and then 50 µM CTAB again.

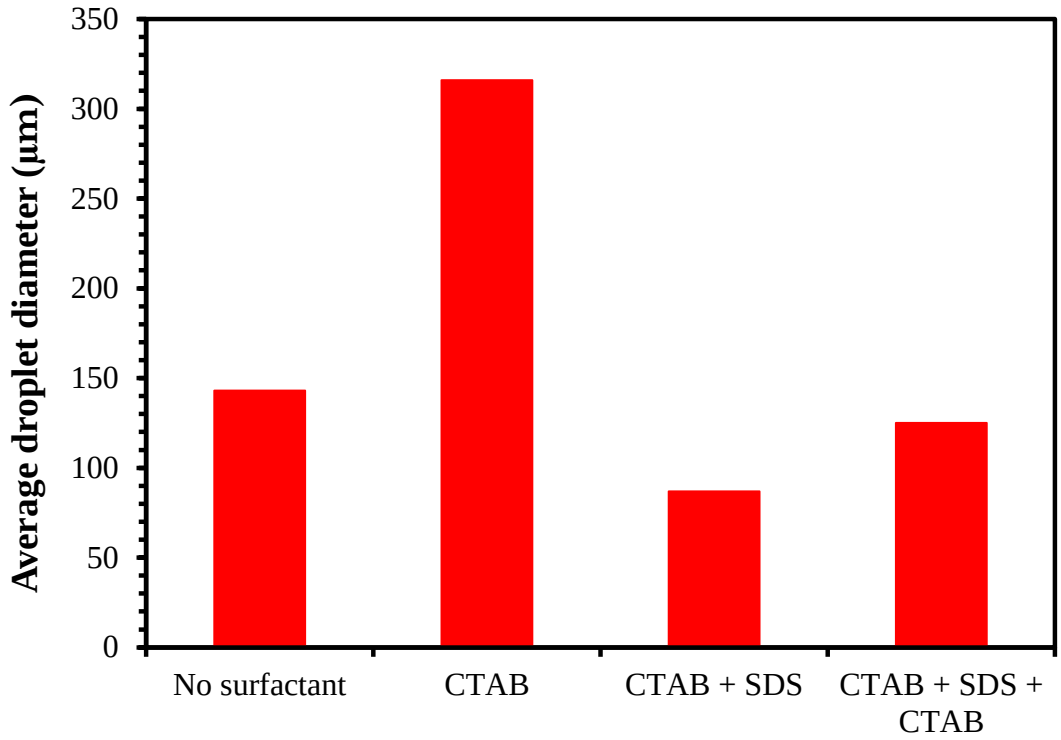

Figure 86: Comparison of emulsion droplet size when adding 125 µM CTAB, then 125 µM SDS, and then 125 µM CTAB again.

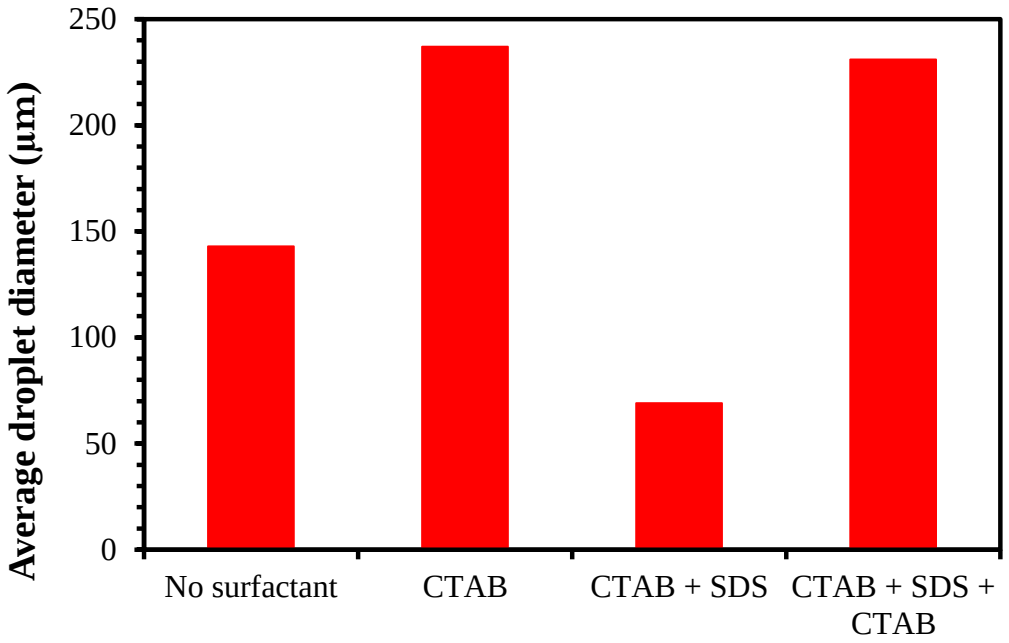

Figure 87: Comparison of emulsion droplet size when adding 175 µM CTAB, then 175 µM SDS, and then 175 µM CTAB again.

Reactions with Palladium supported on multi-walled carbon nanotubes. Reactions were run the same way as in Chapter 5, except CTAB was added. Conversion for the oil soluble reactant increases and the water soluble reactant decreases when using 10 μM CTAB, Figure 88. However, using a higher amount of CTAB, 125 μM, results in a decrease in conversion of the oil and water soluble reactants, but the selectivity remains similar to when using 10 μM of CTAB.

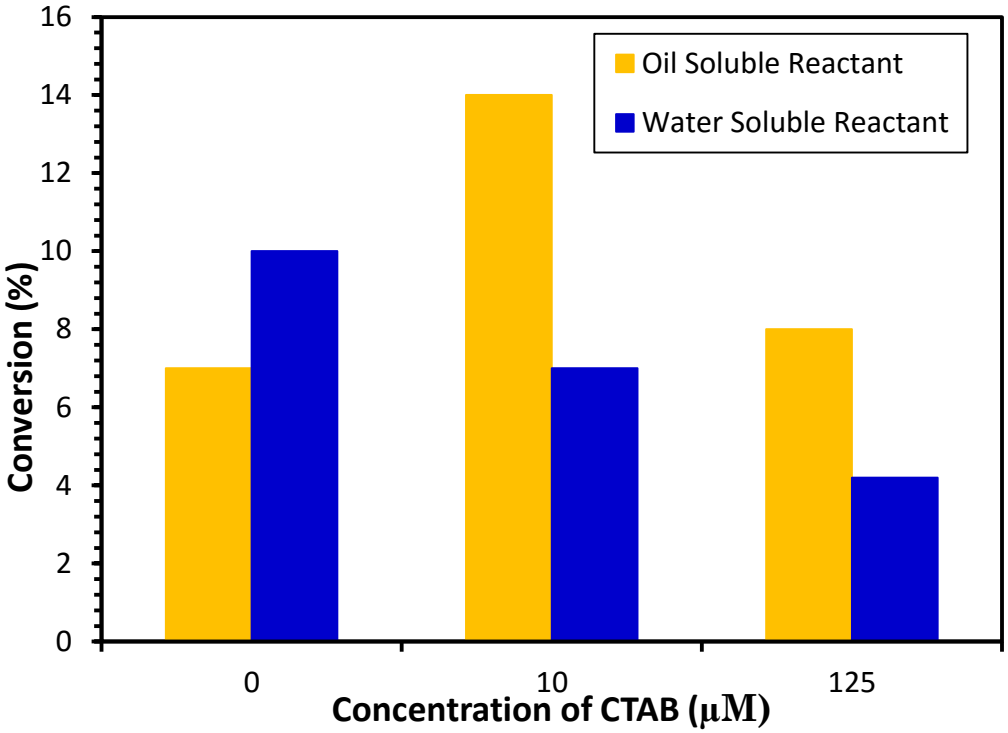

Figure 88: Reaction with Pd/CNT at different concentrations of CTAB in a emulsion.

To test the ability of MWNTs to phase transfer from one phase to another by using CTAB, MWNTs were mixed with aqueous solutions of various concentrations of CTAB. Then either undecanol or decalin was added and the vial inverted several times to mix the two phases together and allow the opportunity for the MWNTs to phase transfer. Undecanol and decalin were chosen as oils because of the difference in surface

tension each has between oil and water.[42,53] Several groups have shown phase transfer of particles between two phases only occurs when the oil-water interfacial tension is significantly low.[148,140,151,356] Using undecanol the MWNTs initially phase transfer to the oil because of their hydrophobicity, but as the concentration of surfactant increases the MWNTs being to phase transfer at a CTAB concentration of μM and appear to completely phase transfer at a concentration of 2500 μM, Figure 89. Using decalin as an oil the MWNTs are initially in both phases after mixing the phases, but with increasing CTAB concentration begin to transfer into the aqueous phase. At the highest CTAB concentration tested the a emulsion appears to form.

Figure 89: 0.03 wt% MWNTs dispersed in aqueous solutions containing various amounts of CTAB and then mixed with undecanol. The concentrations of CTAB in each vial from left to right is 0 μM, 15 μM, 25 μM, 50 μM, 75 μM, 100 μM, 150 μM, 200 μM, 250 μM, 2500 μM. In the photo it may appear the middle vials have MWNTs entirely in the aqueous phase, but this is due to the quality of the photo. Only the vial at the far right do the MWNTs appear to entirely be in the aqueous phase.

Figure 90: 0.03 wt% MWNTs dispersed in aqueous solutions containing various amounts of CTAB and then mixed with decalin. The concentrations of CTAB in each vial from left to right is 0 μM, 15 μM, 25 μM, 50 μM, 75 μM, 100 μM, 150 μM, 200 μM, 250 μM, 2500 μM.

References

[356] Ziegler, Kirk J., et al. "Length-dependent extraction of single-walled carbon nanotubes." *Nano letters* 5.12 (2005): 2355-2359.

Appendix A9: Supporting Information for Chapter 7

Supporting information for this chapter can be found on the RSC Advances journal website where the article was published.

The publication and supporting information can be found using the citation: Briggs, N. M., and S. P. Crossley. "Rapid growth of vertically aligned multi-walled carbon nanotubes on a lamellar support." *RSC Advances* 5.102 (2015): 83945-83952.

Appendix A10: Supporting Information for Chapter 8

Additional Reaction Data

For Pd/MWNT

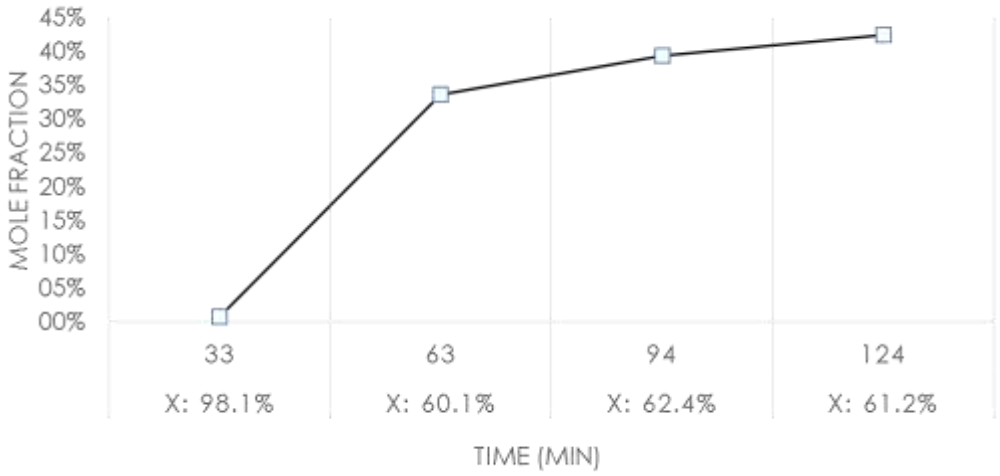

Figure 91: Conversion of furfural for Pd/MWNT

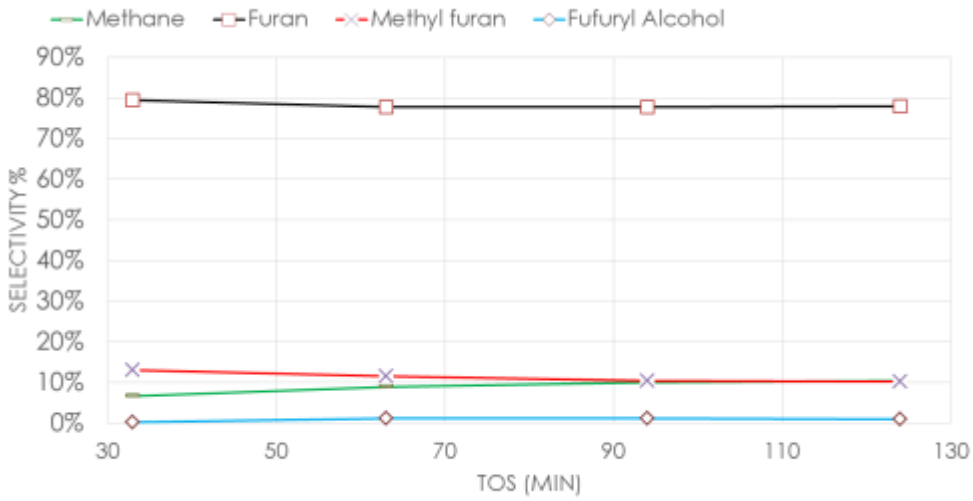

Figure 92: Selectivity using Pd/MWNT

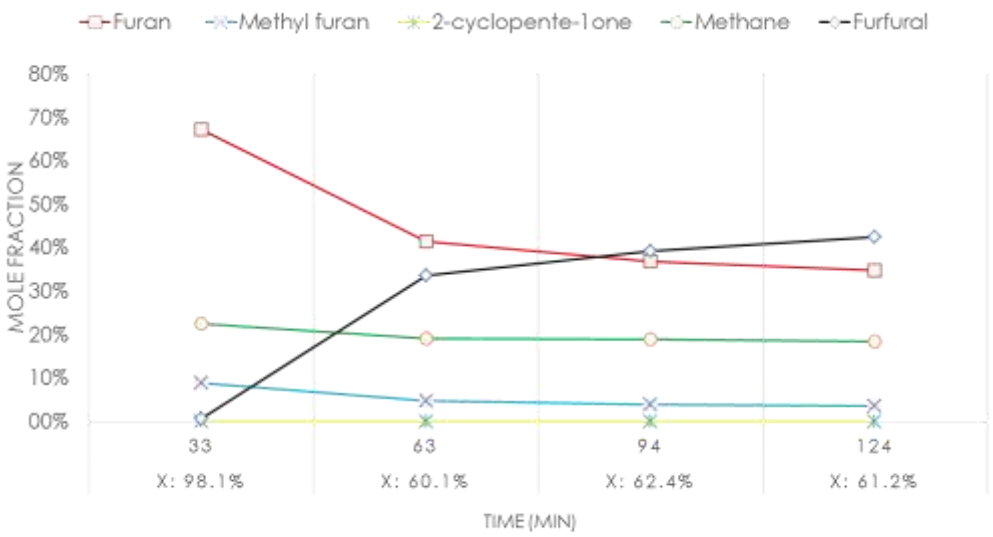

Figure 93: Mole fraction for Pd/CNT

For catalyst Pd/TiO_2/MWNT

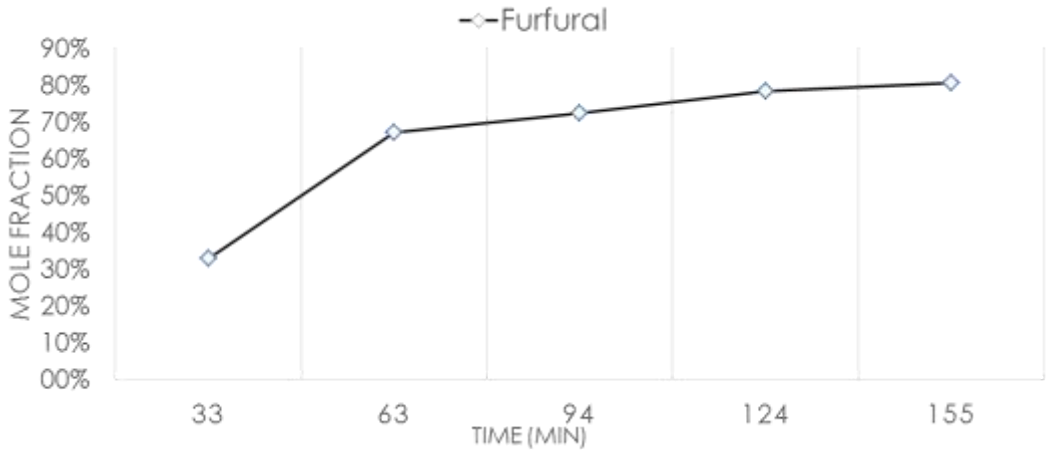

Figure 94: Conversion for Pd/TiO_2/MWNT

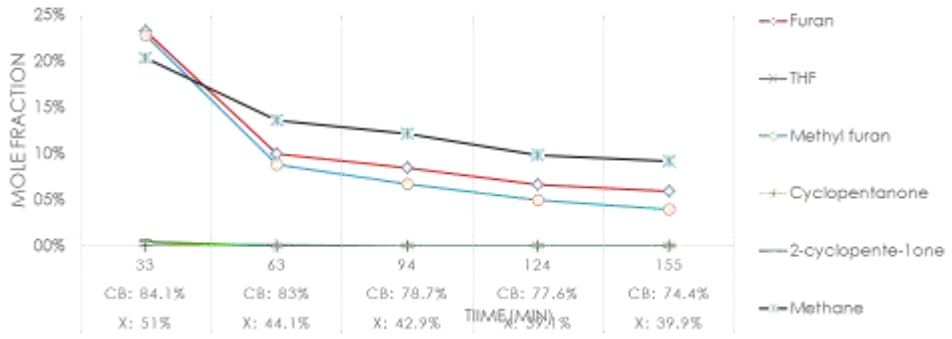

Figure 95: Mole fractions for Pd/TiO_2/MWNT

Pd and TiO_2 separated on MWNTs

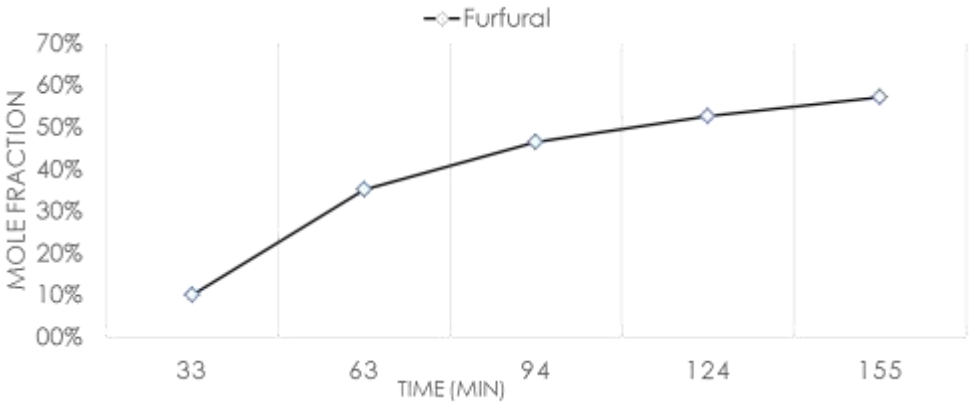

Figure 96: Conversion for Pd and TiO_2 separated on MWNTs

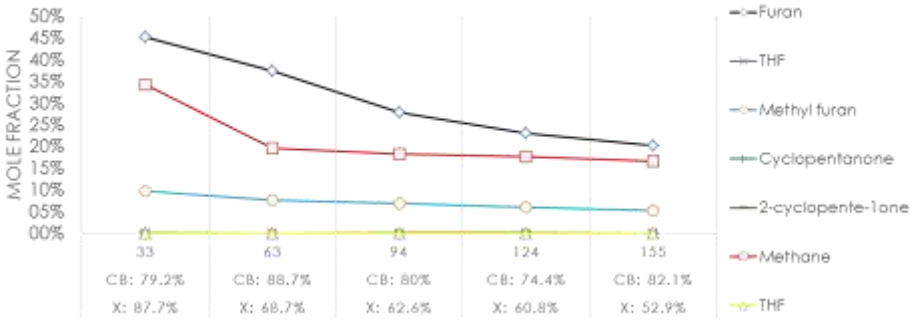

Figure 97: Mole fractions for products of Pd and TiO_2 separated on MWNTs

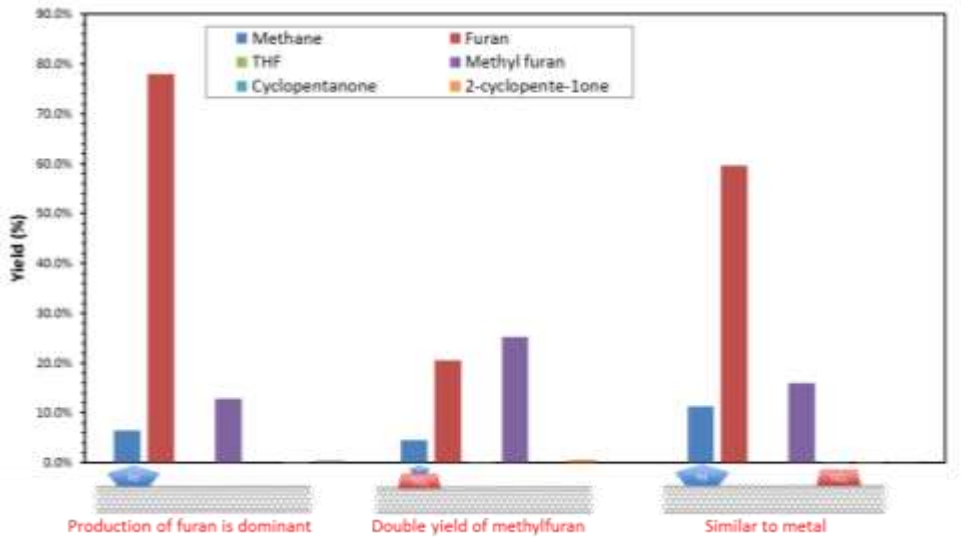

Figure 98: Yields for the three different catalysts.

Partial Masking of VMWNTs using Polymers

A different approach for partially coating VMWNTs is to partially embed VMWNTs in a polymer film.[357,358] With one end of the VMWNTs protected in the polymer the exposed end can be functionalized or have catalyst deposited on. After functionalizing or depositing catalyst on the exposed end a polymer with different solubility than the VMWNTs were initially embedded in can be used to cover the exposed end of the VMWNTs. Then the first polymer can be washed away and the second polymer left intact. This then allows for the now exposed end of the VMWNTs to be functionalized or have a catalyst deposited on. Once the exposed in has been treated the second polymer can be removed. The result is a VMWNT with functional groups on different ends or catalyst particles.

We have repeated this approach by using poly(methyl methacrylate) (PMMA) with a Mw ~ 120,000 and polyvinylpyrrolidone (PVP) with a Mw ~ 55,000. A silicon wafer 21 mm x 21 mm is spin coated with a PMMA solution consisting of PMMA in

toluene. The solution is placed on a silicon wafer and spun using a spin coater at 500 rpm for one minute. Depending on the weight percent of PMMA in toluene the thickness of the film will vary, Figure 99. Using a PVP solution consisting of PVP and isopropanol and spin coating on silicon wafers at the same speed can be used to make a PVP film. The weight percent of PVP in isopropanol can be used to control the PVP film thickness.

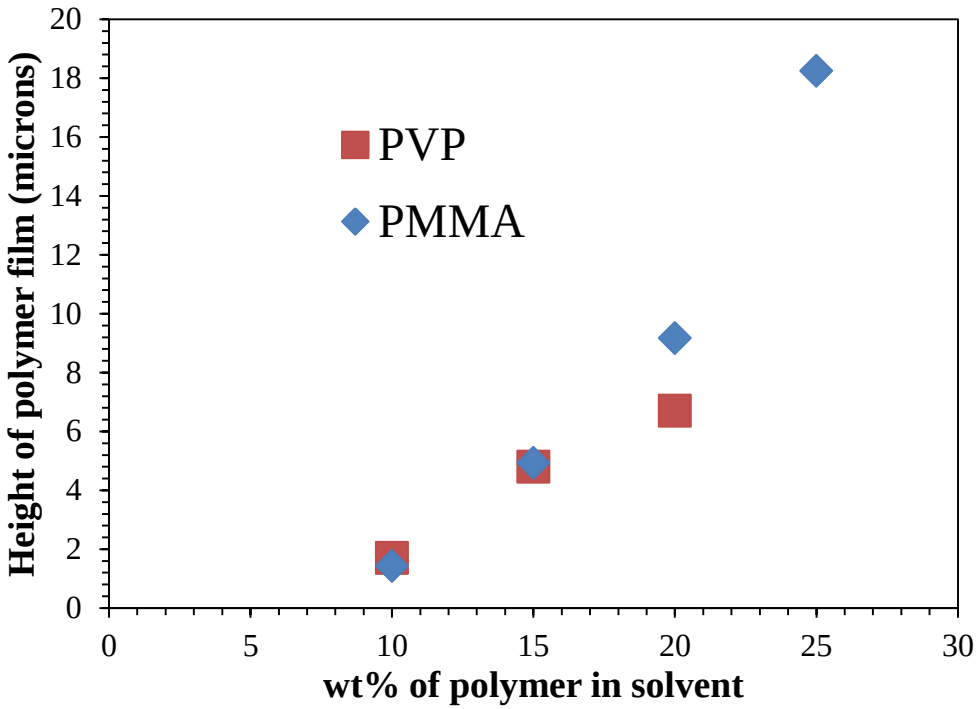

Figure 99: Dependence of polymer film thickness on a silicon wafer with the weight percent of polymer in the solution.

The VMWNTs are embedded in the polymer by placing the silicon wafer with the polymer film on a hot plate and the VMWNTs on the silicon wafer they were grown on the polymer. A weight of 500 g is then placed on top of the two sandwiched silicon wafers. The hot plate is then set to bring the temperature of the silicon wafers to 160°C. After reaching 160°C the temperature is held for 15 minutes. After which the weight is removed and the samples allowed to cool. The silicon wafer the VMWNTs are grown

on is then removed leaving VMWNTs embedded in the polymer film. This can be done with either a PMMA or PVP film. A SEM image of the VMWNTs embedded in the PMMA film can be seen in Figure 100.

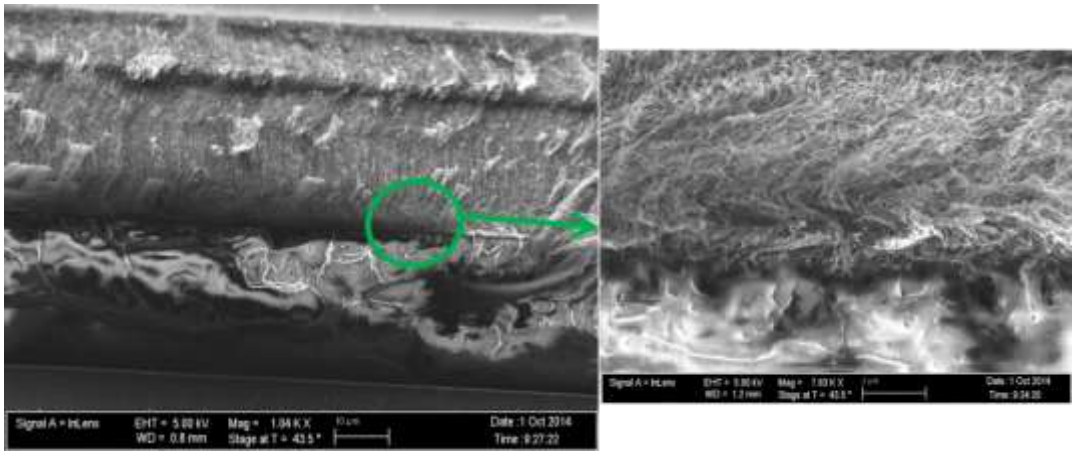

Figure 100: VMWNTs partially embedded in a PMMA film.

Two approaches were used to determine if the VMWNTs are embedded in the polymer and how much of the VMWNTs. For the first approach VMWNTs of nine microns were embedded in a PMMA film. Then the PMMA film thickness and portion of the VMWNTs above the polymer film measured. As can be seen in Figure 101 the a PMMA film made from a 10 wt% PMMA solution yields a polymer film thickness of 1.9 microns and the exposed VMWNTs is 6.3 nm. Indicating the VMWNTs are partially embedded in the polymer. Another example can be seen in Figure 102 where the PMMA film made from a 15 wt% PMMA solution yields a polymer film thickness of 4.0 microns and the portion of VMWNTs exposed is 5.9 microns. These two results indicate the VMWNTs are likely partially embedded in the PMMA film.

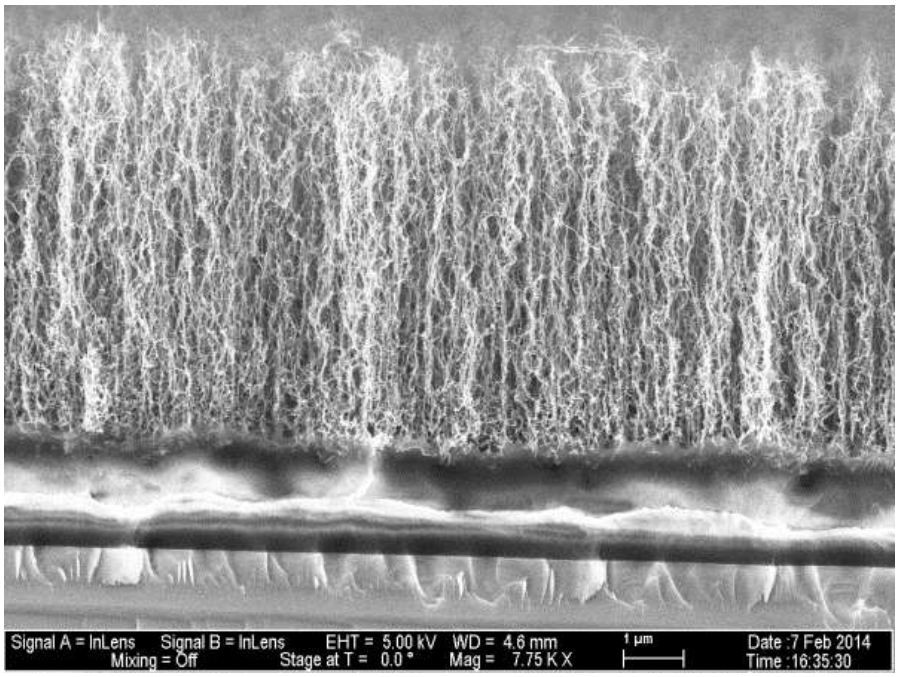

Figure 101: VMWNTs of nine microns in length partially embedded in a PMMA film made from a 10 wt% PMMA solution.

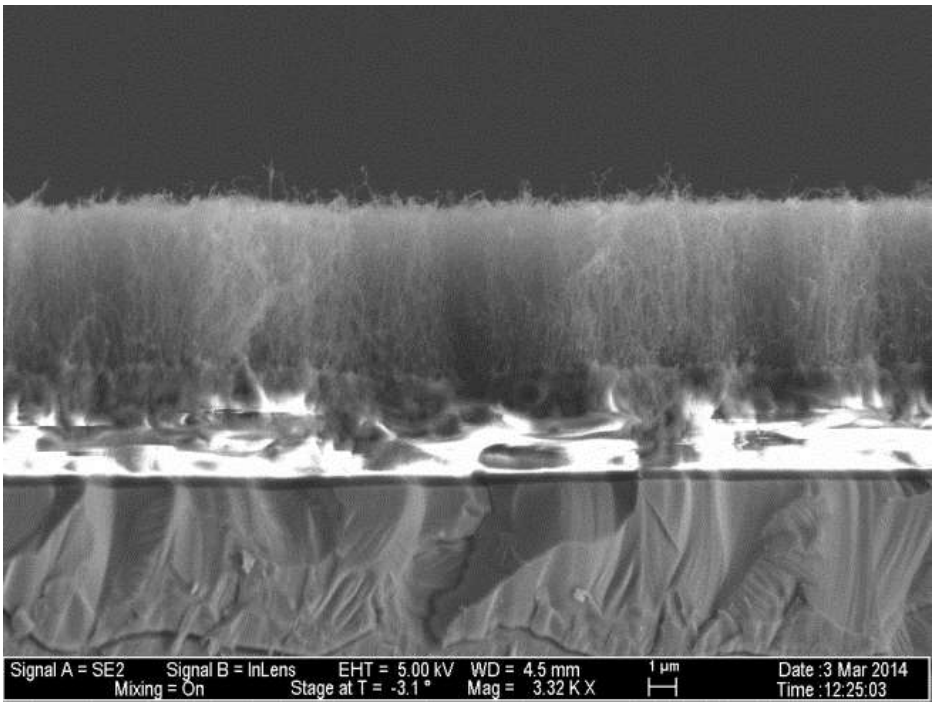

Figure 102: VMWNTs of nine microns in length partially embedded in a PMMA film made from a 10 wt% PMMA solution.

In the second approach after partially embedding the VMWNTs in a PMMA film made with a 10 wt% PMMA solution titanium isopropoxide was deposited on top of the exposed ends of the VMWNTs. The titanium isopropoxide was then hydrolyzed creating titania. Next the PMMA was washed away with toluene. From the resulting SEM images the exposed ends of the VMWNTs are embedded in titania, while the portion of the VMWNTs embedded in polymer are free of a titania coating. Thus, indicating the VMWNTs is partially being embedded in the polymer, Figure 103.

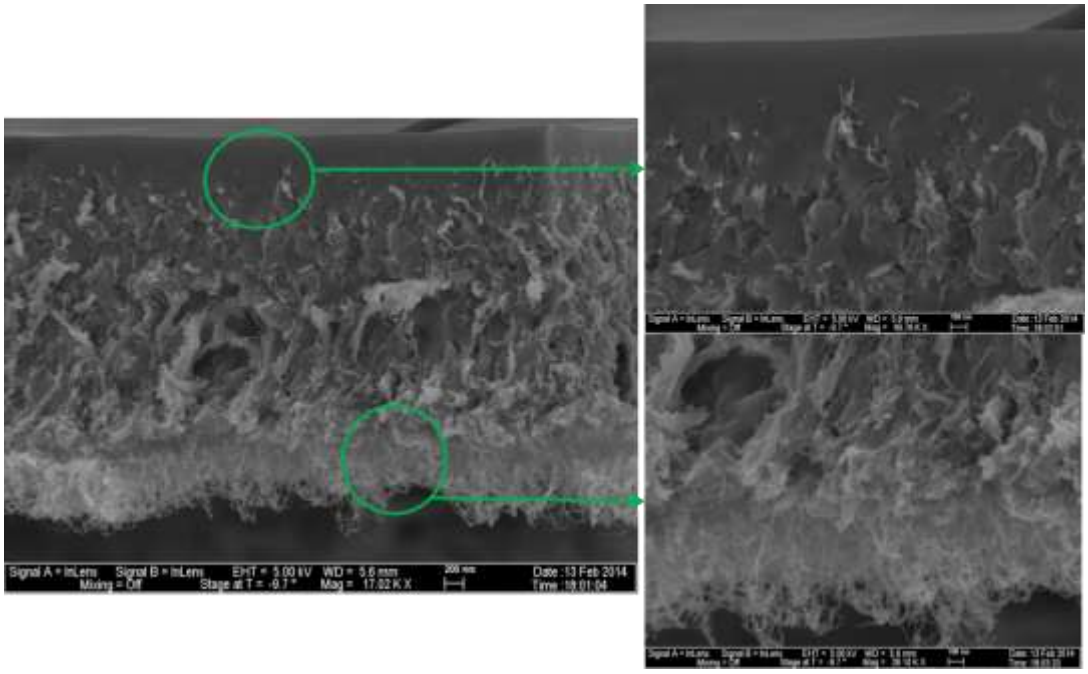

Figure 103: VMWNTs partially coated with titania.

If a barrier is desired to be created between the two ends of where catalyst or functional groups are on the VMWNTs then a second polymer can be used. After spin coating the first polymer, in this case PMMA, a second polymer PVP can be spin coated on top, Figure 104. This creates a two polymer films on top of one another and each with different solubility. A barrier between the two ends of the VMWNTs may be

desirable if catalyst sintering becomes a problem and the different catalysts at opposite ends of the VMWNTs need to be kept from coming in contact. VMWNTs can be partially embedded through both polymer films using the same approach as with a single polymer film.

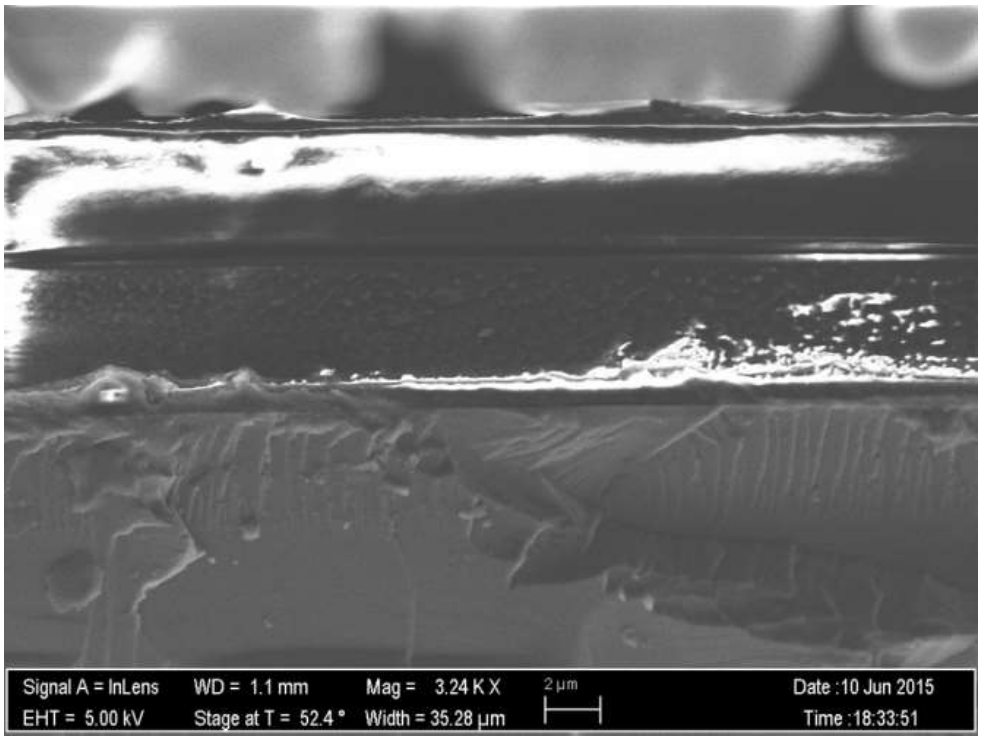

Figure 104: PVP film on top of a PMMA film.

References

[357] Peng, Qiang, et al. "Asymmetrically charged carbon nanotubes by controlled functionalization." *ACS nano* 2.9 (2008): 1833-1840.

[358] Qu, Liangti, and Liming Dai. "Polymer-masking for controlled functionalization of carbon nanotubes." *Chem. Commun.* 37 (2007): 3859-3861.